UTS UNIVERSITY OF TECHNOLOGY SYDNEY

Impact of Structural Pounding on Seismic Behaviour of Adjacent Buildings

by Yazan Jaradat

Thesis submitted in fulfilment of the requirements for the degree of

Doctor of Philosophy

under the supervision of Dr. Harry Far and
Dr. Mina Mortazavi

University of Technology Sydney
Faculty of Engineering and Information Technology

August 2023

CERTIFICATE OF ORIGINAL AUTHORSHIP

I, ***Yazan Jaradat*** declare that this thesis, is submitted in fulfilment of the requirements for the award of *Doctor of Philosophy*, in the *School of Civil and Environmental Engineering* (*Faculty of Engineering and Information Technology*) at the University of Technology Sydney.

This thesis is wholly my own work unless otherwise referenced or acknowledged. In addition, I certify that all information sources and literature used are indicated in the thesis.

This document has not been submitted for qualifications at any other academic institution.

This research is supported by the Australian Government Research Training Program.

Signature: Production Note: Signature removed prior to publication.

Date: 20/08/2023

DEDICATION

To my dear late father Mohammed Jaradat,

Though you never got to see this
you're in every page

May Almighty God rest his soul in eternal peace

ACKNOWLEDGMENT

This degree could not have been possible without the assistance, understanding, and guidance rendered by numerous of people with I would like to give special thanks to those who have influenced my work during my time at University of Technology Sydney.

First and foremost, I would very much like to express my appreciation and gratitude to my principal supervisor, Dr. Harry Far, for his limitless support, tireless contributions, and guidance throughout this work. Throughout the years, I have learned a great deal from him, as his scientific knowledge has always given me great advice for my research and providing me with additional research opportunities. Together with my co-supervisor, Dr. Ali Saleh and Dr. Mina Mortazavi, for their invaluable advice and unfailing assistance providing insightful comments, suggestions, and research advice throughout the research process, with I am greatly appreciate.

Secondly, I would also like to thank members of the UTS Structures Laboratory for their guidance, contributions, and professional support including Rami Haddad and Scott Graham for their extensive support in conducting the experimental works. Especially Peter Brown, for his extraordinary help in all technical matters regarding experimental shaking table tests. My deep sense of appreciation to all the academic and non-academic staff in the Faculty of Engineering and Information Technology for the help provided, their help and rapid support have been noted.

Thirdly, I would like to express my thanks to my dear friends and colleagues for rendered their precious time to cheer up and sharing on the work. Exclusively Dr. Mohammed Al-Zobbi for your kind advice in mathematical and statistical analysis and Dr. Piyush Punetha for the help on many technical aspects. We have spent many hours together, with countless trials, tribulations, and conversations, somehow managing to find our way through. Your friendship and continue support have been touched.

Words are not enough to my wonderful family, my wife and my kids for their love, trust, understanding, cheering and back me up during this long and challenging journey. Lastly, my love and gratitude went through my parent for their unconditional love and encouraging me to the value of learning and provided me an outstanding opportunity throughout the lifetime. Without all your endless support and love, I would not be able to achieve this goal.

LIST OF PUBLICATIONS RELATED TO THIS RESEARCH

Journal Articles

1. **Jaradat, Y**. and Far, H. (2023), "Impact stiffness of linear viscoelastic model for seismic pounding simulation: an experimental evaluation", *Civil Engineering Journal,* 9(6), 1289-1311. http://dx.doi.org/10.28991/CEJ-2023-09-06-01
2. **Jaradat, Y**., Sobhi, P. and Far, H. (2023), "An investigation into adequacy of separation gap to preclude earthquake-induced pounding", *Structural Engineering and Mechanics,* 86(1), 29-48. https://doi.org/10.12989/sem.2023.86.1.029
3. **Jaradat, Y**., Far, H. and Mortazavi, M. (2022), "Experimental evaluation of theoretical impact models for seismic pounding", *Journal of Earthquake Engineering*, 1-21. doi:10.1080/13632469.2022.2131654
4. **Jaradat, Y**. and Far, H. (2020), "Optimum stiffness values for impact element models to determine pounding forces between adjacent buildings", *Structural Engineering and Mechanics,* 77(2), 293-304. https://doi.org/10.12989/sem.2021.77.2.293
5. **Jaradat, Y**., Far, H. and Mortazavi, M. (2023), "A mathematical approach for predicting sufficient separation gap between adjacent buildings to avoid earthquake-induced pounding", *Civil Engineering Journal,* (submitted on April 2023)

Peer-reviewed Conference Papers

6. **Jaradat, Y**., Far, H. and Saleh, A. (2021), "Examining the adequacy of separation gaps between adjacent buildings under near-field and far-field earthquakes", Proceedings *of the thirteenth International Conference on Earthquake Resistant Engineering* Structures (ERES 2021), 26 – 28 May 2021, Online, pp.59-71. doi:10.2495/ERES210061

Table of Contents

List of Figures

List of Tables

LIST OF NOTATIONS

A_b, A_s	Cross-sectional area of the beam and the slab
ABS	Absolute sum method
C	Damping coefficient
C_h	Damping coefficient of the Hertz-damp model
$C(t)$	Impact damping coefficient time history
CQC	Complete quadratic combination method
d	Separation gap between adjacent structures
DDC	Double difference method
DS	Damping ratio of the short building as %
DT	Damping ratio of the tall building as %
$\underline{E}$	Modulus of elasticity
E	Earthquake peak ground acceleration in g
e	Coefficient of restitution
$F_{e,max}$	Maximum impact force from the experimental measurements
$F_{t,max}$	Maximum impact force from the theoretical simulation
F_c	Pounding impact force
FS	Frequency of the short building in Hz
FT	Frequency of the tall building in Hz
H	Building height
HS	Height of the short building in mm
HT	Height of the tall building in mm
k	Stiffness of linear spring
K_b , K_s	Axial stiffness of the beam and the slab
k_h	Stiffness of the nonlinear spring
L_b, L_s	Length of the beam and the slab in the direction perpendicular to the contact surfaces
LD	Laser displacement
m_i , m_j	Colliding masses of objects *i* and *j*
MAE	Mean absolute error
MDOF	Multiple-degree-of-freedom oscillators
MLR	Multiple linear regression analysis

MS	Mass of the short building in kg
MSE	Mean square error
MT	Mass of the tall building in kg
MTS	Multi-axial simulation shaking table
N	The number of observations
PE	Percent error
PGA	Peak ground acceleration
R	Radius of the sphere
R_a, R_b	Ductility factors of the adjacent structures A and B
S	Separation distance
SDOF	Single-degree-of-freedom oscillators
SF	Separation factor
SRSS	Square-root-of-sum-of-squares method
SS	Stiffness of the short building in kN/mm
ST	Stiffness of the tall building in kN/mm
T_a,T_b	Natural period for building *a* and building *b*
T_d	Duration of vibration
t_s	Slab thickness
T_g	Earthquake dominant vibration period
$\dot{u}_i, \dot{u}_j$	Relative velocity of the adjacent masses (m_i, m_j)
$u_a(t)$, $u_b(t)$	Lateral deflection time histories of building A and building B at the collision point
U_a, U_b	Peak displacement response of the adjacent structures A and B
u_i, u_j	Displacement of the adjacent masses (m_i, m_j)
v_i, v_j	Velocities of the colliding masses (m_i, m_j) exactly before impact
v_i', v_j'	Velocities of the colliding masses (m_i, m_j) exactly after impact
W_i	Average width of element *i*
Y_i	The actual data
$\hat{Y}_i$	The predicted data of minimum separation gap
α_y	Amplification factor
β	Impact stiffness for the nonlinear viscoelastic model
δ_1 , δ_2	Material parameters 1 and 2

Δe_a, Δe_b	Elastic displacements of the adjacent structures A and B
Δu_a, Δu_b	Peak inelastic displacements of the adjacent structures A and B
ζ_a, ζ_b	Damping ratio of building *a* and building *b*
ξ	Impact damping ratio for the linear viscoelastic model
$\bar{\xi}$	Impact damping ratio for the nonlinear viscoelastic model
ξ_h	Impact damping ratio of the Hertz-damp model
λ	Scaling factor
ρ	Poisson's ratio
ρ_{ab}	Correlation coefficient between the adjacent structures A and B

ABSTRACT

Investigations into earthquake-related damage reveal that buildings are susceptible to serious damage and/or collapse during moderate to strong ground motions. Among the possible causes of structural damage, seismic induced pounding become noticed in many historical and the current earthquakes due to inadequate separation gaps between neighbouring structures. Countries around the world have compiled building standards to address the pounding issue. One of the strategies recommended is the introduction of the separation gap between structures, as seen in Australian Standard AS1170.4-2007, which requires 1% of the building height as a leased space between buildings to preclude pounding. There is a need to examine this specification to find out whether or not it is adequate to prevent earthquake-induced pounding. Also it is necessary to propose mathematical equation to calculate sufficient separation gap in order to avoid the collision between adjacent mid-rise steel frame buildings.

However, if pounding occurs between adjacent buildings the impact lateral force should be considered in earthquake building design. Aiming to simulate pounding response, selecting the appropriate impact model and the model parameter's especially the impact stiffness k is considered as a critical factor in calculating the impact force during the collision of adjacent structures.

This research presents numerical and experimental results obtained through the shaking table tests under the effect of four scaled earthquakes, which were conducted on the scale models.

The outcomes indicated that the recommended minimum separation gap based on the Australian Standard is inadequate if the short building in a coupled case is utilised under both near-field and far-field earthquakes. The standard is adequate if a tall building is involved but only when a far-field earthquake happens.

Moreover, the results revealed that the theoretical impact parameters differ essentially with the identified experimental value since the supposition for deriving theoretical formulae does not match the actual impact effects. The results indicated that the numerical impact models over-predicted the pounding response. Nevertheless, the prediction results were corresponding with the experimental outcomes. The least variance and most accurate outcomes was produced by the linear viscoelastic model when the predicted results compared to the other models.

Correspondingly, the results revealed that the proposed mathematical equation to predict the separation gap is directly proportional to the height of the short building and earthquake peak ground acceleration. The concluded proposed equations are simplified to enable engineers evaluating the existing mid-rise steel frame buildings with no structural irregularity.

CHAPTER 1 **INTRODUCTION**

1.1 **Background**

Structural pounding is understood as the collisions occurring between neighbouring structures during earthquakes. The collisions occur due to inadequate space between the adjoining structures and their out-of-phase vibrations. In many cities, the gaps between adjacent structures are narrow or non-existent. This irregularity is attributed to financial and architectural constraints. For example, structural statistics from Eskisehir City in Turkey reveal that only around 36% of neighbouring buildings have adequate space or gaps between them (Doğan & Günaydin 2009). If a powerful quake occurs, the collision between the edifices will create a strong impact force and short interval acceleration pulses (spikes) on the adjoining buildings. The lack of adequate space or gaps between buildings is due to flawed engineering design, which can lead to catastrophic consequences (Miari et al. 2019).

The incidence of structural pounding has been recorded in many earthquakes. The largest reported magnitude of destruction associated with pounding happened during the 1985 earthquake in Mexico. There were traces of pounding noted among 15% of the damaged or collapsed buildings. About 20–30% of the damaged or collapsed structures showed that pounding was a key factor (Anagnostopoulos 1995, 1996; Rosenblueth & Meli 1986; Valles-Mattox & Reinhorn 1996). Figure 1.1 shows examples of earthquake-induced pounding damage detected in the 1999 Taiwan, 2008 Wenchuan and 2011 Christchurch earthquakes. Another example of pounding damage comes from the 1971 San Fernando earthquake, which caused permanent tilting of the stairway tower outside Olive View hospital, as shown in Figure 1.2.

Statistical studies from the 1985 Mexico earthquake estimated that about 10,000 people were killed, 50,000 suffered injuries and 250,000 became homeless (Degg 1989). Similar occurrences were noted in the Loma Prieta earthquake in 1989, in which 200 out of the 500 surveyed structures experienced pounding (Kasai & Maison 1997). Pounding between adjoining edifices was also detected in recent earthquakes, such as Lorca (Spain, 2001) (Romão et al. 2013), Wenchuan (Sichuan Province, China, 2008) (Wibowo et al. 2008), Christchurch (New Zealand, 2010) (Cole et al. 2010b), Christchurch (2011) (Cole et al. 2012b), and Gorkha (Nepal, 2015) (Shrestha & Hao 2018). Stonework and concrete

buildings were the most significantly affected by earthquake-induced pounding (Far 2019; Far & Flint 2017). In addition, central business districts of cities are filled with neighbouring buildings of different shapes and plan geometry. It is more likely during an earthquake excitation that asymmetric induced pounding may lead to torsional movements, which can cause critical harm in structures, especially when the shear demand surpasses the shear strength (Karayannis & Naoum 2017a, 2017b, 2018).

Figure 1.1 Detected pounding damage between adjacent structures: (a) 1999 Taiwan earthquake (b) 2008 Wenchuan earthquake (c) 2011 Christchurch earthquake (Hao 2015).

The pounding phenomenon is aggravated when the adjoining edifices throb out of phase. The condition is attributed to the difference in natural periods of adjacent structures, which is a common occurrence as most adjacent structures are of various dynamic properties (Figure 1.3) (Anagnostopoulos 1996; Degg 1992; Isobe et al. 2012).

Pounding scenarios are generally categorised into two classes: slab-to-slab (floor-to-floor) impact and slab-to-column (floor-to-column) impact (Cole et al. 2010a). The slab-to-slab collision takes place when the colliding structures have similar floor heights, while the slab-to-column collision transpires when the colliding edifices have diverse floor elevations (Figure 1.4). The second category of pounding scenario is more critical than the first type. This is because of the large shear forces imposed at the mid-height of the impacted column (Anagnostopoulos 1996).

Researchers have studied the abovementioned earthquakes to highlight the causes of massive damage that occurred due to pounding effects. They classified pounding into the following configurations (Figure 1.5):

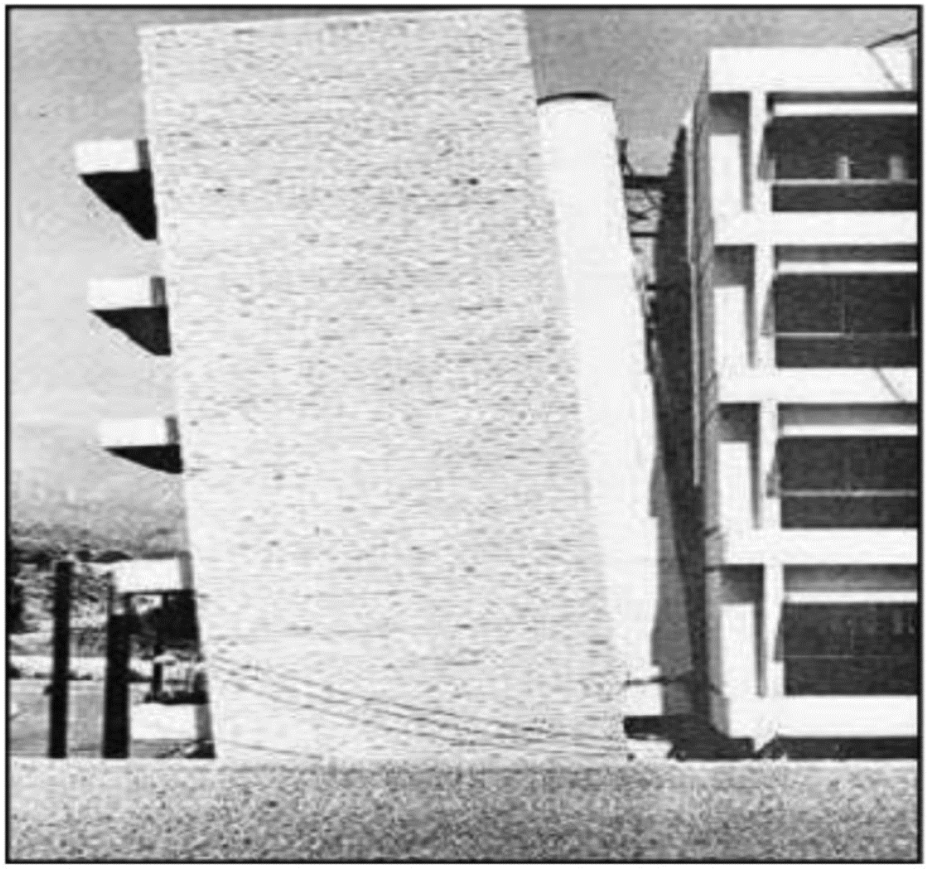

Figure 1.2 Perpetual leaning of a stairway tower; San Fernando earthquake, 1971, adapted from Jankowski (2009)

1. pounding of a lighter building adjacent to a heavier building (Jankowski 2008b; Kazemi et al. 2020)
2. pounding of a shorter building adjacent to a taller building (Cole et al. 2010a)
3. floor-to-column pounding (this type of collision is considered to have more serious consequences that can result in sudden collapse of the structure (Karayannis & Favvata 2005a, 2005b, 2008))
4. end building pounding (pounding between buildings in series) (Anagnostopoulos 1988; Raheem et al. 2018; Skrekas et al. 2014)
5. eccentric or non-eccentric pounding (Leibovich et al. 1996; Polycarpou et al. 2014; Raheem et al. 2019).

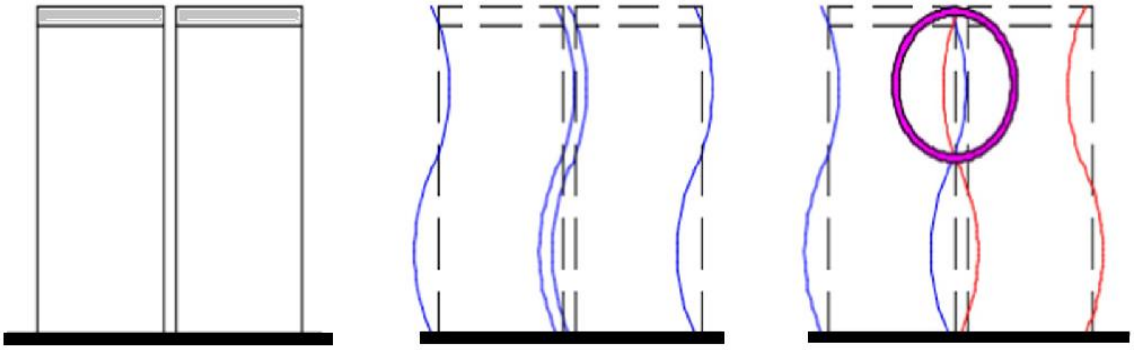

a) Before earthquake b) In-phase vibration c) Out-of-phase vibration

Figure 1.3 Seismic behaviour of adjacent buildings.

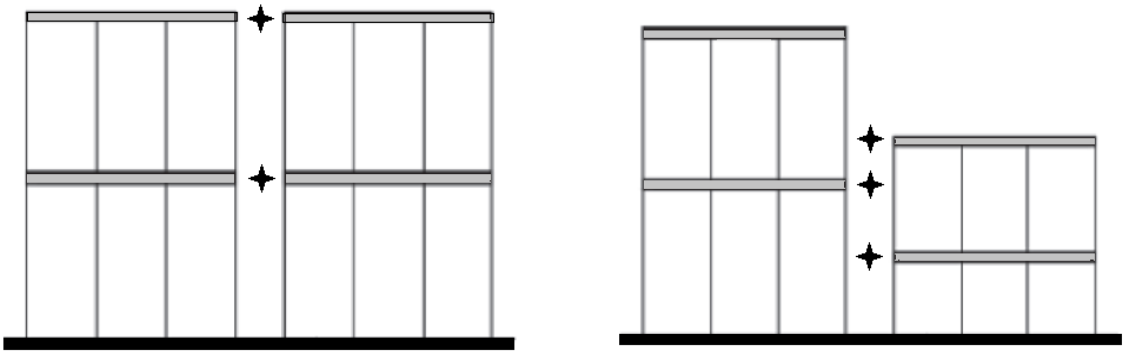

a) Floor-to-floor b) Floor-to-column

Figure 1.4 Pounding scenarios

Some scholars also consider a distinct sixth type of pounding configuration that is totally dedicated to pounding between masonry buildings (Cole et al. 2012b); masonry structures are particularly vulnerable to damage from pounding. Floor-to-column collisions, pounding between taller and shorter buildings, and end building pounding were the major reasons of damage through the Wenchuan earthquake (Sichuan Province in China in 2008) (Wibowo et al. 2008). The influences of these arrangements to pounding during the Christchurch (2011) (Cole et al. 2011a) and Taipei (Jeng & Tzeng 2000) earthquakes created on surveys of 119 and 708 buildings, respectively, are shown in Figure 1.6 (Miari et al. 2019).

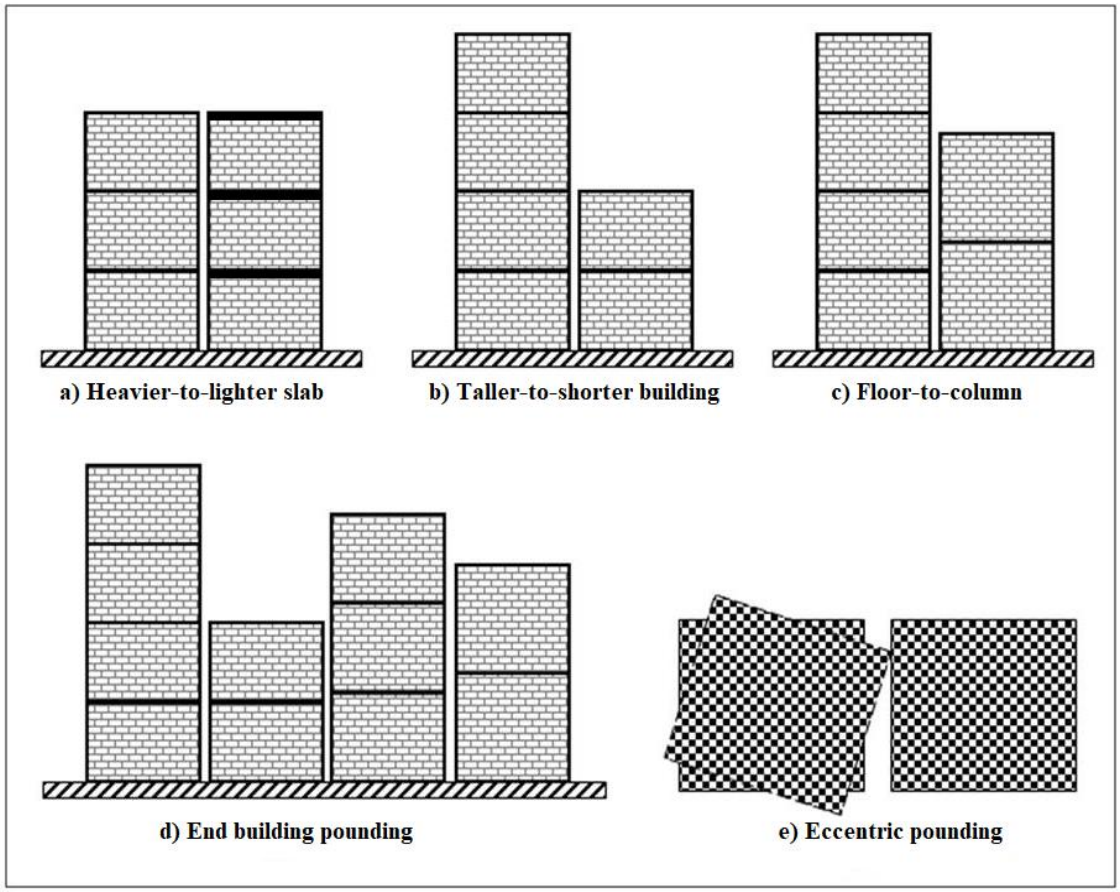

Figure 1.5 Pounding configurations

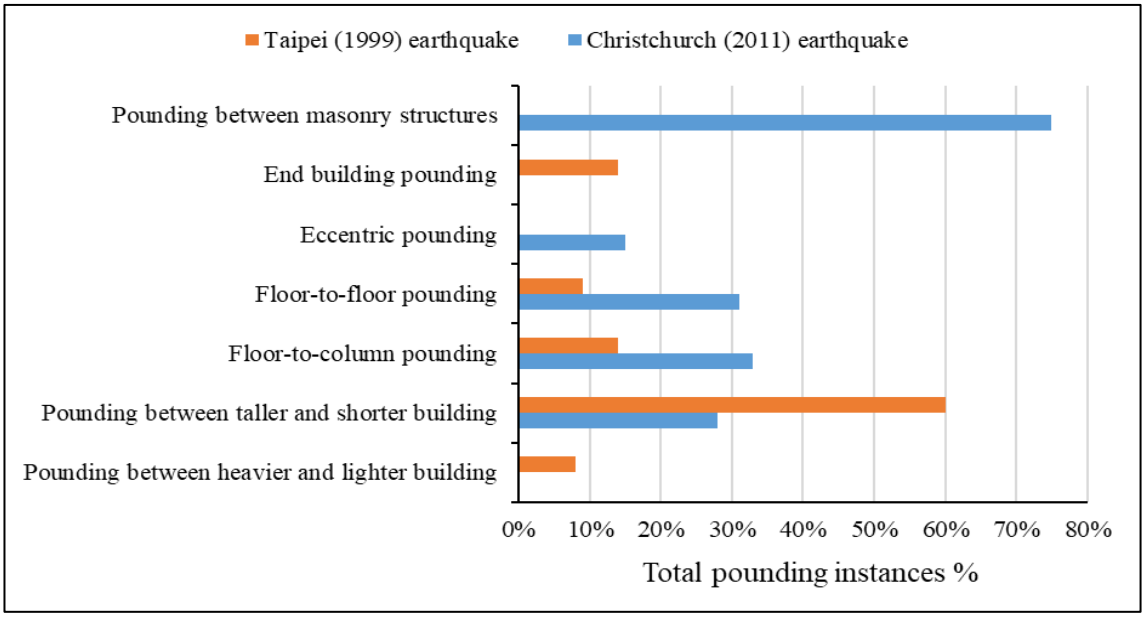

Figure 1.6 Influence of pounding arrangements during the Christchurch (2011) and the Taipei (1999) earthquake

1.2 **Research Significance**

Due to the significant effects of earthquake-induced structural pounding, several researchers have dedicated their studies on this phenomenon to well understand the factors influencing it and recommend the best mitigation methods for it. The ambiguity in the dynamic characteristics of adjacent structures may illustrate non-uniform trends in structural displacement histories. This results in high difficulty of the pounding phenomenon, making it more complex to study. The following research gaps have been identified:

Different impact models adopted to simulate pounding between adjacent buildings have created ambiguity and confusion in the research body. Moreover, engineers do not have clear formulae to follow for finding the impact model. Their numerical analyses have exercised impacts between reinforced concrete structures and the studies on pounding between steel buildings are very limited. Most of their analytical works utilise single-degree-of-freedom systems in order to elucidate the problem.

With the uncertainties in impact stiffness, k, there is no experimentally verified method of determining its value. Several researchers have proposed different methods to calculate the spring stiffness. The large number of methods has led to more confusion around choosing the appropriate value of k when conducting numerical analyses. Defining the appropriate k value is essential to ensure the accuracy of the results. Inappropriate value of k may have direct effects on the peak force and number of impacts between the adjacent buildings.

The Australian Earthquake Standard (AS1170.4-2007) does not provide definite guidelines for estimating the likely minimum building separation essential to preclude pounding. Due to growing building density and rapid property value increases in most Australian major cities in recent years, separation distance clauses for adjacent buildings are sometimes ignored or simply impractical.

The equations specified in literature and building codes involve the determination of lateral displacements of the adjacent buildings. Consequently, analysing both buildings is essential to calculate the gap distance. Therefore, there is a need to develop a simple method that does not require analysis to estimate the minimum separation gap.

1.3 Research Question

What is the appropriate formula that can be used as a standard to determine the minimum distance between adjacent buildings to reduce the impact of earthquake-induced pounding?

This leads to answering the following sub-questions before deriving a final formula

1. Does the Australian Earthquake Standard (AS1170.4-2007) clearly identified the minimum gap between the adjacent buildings?
2. What are the major factors that have direct impact on seismic pounding response between the adjacent buildings?
3. Are the current k values adequate for numerical simulation?

1.4 Research Objectives

The objectives of this study are as follows:

1. Experimentally investigate the safe minimum separation gap between two adjacent buildings to preclude pounding.
2. Examine the adequacy of the minimum separation gap prescribed by AS1170.4 to find out whether or not the minimum separation gap of 1% between two adjacent buildings is enough to preclude pounding under earthquake ground motions.
3. Experimentally develop a formula for the impact stiffness (k) for the linear viscoelastic model to simulate pounding between two adjacent unbraced steel structures.
4. Evaluate experiments to ascertain the efficiency of different analytical models in demonstrating the pounding response of closely spaced adjacent structures.
5. Develop and propose mathematical relationships for determining the minimum separation gap between two adjacent buildings to preclude pounding. The mathematical relationships will include various parameters such as height, mass, stiffness, natural period and damping.

1.5 Thesis Organisation

This thesis is organised into eight chapters. This chapter introduced the research problem, objectives and scope of the present study.

Chapter 2 provides a comprehensive literature review of past research on earthquake-induced pounding between adjacent structures. Previous experimental and numerical studies, impact models, building code recommendations and equations affiliated to the seismic pounding have been addressed.

Chapter 3 describes test frame models, test preparation and set-up and the adopted laboratory shaking table tests procedure for obtaining the experimental measurements of the coupled frames.

Chapter 4 presents experimental and numerical tests to investigate the adequacy of separation gap to preclude earthquake-induced pounding between adjacent buildings and to determine the sufficiency of the minimum separation gap prescribed by AS1170.4.

Chapter 5 develops a formula for the impact stiffness for the linear viscoelastic model using experimental measurements on pounding between multistorey buildings with various heights.

Chapter 6 evaluates the efficiency of different analytical models, namely the linear spring, linear viscoelastic, Hertz, nonlinear viscoelastic and Hertz-damp models in representing the pounding response of closely spaced adjacent structures.

Chapter 7 depicts experimental and numerical analysis using multi-linear regression analysis to develop the mathematical model capable of predicting sufficient separation gap between adjacent structures to avoid earthquake-induced pounding.

Chapter 8 presents the conclusions of the current research and recommendations for further research.

CHAPTER 2 **LITERATURE REVIEW**

2.1 **Overview**

Impact between adjacent structures during an earthquake is a phenomenon that has involved significant research interest in the recent and past. Pounding is a nonlinear problem due to its impact. In this review, previous studies and experiments related to the seismic pounding between adjacent structures will be addressed. Several experiments that were conducted by shaking table will be covered, and then numerical investigations that were conducted by using popular software applications such as Seismo-Struct, DRAIN2D-X and SAP2000 will be described. Furthermore, the analytical studies that pointed out the pounding force against structures in earthquake occurrences will be listed. All of these described studies aim to calculate the minimum separation gaps between adjacent structures by finding the correct values of pounding force.

2.1.1 Experimental Studies

Limited experiments have been performed to check the validity of the previous theoretical models in applying actual poundings between buildings detected in the field. Two major tests on shaking tables have been executed to validate theoretical models for seismic poundings. The experimental studies on pounding are mostly restricted to the elastic range to avoid permanent damage to the models.

Few experimental tests have been carried out to investigate the effects of pounding. Filiatrault et al. (1995) were among the first researchers who conducted shaking table tests on dynamic impact on two adjacent 1/8 scale single-bay moment-resisting steel frame models, 3-storey and 8-storey. The overall floor plan dimensions of both models were 800 × 800 mm, while the heights of the three-storey and the eight-storey frames were 1500 mm and 4000 mm, respectively. Three impact elements were designed to measure the impact force time histories between the first three levels of the frames. Compressive static tests were conducted on each impact element device to determine its element axial stiffness, which was 12.8 kN/mm. This value was used by Filiatrault et al. in a linear spring impact model to mimic collision forces in numerical studies. The frames were subjected to the first ten seconds of the 1940 El Centro earthquake ground motion, whose peak horizontal acceleration (PHA) = 0.15 g with initial separation of 0 and 15 mm gap. The experimental results were compared to results achieved from two software programs, SLAM2 and PC-ANSR. The amplitude and phase of the displacement and

impact force time histories showed good agreements. Acceleration at contact points were not predicted accurately for the specified period, although a malfunction of the impact element on the second floor disallowed any measurement of impact force time histories at this location.

Shaking table test conducted by Chau et al. (2003) to examine the pounding between two steel towers (2 m tall). The steel towers were constructed by four columns each, and spacing along the shaking direction and the orthogonal direction was 400 mm and 600 mm respectively. The two towers were of different natural frequencies, damping ratios and standoff distance. The frames were subjected to both harmonic excitation and ground motion from the 1940 El Centro earthquake. The experimental results were compared with theoretical prediction of nonlinear pounding using the Hertz contact law (Nonlinear elastic model), with an impact stiffness parameter, $\beta_e = 2.36 \times 10^{10}\ N/m^{\frac{3}{2}}$. The pounding occurrences have comparatively caused a relative impact velocity, excitation frequency and maximum standoff distance in both experiment and analytical findings. Also, periodic and chaotic pounding between structures were observed, which depends on the changes in the ground motion and the parameters of the two steel towers' characteristics. Numerical calculations showed that the relative impact velocity is less responsive to whether the contact is elastic or plastic. This shaking table experiment adopted a single-degree-of-freedom (SDOF) oscillator or steel tower to provide a simple technique for estimating the pounding hazard between two adjacent buildings.

Papadrakakis & Mouzakis (1995) used a shaking table to test pounding between two 2-storey reinforced concrete buildings with zero-gap separation. One building was designed to be flexible and the other was designed to be stiff. The overall frame dimensions were 2.7 × 1.6 × 5.4 m and 2.7 × 1.7 × 5.4 m for the flexible and stiffer structures respectively. A rigid slab response was assumed at each floor. The adjacent frames were subjected to sinusoidal and random motions. The experimental outcomes were compared to the predictions by the Lagrange multiplier method (corresponding to the stereo-mechanical method with $e = 1$). Overall, a good agreement between both results was achieved. It can be observed from the study that when a peak acceleration occurred in one level, during pounding, the consistent acceleration of the other level is not affected. This is true for during and after the impact occurrences. It is believed that peak acceleration or impulse that occurs at the pounding level may affect the equipment and the secondary components of a short natural period. This experiment can be considered as a unique full-

scale structure, which has not been repeated since. However, the pounding force was not tested in this experiment; therefore, the impact force calculations were missing.

Jankowski (2007) examined the interaction between several building materials (steel, concrete, timber and ceramics) by dropping relatively small balls on a rigid surface. The material's restitution coefficient and impact stiffness parameters for the nonlinear viscoelastic model were obtained. The results indicated that the restitution coefficient e value does not depend on the mass of the balls tested but it is much sensitive to the prior-impact velocity. For example, for the steel ball when prior-impact velocity were 0.2 and 2.0 m/s the coefficient of restitution was ranged between (0.64 - 0.74) and (0.48 - 0.51) respectively. Furthermore, the results obtained indicate that the impact stiffness parameter does depend on mass of the tested balls and does not depend on the prior-impact velocity. For example, for the steel ball when the ball mass was 0.053 and 2.013 kg Impact stiffness parameter $\beta[N/m^{\frac{3}{2}}]$ was 1.3×10^{10} and 5.44×10^{10} respectively. The results of the study can be applied to study the impact between different types of colliding bodies in different conditions.

Rezavandi & Moghadam (2007) performed shaking table tests on pounding between 1/10 scaled 3-storey and 6-storey / single-bay moment-resisting steel frame structures. The frames were considered as 2D models; the heights of the 3-storey and the 6-storey frames were 900 and 1800 mm respectively. The impact element consisted of a steel box and a No.8 bolt of 60 mm length used to change the distance between the two adjacent frames. According to the test results, an element axial stiffness value of 0.55 kN/mm was used in the numerical studies. The frames were subjected to harmonic excitation and three different earthquake ground motion records. A 40% scale factor was applied to the records to prevent any damage. Different separation gaps were used in this experiment. The experimental results were compared to results obtained by SAP2000 version 7.21. The in-phase motion and maximum absolute displacement showed acceptable agreement for the no-pounding condition, while it showed poorly estimated acceleration responses for the pounding condition. Also, more impacts occurred experimentally than were obtained numerically. This was due to the sensitivity of the impact element stiffness. The use of dissipating materials can decrease induced acceleration when pounding happens. Referring to their experiment, Rezavandi and Moghadam found that error sources include the probability of inelastic activities in the frame models due to collisions, errors in

responses measurement, sensors limitations, differences between actual applied motions and the intended ones, connection and impact elements characteristics. However, the study did not show the impact pounding force between the contact levels.

In an extensive laboratory experiment, Van Mier & Lenos (1991) studied concrete-to-concrete pounding between breakwater armour elements. A sequence of dynamic experiments were carried out as pendulum tests between a prestressed concrete pile and a concrete striker of variable mass, contact surface geometry, geometries, velocity at impact and concrete quality. The load-time histories during contact were obtained from the experiment and an impact stiffness parameter was derived using the Hertz law. It was found that all parameters are size dependent. In principle, all parameters can be derived from static experiments, except the restitution contact stiffness. Currently, the most reliable results are those for the spherical/planar geometry.

Although valuable insight into the pounding problem attracted highway bridge researchers. To evaluate the accuracy of the theoretical impact stiffness parameters used in contact-element models, Guo et al. (2012) used a shaking table to examine seismic-induced pounding responses of a steel highway bridge model with two segments. 1:30 scaled length bridge model has been designed based on a typical prototype structure. A rectangular shape was designed for each deck of the steel bridge model, thickness and mass with 1000 mm × 400 mm in plane, 20 mm and 62.4 kg, respectively. Three frames used in order to support the two decks with six columns. A series of harmonic excitation waves and a series of ground motions from the 1940 El Centro, 1995 Kobe and 1994 Northridge earthquakes were used for the shaking table inputs. The impact stiffness for four commonly used impact models obtained theoretically was compared with the experimental results and was found to be significantly different. The analytical results reveal that the impact stiffness accomplished from the theoretical methods deviates substantially from the experimental outcomes, with approximately 70 times and 300 times difference for the nonlinear and linear impact models, respectively. The theoretical impact stiffness of the impact models based on the linear spring is farther to the experimental outcomes than those based on the nonlinear spring. Nevertheless, due to the constraints of the experimentation technology, there isn't an appropriate sensor for directly determining the impact force. Consequently, an indirect technique is adapted in this study to determine the impact force during pounding of the highway bridge model.

2.1.2 Numerical Studies

Maison & Kasai (1992) conducted a parametric study to analyse pounding between two non-equal-height, multistorey buildings – 15-storey and 8-storey – subjected to the 1940 El Centro ground motion. They used the microcomputer program SLAM2. In this study, to simulate the pounding force between storey levels, linear spring element model was used. The spring stiffness was equivalent to the axial stiffness of a concrete floor slab having the same thickness and width as that in the adjacent building. It was found that pounding occurring at building mid-height can increase the peak storey responses over the entire building height. Also, pounding resulted in larger adverse effects on the lighter structure with increase in the relative mass.

Using a finite element analysis software, SAP2000, Shakya et al. (2008) demonstrated the effects of mid-column collisions of reinforced concrete buildings considering soil–structure interaction effect. Pounding force is modelled with a Kelvin–Voigt contact element and gap element. Soil flexibility is modelled by mass-spring-damper discrete models positioned at the foundation. To simulate contact of buildings and pounding force, the impact element is created by combining a gap element with a Kelvin–Voigt element. The impact stiffness and the damping coefficient of the Kelvin–Voigt model were obtained from Jankowski (2005) for concrete-to-concrete impact $k_k = 93{,}500\ kN/m$ and the stiffness of gap element k_G is considered as $100k_k$. Again, the stiffness values were chosen from previous study.

Pant et al. (2010) compared two recently proposed linear contact element models, the amended Kelvin–Voigt (MKV) model and the amended Kelvin (MK) model, for seismic pounding between 8-storey and 10-storey reinforced concrete moment-resisting frame buildings. The impact stiffness and the damping coefficient of the Kelvin–Voigt model were obtained from Jankowski (2005) for concrete-to-concrete impact $k_k = 93{,}500\ KN/m$ and damping ratio $\xi = 0.35$ and the coefficient of restitution $e = 0.65$. It was determined that the MKV model was more appropriate than the MK model for simulating earthquake-induced pounding.

Mate et al. (2012) conducted a comparative study on linear and nonlinear contact element models for three adjacent single-degree-of-freedom and multi-degree-of-freedom structures. The impact models were linear-based spring (linear spring element, Kelvin–Voigt model, and modified KV model) and nonlinear-based spring (Hertz contact model, Hertz-damp model, nonlinear viscoelastic model). The value of gap element stiffness for

the linear spring contact element models was taken from Jankowski (2006) as $K_l = 9.74 \times 10^6 N/m$, while for the nonlinear contact element models it was dependant on the Hertz law. The results obtained by both SAP2000 and MATLAB reveal that all contact element models anticipate the pounding response of closely spaced structures, which is acceptable agreement with each other. In addition, the pounding outcomes depend on the earthquake characteristics and the relationship between the buildings' fundamental periods.

Pounding response was simulated with the use of the Kelvin–Voigt model in a study performed by Cole et al. (2012a). The contact element stiffness K_k was calculated by setting the contact element stiffness equal to the smaller axial stiffness of the colliding slabs at the examined nodes. These stiffness values were calculated by taking tributary width measurements. When beams were affiliated parallel to the direction of the predicted contact force, and were located at the examined node, their stiffness was added to that considered in the diaphragm.

Sołtysik & Jankowski (2015) conducted nonlinear dynamic analysis on earthquake-induced pounding between two adjacent steel buildings, three and four storeys with different geometry. Six three-dimensional gap-friction elements were utilised (two for each storey) to investigate the pounding-involved response of the buildings. The friction coefficient of 0.5 was applied in the analysis. The structure was subjected to the 1940 El Centro ground motion. The results of the study indicated that the peak response of the 3-storey structure declines due to pounding by 6.8% and 21.7% in the longitudinal and transverse directions, respectively. On the other hand, it leads to the increase in the peak displacement of the 4-storey building by 86.7% and 95.5% for the longitudinal and transverse direction, respectively. Gap-friction elements are rarely used by researchers.

A numerical study on earthquake-induced pounding between two single-degree-of-freedom adjacent buildings was conducted by Naderpour et al. (2016). Dynamic analyses of the 1966 Parkfield, the 1971 San Fernando, the 1995 Kobe and the 1940 El Centro earthquake records were performed. Nonlinear viscoelastic model was used to simulate the pounding response. The results of the study point out that the impact force time history depends significantly on the earthquake excitation analysed. Furthermore, the peak impact force throughout collision is very dependent on such factors as gap size, coefficient of restitution, impact velocity and the impact element spring' stiffness. This

study gives special attention to calculating values of impact forces during collisions and does not show how the model impact parameters were chosen.

Another numerical analysis of earthquake-induced pounding between inelastic 3-storey adjacent buildings subjected to the 1940 El Centro ground motion was conducted by Jankowski (2016). In this study, to simulate impact force due to earthquake-induced pounding between storey levels, nonlinear viscoelastic model has been employed and the model's parameters were selected from an earlier study. The impact stiffness parameter $\beta = 2.75 \times 10^9 N/m^{\frac{3}{2}}$ and damping ratio $\xi = 0.35$ and coefficient of restitution $e = 0.65$ (Mahmoud & Jankowski 2011). The results of the study indicate that the response of the lighter and more flexible inelastic building can be considerably influenced by structural interactions and collisions. This may cause permanent deformation of the structure.

López-Almansa & Kharazian (2018) proposed a new formula for estimating the damping parameter for the Kelvin–Voigt model for seismic pounding simulation. The proposed formula was based on an approach presented by Anagnostopoulos (Anagnostopoulos 2004). The dynamic behaviour of the colliding frames is simulated using Seismo-Struct software. When compared with the proposed formula, the numerical results for Anagnostopoulos's approach showed significant differences in some cases, even though the accuracy of the Anagnostopoulos formulation is enhanced at a reduced computational cost, given that the suggested algorithm needs to be calculated only once for each analysis.

2.1.3 Analytical Studies

Lin (1997) analysed the ambiguity of the separation gap required to preclude earthquake-induced pounding of two adjacent buildings. The analytical techniques were based on arbitrary vibrations. The outcome of this study indicated that the theoretical results adequately reflect the simulated results. Wider separation gap is essential for both adjacent buildings having a longer fundamental period.

Lin & Weng (2002) examined the pounding probability of buildings designed according to the 1997 Taiwan Building Code (TBC) to gain understanding into the validity of the pounding-related provisions. A total of 36 cases of adjacent buildings A and B were studied. The conditional probabilities of adjacent buildings parted by minimum code-specified separation distance under earthquakes with different peak ground acceleration

(PGA) were examined under 1000 artificial earthquakes. Results revealed that the building separation indicated by the TBC is approximately 1.6 times that indicated by the Uniform Building Code (UBC) for the same building and soil properties. The probability of surpassing the design basis ground motion indicated in UBC-94 during a 50-year period is 10%.

To calculate critical separation gap between adjacent nonlinear hysteretic structures, a novel method has been anticipated by Garcia (2004). A pair of single-degree-of-freedom (SDOF) arrangements was investigated, and the mean peak displacement responses were obtained through numerical simulations (nonlinear time history analysis). He investigated the correlation coefficient ρ, which was obtained for calculating the separation distance anticipated by Filiatrault, Penzien, Kasai and Valles. Results were expressed in terms of the ratio minimum separation to peak relative displacement response. The outcomes of the anticipated method indicated that, this method delivers reliably conventional estimates of critical separation distances, the degree of conventionalism generally being minor in most cases. When matched to other existing approaches, the anticipated approach demonstrated a number of appropriate advantages. The foremost disadvantage was the fact that the anticipated values of ρ are obtainable only in charts.

Ye et al. (2009) re-examined the derivation of the equation for the damping constant ξ_h in the Hertz-damp contact model. It was found that the derivation is established on the following assumptions: (1) that the energy dissipated throughout impact is insignificant compared with maximum absorbed elastic energy, and (2) that the penetration velocities throughout the compression and restitution are alike. To make the Hertz-damp model valid for pounding analysis in structural engineering, the modified expression for the damping constant ξ_h should be derived again. Through numerical investigation, the accuracy of the formula and its corresponding theoretical derivation has been confirmed. Further reliable results of pounding simulation in structural engineering can be provided by using the Hertz-damp model with the modified formula for the damping constant.

The correctness of the double difference combination (DDC) rule was assessed by Lopez-Garcia & Soong (2009) in order to predict the separation distance necessary to avoid seismic pounding between linear structural systems. Adjacent structures, structure A and structure B, were modelled as 5%-damped SDOF systems with the natural periods T_A , T_B and damping ratios ζ_A , ζ_B. The results indicated that, when the value of the T_A/T_B ratio

is greater than 0.75, the DDC rule is always conservative, and when the value of the T_A/T_B ratio is less than 0.75, the DDC rule is always un-conservative. Furthermore, the accuracy of the DDC rule depends on the relationship between the values of the natural periods of the structures and the value of the period allied with the main excited frequency.

In the abovementioned experimental studies, several gap-separation (distances) were considered. However, none of these shaking table tests provided the maximum stand-off distance as a function of the excitation frequency. Another limitation of the above experimental studies is that the parameters of the adjacent buildings have been fixed, such as the structure mass, stiffness and height.

Moreover, it is observed that the past numerical studies on pounding between adjacent structures are modelled as linear systems using link and beam elements. They were considered multiple-degree-of-freedom (MDOF) systems, where the mass is concentrated at each floor. The local effects, such as damage to a column being pounded by a slab of an adjacent building, were not considered, whereas the effects of collision on the whole structural response were considered.

Due to the difficulty and nonlinearity affiliated with colliding process (inelasticity, plasticity, viscoelasticity, frictions and numerous methods of energy dissipation), several simplified impact force models have been anticipated to simulate pounding force between two colliding adjacent structures. Commonly, contact is modelled using either a continuous force model or via a stereo-mechanical (coefficient of restitution) approach. The analytical formulations of the various impact models are outlined below.

2.2 **Impact Numerical Models**

Typically, pounding is modelled using either a continuous force model or via a stereo-mechanical (coefficient of restitution) approach. The analytical formulations of the several impact models are defined below.

2.2.1 Stereo-mechanical Model

This approach uses the momentum conservation principle and the coefficient of restitution to model impact. The interval of impact is ignored. The coefficient of restitution (e) is defined as the ratio of separation velocities of the bodies after impact to their approaching velocities before impact (Goldsmith 2001a). The post-collision velocities are calculated using the following equation:

$$v_i' = v_j - (1+e)\frac{m_j(v_i - v_j)}{m_i + m_j} \quad 2.1$$

$$v_j' = v_j - (1+e)\frac{m_i(v_i - v_j)}{m_i + m_j} \quad 2.2$$

where v_i', v_j' are velocitites of the colliding masses (m_i , m_j) after impact, v_i, v_j are the velocities before impact and e is the coefficient of restitution, which is defined as

$$e = \frac{v_j' - v_i'}{v_i - v_j} \quad 2.3$$

This coefficient defines the level of plasticity in the collision: when $e = 1.0$, the collision is entirely elastic, while $e = 0.0$ corresponds to an entirely plastic collision. Since this not a force-based approach, it is not recommended when a precise pounding-involved structural response is required (Jankowski 2005; Mate et al. 2012). Moreover, the stereo-mechanical method is not frequently used in pounding analyses; hence, it is unsuitable for finite element (FE) analysis.

2.2.2 Linear Spring Model

Applying Hooke's law, a simple contact element consisting of a linear spring with high stiffness (k) is used to simulate is used to simulate the pounding force once the gap between adjacent bodies closes (Flores & Lankarani 2016). The force in the contact element is shown in Equation 2.4,

$$F_c = \begin{cases} k\left(u_i - u_j - d\right); & u_i - u_j - d > 0 \\ 0\,; & u_i - u_j - d \leq 0 \end{cases} \quad 2.4$$

with u_i, u_j representing the displacement of the adjacent structural components and d representing the separation gap between the structures, shown in Figure 2.1. Several researchers used this model (Filiatrault et al. 1995; Maison & Kasai 1992). This approach is simple and can easily be employed in commercial software. Yet, the model excludes the effect of energy dissipation during impact.

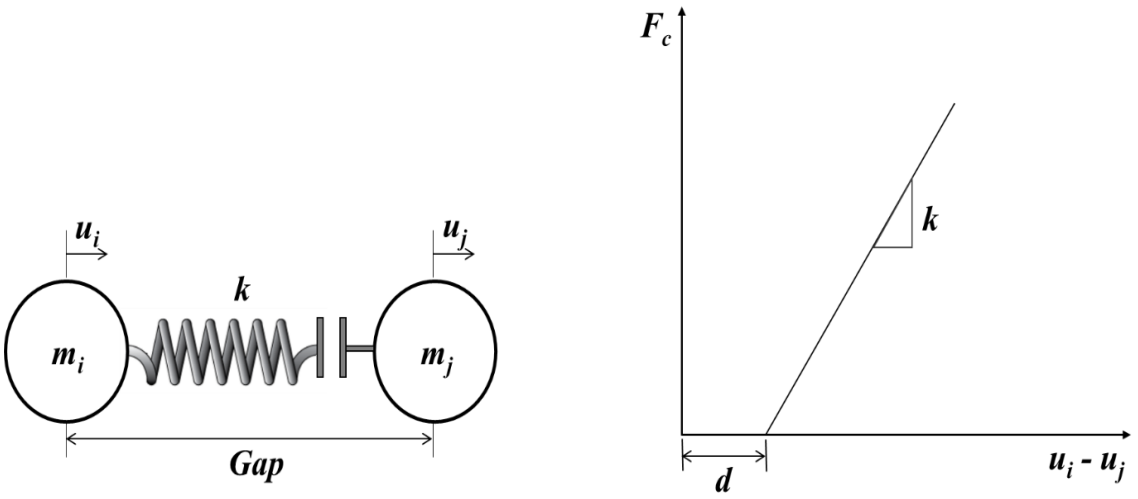

Figure 2.1 Linear spring model and contact force relation

2.2.3 Linear Viscoelastic Model

The linear viscoelastic model presented in Figure 2.2 (known as the Kelvin–Voigt model) is a well-known model and is often used in earthquake-induced pounding simulation. To define the energy dissipation during impact, this model uses a linear spring to measure the impact in parallel with a damper. This model has been implemented by numerous scholars (Anagnostopoulos & Spiliopoulos 1992; Crozet et al. 2017; López-Almansa & Kharazian 2018; Polycarpou & Komodromos 2010). Equations 2.5 – 2.8 demonstrated the impact force, F_c, based on this model.

$$F_c = \begin{cases} k(u_i - u_j - d) + C(\dot{u}_i - \dot{u}_j); & u_i - u_j - d \geq 0 \\ 0; & u_i - u_j - d < 0 \end{cases} \quad 2.5$$

$$C = 2\xi\sqrt{k\,\frac{m_i m_j}{m_i + m_j}} \quad 2.6$$

$$\xi = -\frac{\ln e}{\sqrt{\pi^2 + (\ln e)^2}} \quad 2.7$$

$$e = \frac{v_j' - v_i'}{v_i - v_j} \quad 2.8$$

where $(\dot{u}_i - \dot{u}_j)$ is the relative velocity of the colliding bodies at time t. The damping coefficient c is associated to the coefficient of restitution e by equating the energy losses during impact. Conversely, m_i and m_j are the masses of the colliding bodies and ξ is the damping ratio. v_i', v_j' are velocities of the colliding masses after impact, while v_i, v_j are

the velocities before impact. The disadvantage of the linear viscoelastic model is the damping-initiated negative pounding forces before separation that pull the colliding structures. This results in inconsistent uniform dissipation during the approach and restitution periods (Hao et al. 2013; Jankowski 2005). The linear viscoelastic model is widely used in many commercial software applications for the purpose of structural pounding simulation.

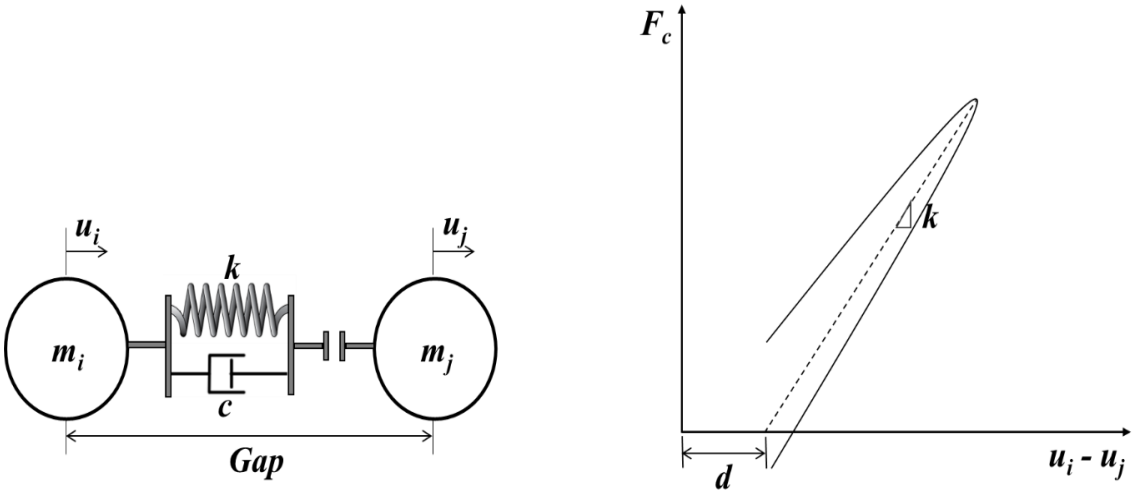

Figure 2.2 Linear viscoelastic model and contact force relation

2.2.4 Hertz Model or Nonlinear Elastic Model

This model, which uses a nonlinear spring of stiffness, k_h based on the Hertz law of contact, has been adopted by a number of scholars (Abdel Raheem 2006; Chau et al. 2003; Mate et al. 2012). The pounding force, F_c, for this model is expressed through Equation 2.9.

$$F_c = \begin{cases} k_h(u_i - u_j - d)^{1.5}; & u_i - u_j - d > 0 \\ 0\,; & u_i - u_j - d \leq 0 \end{cases} \qquad 2.9$$

The impact stiffness parameter, k_h, depends on the material properties of the colliding structures and the contact surface geometry. Elastic contact between a sphere of radius R and a flat plate, k_h, is expressed in Equations 2.10 and 2.11

$$k_h = \frac{4\sqrt{R}}{3\pi}\left(\frac{1}{\delta_1 + \delta_2}\right) \qquad 2.10$$

in which the material parameters δ_1 and δ_2 are given by

$$\delta_i = \frac{1-\rho_i^2}{\pi E_i} \; ; \quad i = 1,2 \tag{2.11}$$

Here, ρ_i and E_i are the Poisson's ratio and modulus of elasticity, respectively. The model does not consider energy loss during impact as the spring is fully elastic. This model is shown in Figure 2.3:

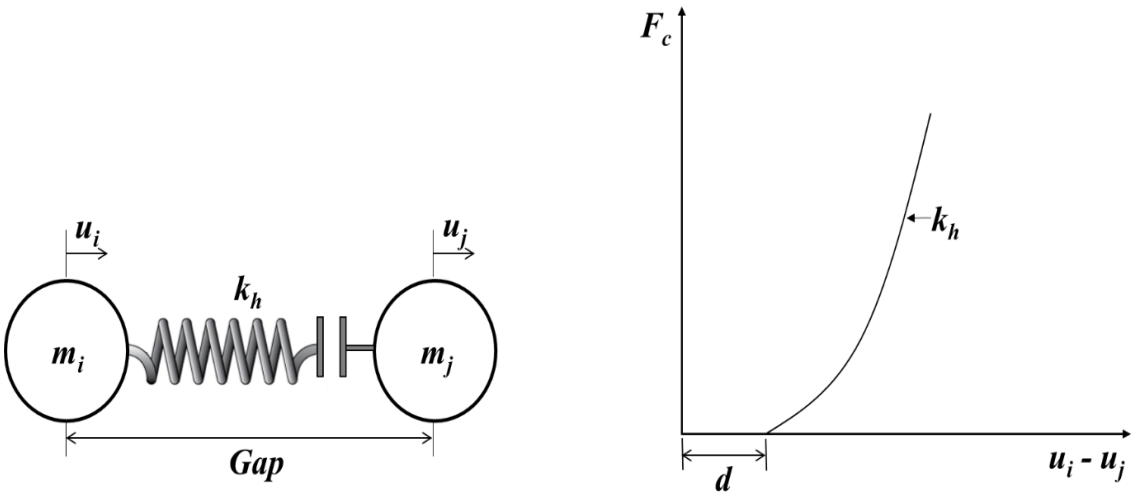

Figure 2.3 Hertz model and contact force relation

2.2.5 Nonlinear Viscoelastic Model

Jankowski developed the nonlinear viscoelastic concept as shown in Figure 2.4 to improve the Hertz model. The model is commonly used by Jankowski (2008a), Mahmoud & Jankowski (2011) and Naderpour et al. (2016). Based on this model, the impact force is presented in Equation 2.12,

$$F_c = \begin{cases} \beta\delta(t)^{\frac{3}{2}} + C(t)\dot{\delta}(t) & ; \; \delta(t) > 0 \; and \; \dot{\delta}(t) > 0 \quad approach \; period \\ \beta\delta(t)^{\frac{3}{2}} & ; \; \delta(t) > 0 \; and \; \dot{\delta}(t) \leq 0 \quad restitution \; period \\ 0 & ; \; \delta(t) \leq 0 \quad no \; contact \; period \end{cases} \tag{2.12}$$

where $\delta(t)$ defines the deformation of colliding structural members, $\dot{\delta}(t)$ represents the relative velocity between them, β is the impact stiffness parameter and $C(t)$ is the impact element damping coefficient as computed based on the formula:

$$C(t) = 2\bar{\xi}\sqrt{\beta\sqrt{\delta(t)}\frac{m_i m_j}{m_i + m_j}} \tag{2.13}$$

Here, $\bar{\xi}$ is the impact damping ratio corresponding to a coefficient of restitution e, which can be defined as:

$$\bar{\xi} = \frac{9\sqrt{5}}{2} \frac{1 - e^2}{e(e(9\pi - 16) + 16)} \tag{2.14}$$

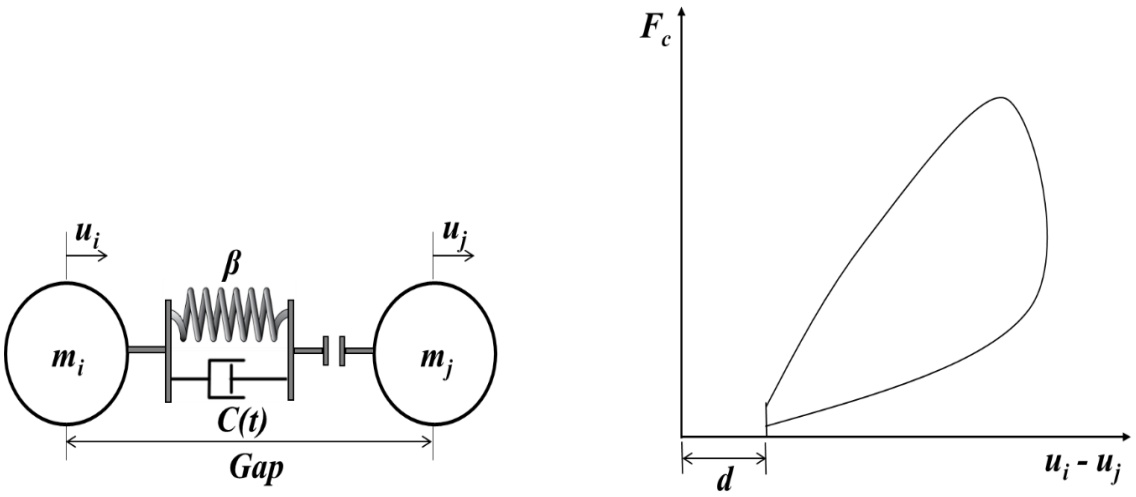

Figure 2.4 Nonlinear viscoelastic model and contact force relation

This model can capture the energy dissipation mechanism during the impact. However, the impact force-time curve does not smoothly fluctuate between the approach phase and the restitution period of the collision (Jankowski 2006).

2.2.6 Hertz-damp Model or Hertz Model with Nonlinear Damper

To address the limitation of the Hertz model in terms of its inability to present the energy dissipation during contact, the Hertz-damp model is suggested. This model is an improved version of the Hertz model, whereby the nonlinear damper is used in combination with the Hertz spring as shown in Figure 2.5. Muthukumar & Desroches (2006) proposed the improved version and it was used by Khatiwada et al. (2013) and Mate et al. (2012). Equation 2.15 showed the impact force estimated by this model.

$$F_c = \begin{cases} k_h\left(u_i - u_j - d\right)^{1.5} + C_h(\dot{u}_i - \dot{u}_j) & u_i - u_j - d > 0 \\ 0\,; & u_i - u_j - d \leq 0 \end{cases} \tag{2.15}$$

$$C_h = \xi\left(u_i - u_j - d\right)^{1.5} \tag{2.16}$$

$$\xi_h = \frac{3k_h(1 - e^2)}{4(\dot{u}_i - \dot{u}_j)} \tag{2.17}$$

Ye et al. (2009) indicated that the Hertz-damp model using Equation 2.17 to determine the damping ratio, ξ_h , leads to inacurate pounding results. Therefore, an equation was proposed for the impact damping ratio of the Hertz-damp model; see Equation 2.18.

$$\xi_h = \frac{8k_h(1-e)}{5e(\dot{u}_i - \dot{u}_j)} \qquad 2.18$$

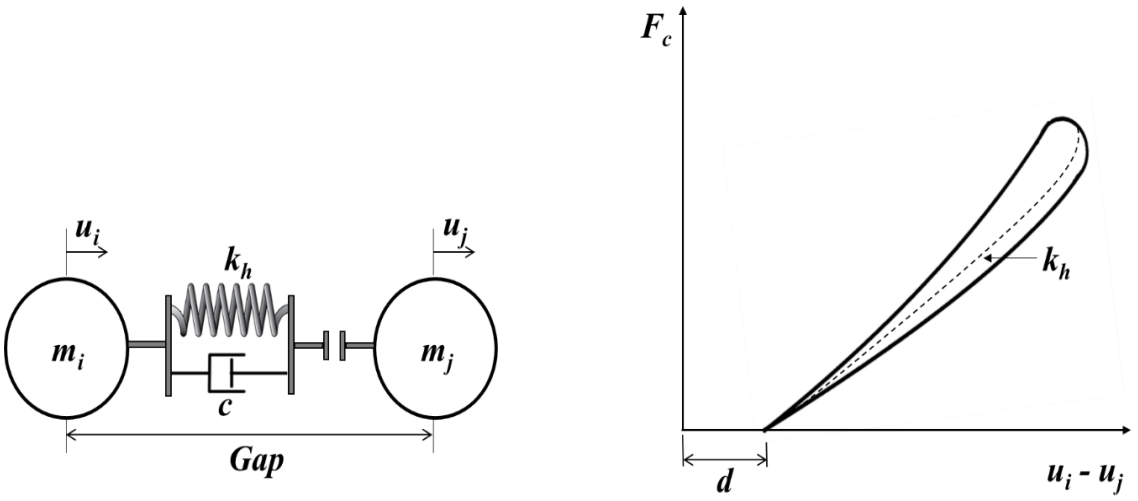

Figure 2.5 Hertz-damp model and contact force relation

Jankowski claimed that the nonlinear viscoelastic model, compared with other models, is the most accurate one in simulating the impact force throughout collisions. The Hertz element, Hertz-damp element and nonlinear viscoelastic element cannot be easily employed in available commercial software. Thus for more accurate prediction of impact forces, collision between adjacent structures needs to be analysed by a separate developed program.

Nevertheless, some drawbacks can be found in these pounding analytical models. The stereo-mechanical approach is not valid if the impact duration is large enough that substantial changes occur in the configuration of the system. Energy loss during impact is not considered in the linear elastic and Hertz models. The linear viscoelastic model shows an initial jump in the impact force values upon pounding due to the damping term. Moreover, the damping force can cause negative impact forces before separation that pull the colliding bodies. In the case of the nonlinear viscoelastic model, the pounding force-time curve is not smoothly varied between the approaching and restitution phases during the collision.

2.3 **Stiffness of Contact Element**

Stiffness of impact spring element is considered to be one of the most significant parameters when the impact force during collision is calculated. Regrettably, there is no acknowledged method of defining its value (Khatiwada & Chouw 2014). The only analytical formula for k was derived by Hertz's law (Lankarani & Nikravesh 1992) and used by Abdel Raheem (2006) and Chau et al. (2003). Many studies have been carried out suggesting numerous assumptions for assigning stiffness to the spring element; they are described in this section.

Wada et al. (1984) integrated a gap element with stiffness equal to the axial stiffness of the beams and slab at the impact level as follows:

$$k = K_b + K_s = \frac{EA_b}{L_b} + \frac{EA_s}{L_s} \tag{2.19}$$

where A_b is the cross-sectional area of the beam, A_s is the cross-sectional area of the slab, E is the modulus of elasticity, and L is the length of the element in the direction perpendicular to the contact surfaces, as shown in Figure 2.6.

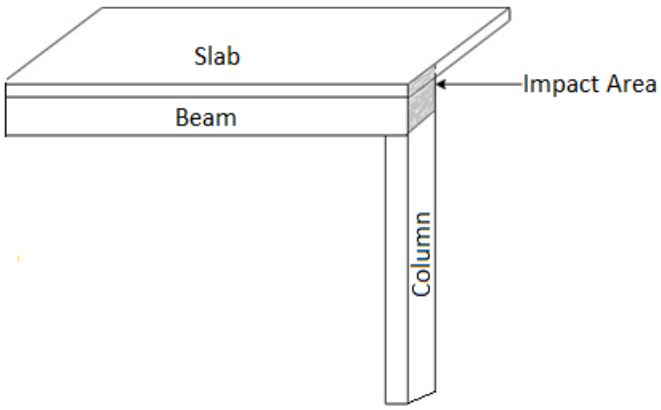

Figure 2.6 Wada method for calculating stiffness of contact element

Anagnostopoulos (1988) suggested a gap element with stiffness twenty times larger than the lateral stiffness of the rigid SDOF system (Figure 2.7), as expressed in Equation 2.20:

$$k = \frac{Lateral\ Load}{Displacement} \times 20 \tag{2.20}$$

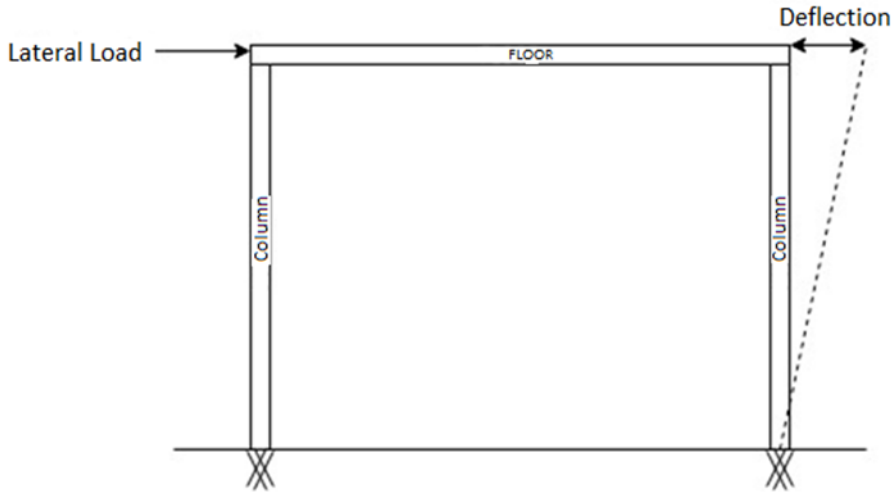

Figure 2.7 Anagnostopoulos' method for calculating stiffness of contact element

Maison & Kasai (1992) proposed a spring stiffness equivalent to the axial stiffness of a floor slab having the width of the adjacent building at the impact level:

$$k = \frac{EA_s}{L} \tag{2.21}$$

where A_s is the cross-sectional area of the slab, E is the modulus of elasticity, and L is the length of the element in the direction perpendicular to the contact surfaces, as depicted in Figure 2.8.

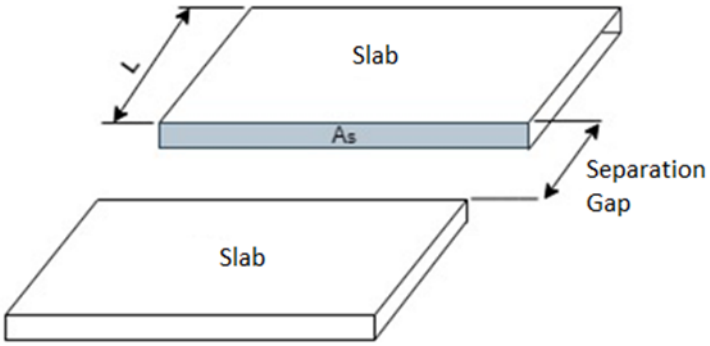

Figure 2.8 Maison and Kasai's method for calculating stiffness of contact element

Based on an experimental study carried out by Jankowski (2005) and Van Mier & Lenos (1991), the impact stiffness parameter value for concrete to concrete was $\beta = 2.75 \times 10^9 N/\text{m}^{3/2}$ and $k = 93.5\ \text{kN/mm}$ for the nonlinear viscoelastic model and linear viscoelastic models, respectively; values for steel-to-steel impact were $\beta =$

$9.9 \times 10^{10} N/m^{3/2}$ and $k = 1400\ kN/mm$ for the nonlinear viscoelastic model and linear viscoelastic model, respectively.

Cole et al. (2012a) adopted a spring with stiffness equivalent to the smaller axial stiffness of the colliding floor at point of contact. These stiffness values were calculated by taking tributary width measurements when beams were aligned. The parallel beam aligned to the direction of the expected contact force is considered in calculation, while the perpendicular beam is ignored (see Figure 2.9). Their stiffness was added to that calculated in the diaphragm.

$$K_i = EA_i/L \; and \; A_i = W_i t_s \tag{2.22}$$

$$k = K_s + K_b = \frac{EA_s}{L} + \frac{EA_b}{L} \tag{2.23}$$

where E, t_s and W_i are the modulus of elasticity, slab thickness and average element width respectively.

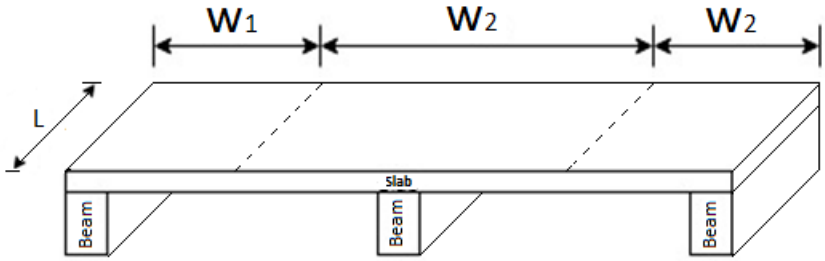

Figure 2.9 Cole's method for calculating stiffness of contact element

Moreover, based on the experiment performed by Jankowski (2008a), the impact stiffness parameter value for steel-to-steel impact was $k = 482\ kN/mm$ under the linear viscoelastic model.

Concurrently, as expressed in Equation 2.24, according to Naserkhaki et al. (2012) the impact stiffness of the impact element should be 50–100 times more than the building's lateral stiffness.

$$k = Building\ stiffness \times (50 - 100) \tag{2.24}$$

Furthermore, Xu et al. (2016) developed the following formula (Equation 2.25) for the impact stiffness of the linear viscoelastic model:

$$k = \frac{m_j}{m_i + m_j} k_1 e^{(2\ln e/\pi)\left(\arcsin\left(\pi/\sqrt{\pi^2+(\ln e)^2}\right)\right)} \quad 2.25$$

where $k_1$is calculated based on Equation 2.21.

At present, there is no relationship developed to bridge the gap in terms of impact modelling. Therefore, the subject of how to select the suitable impact stiffness to successfully calculate the pounding responses between two colliding adjacent buildings should be further investigated.

2.4 **Review on Codal Provisions**

Globally, building standards in seismically active regions recommend construction guidelines to mitigate the influence of earthquake-induced pounding on structural frames. The most common provision integrated into building codes is to separate the structures to prevent interactions between adjacent edifices. Some building standards base their separation gap requirements on the resulting displacements while other code provisions take into consideration the building height or a combination of the building height and the separation gap requirements. Other countries go further by taking into account the type of soil where the edifices are constructed as well as the design of the structure. As stated in the International Building Code (IBC 2009) and Eurocode 8 (Eurocode-8 2005), the required separation gap is given by:

$$S = U_a + U_b \quad 2.26$$

$$S = \sqrt{{U_a}^2 + {U_b}^2} \quad 2.27$$

Equations 2.26 and 2.27 are commonly referred to as the absolute sum (ABS) and square-root-of-sum-of-squares (SRSS) methods, respectively. If the adjacent building separated by a proper line or located on the same property, the ABS and SRSS methods will be used accordingly (Lopez-Garcia & Soong 2009).

Moreover, in the National Building Code of Canada (NBCC 2010) the formula is calculated using the following expression:

$$S = \sqrt{U_a + U_b} \quad 2.28$$

where S, U_a , U_b are separation distance and peak displacement response of the adjacent structures A and B, respectively, in the location where pounding is expected to occur

(Lopez-Garcia & Soong 2009). A similar requirement can be observed in American Society of Civil Engineers ASCE7–10 (ASCE 2013).

Referring to the Chinese earthquake standard GB5001, the minimum gap for buildings up to 15 m high is 0.07 m, which increases 0.02 m for seismic intensity levels of 6 to 9 (GB50011 2001). However, the provision has been upgraded in GB50011-2010 to 100 mm in concrete-framed buildings. The 1997 Taiwan Building Code (TBC 1997) suggested the following formulae when considering the construction of the same type of structures:

$$S_{code} = 0.6(\Delta u_a + \Delta u_b) \tag{2.29}$$

where

$$\Delta u_a = 1.4\alpha_y R_a \Delta e_a \tag{2.30}$$

$$\Delta u_b = 1.4\alpha_y R_b \Delta e_b \tag{2.31}$$

where $\Delta u_a$and Δu_b are the displacements with 0.6 and 1.4 representing the factors of reduction and over strength, respectively. R_a and R_b are the ductility factors, α_y is the amplification factor, and Δe_a and Δe_b are the elastic displacements (Lin & Weng 2002). In other words, the required separation distance is equal to 60% of the absolute sum of the peak inelastic displacements of the two adjacent buildings.

According to Federal Emergency Management Agency (FEMA: 273-1997), pounding may be assumed not to happen whenever the buildings are separated at any level *i* by a distance greater than or equal to S_i. The value of S_i need not surpass 0.04 times the height of the building above grade at the zone of possible impacts where S_i follows the SRSS method.

The Iranian Code of Practice for Seismic Resistant Design of Buildings (ISC 2005) and Australian Earthquake Standard (AS1170.4 2007) both follow a similar approach by recommending a gap of 0.01 of the building height. Hao (2015) agreed with this approach, which is similar to the ISC-2005 specification, and is expressed in Equation 2.32:

$$S = 0.01H \tag{2.32}$$

where H is the building height.

The Australian Earthquake Standard (AS1170.4-2007) states that pounding needs to be considered for structures over 15 m for design category II or III. Clauses 5.4.5 and 5.5.5 for design categories II and III states 'This clause is deemed to be satisfied if the setback from a boundary is more than 1% of the structure height.' However, AS1170.4-2007 does not clearly describe accurate values for minimum separation gaps. Many factors that have direct impact on the adjacent buildings were ignored. For instance, reinforced concrete or steel structure, parameters such as stiffness, mass and soil deposit (soft, hard etc.) were not considered. As a result, it has been recognised that there is a strong necessity to develop design tools for adjacent buildings. The tools should consider structural pounding effect in seismic design of adjacent building frames with varying frequencies.

The gap required to preclude earthquake-induced collision between closely spaced buildings has been investigated for many decades. Many cases were studied during this period with researchers suggesting various methods, one of which is to separate adjacent buildings by SDOF oscillators (Anagnostopoulos 1988; Garcia 2004; Hao & Liu 1998; Kasai et al. 1996) or multiple-degree-of-freedom (MDOF) oscillators (Abdel Raheem 2014; Anagnostopoulos & Spiliopoulos 1992; Favvata 2017; Jeng et al. 1992a; Lin & Weng 2001; Maison & Kasai 1992) while considering structural responses in either elastic or inelastic phases.

2.5 **Separation Distance Equations**

To determine the essential separation gap between two adjacent buildings, the ABS and SRSS were commonly used by previously mentioned seismic codes. Previous studies have shown that this method provides conservative results (Jeng et al. 1992b; Penzien 1997). Consequently, Jeng et al. (1992b) suggested a new method on the basis of the spectral difference method, acknowledged as the double difference method (DDC) or the complete quadratic combination (CQC) method (Equation 2.33). The method is response spectrum-based and requires a correlation coefficient, ρ_{ab}, depending on the period and damping ratios of the structures (Equation 2.34).

$$S = \sqrt{U_a^2 + U_b^2 - 2\rho_{ab}U_aU_b} \qquad 2.33$$

$$\rho_{ab} = \frac{8\sqrt{\zeta_a \zeta_b}\ \left(\xi_a + \xi_b \frac{\mathrm{T}_a}{\mathrm{T}_b}\right)\left(\frac{\mathrm{T}_a}{\mathrm{T}_b}\right)^{1.5}}{\left[1 - \left(\frac{\mathrm{T}_a}{\mathrm{T}_b}\right)^2\right]^2 + 4\zeta_a\zeta_b\left[1 + \left(\frac{\mathrm{T}_a}{\mathrm{T}_b}\right)^2\right]\left(\frac{\mathrm{T}_a}{\mathrm{T}_b}\right) + 4(\zeta_a^2 + \zeta_b^2)\left(\frac{\mathrm{T}_a}{\mathrm{T}_b}\right)^2} \quad 2.34$$

where S is the seismic separation gap, U_a, ζ_a and T_a are the maximum displacement responses, damping ratio and natural period for building 'a', and U_b, ζ_b and T_b are the maximum displacement responses, damping ratio and natural period for building 'b', respectively. The DDC method has been studied by numerous scholars (Filiatrault & Cervantes 1995; Lopez-Garcia & Soong 2009; Penzien 1997). Garcia (2004) studied the accurateness of the DDC method using nonlinear systems and concluded that the DDC formula provided both conservative and un-conservative results depending on the period ratios of adjacent buildings. Hong et al. (2003) and Wang & Hong (2006) enhanced the DDC technique by multiplying the coefficient based on the period ratios of the edifices.

Naderpour et al. (2017) created a new method anchored on the era of adjacent buildings by altering the coefficient of correlation in the DDC method, which consider the in-phase and out-of-phase vibrations (Equation 2.35),

$$S = \sqrt{U_a^2 + U_b^2 - 2SFU_aU_b} \quad 2.35$$

where $U_a$and U_b are the design displacements (peak displacements without pounding), and *SF* denotes the separation factor, which based on the periods of both buildings, as presented in Equation 2.36:

$$SF = \left(\frac{T_b}{T_a}\right) - 10.5(T_b - T_a)\ ;\ T_a < T_b \quad 2.36$$

Shrestha (2013) contrasted the ABS, SRSS and DDC calculations based on the analytical required gap using linear and nonlinear versions. The findings revealed that the ABS approach is conservative and overrates the gap. For the SRSS method, the outcomes were also found to be conservative when the natural periods of the adjacent structures were close to each other and not conservative when the natural periods were not similar. The DDC equation was deemed as the best method for forecasting the separation. However, only a single ground motion was applied in the research. Thus, there is a need to conduct more studies using other ground motions to validate the results. Also, Barbato & Tubaldi

(2013) considered the DDC formula as the most accurate, whereas ABS and SRSS methods had un-conservative results.

The above-described formulae for the seismic distance between adjacent buildings concern fixed-base structures. In contrast, flexible-base structures (due to SSI or seismic isolation) involve a larger distance to be provided (the adequate gap in the case of soft soil might be even three times larger than the suggested one) (Ghandil & Aldaikh 2017; Li et al. 2017; Naserkhaki et al. 2013).

The methods in the related literature, laws and regulations necessitate the identification of lateral displacements of the adjacent structures. The DDC method, which gives more accurate findings, encompasses a correlation coefficient based on the time and damping ratios of the edifices. If an engineer wants to measure the required distance using these methods for evaluation or design, they must analyse both buildings.

2.6 **Summary**

In this chapter, a comprehensive literature review has been conducted regarding earthquake-induced pounding between adjacent structures. Based on the presented literature, the past researchers accomplished efficient research studies in the field of seismic pounding. Most of the experimental investigations available in published researches are carried out on structural models assembled with contact points. There are commonly two explanations for this. One is to assure the axial impact with point contact to eliminate the torsional influence of the structural model due to the ambiguity of the materials, manufacture and installation. The second explanation is to be consistent with the assumption of the Hertz impact model. Though, additional experimental studies are essential to verify the validity of numerical models of collisions. This impact force acting on structures due to pounding, which is not considered in a standard design, might increase shear forces and overturning moments in structures.

Moreover, the past studies and building codes provide recommendations on the minimum required separation gap between adjacent structures to prevent pounding. These recommendations are based on the structural displacements calculated by equivalent static analysis or on the building heights and ground excitation intensity. Hence, it is very important to evaluate the adequacy of the code specification to avoid pounding of adjacent steel frame structures experimentally.

In general, considering the abovementioned studies and other available literature, pounding is a complex, highly nonlinear phenomenon that can develop between high-rise

buildings and between low-rise buildings, and between both during strong earthquakes, and may amplify the overall dynamic response of structures. Therefore, the results of the abovementioned numerical and experimental investigation on earthquake-induced pounding between adjacent structures can be significantly improved.

Hence, the succeeding research gaps have been identified:

Different impact models implemented to simulate earthquake-induced pounding between adjacent buildings have produced uncertainty and confusion in research area. Furthermore, engineers do not have clear formulae to follow for finding the impact model. Their numerical analyses have concerned impacts between reinforced concrete structures and the studies on pounding between steel structures are very limited. Most of their analytical works utilise single-degree-of-freedom systems in order to simplify the problem.

Through the uncertainties in impact stiffness, k, there is no experimentally confirmed method of determining its value. Numerous researchers have suggested different methods to calculate the spring stiffness. The large number of methods has led to more confusion around choosing the suitable value of k when conducting numerical analyses. Defining the appropriate k value is vital to ensure the accuracy of the results. Unsuitable value of k may have direct effects on the peak force and number of impacts between the adjacent buildings.

The Australian Earthquake Standard (AS1170.4-2007) does not provide definite guidelines for estimating the likely minimum building separation necessary to preclude pounding. Due to growing building density and rapid property value increases in most Australian major cities in recent years, separation distance clauses for adjacent buildings are sometimes ignored or simply impractical.

The equations specified in literature and building codes require the determination of lateral displacements of the adjacent buildings. Accordingly, analysing both buildings is essential to calculate the gap distance. Thus, there is a need to develop a simple formula to estimate the minimum required separation gap without any analysis.

The subsequent chapters seek to address these research gaps to better understand earthquake-induced pounding phenomena.

CHAPTER 3
EXPERIMENTAL STUDY

3.1 Introduction

This chapter describes the experimental test program using an independent lab platform conducted at the Structural Testing Facility at the University of Technology, Sydney. Five steel frame structures were designed as test specimens to represent adjacent equal-height frames and adjacent unequal-height frames. A special impact device was used to simulate the colliding between the frames. All testing took place using recorded ground motions that were scaled based on the peak ground acceleration (PGA) level to different intensities, two far-field and two near-field. Structural responses in term of acceleration, displacement and impact force were measured using accelerometers, laser displacement and force sensor, respectively for all configurations. The results of the earthquake simulator tests were then processed and used later to calibrate and compared with the numerical model.

3.2 Earthquake Simulator

The experimental work was carried out on an MTS 354.20 multi-axial simulation table at the structural testing facility in the state-of-the-art Tech Lab at the University of Technology, Sydney. The shaking table has plane dimensions of 2.2 m × 2.2 m with six degrees of freedom, as shown in Figure 3.1. This shaking table is capable of testing samples of two tonnes at 5 g acceleration, 1000 mm/s velocity and up to +/–200 mm stroke. The system can be used as an earthquake simulator and is powered by six hydraulic actuators in a hexapod arrangement with a highly sophisticated control system to ensure the waveform is accurately reproduced.

3.3 Steel Frame Models

Five 1/30 scale single-bay moment-resisting steel frame models were constructed: two 15-storey, one 10-storey and two 5-storey structures. Associated building frames were analysed to the requirements of AS4100 (Steel Structures) with the connecting base plates in accordance with AS 3678-2011. The tested frames were designed following a similar approach by Tabatabaiefar & Mansoury (2016) and Tabatabaiefar et al. (2014). The overall floor plan dimensions of all models are 0.4 m × 0.4 m. The common height of each floor is 100 mm. The heights of the 15-storey, 10-storey and 5-storey frames are 1.5 m, 1.0 m and 0.5 m, respectively. In all models, columns and floors are made of rectangular flat steel sections of 40 mm × 2 mm and 400 mm × 5 mm, respectively.

Detailed drawings of the scaled models are illustrated in Appendix A. The steel frames were first assembled on the hard floor at the structural testing area. Then several primary tests were conducted on each frame independently to determine the dynamic properties of each steel frame. Next, the test frames were placed at the shaking table surface using a crane lift, as shown in Figure 3.2. Each test model was then attached to the shaking table surface by nine 12 mm bolts and nuts to ensure complete base fixity of the models (Figure 3.3).

Figure 3.1 Multi-axial seismic simulator at the UTS structural testing facility

3.4 **Instrumentation and Data Acquisition System**

Three different classes of measuring instruments were adapted in the current shaking table test program, namely, accelerometers (Figure 3.4a), laser displacement (Figure 3.4b) and a force sensor (Figure 3.4c) in order to measure structural accelerations, deformations and impact force, respectively. The adapted measuring instruments have the following specifications:

- Accelerometers
  - Model: PCB 352C34 uniaxial accelerometer
  - Frequency range: ∓5%
  - Measurement range: ∓50 g
  - Measurement accuracy: ∓0.006 m/s²
  - Operating temperature range: -54 to + 121 ℃

- Laser displacement
  - Model: ZX1-LD100A81, ZX1-LD300A81, ZX1-LD600A81
  - Measurement range: 100∓35 mm, 300∓150 mm, 600∓400 mm
  - Response time: 200 ms max
  - Resolution: 7 μm, 30 μm, 80 μm
- Force sensor
  - Model: PCB 208C05
  - Sensitivity: ∓15% (224.82 mV/kN)
  - Measurement range (Compression): 22.24 kN
  - Measurement range (Tension): 2.224 kN
  - Upper Frequency Limit: 36000 Hz
  - Operating temperature range: -54 to +121 ℃
  - Stiffness: 1.05 kN/μm
  - Weight: 22.7 gm

Data acquisition system is managed by some integrated software packages. The software is directly connected to instruments. The control system is a computerised system with an MTS (MTS System Corp) interface that is connected to the shaking table. Accelerometers, laser displacement devices and the load cell were calibrated before installation to increase the accuracy before the shaking table test, calibration check should be performed online. This is important to verify the system liability and to avoid any malfunctioning. During the experiment, data acquisition is selected according to the software system requirements. The acquired data will be automatically transformed in to the engineering unit.

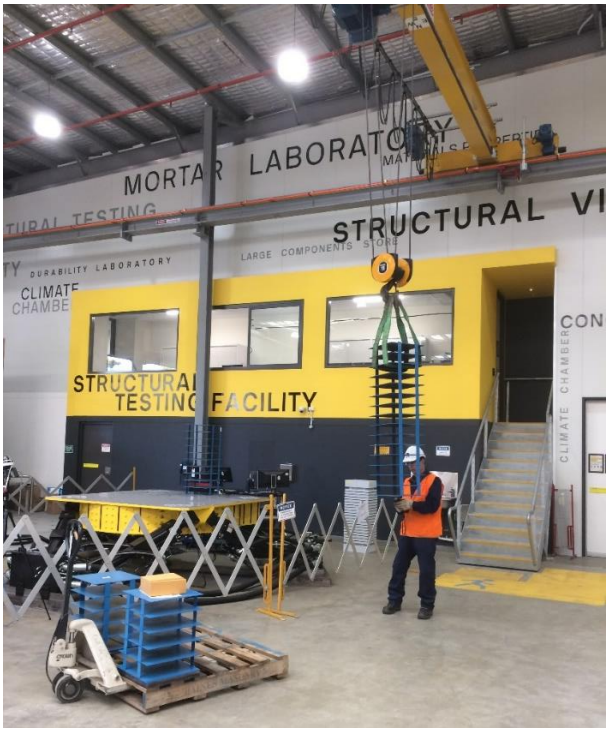

Figure 3.2 Crane lift procedure

Figure 3.3 Bolted base plate

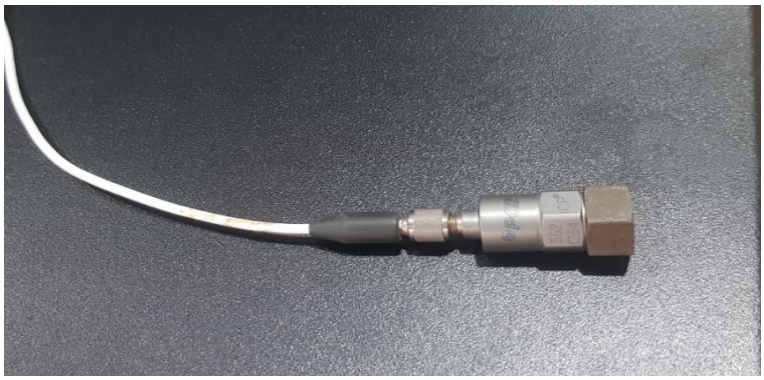

(a)

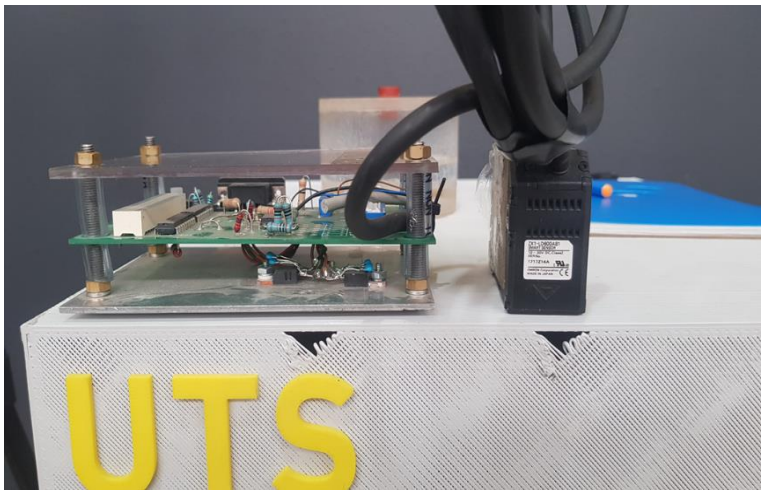

(b)

(c)

Figure 3.4 Adapted measuring instruments in the shaking table tests; (a) accelerometers, (b) laser displacement, (c) force sensor

3.5 **Numerical Model**

A three-dimensional numerical model has been generated in SAP2000 version 20 (SAP 2000) software using two-dimensional shell elements to model columns and floors, as presented in Figure 3.5. The numerical model consists of 15, 10 and 5 horizontal steel plates as the floors and four vertical steel plates as the columns for the fifteen, ten, and five-storey frame, respectively.

Simplistic models of multi-storeyed buildings, consisting of five, ten and fifteen storey frames, are generated taking into account the material nonlinearities. The material behaviour is considered elasto-plastic and its stress-strain relation is shown in Appendix B.

The frames consist of four columns, which are modelled using vertical steel plates, with fixed boundary conditions considered at the column bases. The slabs/floors are represented using horizontal steel plates. Shell element of 2 mm and 5 mm thickness were used for the column and slap respectively.

Steel plate grade 250, according to AS/NZS 3678-2011 (Structural Steel), with a minimum yield stress of 280 MPa and a minimum tensile strength of 410 MPa, has been implemented in the design. Moreover, the Young's modulus, Poisson's ratio and mass density are taken as 200 GPa, 0.3, and 7850 kg/m^3, respectively. It is assumed that building floors are rigid in the plane level, with an even distribution of the floor mass.

The flexibility of the modelled joints can significantly impact the overall behaviour of a frame structure; thus it is essential to correctly model the structure joints. SAP2000 offers the ability to easily fine-tune the flexibility at these joints using panel zones which are assigned to the joints themselves (Far & Flint 2017). This includes the effects of panel zone deformation, that is, how the zone located at the intersection of a column and beam deforms. Panel zone behaviour is modelled using springs that connect the joints. In panel zone, elastic properties from column option have been used.

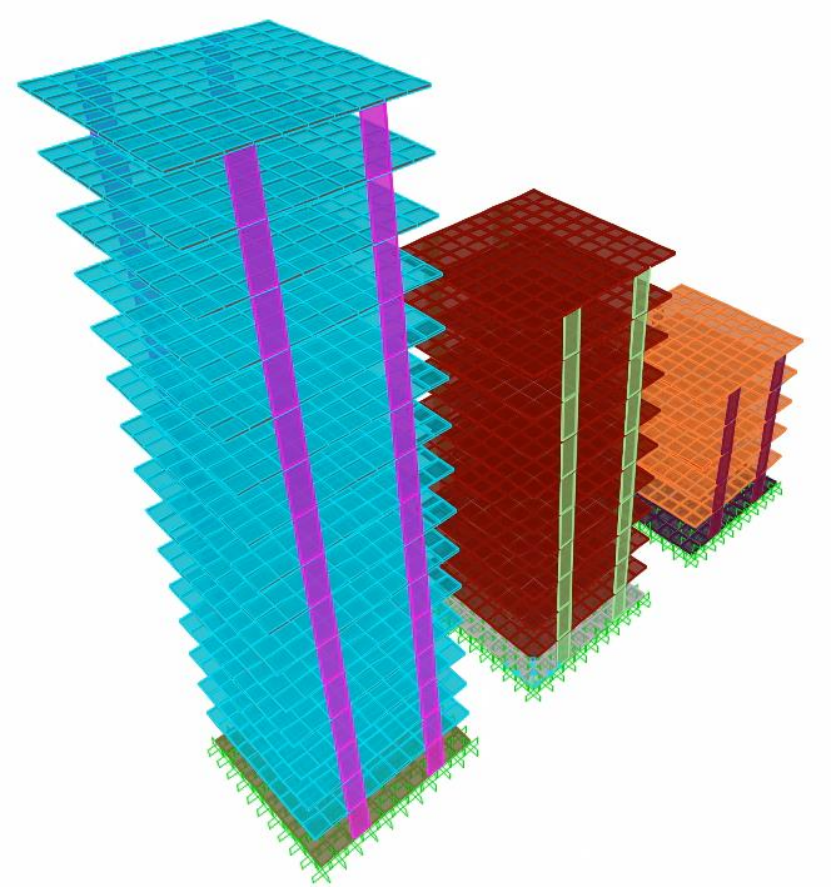

Figure 3.5 3D numerical model of the structural models in SAP2000

3.6 **Preliminary Identification Tests**

3.6.1 Free Vibration Tests

The dynamic characteristics of each steel frame were identified by conducting several preliminary tests including free vibration, stiffness and sine sweep tests. In the free vibration tests, the experiment aimed to measure the fundamental period and damping of the structures. Each structure was excited manually in its first mode by displacing and releasing its roof level. The fundamental periods and natural frequencies were established from the acceleration decay time histories using an accelerometer attached to the structure's top level, as presented in Figure 3.6. Fourier amplitude spectra and frequency response curves were generated from the recorded data of the free vibration tests, and the natural frequencies were determined from the peaks of these plots and presented in Figure 3.8. Here, damping is calculated through using the half-power bandwidth method (Chopra 2007; Papagiannopoulos & Hatzigeorgiou 2011), which is explained in Figure 3.9.

3.6.2 Frame Stiffness Tests

Load-deflection tests were carried out on all these models. The experiment focused on calculating the stiffness parameter for the frame structures. A hydraulic pressure device was used to measure this value, as shown in Figure 3.7. The scaled models were subjected to a lateral loading at the top level to deduce a resulting deflection in the three cases, where frame stiffness is expressed as $K = \frac{Lateral\ Load}{Deflection}$. Appendix C shows the relationship between lateral load and deflection. From the resulting diagrams, it was possible to obtain the stiffness value by mathematically calculating the linear regression line. However, the relationship diagrams show a low divergence and a linear relationship. This facilitates the calculation of finding the regression line.

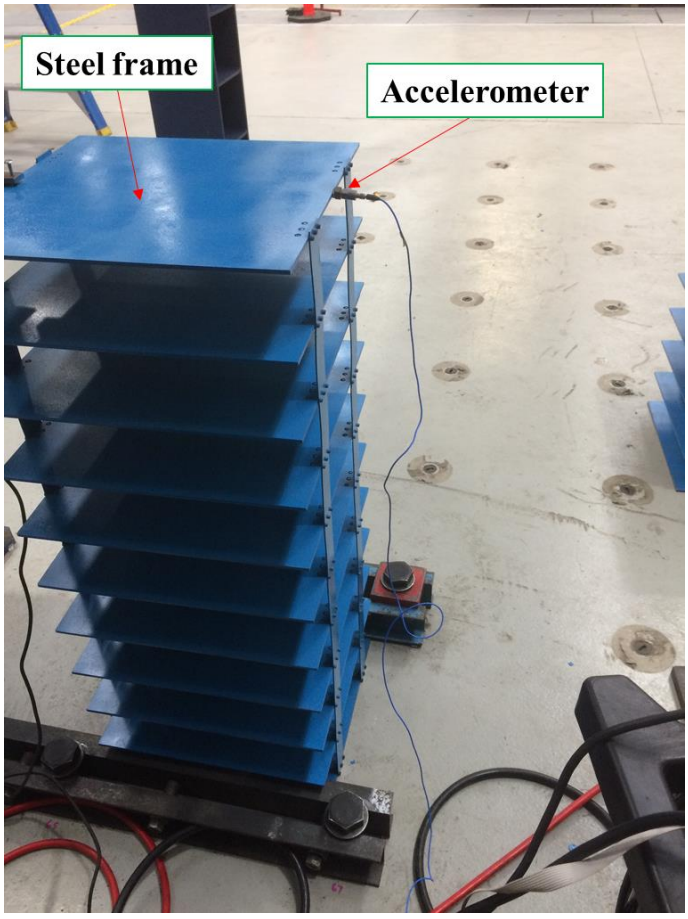

Figure 3.6 Free vibration test using accelerometer

Figure 3.7 Load-deflection test using hydraulic pressure device

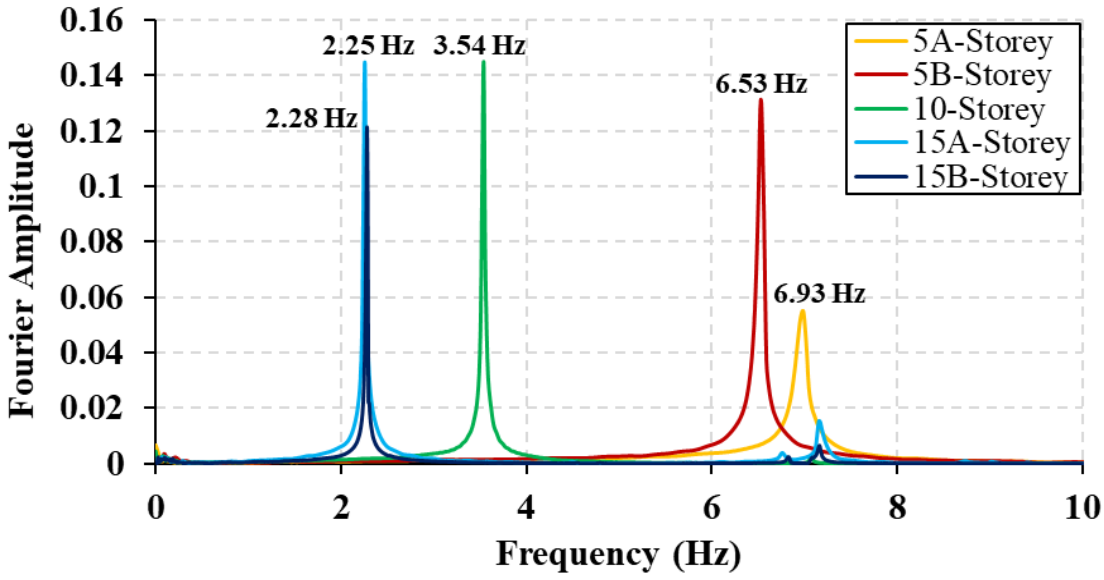

Figure 3.8 Fourier amplitude frequency response curve for all steel frames

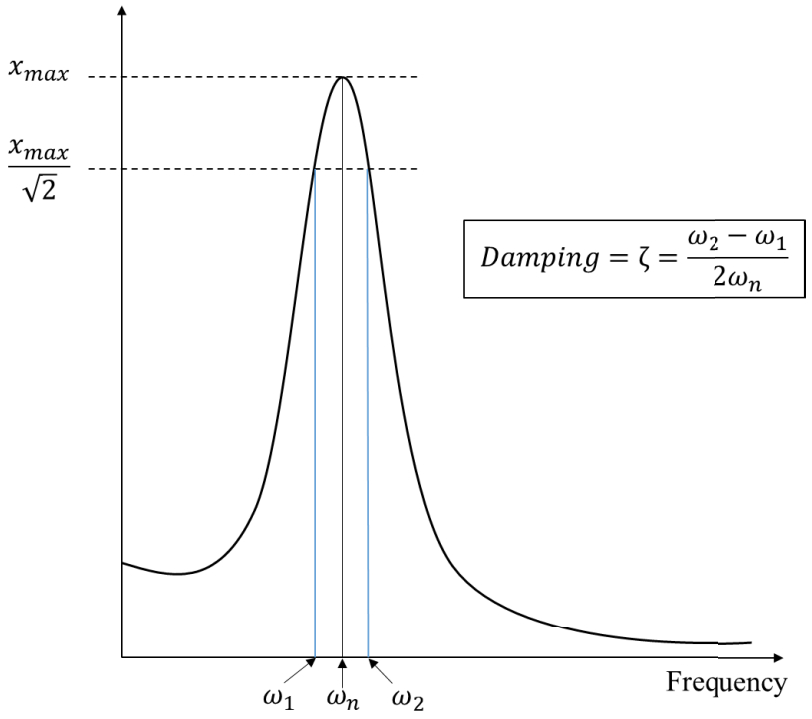

Figure 3.9 Half-power bandwidth method

3.6.3 Sine Sweep Tests

Finally, sine sweep tests were performed on these scaled models. The purpose of the sine sweep tests was to determine the modes of vibration, especially modes 1, 2 and 3, as these could not be verified during the free vibration test. Sine sweep tests involve a logarithmic frequency sweep holding a specified acceleration constant at the base of the structure. The frequency of the shaking table was increased from 0.1 Hz to 50 Hz in order to achieve the aim of the sine sweep test. The first resonance between the shaking table and structural model frequencies indicated the fundamental natural frequency of the model (Dossogne et al. 2019). In Appendix D, the acceleration time history measured on all experimental steel models is plotted for sine-sweep excitations. Several attempts were required to achieve more accurate results, which are tabulated in Table 3.1. The comparison showed that these results were similar to the models' frequency obtained from the free vibration tests presented in Table 3.1.

Table 3.1 summarises the dynamic characteristics of the experimental and numerical results for all the tested frame models. Results are closely similar in natural period and stiffness values.

3.7 **Selected Earthquake Acceleration Records**

Four scaled earthquake acceleration records – El Centro, 1940 (Figure 3.10(b)), Hachinohe, 1968 (Figure 3.11(b)), Northridge, 1994 (Figure 3.12(b)) and Kobe, 1995 (Figure 3.13(b)) – are utilised in shaking table tests. The time duration of the original ground motion was scaled by $\sqrt{\lambda}$, where λ is the scale factor of 1 /30 resulted in a time scale factor of 0.182. More details about scaling of adopted earthquake time histories can be found in Tabatabaiefar & Mansoury (2016). The abovementioned earthquakes have been selected by the International Association for Structural Control and Monitoring for standard seismic studies (K-Karamodin & H-Kazemi 2010). Frequencies, time history and accelerations were included in the adopted results. Moreover, these are considered diverse in relation to epicentre distance. The El Centro and Hachinohe earthquakes are far-field in nature, whereas the Northridge and Kobe earthquakes are near-field. Adverse behaviour of adjacent buildings during these types of earthquakes was a main factor in the seismic design (Yaghmaei-Sabegh & Jalali-Milani 2012). Hatzigeorgiou (2010) and Yaghmaei-Sabegh & Tsang (2011) emphasised the significance of these motions under the effect of dynamic elastic and inelastic analysis.

The Northridge earthquake had the uppermost PGA among the four cases discussed, with a PGA equalling 0.843 g and an epicentre distance of less than 9.2 km. The Kobe earthquake was lesser in both PGA and the distance from the epicentre, measuring 0.833 g and 7.4 km, respectively. However, the PGA values decreased even further for the El Centro and Hachinohe earthquakes, equating to 0.349 g and 0.229 g, respectively, but they were far away from their respective epicentres, with distances measuring 15.7 and 14.1 km respectively.

Since the experimental study was designed to be a non-destructive test, frames were not supposed to yield during excitation so that they could be tested again using different records.

Table 3.1 Experimental and numerical dynamic characteristics of the structural models

	Experiment						Numerical				
	Free Vibration Test		Sine Sweep Test			Stiffness kN/mm	Modal Load Analysis			Stiffness kN/mm	Mass kg
	Natural Frequency Hz	Damping %	Mode1 Hz	Mode2 Hz	Mode3 Hz		Mode1 Hz	Mode2 Hz	Mode3 Hz		
5-Storey/A	6.93	0.664	6.90	21.88	35.35	0.0284	6.90	20.69	33.89	0.0287	37
5-Storey/B	6.531	0.467	6.43	19.99	35.912	0.0275	6.42	19.275	31.54	0.0278	36.5
10-Storey	3.54	0.431	3.46	11.13	18.44	0.0144	3.529	10.571	17.556	0.0149	72
15-Storey/A	2.25	0.508	2.03	6.479	10.82	0.0082	2.078	6.226	10.35	0.00816	104.4
15-Storey/B	2.28	0.503	2.113	6.695	11.56	0.0081	2.0976	6.285	10.455	0.00831	104

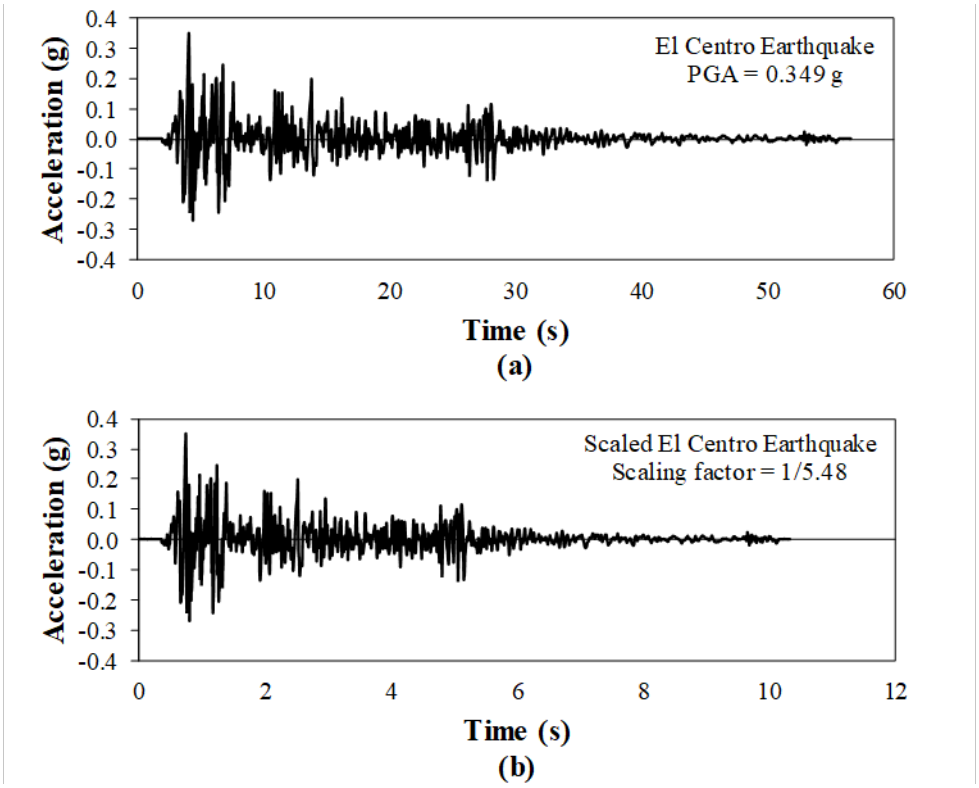

Figure 3.10 El Centro earthquake 1940; (a) Original record; (b) Scaled record

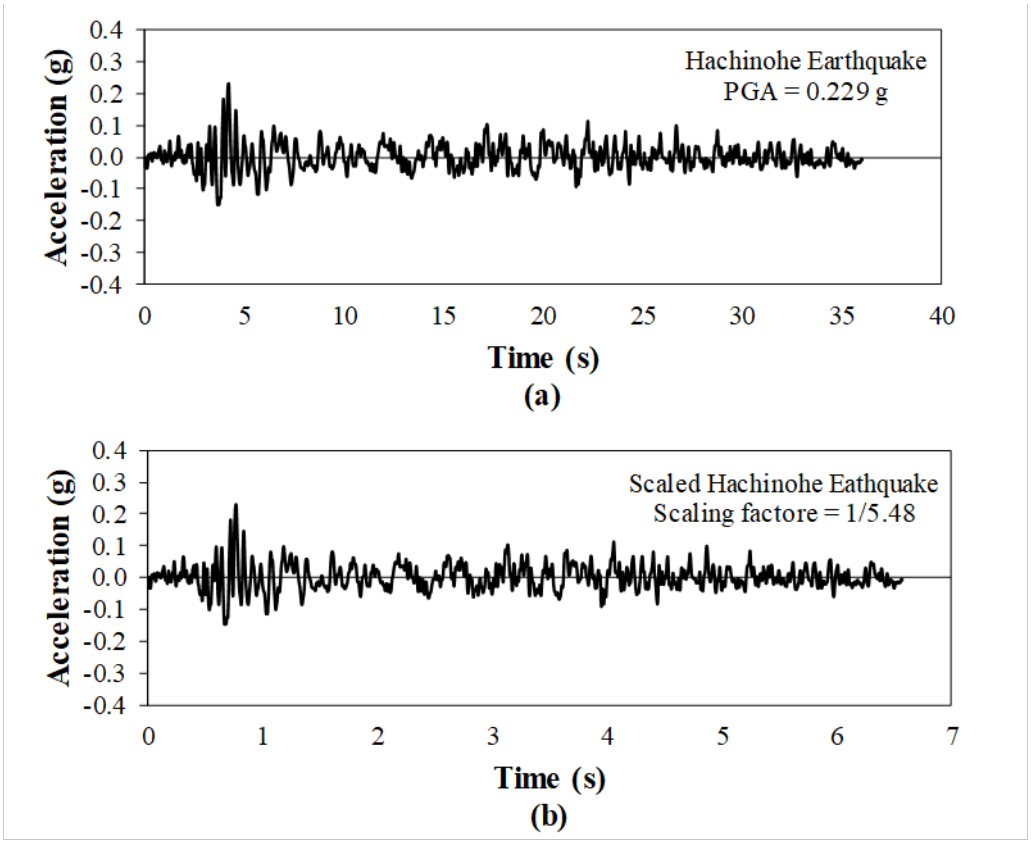

Figure 3.11 Hachinohe earthquake 1968; (a) Original record, (b) Scaled record

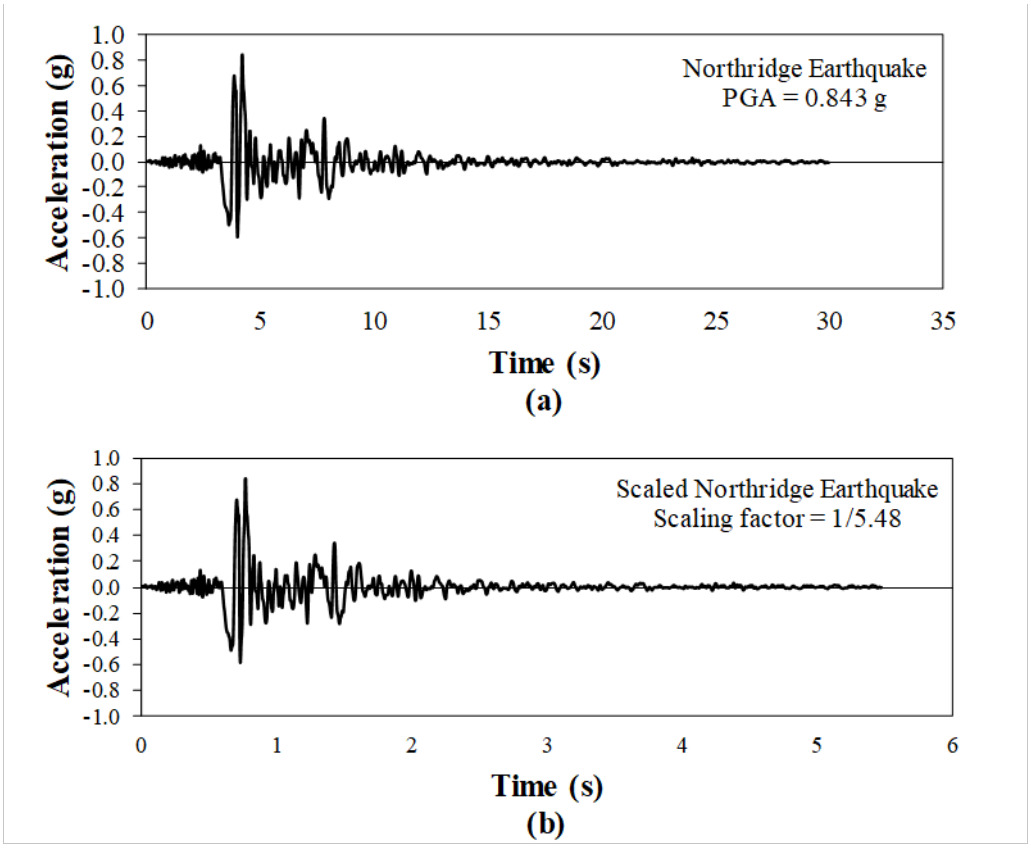

Figure 3.12 Northridge earthquake 1994; (a) Original record, (b) Scaled record

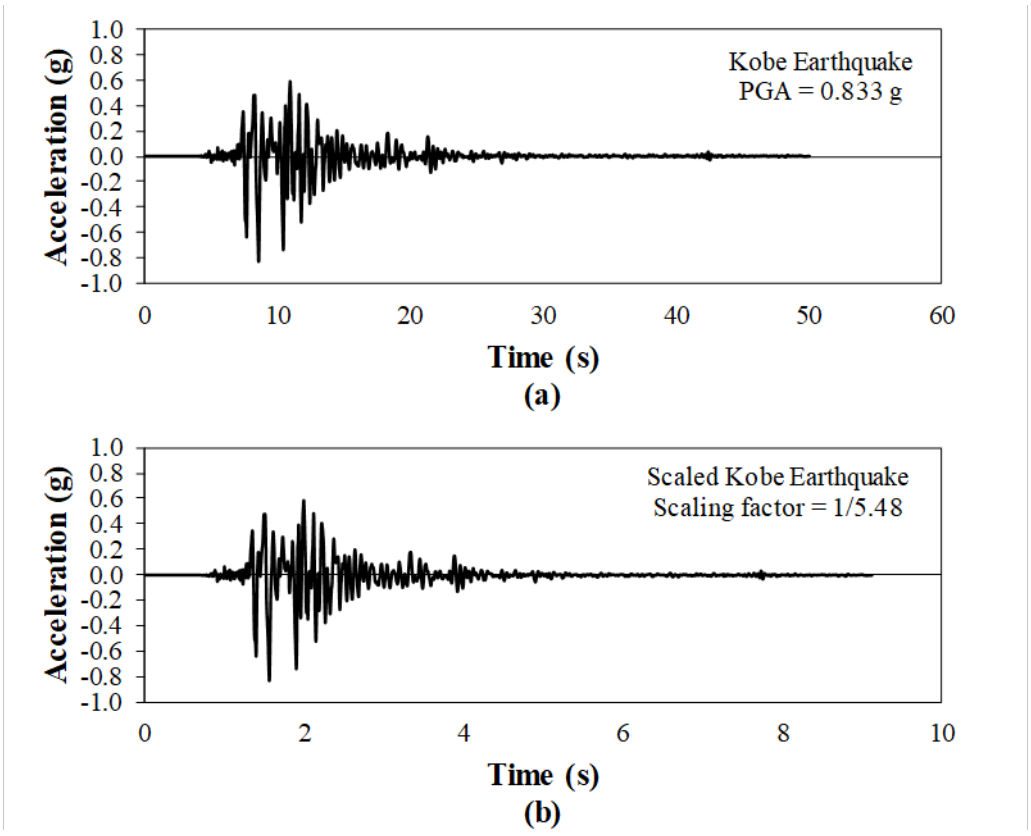

Figure 3.13 Kobe earthquake 1995; (a) Original record, (b) Scaled record

3.8 **Experimental Testing Program**

The structural models were fixed and secured on the shaking table with the following coupled configuration: 15B-storey and 10-storey; 15B-storey and 5B-storey; 10-storey and 5B-storey; 5A-storey and 5B-storey; 15A-storey and 15B-storey (see Figures 3.14–3.18). After securing the structural models on the shaking table, the accelerometers and laser displacement (LD) sensors were installed. In addition, a force sensor was mounted at contact level of impact. The impact pounding force, acceleration and displacement response data were obtained using the sensors. Shaking table tests were carried out by applying the abovementioned scaled earthquake acceleration records, which are depicted in Figures 3.10(b), 3.11(b), 3.12(b) and 3.13(b)). The reference frames were based outside the shaking table. Hence, the recorded displacements have been the absolute displacement time history.

The arrangement of the sensors was as follows: for 15B-storey frames adjacent to 10-storey frames, PCB 352C34 (±50 g) accelerometers were attached to the tenth and fifteenth floors of the 15B-storey frame and to the tenth floor of the 10-storey frame. Laser displacement sensors were attached to reference frames as follows: two LD300 ((±150 mm) opposite the tenth floor of both frames and an LD400 ((±200 mm) opposite the fifteenth floor of the 15B-storey frame. A load cell was mounted on the tenth floor of the flexible left frame directly opposite the steel plate of the rigid right frame as the receiving side of the impact. An enlargement of the contact point between the two frames is shown in Figures 3.19. A force sensor model PCB 208C05 (with measurement range of 22.24 kN) was used to record the impact force induced by pounding. The procedure was repeated, with sensor location levels changed, for the coupled configurations: 15B-storey and 5B-storey; 10-storey and 5B-storey; 5A-storey and 5B-storey; 15A-storey and 15B-storey.

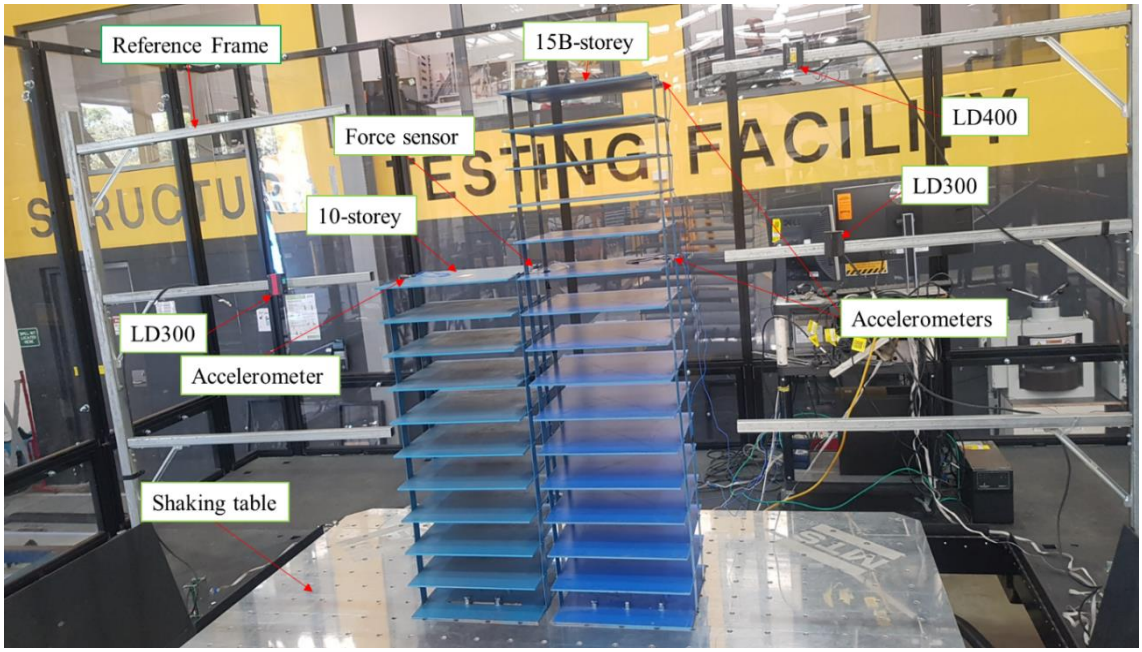

Figure 3.14 Test frames on the shaking table: 15B-storey adjacent to 10-storey

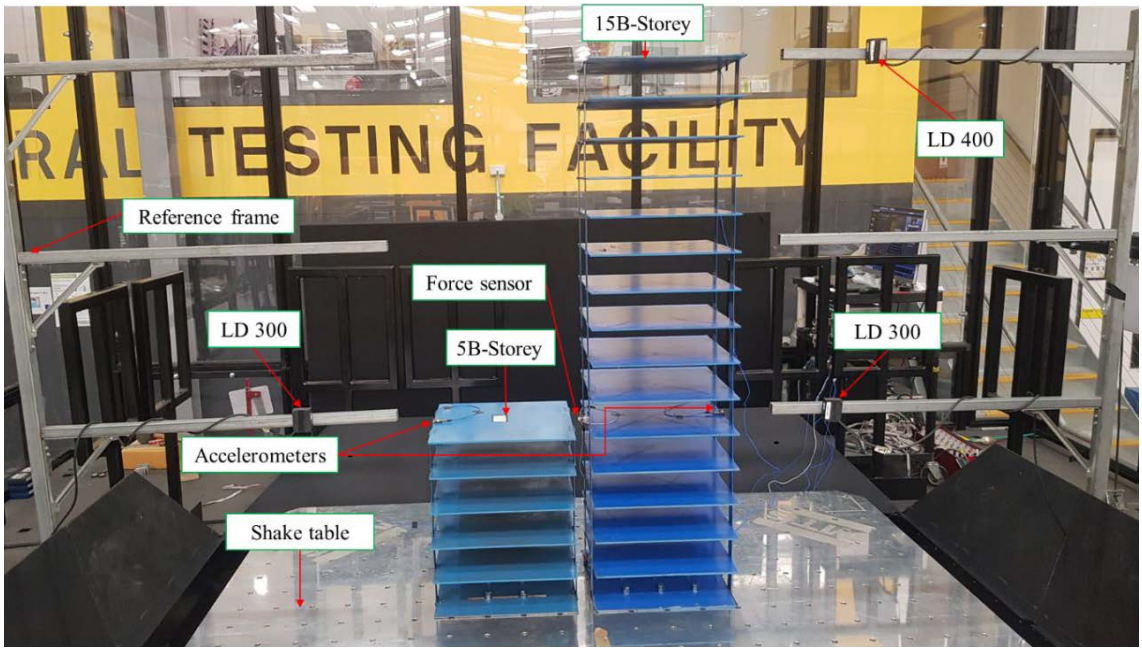

Figure 3.15 Test frames on the shaking table: 15B-storey adjacent to 5B-storey

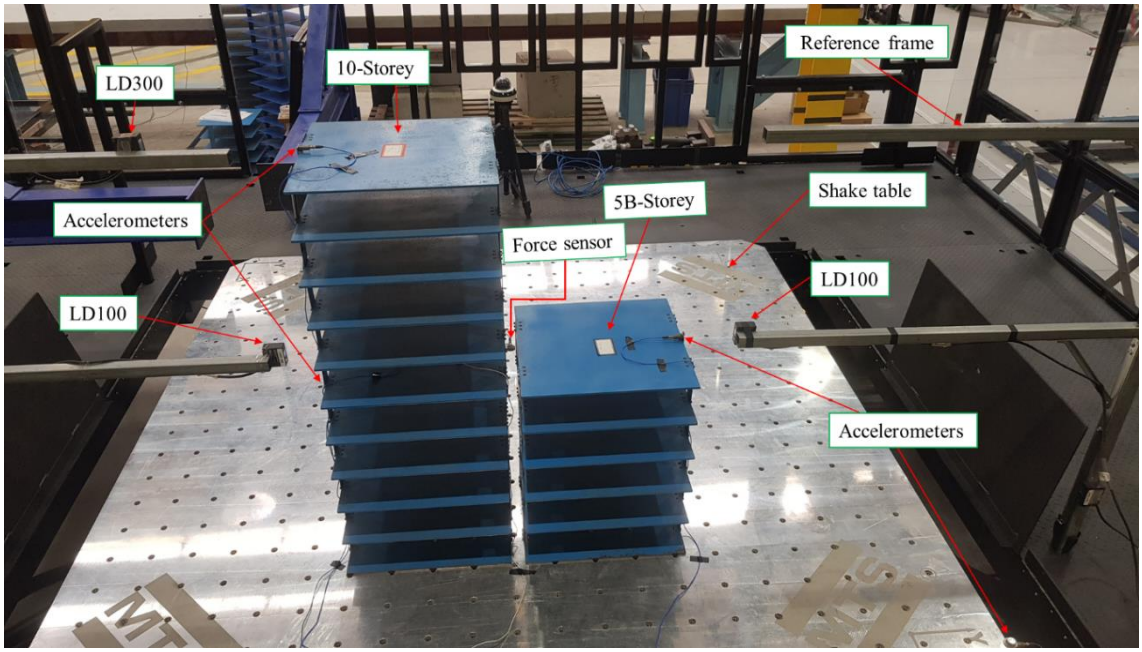

Figure 3.16 Test frames on the shaking table: 10-storey adjacent to 5B-storey

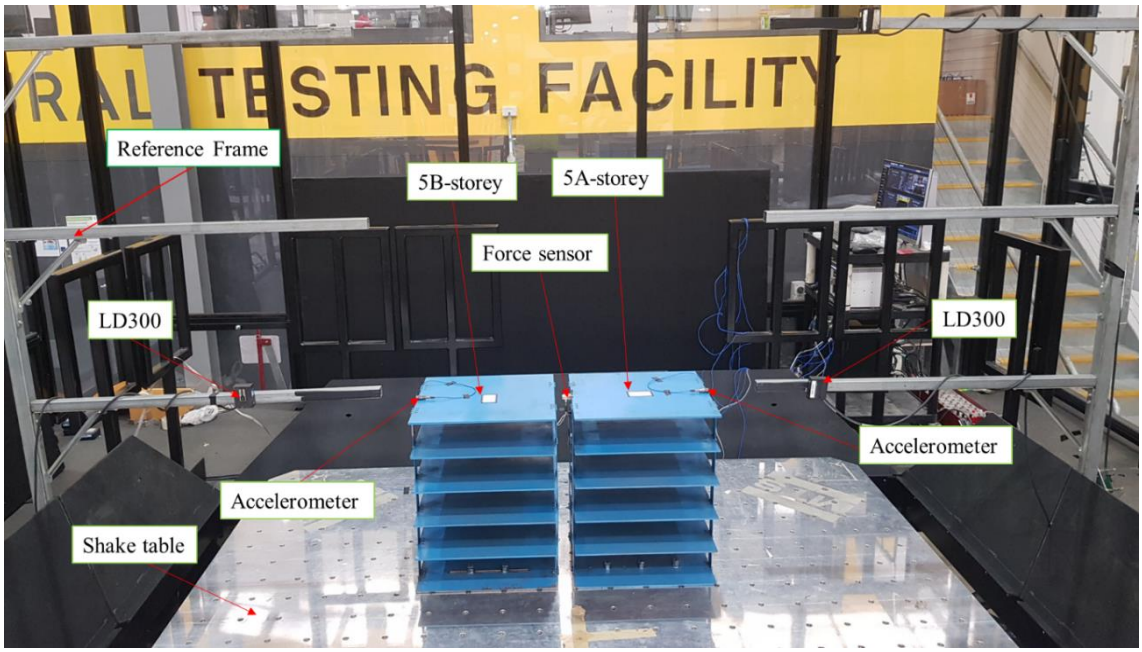

Figure 3.17 Test frames on the shaking table: 5B-storey adjacent to 5A-storey

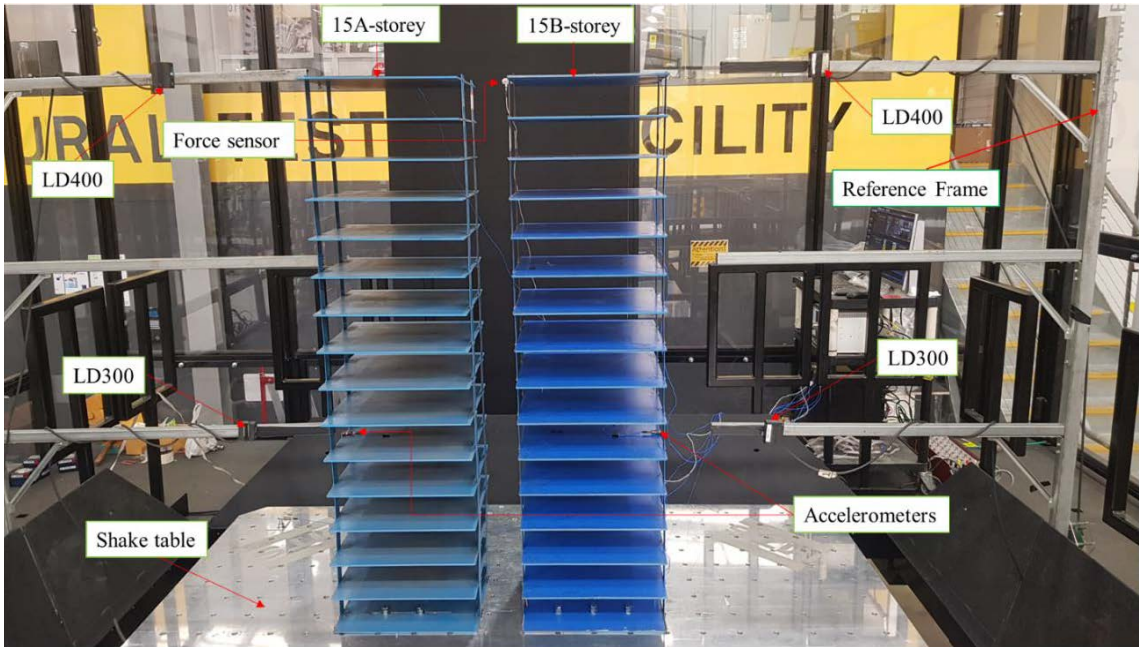

Figure 3.18 Test frames on the shaking table: 15A-storey adjacent to 15B-storey

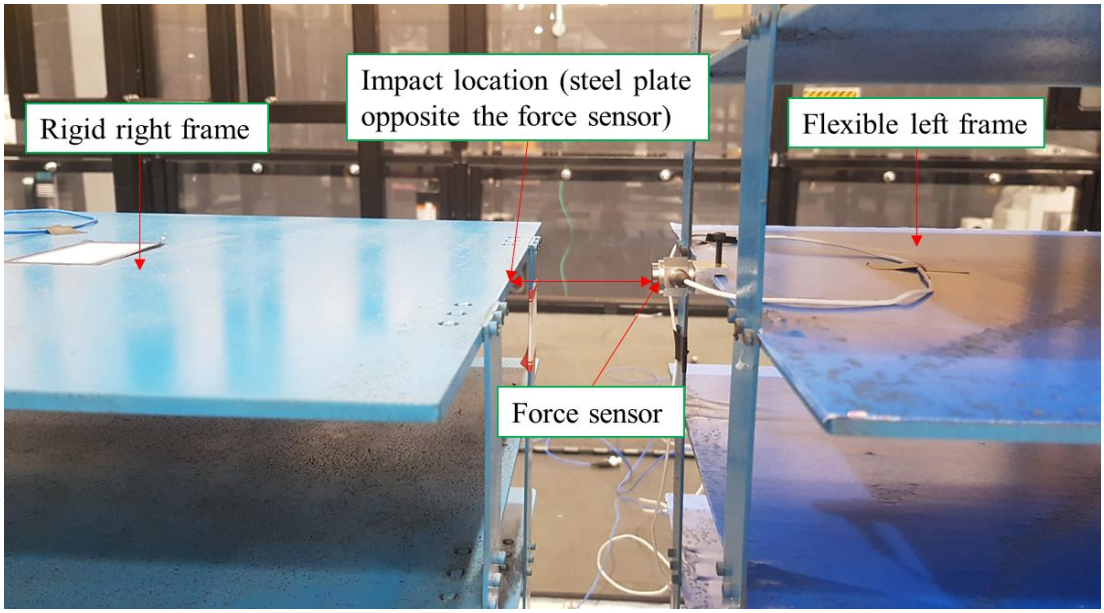

Figure 3.19 Force sensor at contact location

3.9 **Summary**

In this chapter, five scaled single-bay moment-resisting steel frame models were selected. The building frames were modelled with two 15-storey steel models 1500 mm in height, one 10-storey steel model 1000 mm in height and two 5-storey steel models 500 mm in height.

Several preliminary tests were carried out on the model frames to determine their basic dynamic properties; the five structures were tested separately. The dynamic characteristics of the experimental and numerical models showed similar results in natural frequency and stiffness values.

The results of the shaking table tests excited under the effect of four scaled earthquake acceleration records will be discussed in the following chapters. The results in terms of relative displacement, acceleration and impact force time histories are measured and compared with the numerical data.

CHAPTER 4
INVESTIGATION INTO ADEQUACY OF SEPARATION GAP TO PRECLUDE EARTHQUAKE-INDUCED POUNDING BETWEEN ADJACENT BUILDINGS

4.1 Introduction

Previous investigations have shown that the collision of adjacent structures can cause severe damage during an earthquake excitation (Shrestha & Hao 2018). The resulting collision is commonly known as 'structural pounding'. Pounding of adjacent edifices has caused a lot of damage and in many instances led to the total collapse of structures. According to Raheem (2013), pounding is a phenomenon in which two buildings strike due to their lateral movements, induced by lateral forces. Cole et al. (2011a) consider seismic pounding as the collision of adjacent buildings during earthquakes. Jeng et al. (1992a) stated that the difference in the dynamic characteristics of each structure and the existing distance between the buildings were common causes of structural pounding. The said factors are often the results of an out-of-phase vibration.

Over the years, researchers have considered insufficient separation gap as the main reason for structural pounding (Jankowski & Mahmoud 2016; Jeng et al. 1992a; Lopez-Garcia & Soong 2009). Many studies proved that providing sufficient gap is a reasonable approach to mitigate the incidence of pounding (Hao 2015). Based on these studies, providing a sufficiently larger gap between adjacent buildings appears to be a reasonable solution to prevent collision. However, even though providing a sufficient gap is considered one of the best solutions for decreasing the occurrence of collision between structures, many property owners and engineers do not adopt this strategy because it is costly and architecturally difficult. Within this purview, there are other techniques recommended to reduce the incidence of pounding, which will be discussed later.

This chapter aims to determine the adequacy of the minimum separation gap prescribed by AS1170.4 to mitigate the incidence of structural earthquake-induced pounding between adjacent structures. Specifically, the main purpose was to find out whether or not the minimum separation gap of 1% between two adjacent steel frame structures is adequate to preclude pounding under earthquake ground motions. Figure 4.1 illustrates two different examples of adjacent buildings in Sydney, Australia. Figure 4.1a shows that the 1% separation gap has been applied in recently constructed buildings. This application has not been implemented for older buildings, as shown in Figure 4.1b.

Figure 4.1 Case of neighbouring buildings in Sydney, Australia (a) with separation gap, (b) with zero separation gap (image by Yazan Jaradat)

4.2 **Shaking Table Test Results and Numerical Investigation**

During the experiment, the structural models were fixed and secured to the shaking table with the coupled configuration of 15B-storey with 10-storey, 15B-storey with 5B-storey, 10-storey with 5B-storey, 5A-storey with 5B-storey and 15A-storey with 15B-storey, as shown in Figures 3.10–3.14. In this section only acceleration and displacement response data were recorded for no-pounding scenarios. As mentioned previously, the numerical models were created in SAP2000 Version 20 (SAP 2000), as shown in Figure 4.2. Numerical analysis involving time history used the Ritz modal loading analysis (Jaradat & Far 2020) to measure lateral deflection and acceleration. Ritz vectors typically capture more response when compared with the same number of eigenvectors. Mode numbers were selected targeting dynamics check modal participating mass ratios. Nonlinear time history dynamic analyses (fast nonlinear analysis, FNA) were conducted by applying a range of 6000–11,000 time steps from the subject earthquakes (Figure 3.5(b), Figure 3.6(b), Figure 3.7(b) and Figure 3.8(b)).

FNA allows for extremely efficient and fast nonlinear analysis when nonlinear behaviour is limited to predefined location. FNA is nonlinear modal time history analysis using load-dependent Ritz vectors. Using Ritz vectors to perform a nonlinear time history analysis can be significantly more computationally efficient than using direct integration. However, geometric nonlinearity parameters such as P-Delta effects have been omitted since direct integration solution was not considered.

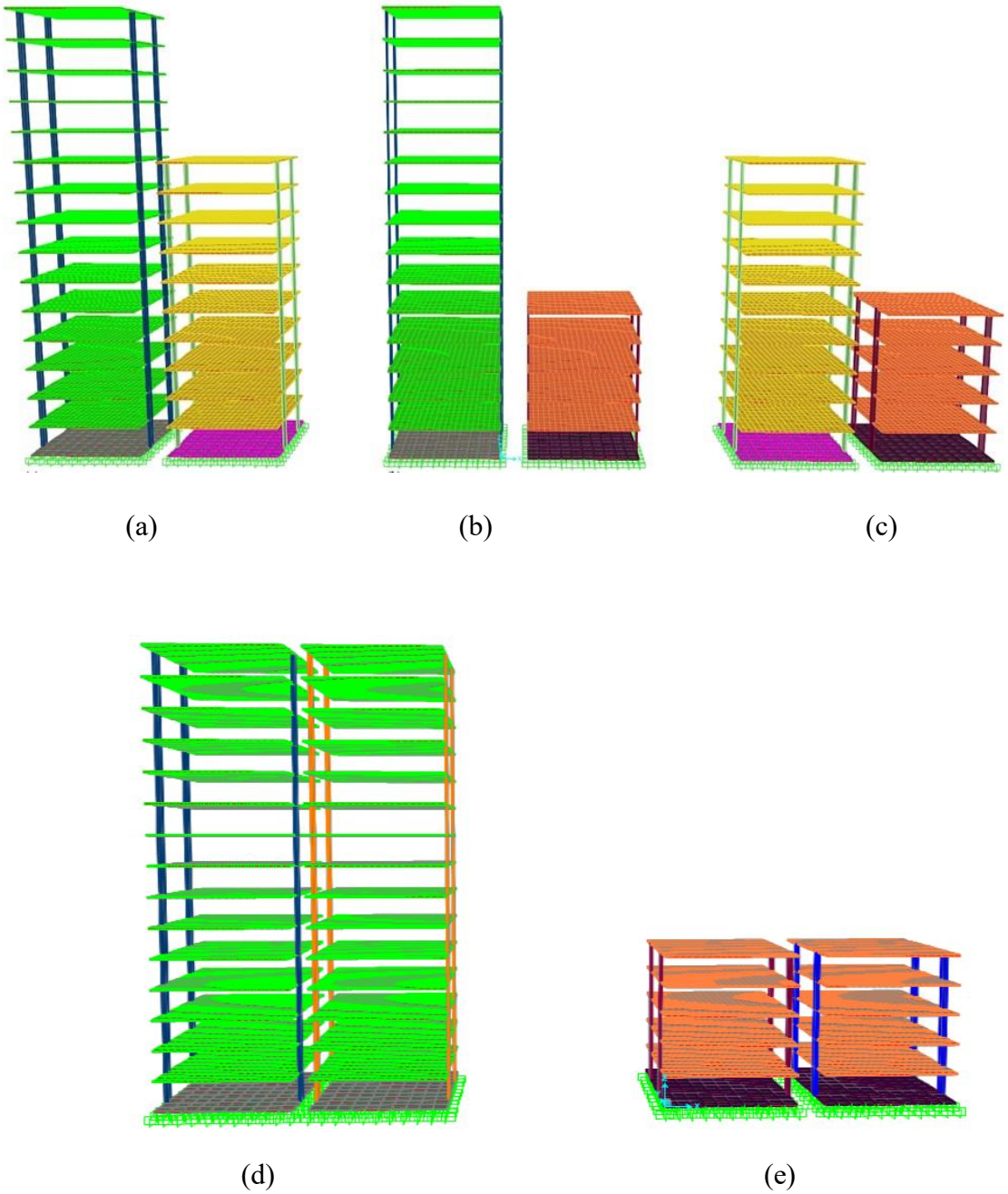

Figure 4.2 3D numerical model of the structural models in SAP2000; (a) 15B-storey adjacent to 10-storey, (b) 15B-storey adjacent to 5B-storey, (c) 10-storey adjacent to 5B-storey, (d) 15A-storey adjacent to 15B-storey, (e) 5A-storey adjacent to 5B-storey

4.2.1 Relative Displacement Time history

Results are depicted in Figures 4.3–4.10. In Figures 4.3 and 4.4, experimental and numerical relative displacement time histories subjected to the four scaled seismic excitations utilised in this study are compared with each other. For the top floor of the 5A and 5B-storey frames, the highest relative displacement was caused by the Kobe earthquake. In contrast, in Figure 4.6 it can be seen that the peak relative displacement for the 10-storey frame was caused by the Northridge earthquake. Figures 4.7 and 4.10 show time histories and lateral deflection at the top floor of the 15A and 15B-storey frames. Similarly, the highest relative overall displacement belongs to the Northridge earthquake (1994).

4.2.2 Acceleration Time History

Experimental and numerical acceleration time histories for the top floor of each frame model are shown in Appendix E.

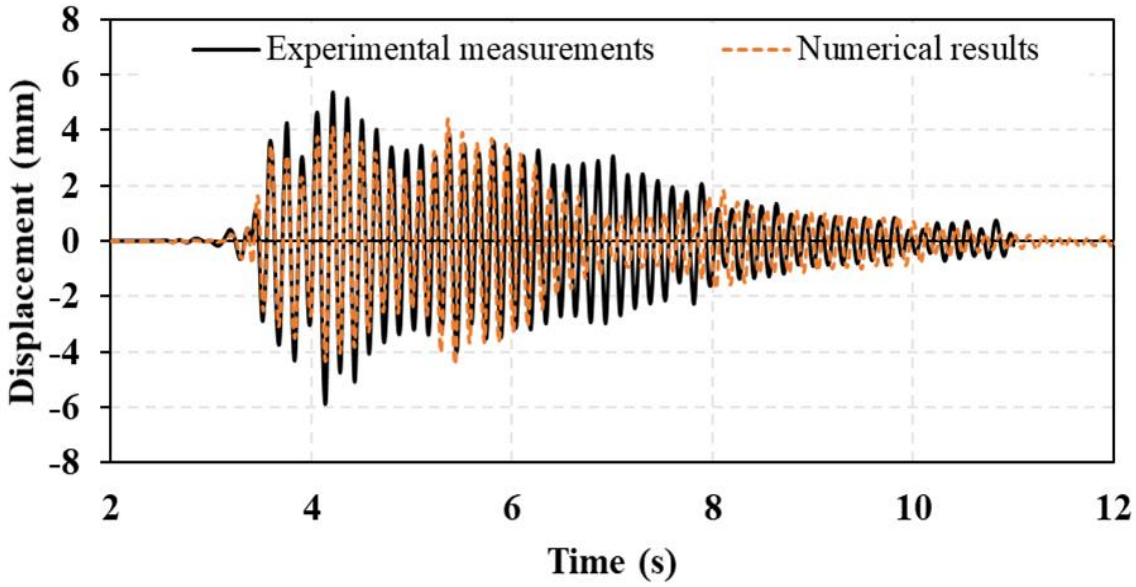

Figure 4.3(a) Experimental and numerical relative displacement time histories for 5A-storey frame (5th floor) under scaled El Centro earthquake

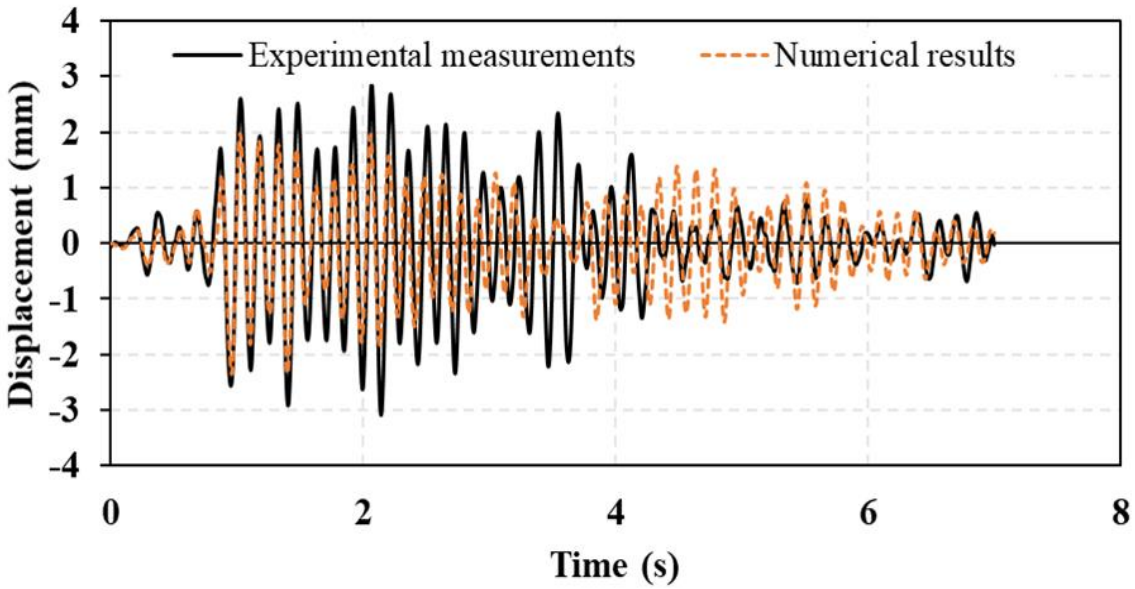

Figure 4.3(b) Experimental and numerical relative displacement time histories for 5A-storey frame (5th floor) under scaled Hachinohe earthquake

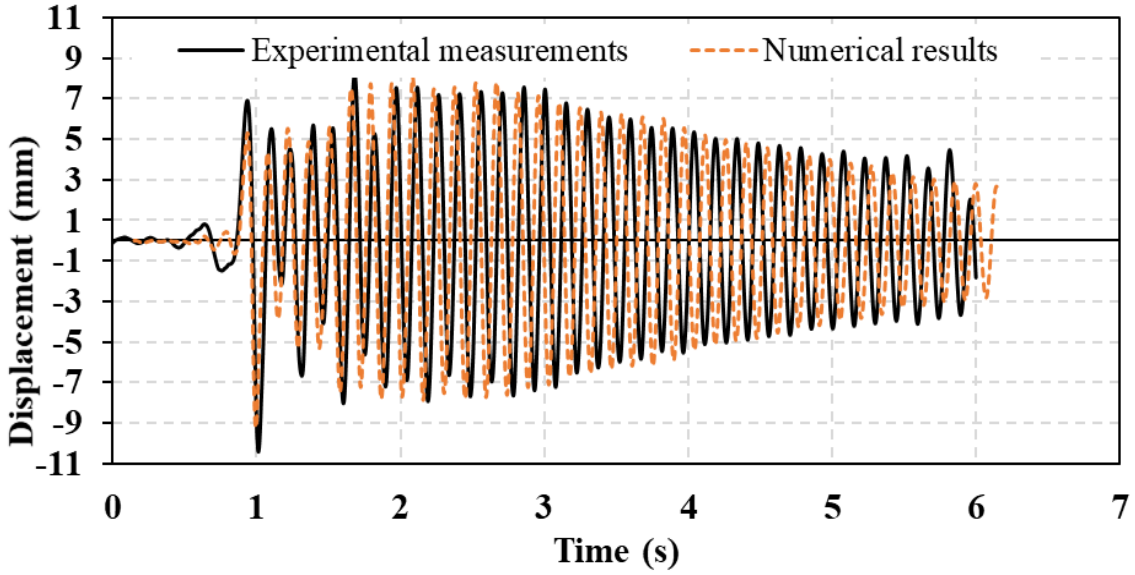

Figure 4.3(c) Experimental and numerical relative displacement time histories for 5A-storey frame (5th floor) under scaled Northridge earthquake

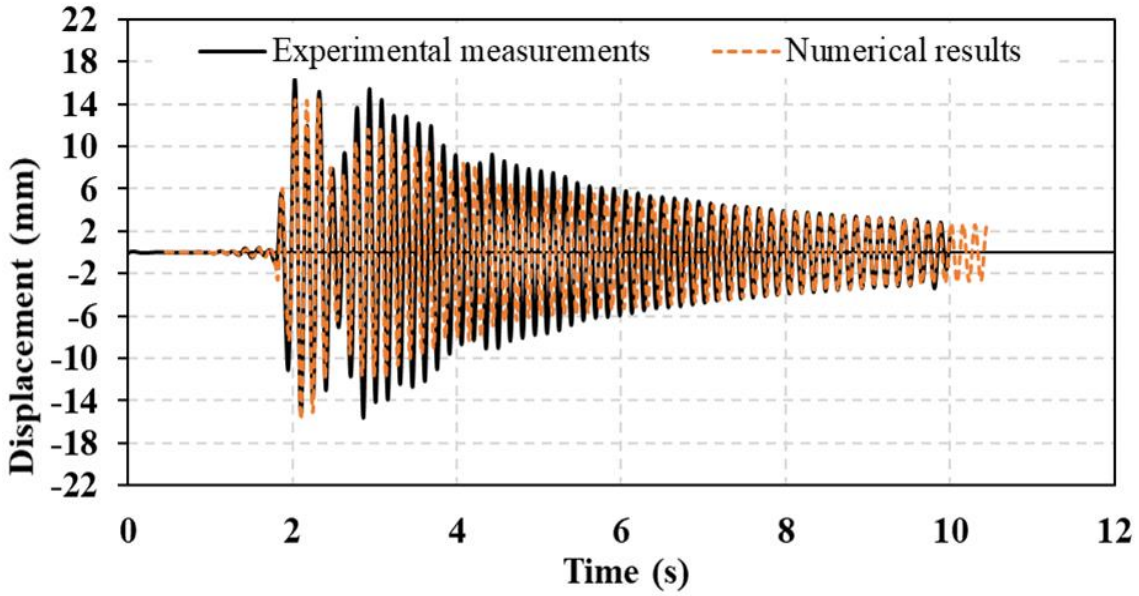

Figure 4.3(d) Experimental and numerical relative displacement time histories for 5A-storey frame (5th floor) under scaled Kobe earthquake

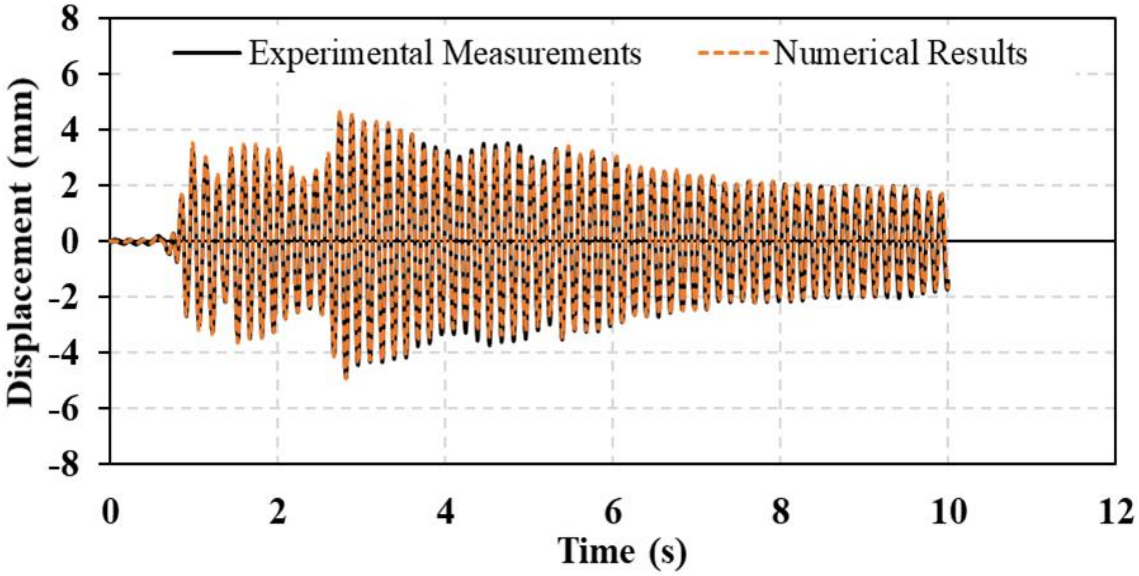

Figure 4.4(a) Experimental and numerical relative displacement time histories for 5B-storey frame (5th floor) under scaled El Centro earthquake

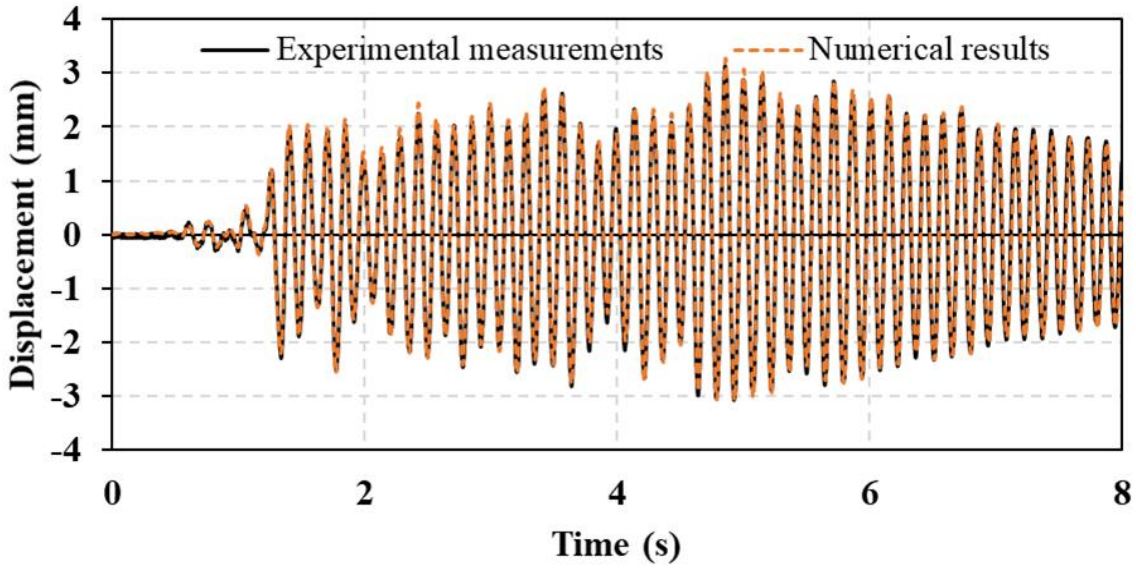

Figure 4.4(b) Experimental and numerical relative displacement time histories for 5B-storey frame (5th floor) under scaled Hachinohe earthquake

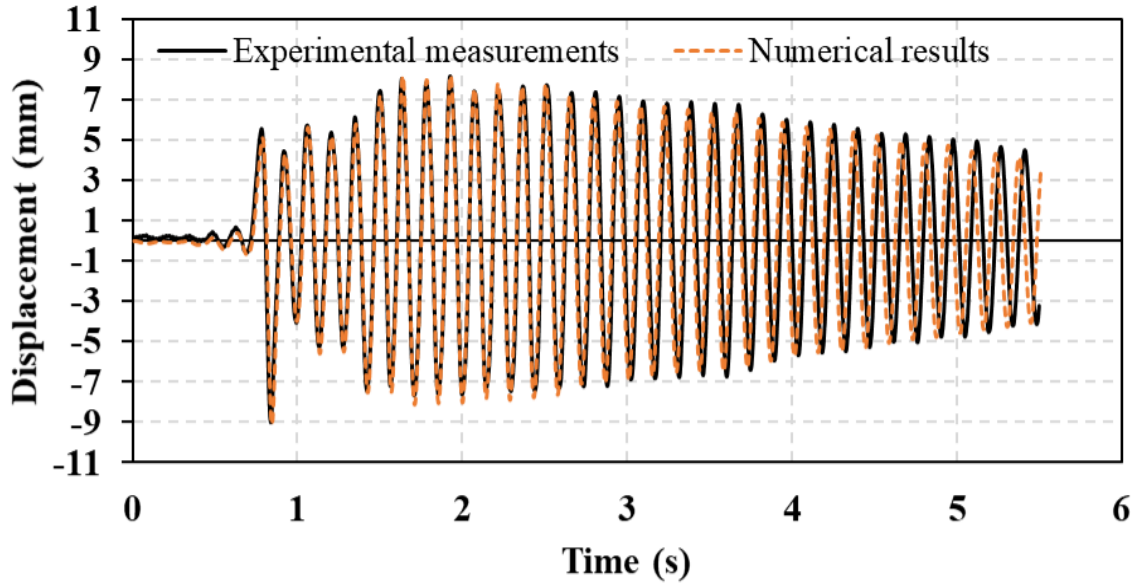

Figure 4.4(c) Experimental and numerical relative displacement time histories for 5B-storey frame (5th floor) under scaled Northridge earthquake

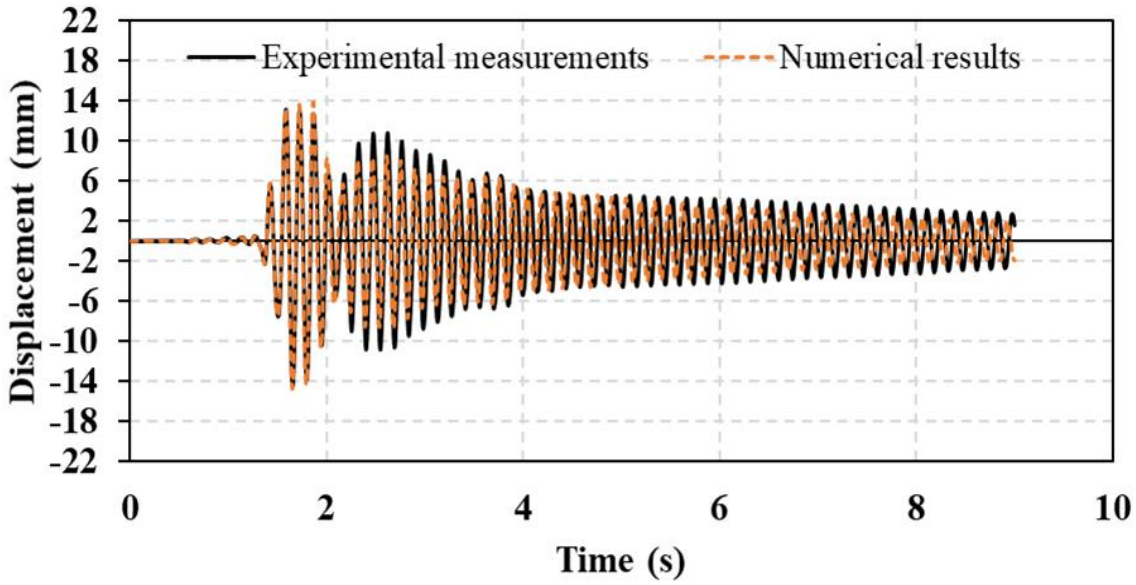

Figure 4.4(d) Experimental and numerical relative displacement time histories for 5B-storey frame (5th floor) under scaled Kobe earthquake

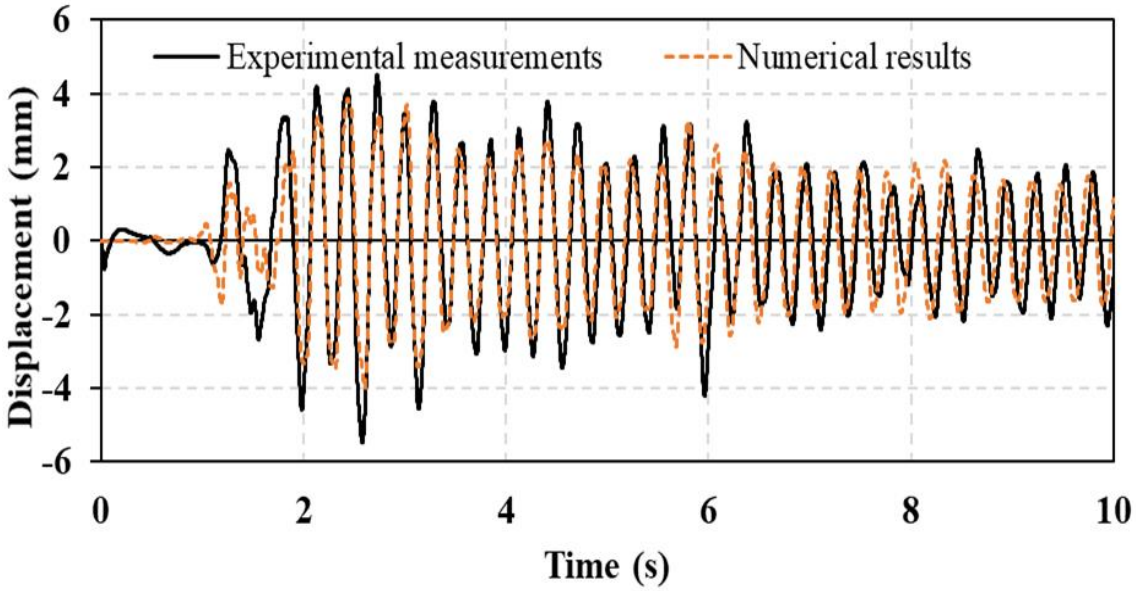

Figure 4.5(a) Experimental and numerical relative displacement time histories for 10-storey frame (5th floor) under scaled El Centro earthquake

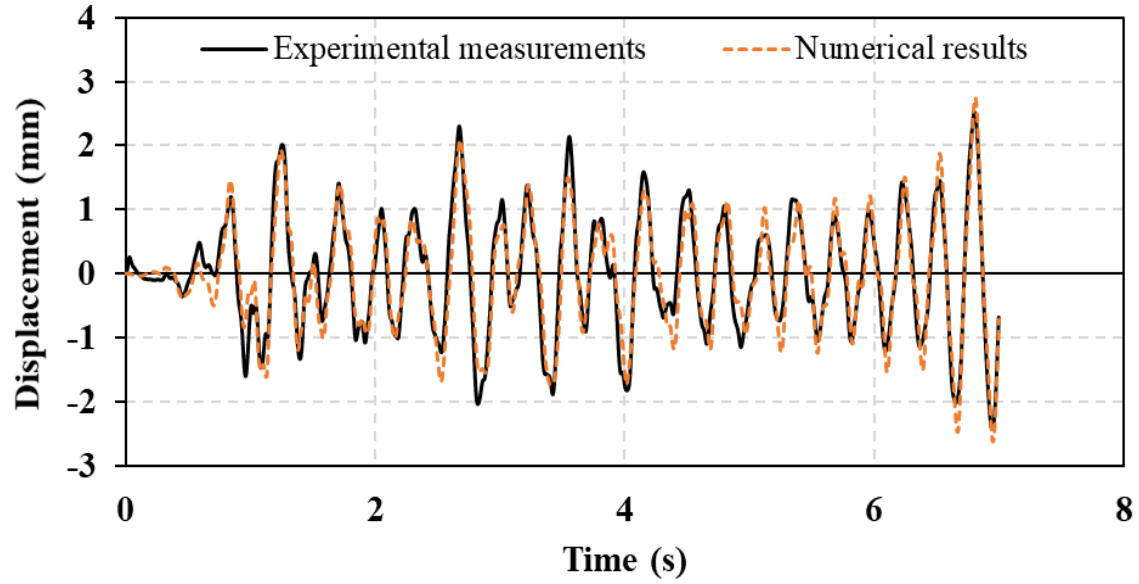

Figure 4.5(b) Experimental and numerical relative displacement time histories for 10-storey frame (5th floor) under scaled Hachinohe earthquake

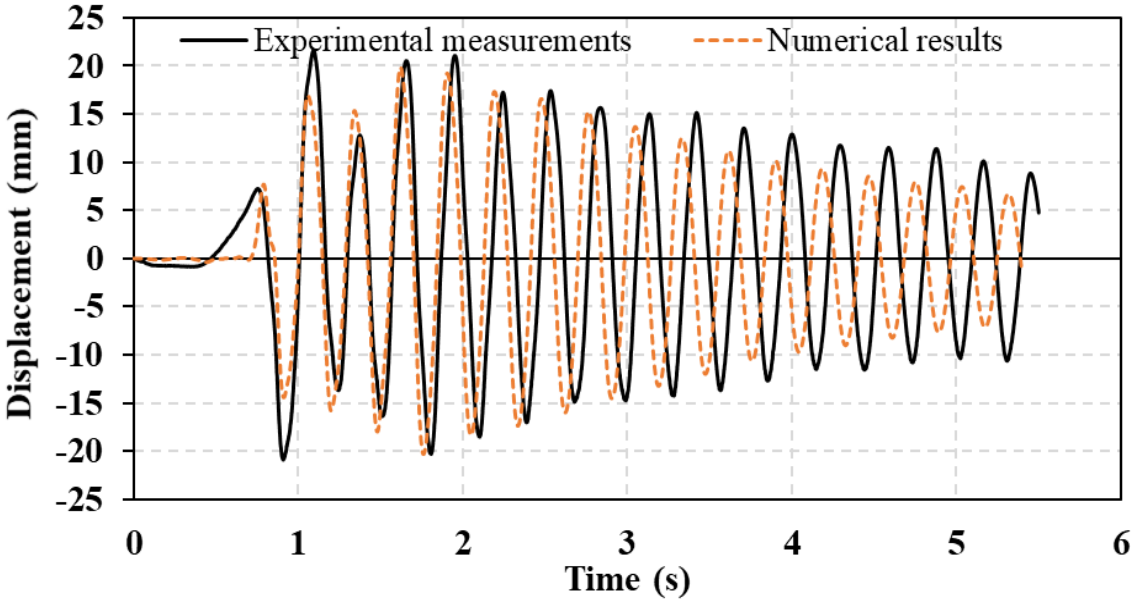

Figure 4.5(c) Experimental and numerical relative displacement time histories for 10-storey frame (5th floor) under scaled Northridge earthquake

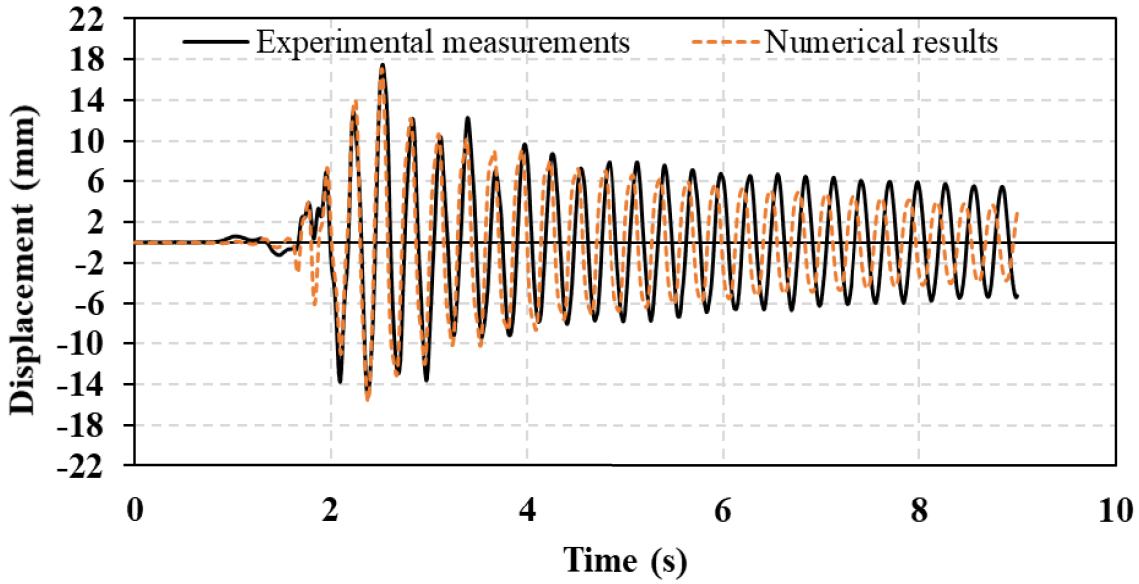

Figure 4.5(d) Experimental and numerical relative displacement time histories for 10-storey frame (5th floor) under scaled Kobe earthquake

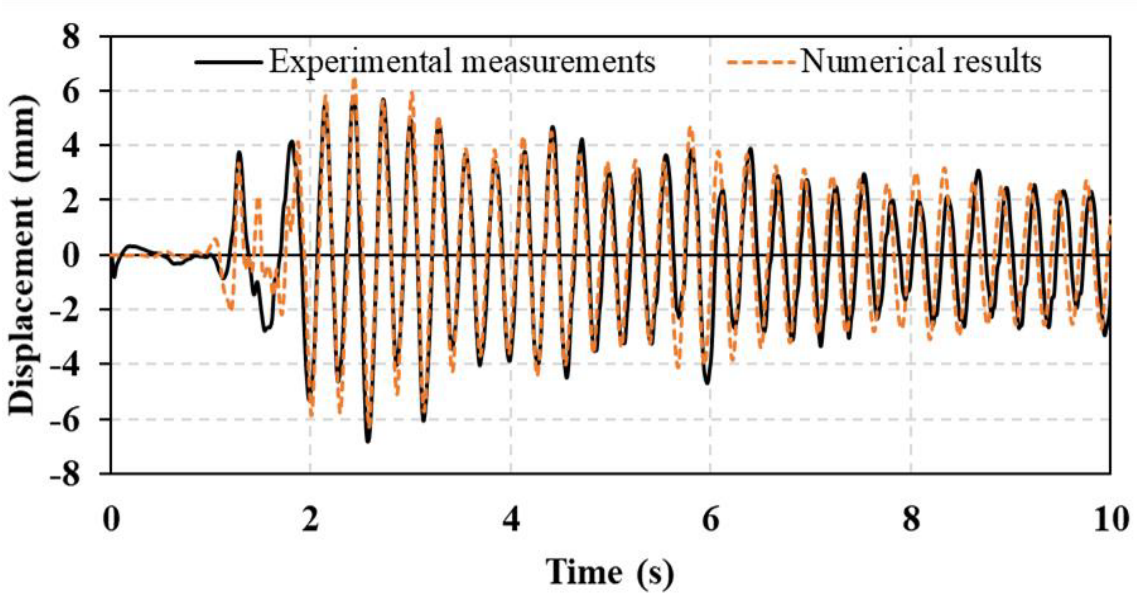

Figure 4.6(a) Experimental and numerical relative displacement time histories for 10-storey frame (10th floor) under scaled El Centro earthquake

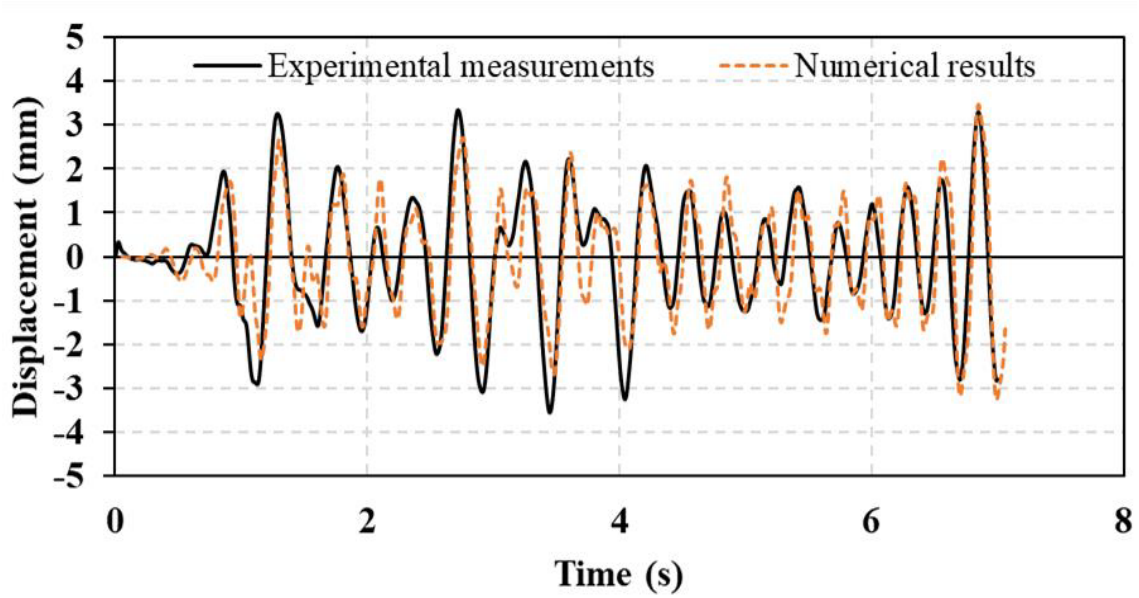

Figure 4.6(b) Experimental and numerical relative displacement time histories for 10-storey frame (10th floor) under scaled Hachinohe earthquake

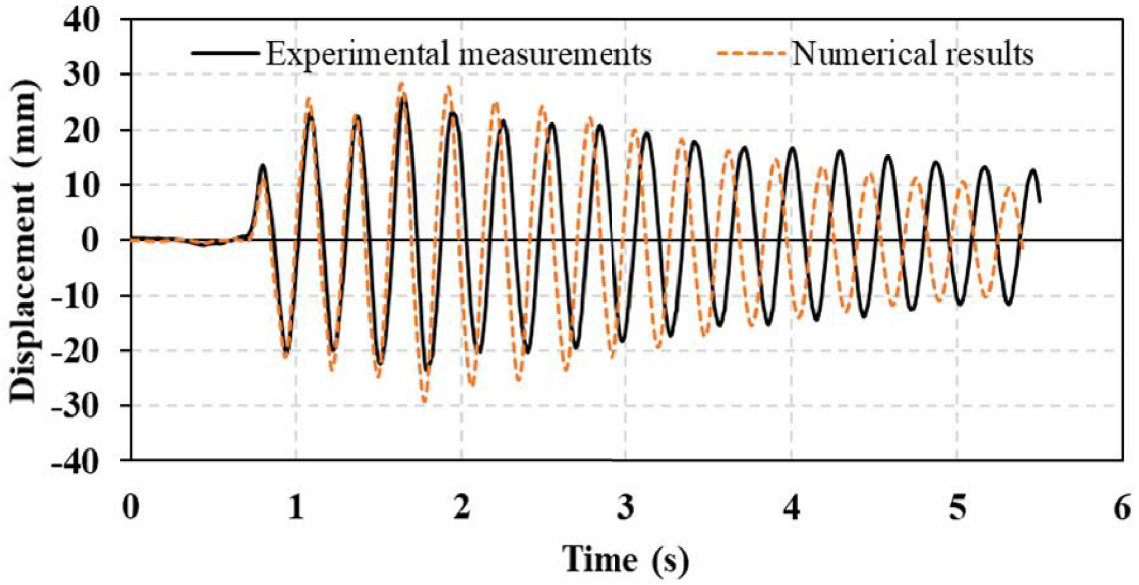

Figure 4.6(c) Experimental and numerical relative displacement time histories for 10-storey frame (10th floor) under scaled Northridge earthquake

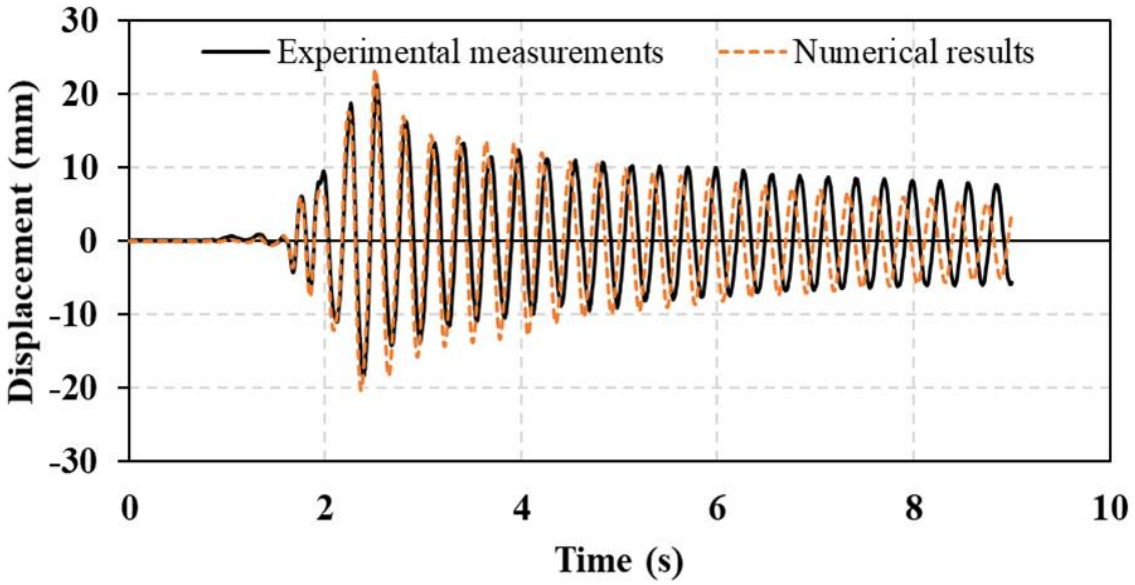

Figure 4.6(d) Experimental and numerical relative displacement time histories for 10-storey frame (10th floor) under scaled Kobe earthquake

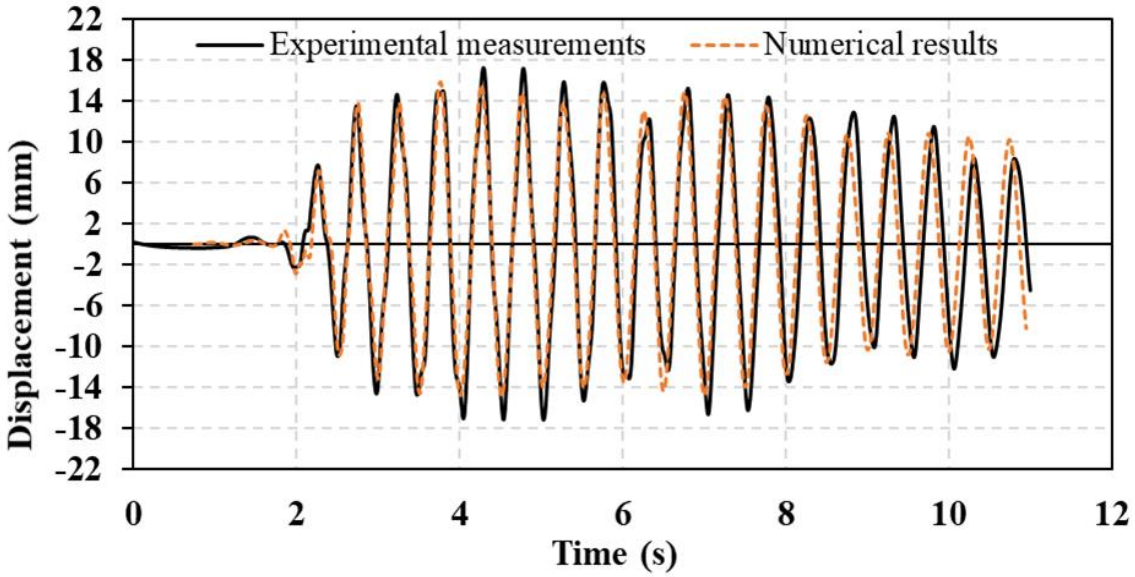

Figure 4.7(a) Experimental and numerical relative displacement time histories for 15A-storey frame (15th floor) under scaled El Centro earthquake

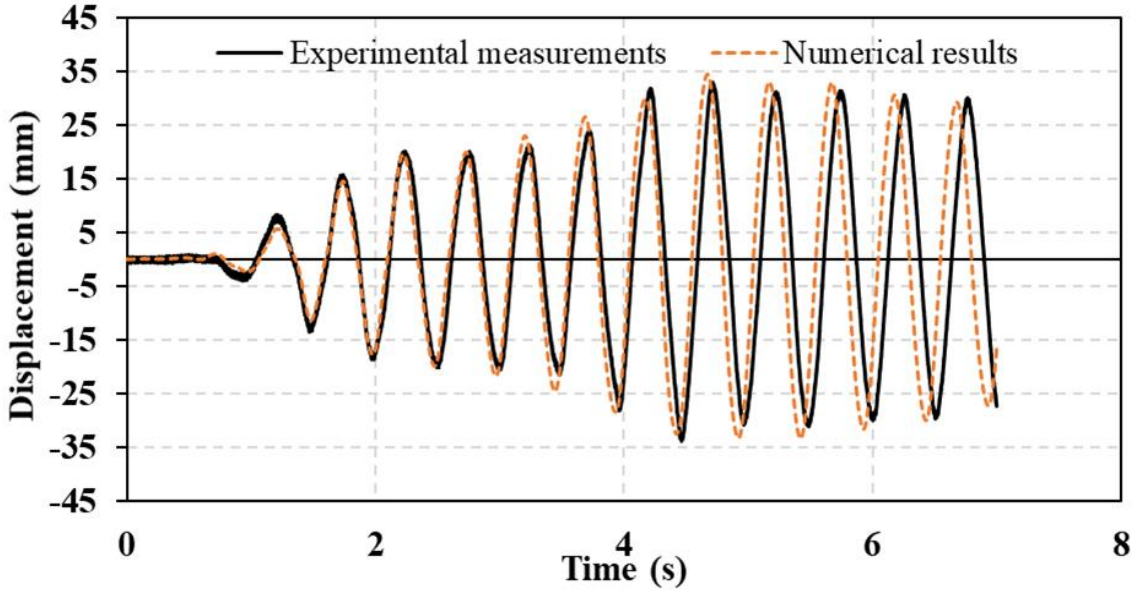

Figure 4.7(b) Experimental and numerical relative displacement time histories for 15A-storey frame (15th floor) under scaled Hachinohe earthquake

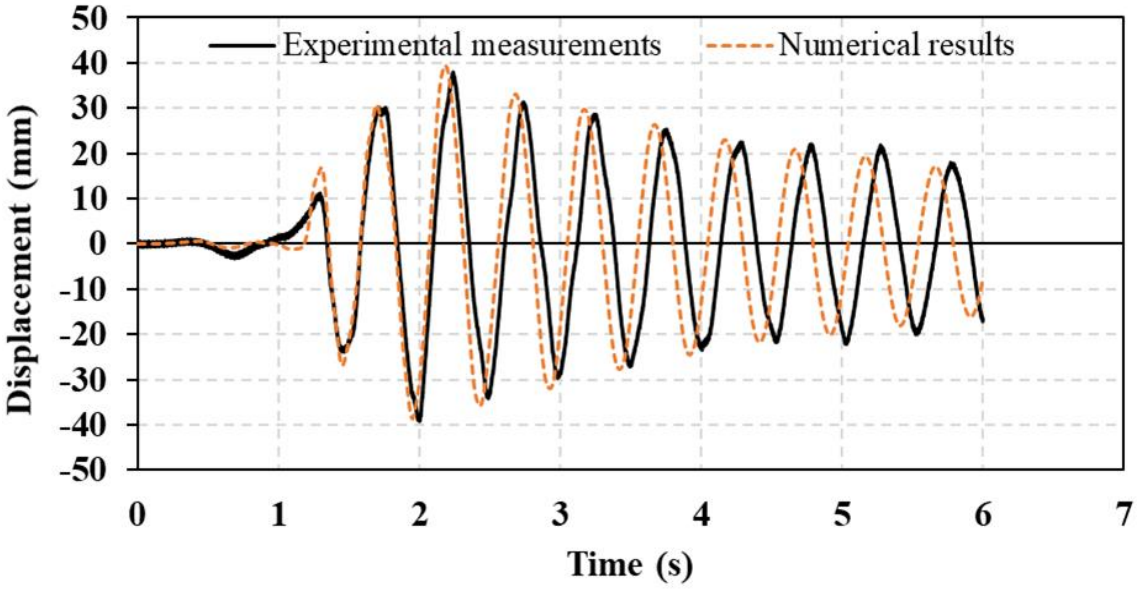

Figure 4.7(c) Experimental and numerical relative displacement time histories for 15A-storey frame (15th floor) under scaled Northridge earthquake

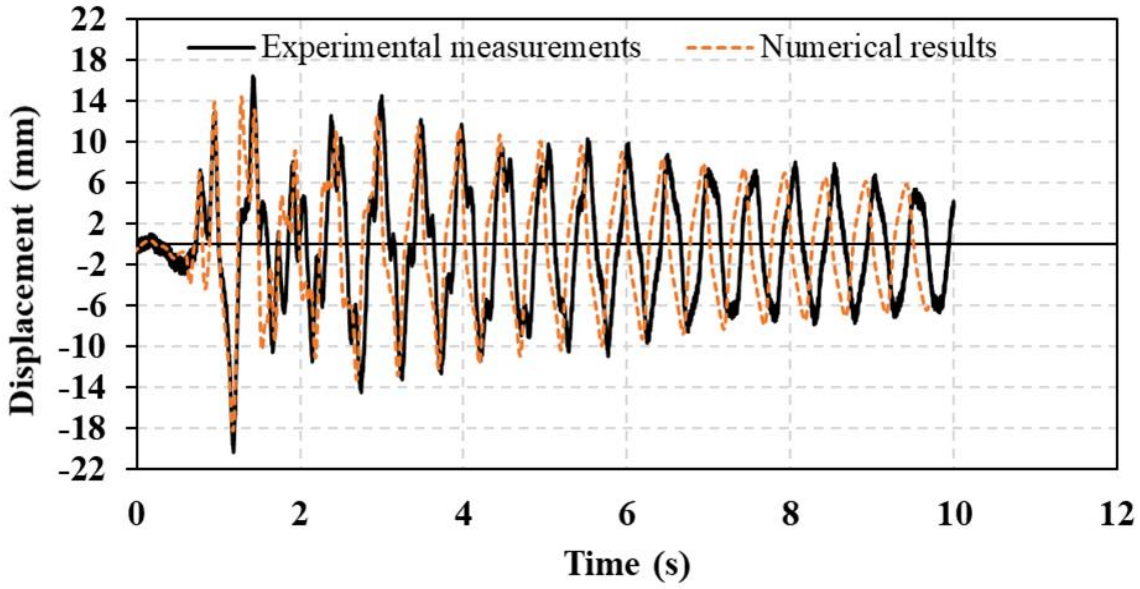

Figure 4.7(d) Experimental and numerical relative displacement time histories for 15A-storey frame (15th floor) under scaled Kobe earthquake

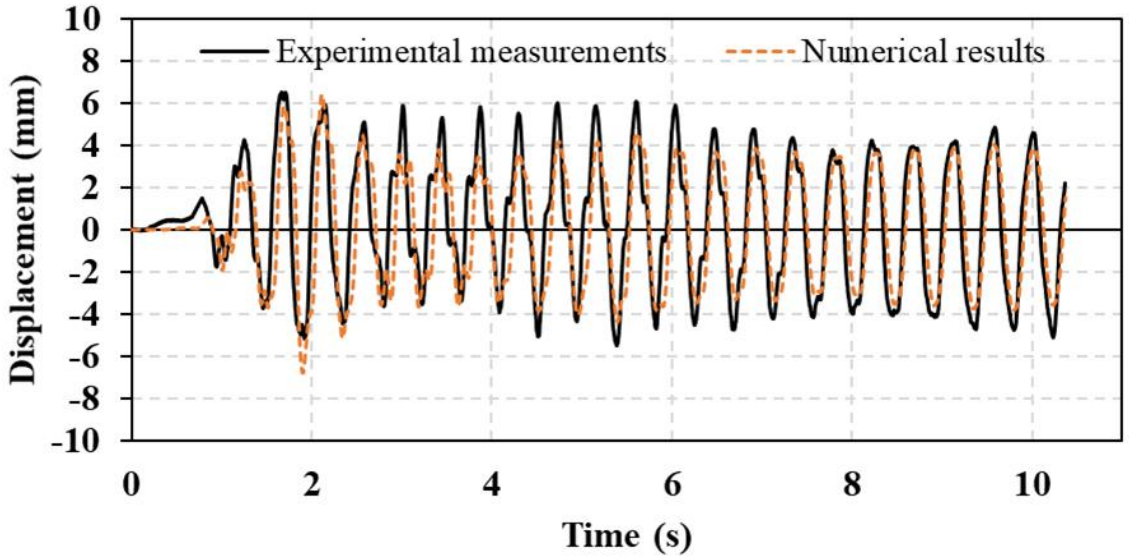

Figure 4.8(a) Experimental and numerical relative displacement time histories for 15B-storey frame (5th floor) under scaled El Centro earthquake

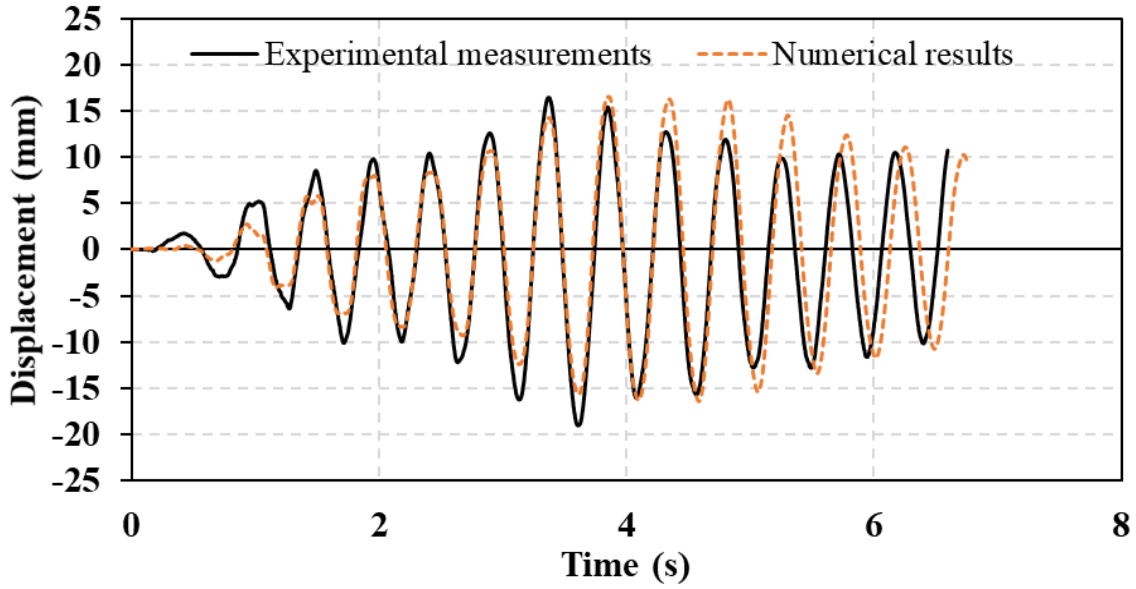

Figure 4.8(b) Experimental and numerical relative displacement time histories for 15B-storey frame (5th floor) under scaled Hachinohe earthquake

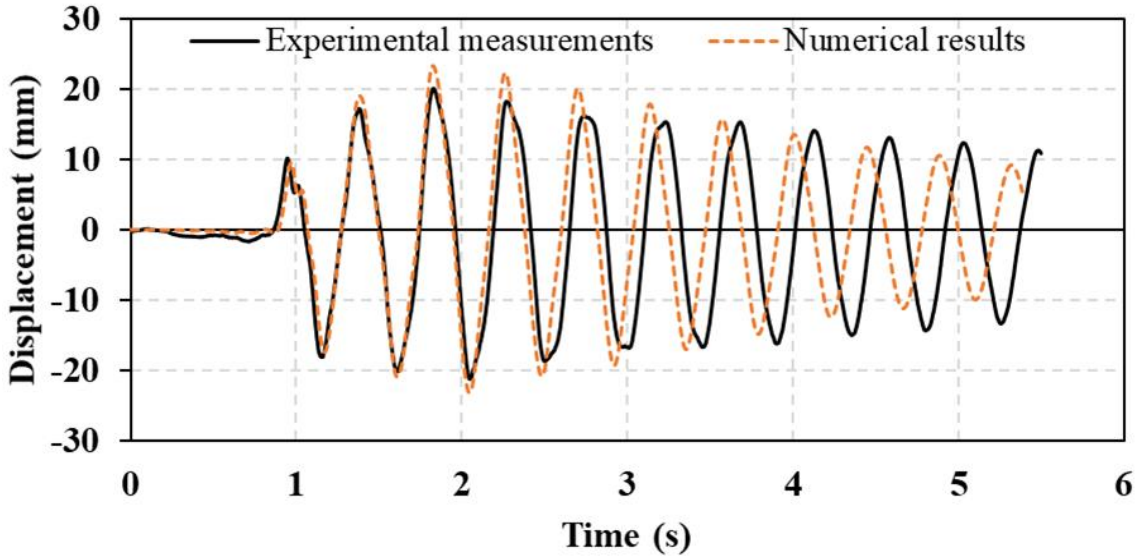

Figure 4.8(c) Experimental and numerical relative displacement time histories for 15B-storey frame (5th floor) under scaled Northridge earthquake

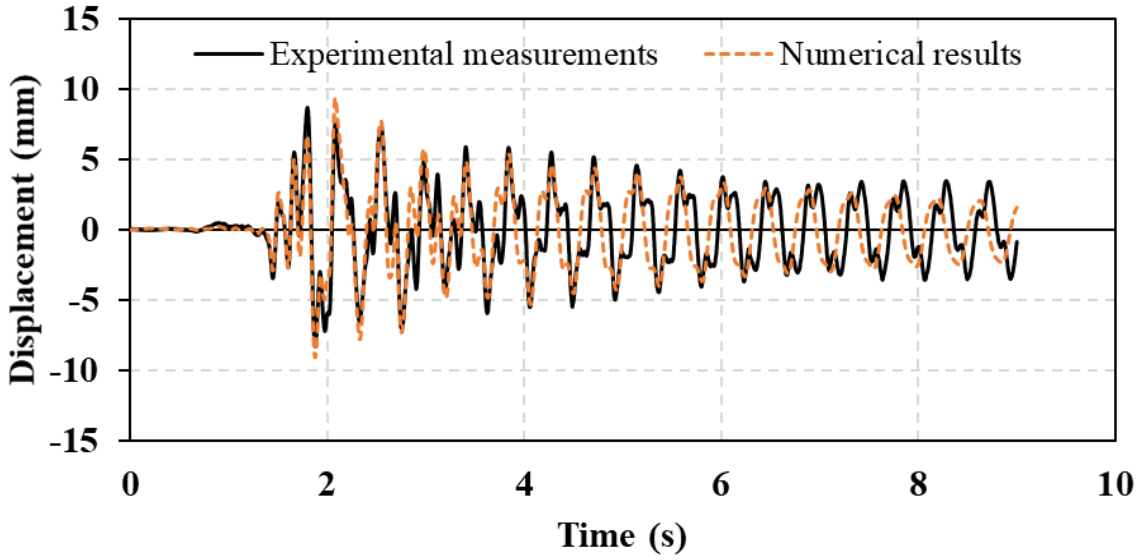

Figure 4.8(d) Experimental and numerical relative displacement time histories for 15B-storey frame (5th floor) under scaled Kobe earthquake

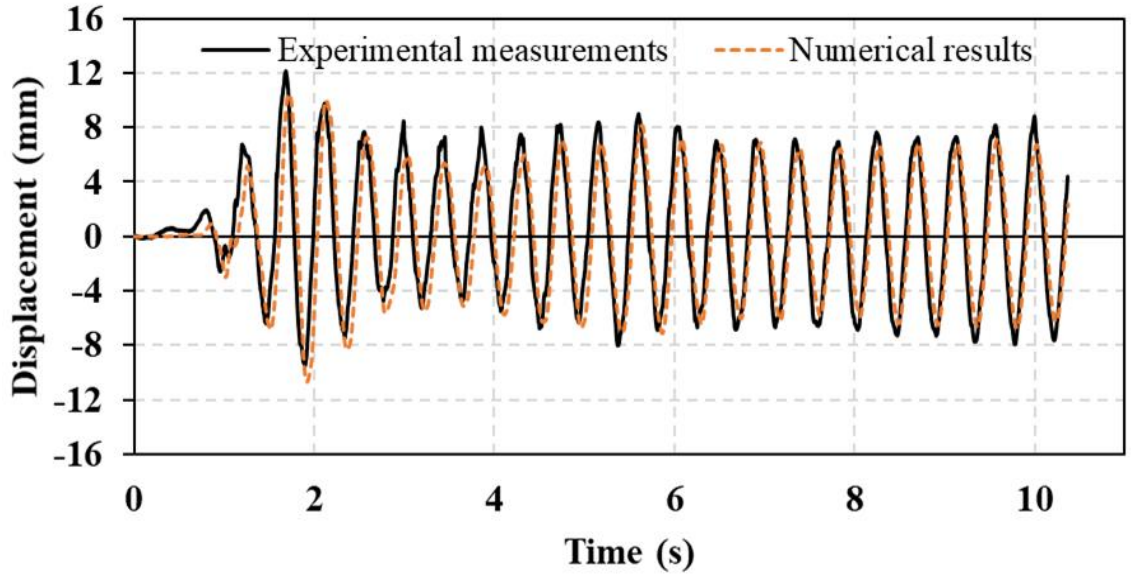

Figure 4.9(a) Experimental and numerical relative displacement time histories for 15B-storey frame (10th floor) under scaled El Centro earthquake

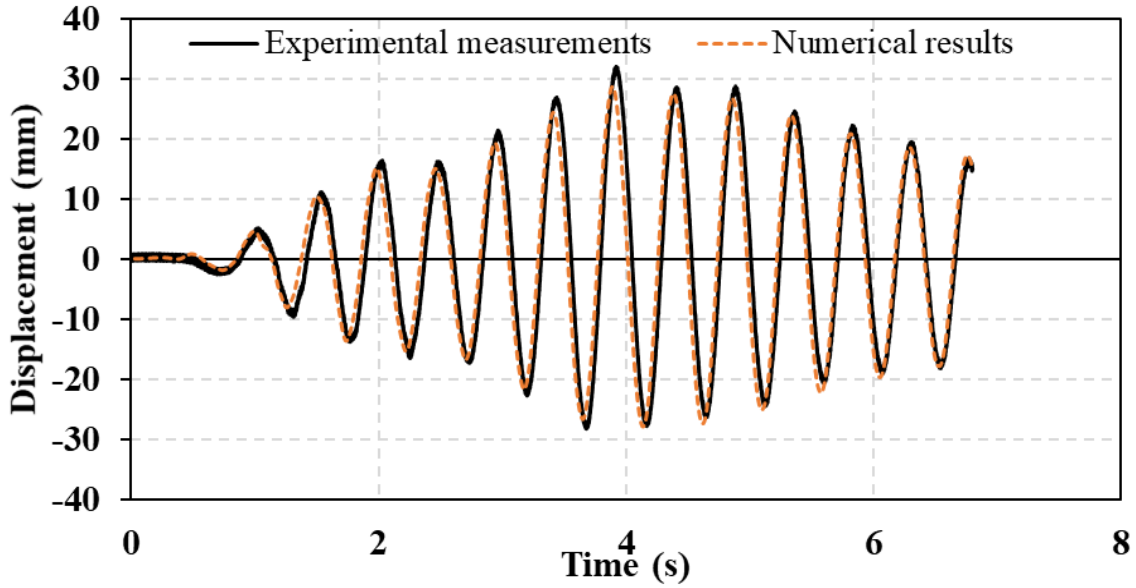

Figure 4.9(b) Experimental and numerical relative displacement time histories for 15B-storey frame (10th floor) under scaled Hachinohe earthquake

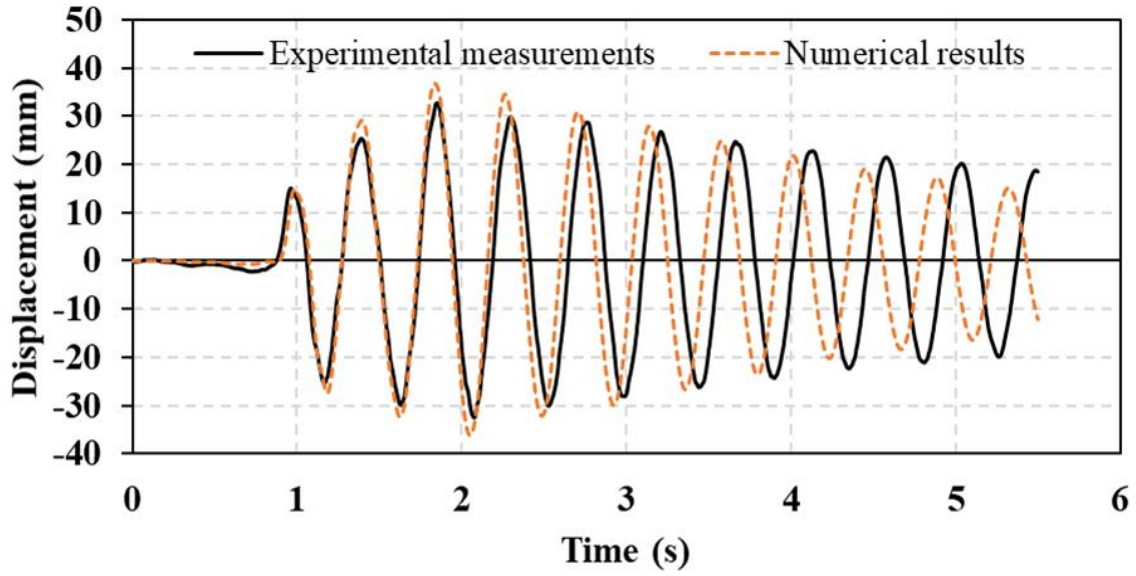

Figure 4.9(c) Experimental and numerical relative displacement time histories for 15B-storey frame (10th floor) under scaled Northridge earthquake

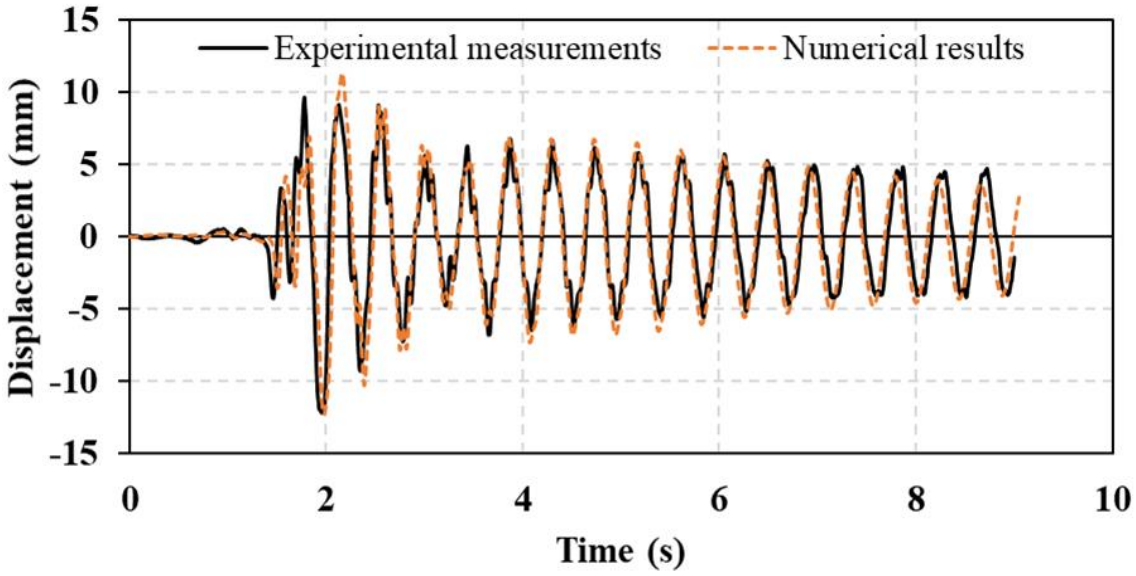

Figure 4.9(d) Experimental and numerical relative displacement time histories for 15B-storey frame (10th floor) under scaled Kobe earthquake

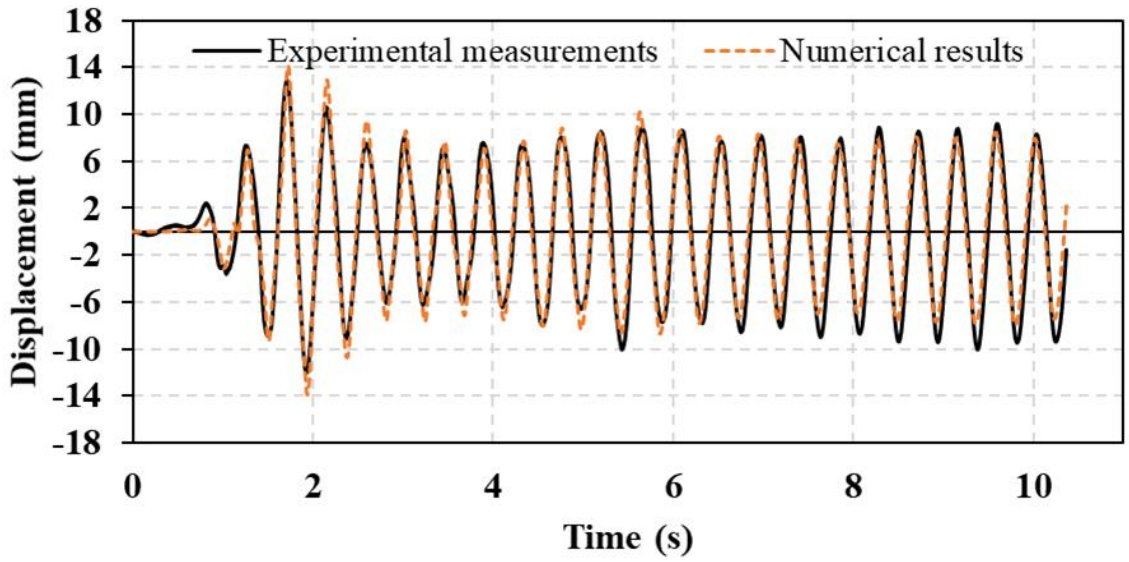

Figure 4.10(a) Experimental and numerical relative displacement time histories for 15B-storey frame (15th floor) under scaled El Centro earthquake

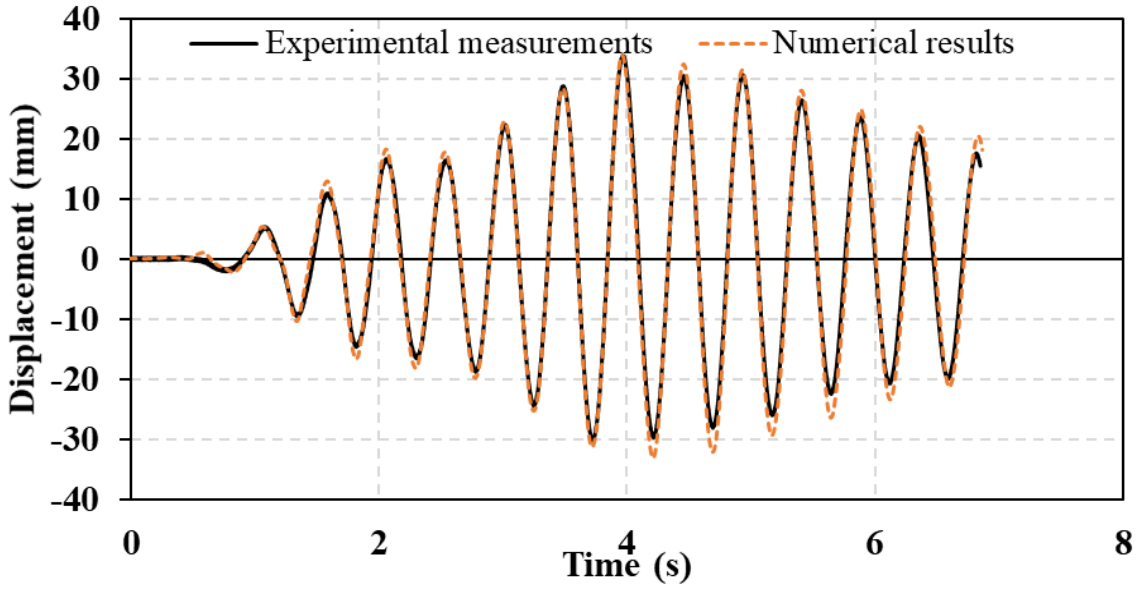

Figure 4.10(b) Experimental and numerical relative displacement time histories for 15B-storey frame (15th floor) under scaled Hachinohe earthquake

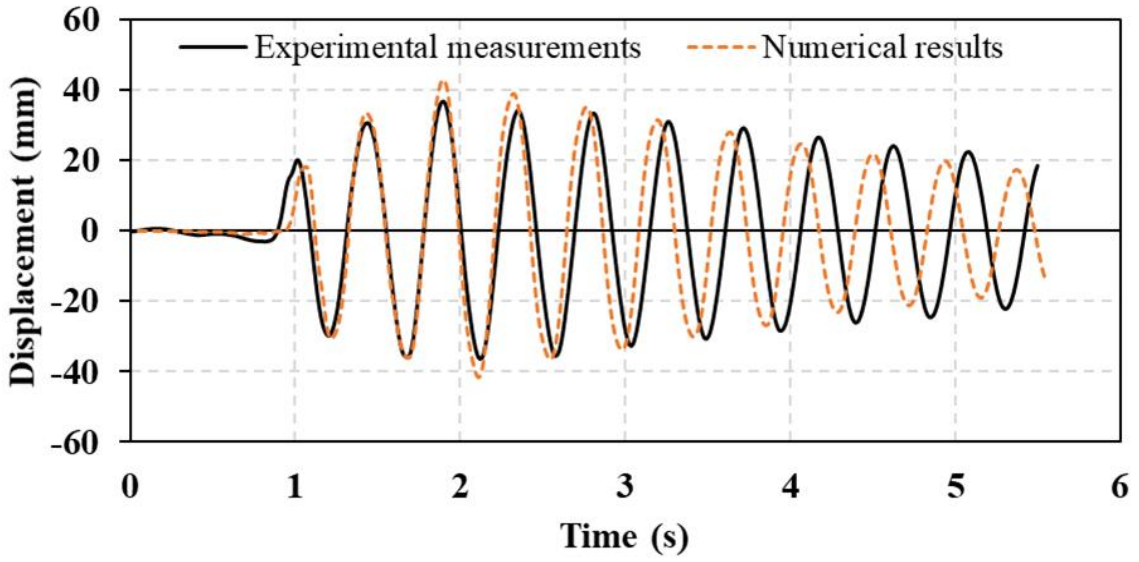

Figure 4.10(c) Experimental and numerical relative displacement time histories for 15B-storey frame (15th floor) under scaled Northridge earthquake

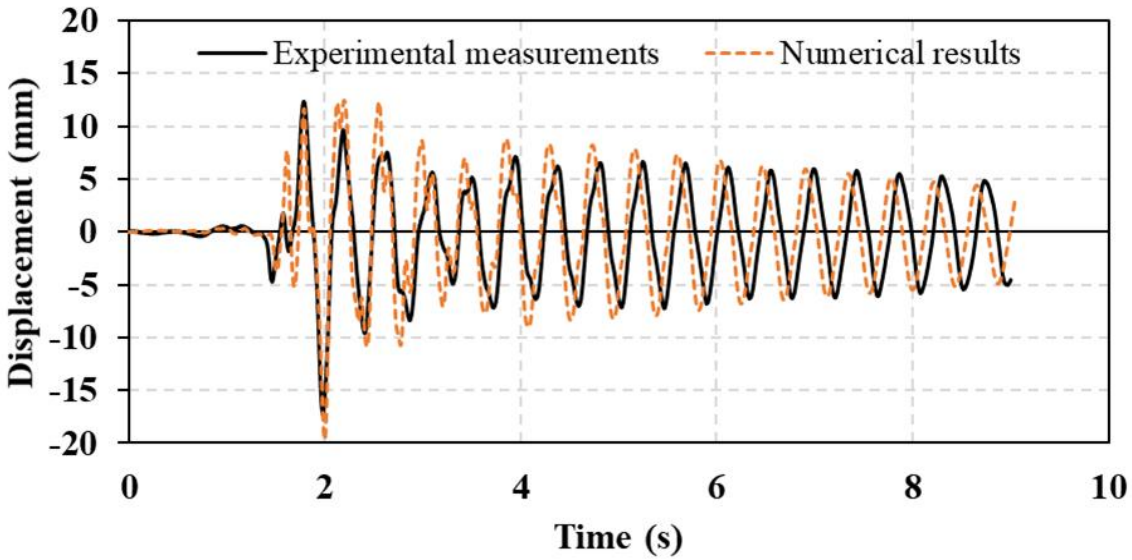

Figure 4.10(d) Experimental and numerical relative displacement time histories for 15B-storey frame (15th floor) under scaled Kobe earthquake

Table 4.1 tabulates the peak minimum and maximum displacement values for each earthquake. The results are classified according to the combination of the building heights, which are: level 15 of the 15A-storey frame; level 15, level 10 and level 5 of the 15B-storey frame; level 5 and level 10 of the 10-storey frame; and level 5 of the 5A and 5B-storey frames.

Table 4.1 Peak relative displacement, in mm

	El Centro				Hachinohe				Northridge				Kobe			
	Experiment		Numerical		Experiment		Numerical		Experiment		Numerical		Experiment		Numerical	
	Max	(-)Min	Max	(-)Min	Max	(-)Min	Max	(-)Min	Max	(-)Min	Max	(-)Min	Max	(-)Min	Max	(-)Min
15AS / Level 15	17.2	17.16	15.8	14.8	33	33.9	34.5	33.4	37.97	39.2	39.3	38.6	16.4	20.3	14.4	18.2
15BS / Level 15	12.9	12.0	14.2	14.2	33.8	30.3	33.9	33.1	36.8	36.3	37.7	37.5	12.3	17.3	12.7	19.0
15BS / Level 10	12.1	9.5	10.5	10.9	32.0	28.3	28.6	27.9	32.7	32.5	33.3	33.5	9.6	12.2	11.6	11.8
15BS /Level 5	6.5	5.5	6.5	6.8	16.4	19.0	16.5	16.4	20.0	21.2	22.6	22.7	8.7	8.3	9.8	9.5
10S / Level 10	5.8	6.8	5.8	6.1	3.3	4.7	3.5	3.3	26.4	23.5	27.8	28.6	21.4	18.3	24.8	22.1
10S / Level 5	4.5	5.5	4.0	4.2	2.5	3.5	2.7	2.6	21.6	20.9	21.8	22.1	17.5	15.2	17.1	15.7
5AS / Level 5	5.7	5.9	4.3	4.47	2.8	3.1	1.97	2.35	8.2	10.4	8.05	9.2	16.4	15.6	14.4	15.7
5BS / Level 5	4.5	4.9	4.8	5.0	3.1	3.1	3.2	3.0	8.2	9.0	8.1	8.9	13.1	14.4	13.7	14.5

4.3 **Discussion**

4.3.1 Effects of Ground Motion Characteristic on the System Response

The building response increases when the characteristic period of the ground motion is close to its fundamental period (Abdel Raheem 2006; Yaghmaei-Sabegh & Jalali-Milani 2012). Table 4.1 illustrates a similar concept; it is apparent that the minimum and maximum displacements in the Northridge earthquake (1994) were higher than the rest of the earthquakes in most cases. This explains Abdel Raheem's (Abdel Raheem 2006) concepts of ground motion and fundamental period, which demonstrate the impacts of earthquakes on the building's response. If the earthquake movement happens in harmony with the building motion, the displacement will be higher because of the momentum exerted into the building motion. Moreover, it is apparent from Figure 4.11(c) that the response of the 15A, 15B and 10-storey buildings increased when the dominant and fundamental period values were close during the Northridge earthquake (1994). This can be seen in the 5A and 5B-storey buildings during the Kobe earthquake (Figure 4.11(d)) and Northridge earthquake (1994). This is not the case for the other two earthquakes, as depicted in Figures 4.11(a) and 4.11(b).

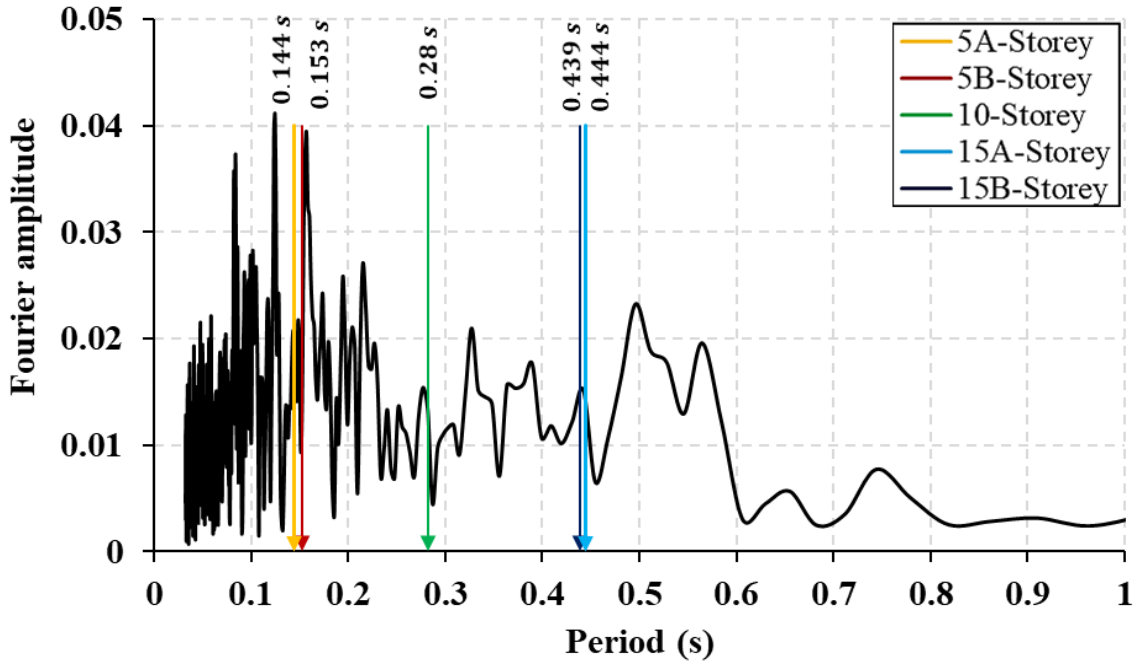

Figure 4.11(a) Fundamental period of all steel frames and Fourier spectrum of ground motion of scaled El Centro earthquake

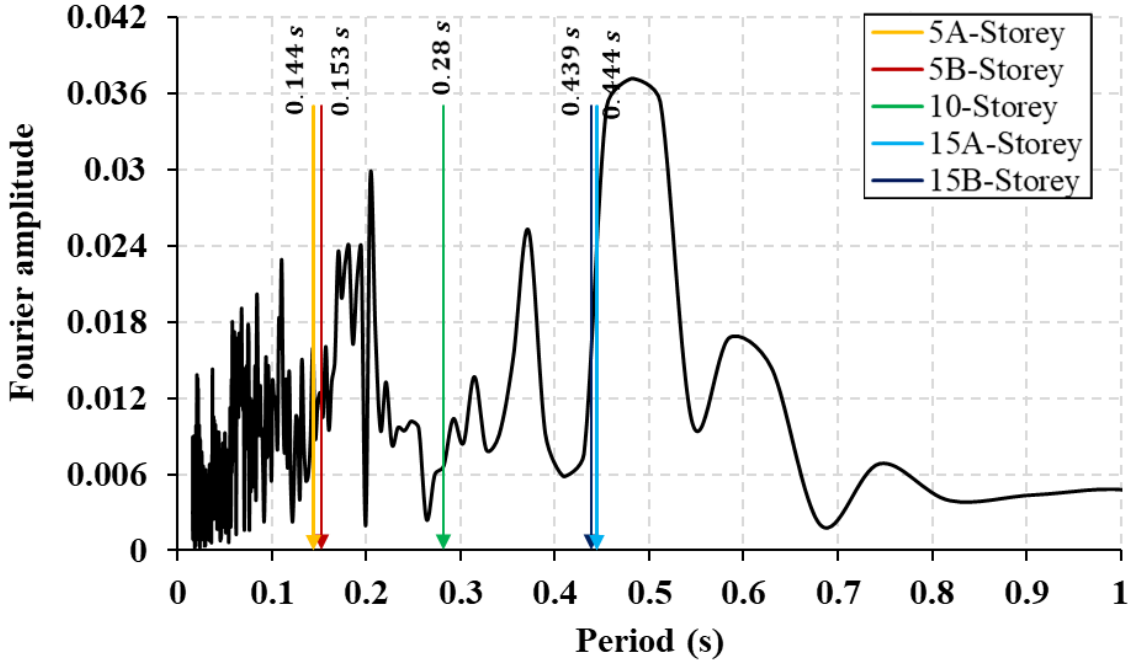

Figure 4.11(b) Fundamental period of all steel frames and Fourier spectrum of ground motion of scaled Hachinohe earthquake

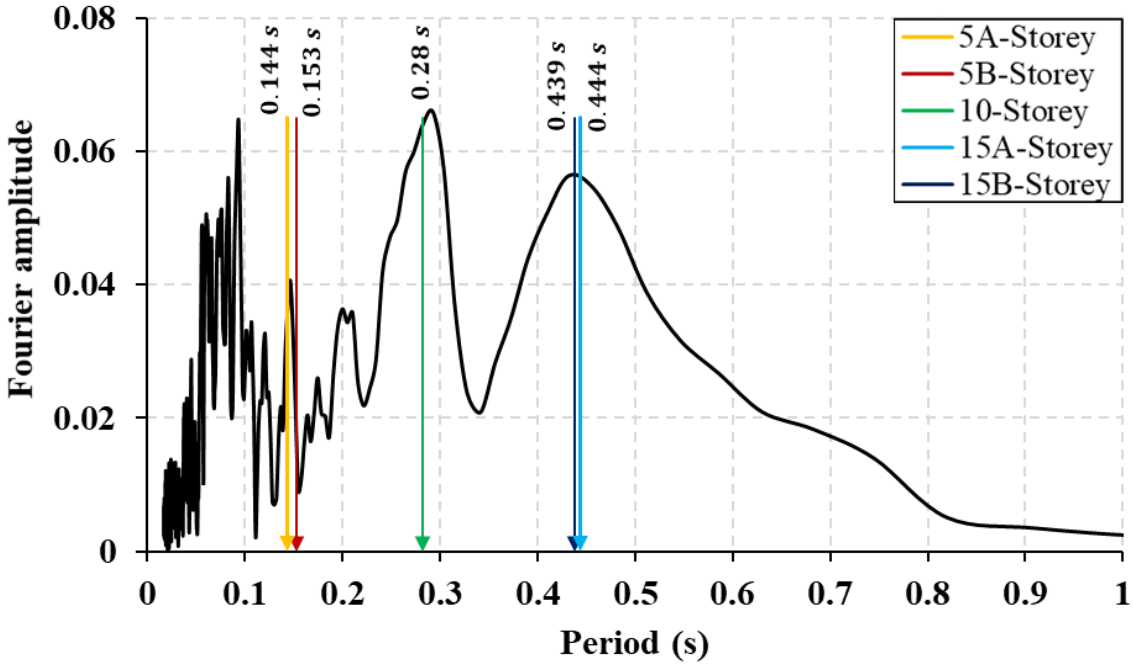

Figure 4.11(c) Fundamental period of all steel frames and Fourier spectrum of ground motion of scaled Northridge earthquake

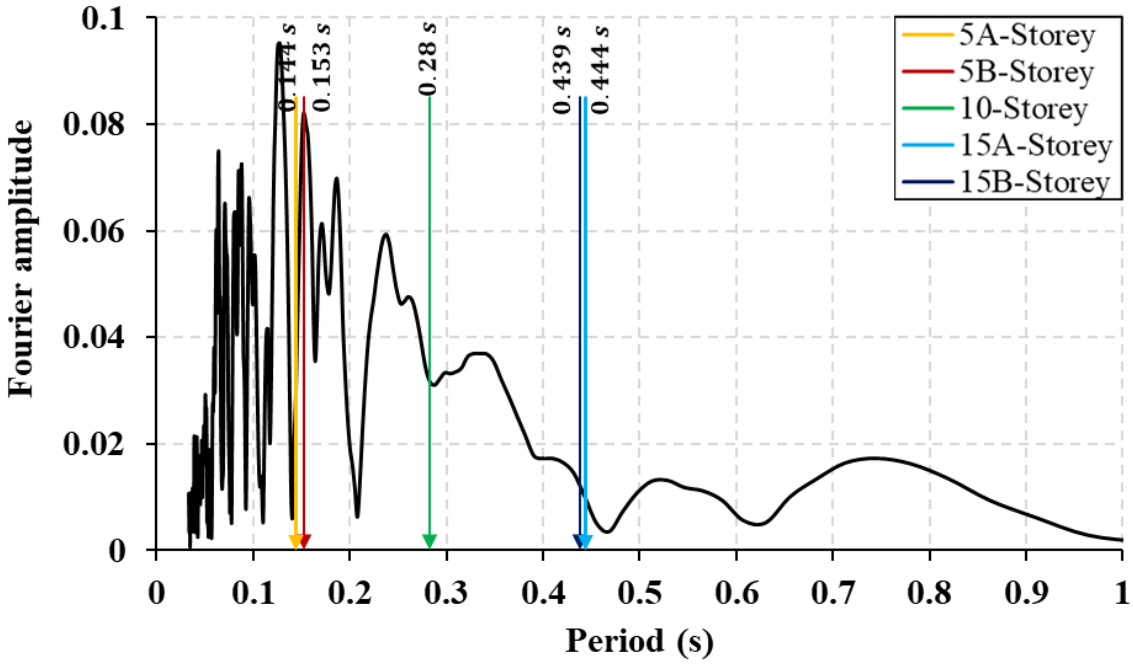

Figure 4.11(d) Fundamental period of all steel frames and Fourier spectrum of ground motion of scaled Kobe earthquake

4.3.2 Required Separation Distance to Avoid Structural Pounding

Lateral movement in adjacent buildings has been acknowledged as an important factor in earthquake-induced structural pounding issues. Lin & Weng (2002) generated a relationship in which they assumed $u_a(t)$ and $u_b(t)$ as the lateral deflection, and time histories of Building A and Building B at the collision point are depicted in Figure 4.12. On that, the least gap required S was expressed as:

$$S = max|u_a(t) - u_b(t)|_{T_d} \quad 4.1$$

where T_d is the duration of vibration. Hence, the collision occurs once the deducted displacement of the two buildings from the gap value is greater than zero and is avoided once the value is negative. In other words, the minimum gap is the maximum value of the difference between $u_a(t)$ and $u_b(t)$. The minimum separation distances to avoid pounding between the 15B-storey and 10-storey frames, the 15B-storey and 5B-storey frames, the 10-storey and 5B-storey frames, the 15A-storey and 15B-storey frames, and the 5A-storey and 5B-storey frames, under the aforementioned scaled earthquakes, are presented in Figures 4.13–4.17.

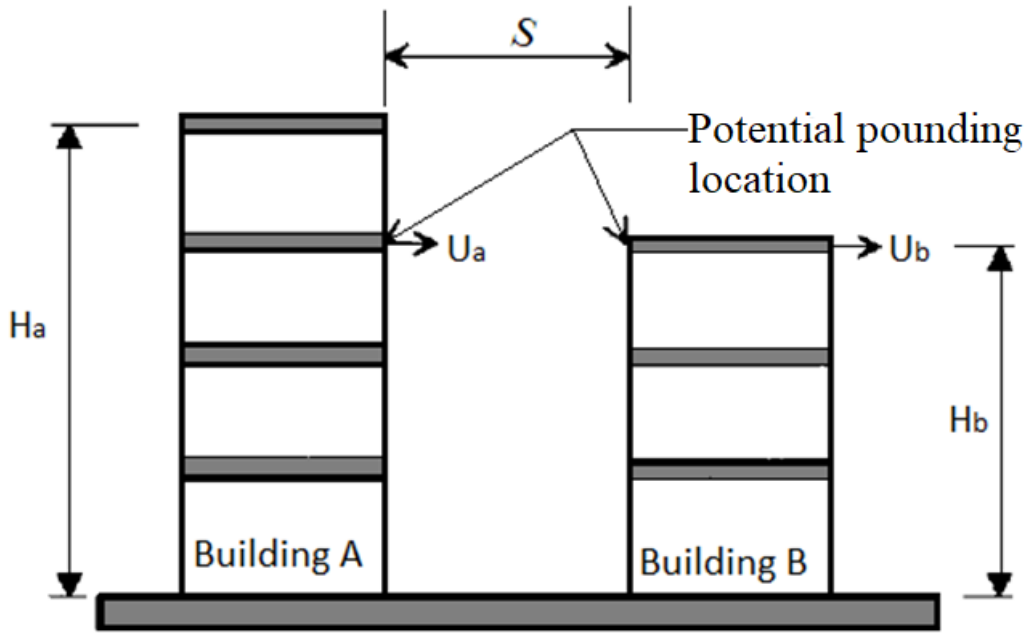

Figure 4.12 Potential pounding location between adjacent buildings of different heights

Numerical minimum separation distance to preclude pounding when a 15-storey frame is adjacent to a 10-storey frame is 16 mm for El Centro (1940), 19 mm for Hachinohe (1968), 52 mm for Northridge (1994) and 30 mm for Kobe (1995). The minimum required separation gap in a 15-storey and 5-storey coupled case was reduced by 44–49%, being 9 mm, 10.5 mm, 25 mm and 17 mm, respectively. However, in the coupled case of 10-storey and 5-storey, this number hardly changed for El Centro (1940), but decreased significantly for Hachinohe (1968) and remarkably increased in the Northridge (1994) and Kobe (1995) earthquakes, being 8.5 mm, 5 mm, 31 mm and 24.5 mm, respectively. Furthermore, numerical minimum separation gaps were different in coupled cases where buildings were of the same height. A comparison of these values with the actual experimental results is shown in Table 4.2.

In the experiment, the two buildings in each adjacent pair are kept close to one another for pounding to occur. The results showed that the pounding finally occurred when the separation distance was less than 18 mm for the coupled case of the 15B-storey and 10-storey frames while subjected to the El Centro earthquake (1940), but decreased to less than 21 mm, 53 mm and 29 mm while under the influence of the Hachinohe (1968), Northridge (1994) and Kobe (1995) earthquakes, respectively.

For the 15B-storey and 5B-storey coupled case, the pounding occurred when the distance was less than 11 mm and 13 mm for the El Centro (1940) and Hachinohe (1968) excitations, respectively, and 27 mm and 17 mm under the influence of the Northridge (1994) and Kobe (1995) excitations, respectively. For the 10-storey and 5B-storey case, though, the pounding occurred when the separation gap was less than 12 mm under the El Centro earthquake (1940), less than 6 mm for Hachinohe (1968) (a decrease of more than half from the previous case), but remained unchanged with 28 mm for Northridge (1994) and increased to 26 mm for Kobe (1995), respectively.

For the 15A-storey and 15B-storey coupled case, the pounding occurred when the distance was less than 20 mm and 46 mm for El Centro (1940) and Hachinohe (1968), while 41 mm and 13 mm under the influence of the Northridge (1994) and Kobe (1995) excitations, respectively. Lastly, for the coupled 5A-storey and 5B-storey, the pounding occurred when the separation gap was less than 10 mm under El Centro earthquake (1940), less than 5 mm for Hachinohe (1968) (a decrease of more than half from the previous case), less than 9 mm for Northridge (1994) and increased to 24 mm for Kobe (1995). All the experimental results for pounding and no-pounding cases have been recorded and listed in the references (Jaradat & Far 2021).

It is worth mentioning that after each pounding test, no local or global damage was detected in the frames. This observation indicates that the frames remained structurally intact and did not experience any detrimental effects as a result of the testing process.

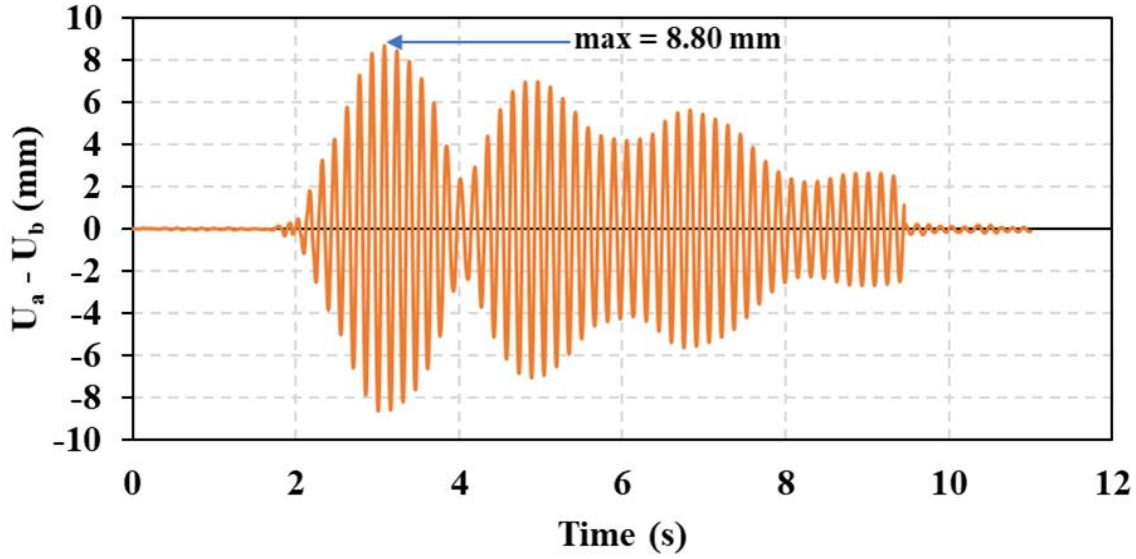

Figure 4.13(a) Numerical minimum separation distance to avoid pounding between the coupled 5A-storey and 5B-storey under scaled El Centro earthquake

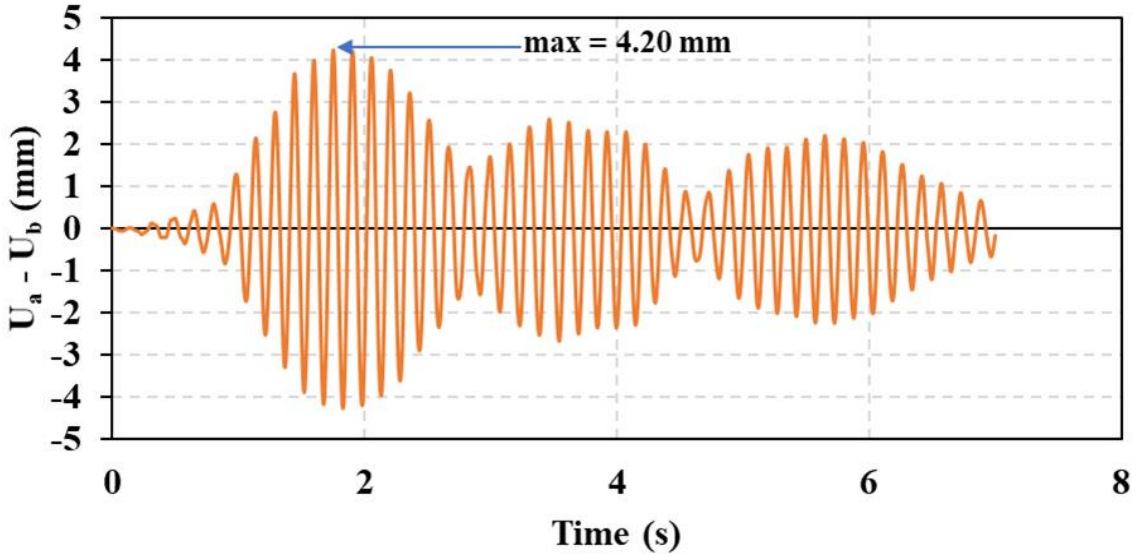

Figure 4.13(b) Numerical minimum separation distance to avoid pounding between the coupled 5A-storey and 5B-storey under scaled Hachinohe earthquake

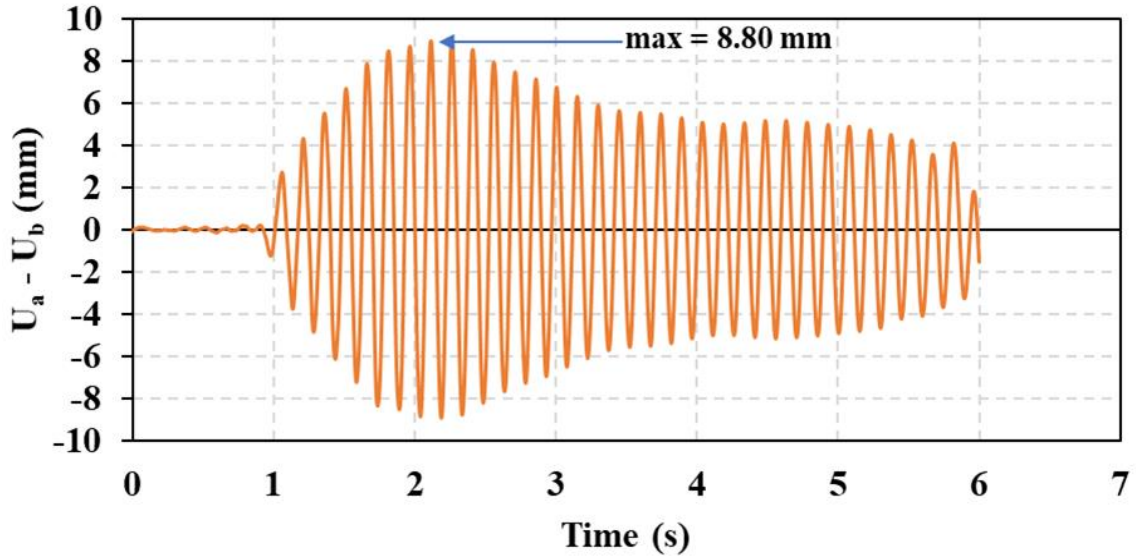

Figure 4.13(c) Numerical minimum separation distance to avoid pounding between the coupled 5A-storey and 5B-storey under scaled Northridge earthquake

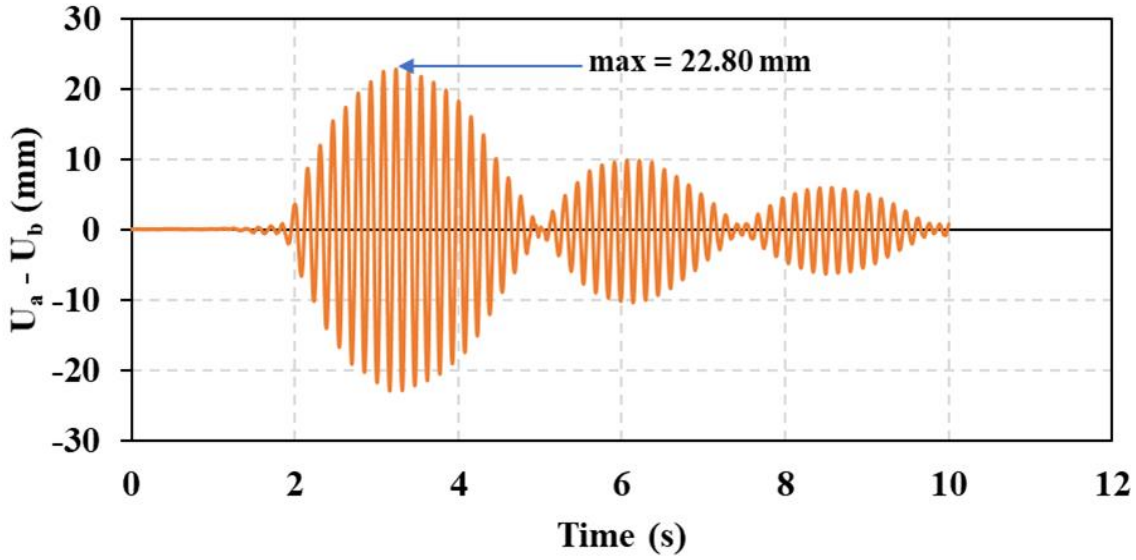

Figure 4.13(d) Numerical minimum separation distance to avoid pounding between the coupled 5A-storey and 5B-storey under scaled Kobe earthquake

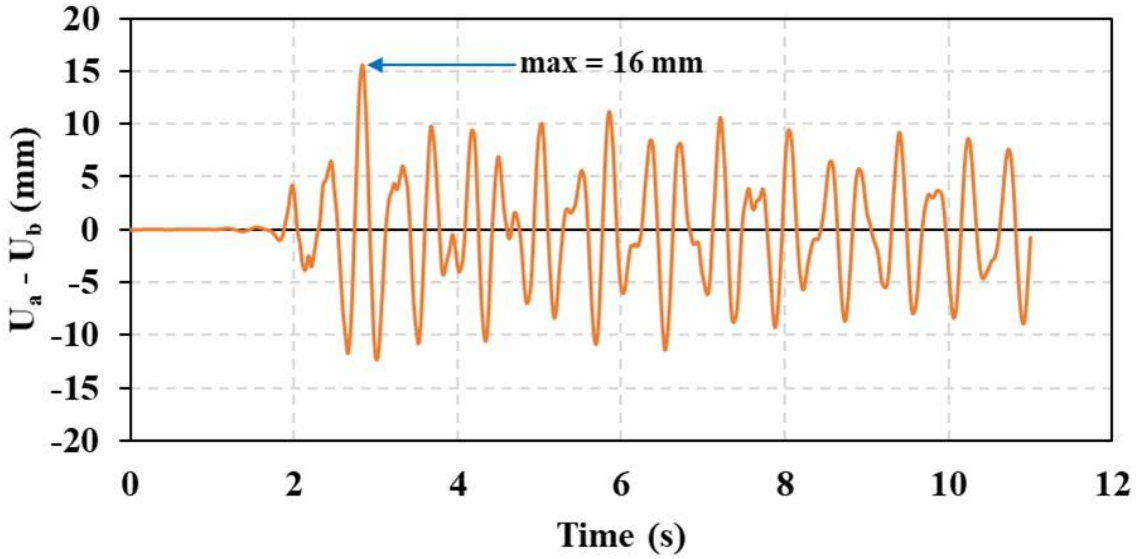

Figure 4.14(a) Numerical minimum separation distance to avoid pounding between the coupled 15B-storey and 10-storey under scaled El Centro earthquake

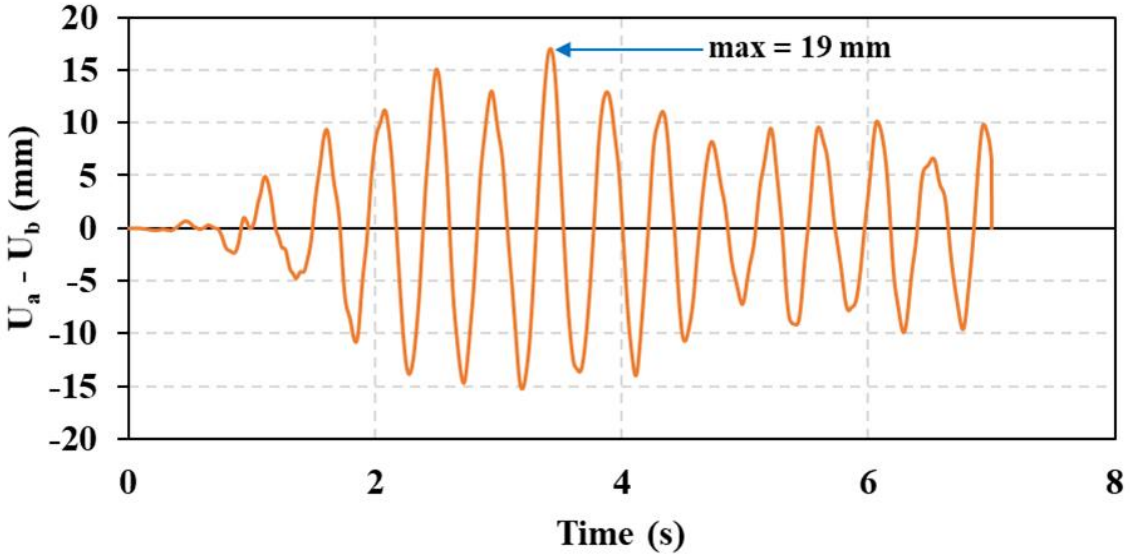

Figure 4.14(b) Numerical minimum separation distance to avoid pounding between the coupled 15B-storey and 10-storey under scaled Hachinohe earthquake

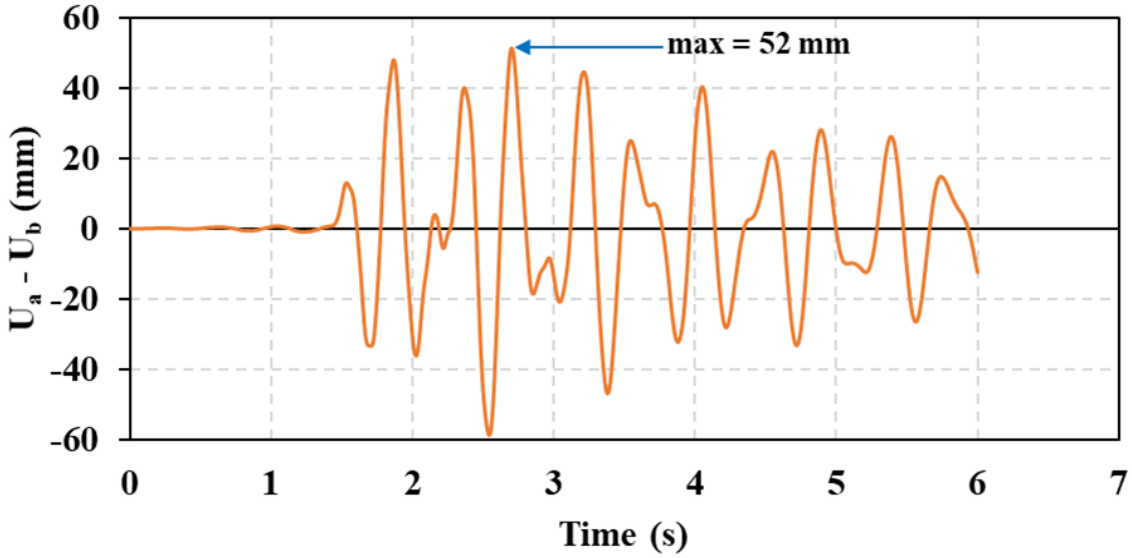

Figure 4.14(c) Numerical minimum separation distance to avoid pounding between the coupled 15B-storey and 10-storey under scaled Northridge earthquake

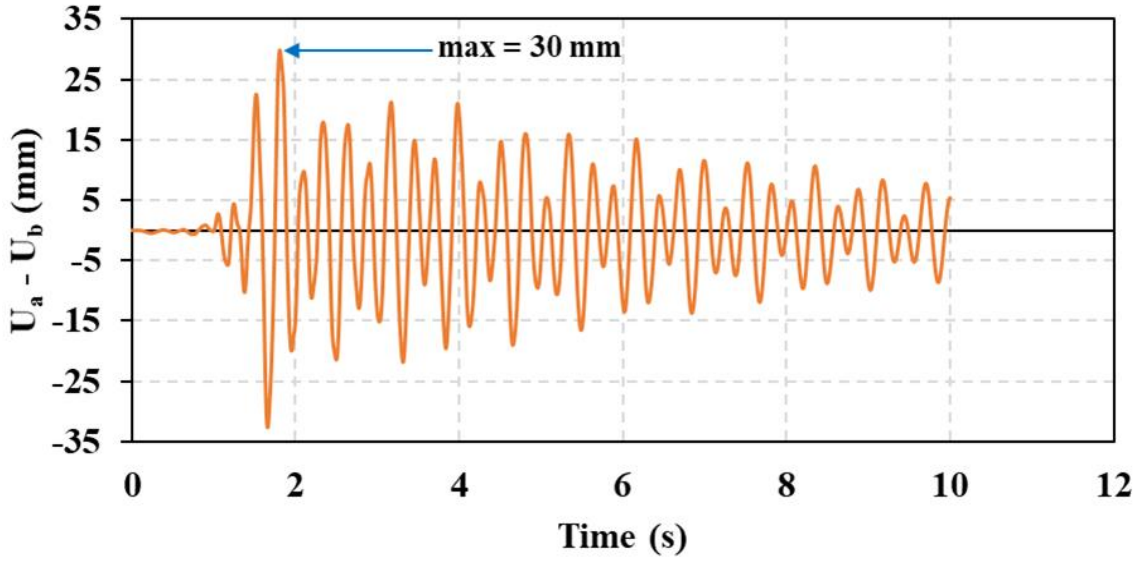

Figure 4.14(d) Numerical minimum separation distance to avoid pounding between the coupled 15B-storey and 10-storey under scaled Kobe earthquake

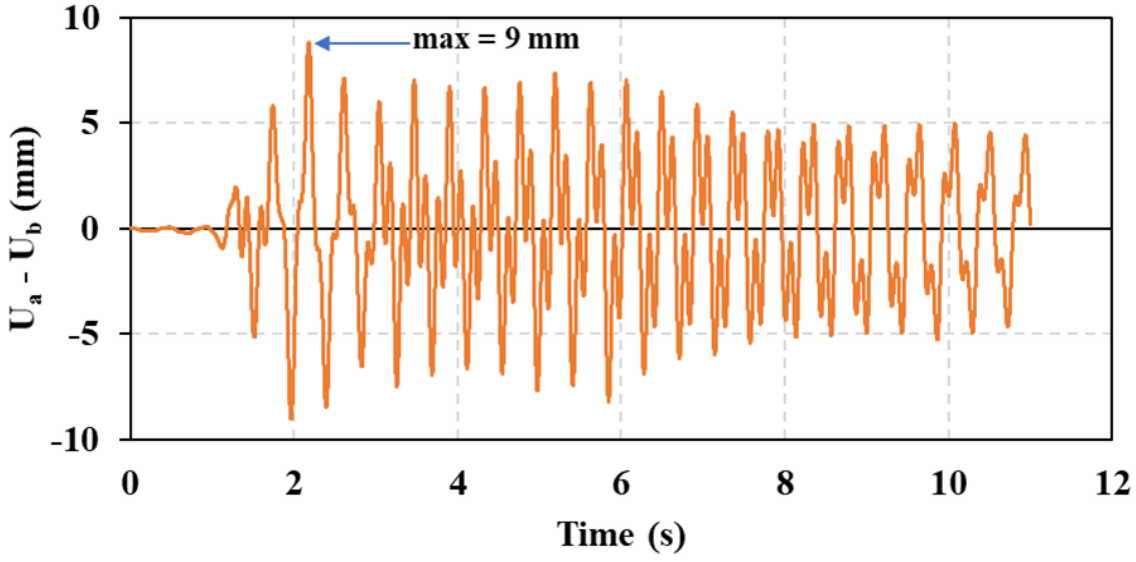

Figure 4.15(a) Numerical minimum separation distance to avoid pounding between the coupled 15B-storey and 5B-storey under scaled El Centro earthquake

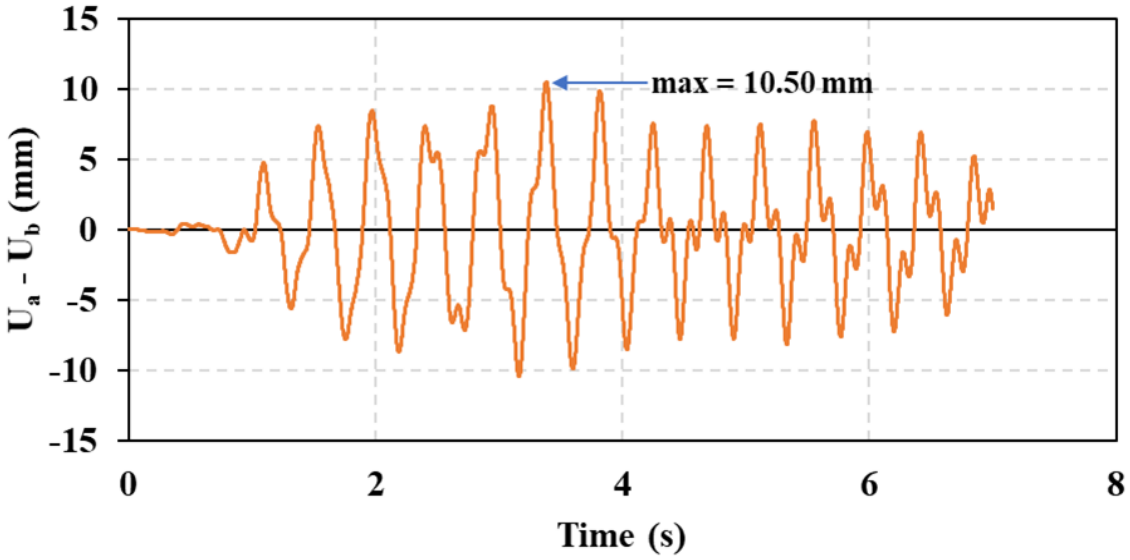

Figure 4.15(b) Numerical minimum separation distance to avoid pounding between the coupled 15B-storey and 5B-storey under scaled Hachinohe earthquake

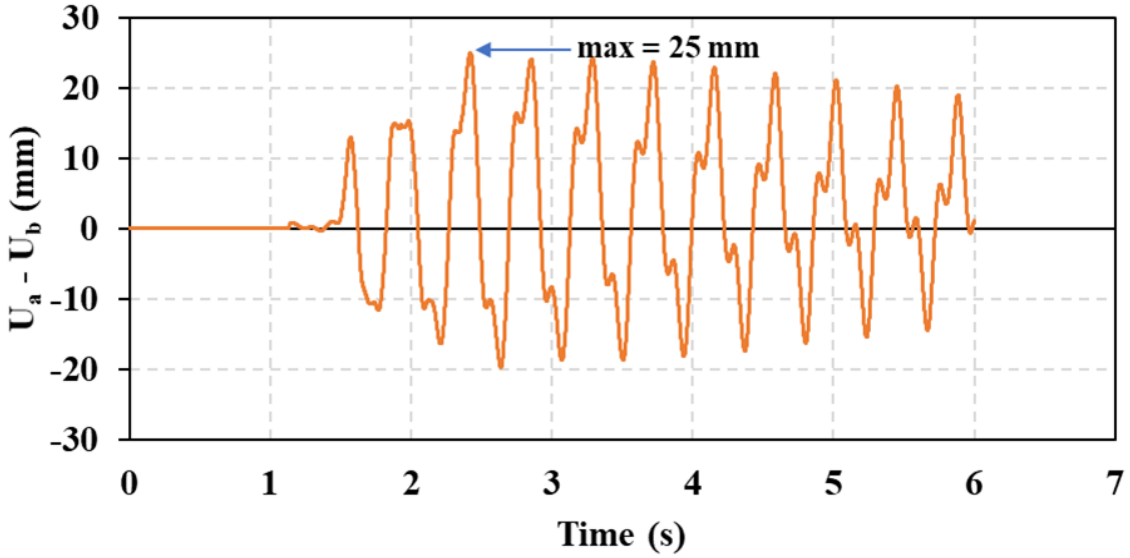

Figure 4.15(c) Numerical minimum separation distance to avoid pounding between the coupled 15B-storey and 5B-storey under scaled Northridge earthquake

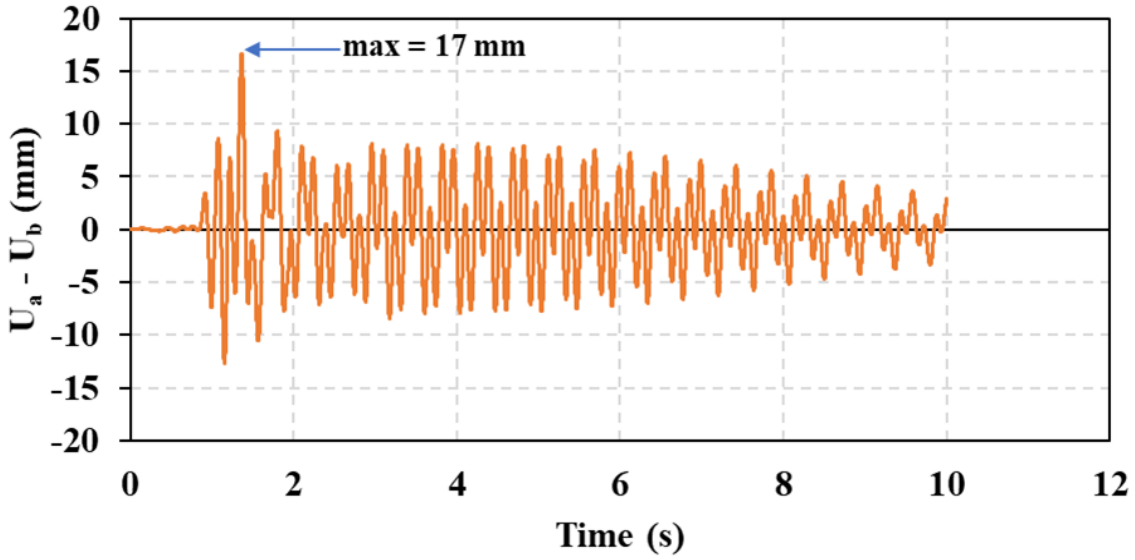

Figure 4.15(d) Numerical minimum separation distance to avoid pounding between the coupled 15B-storey and 5B-storey under scaled Kobe earthquake

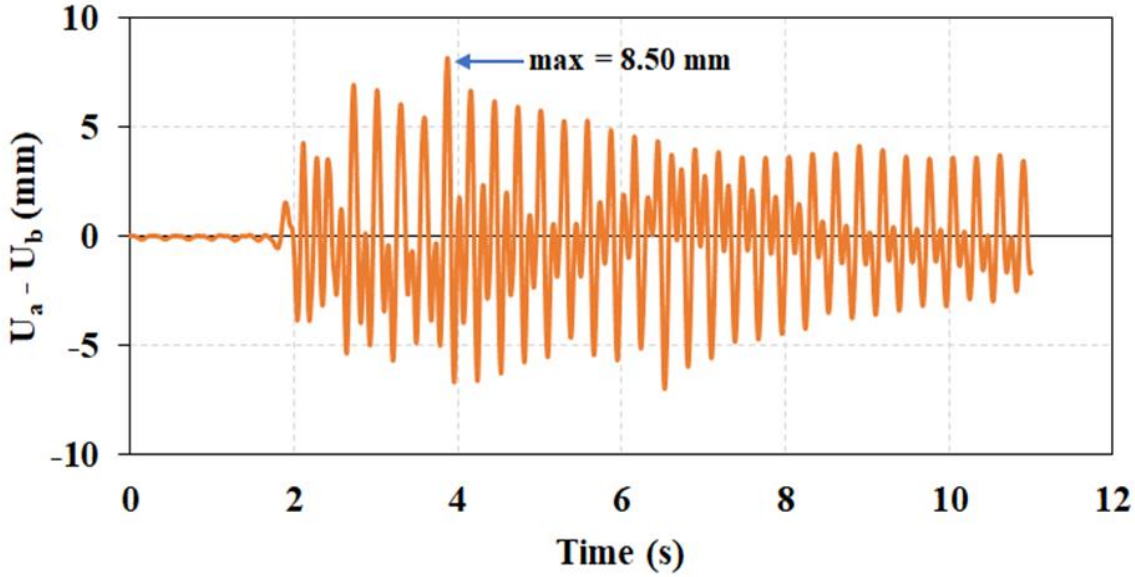

Figure 4.16(a) Numerical minimum separation distance to avoid pounding between the coupled 10-storey and 5B-storey under scaled El Centro earthquake

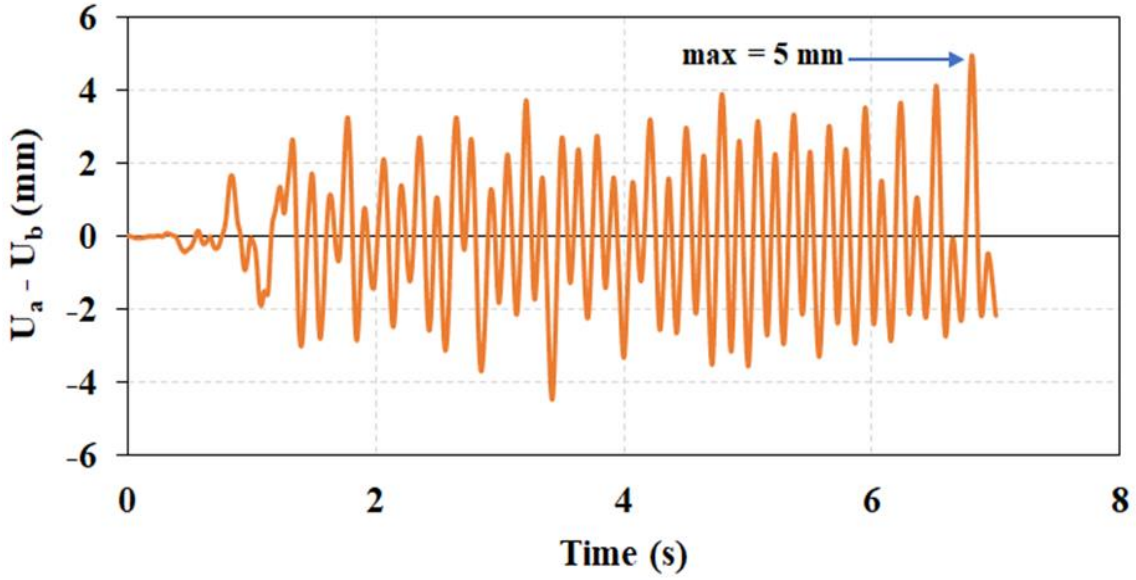

Figure 4.16(b) Numerical minimum separation distance to avoid pounding between the coupled 10-storey and 5B-storey under scaled Hachinohe earthquake

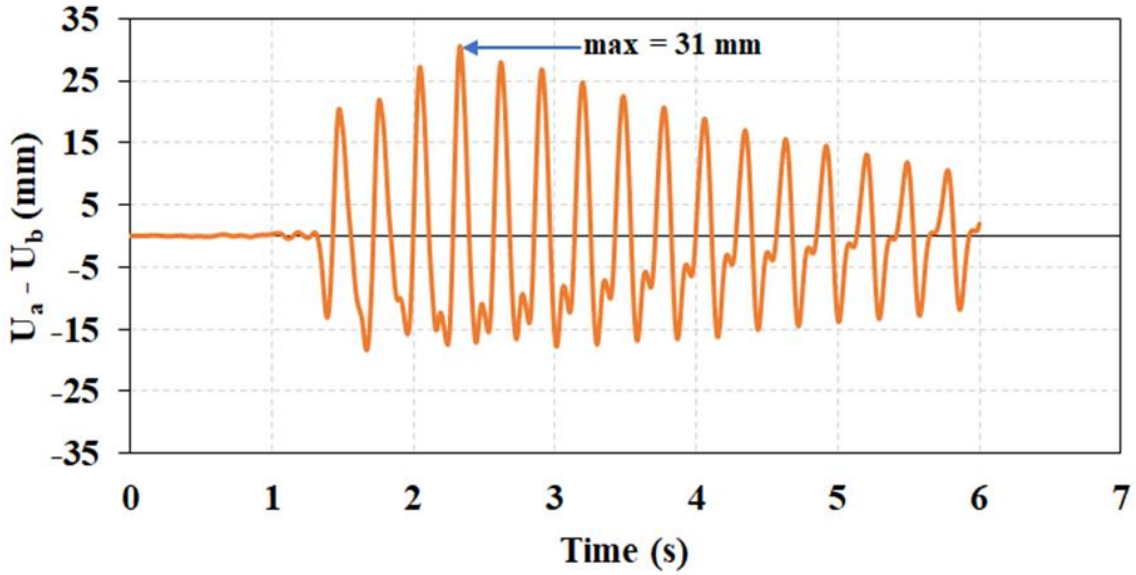

Figure 4.16(c) Numerical minimum separation distance to avoid pounding between the coupled 10-storey and 5B-storey under scaled Northridge earthquake

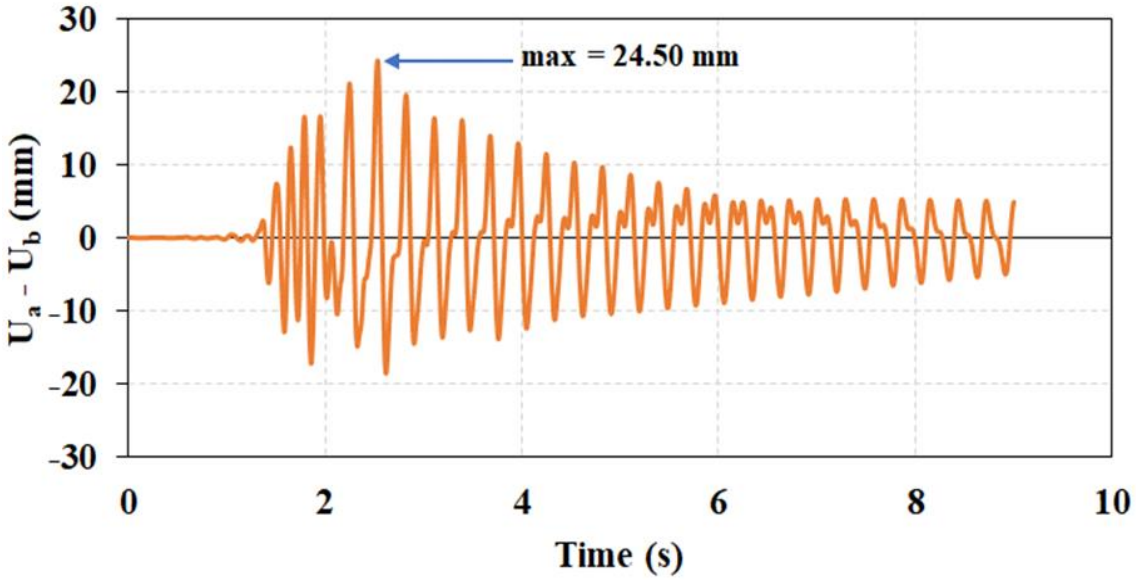

Figure 4.16(d) Numerical minimum separation distance to avoid pounding between the coupled 10-storey and 5B-storey under scaled Kobe earthquake

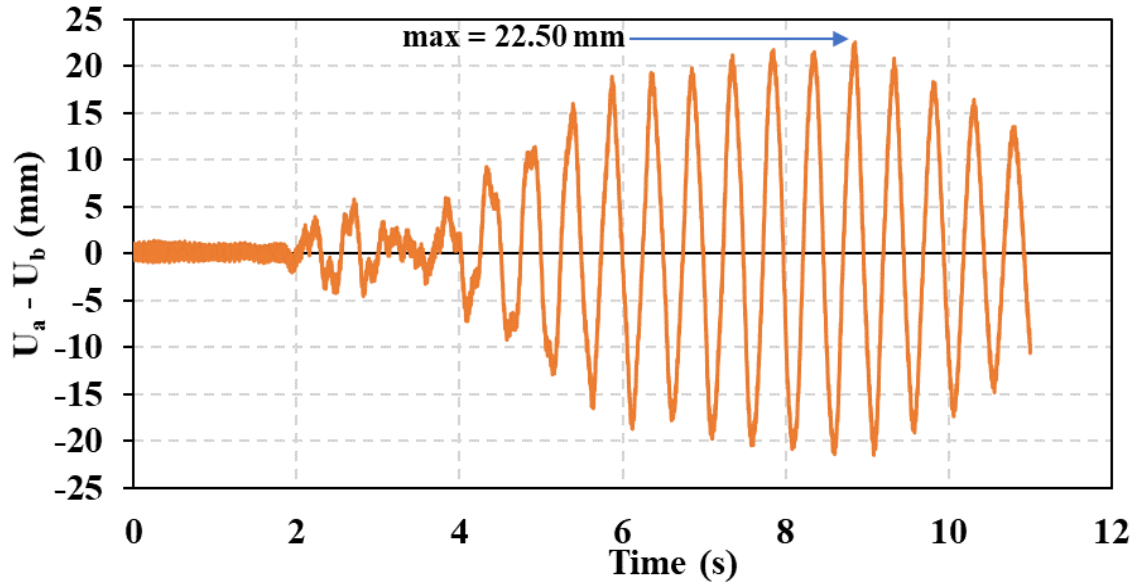

Figure 4.17(a) Numerical minimum separation distance to avoid pounding between the coupled 15A and 15B-storey under scaled El Centro earthquake

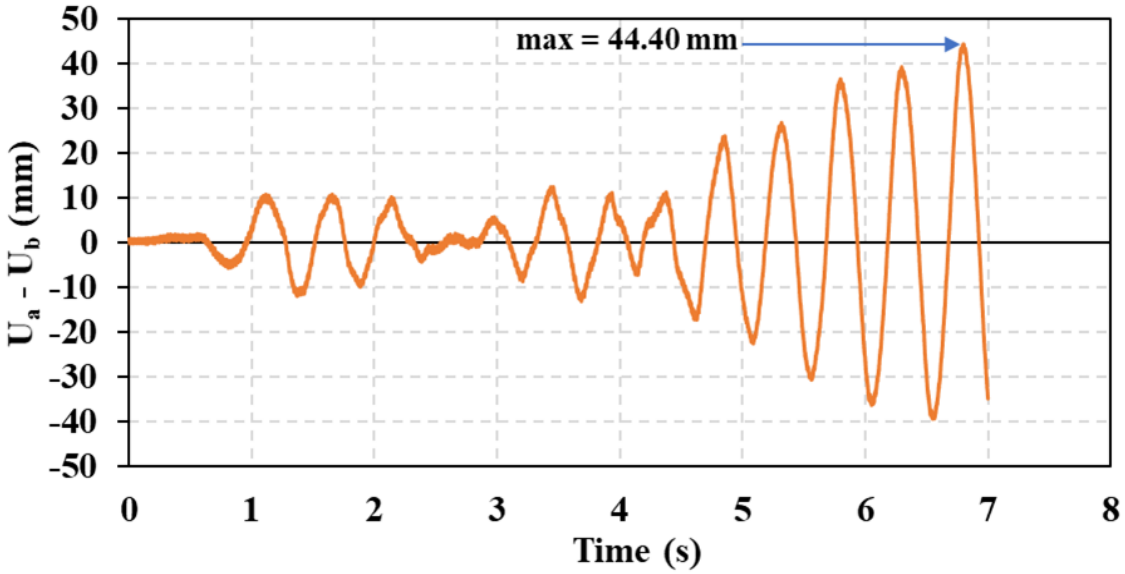

Figure 4.17(b) Numerical minimum separation distance to avoid pounding between the coupled 15A-storey and 15B-storey under scaled Hachinohe earthquake

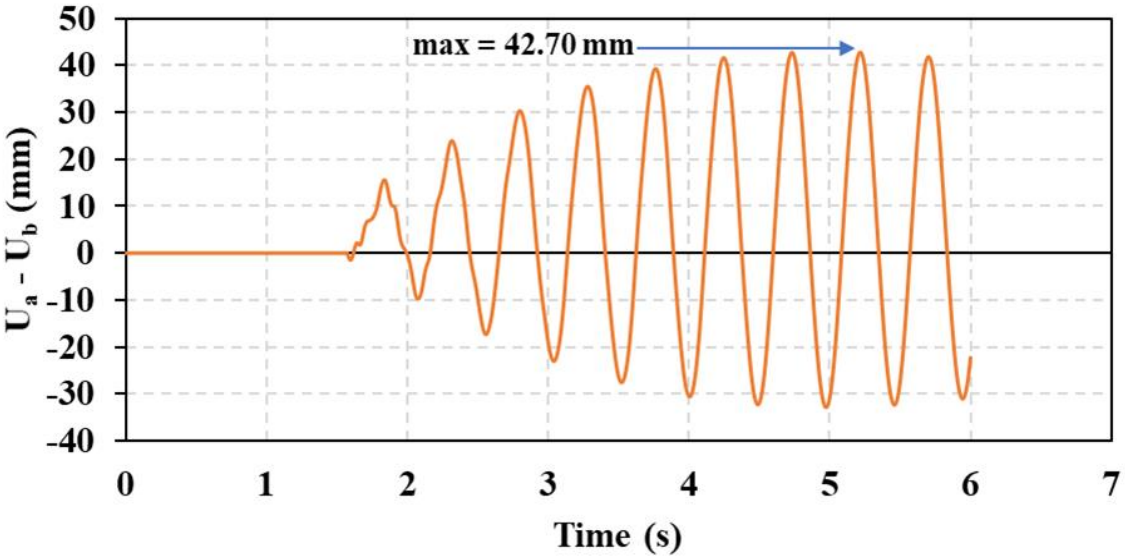

Figure 4.17(c) Numerical minimum separation distance to avoid pounding between the coupled 15A-storey and 15B-storey under scaled Northridge earthquake

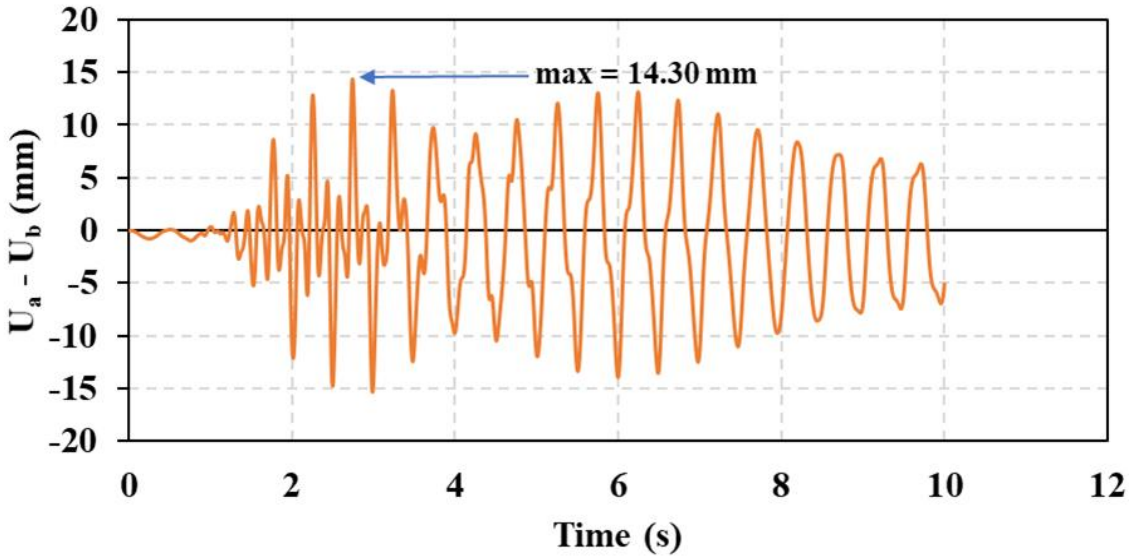

Figure 4.17(d) Numerical minimum separation distance to avoid pounding between the coupled 15A-storey and 15B-storey under scaled Kobe earthquake

4.3.3 Comparison with Code Specifications

Australian Standard AS 1170.4-2007 requires that any adjacent buildings affiliated with Category II design, with height greater than 15 m, and adjacent buildings associated with Category III design, must be separated by 0.01H to prevent collision impact.

Considering two adjacent buildings, the required separation gap in this standard is calculated as a setback distance from the second building. In adjacent buildings of equal heights case, the code still recommends 0.01H. However, uncertainty arises about which structure's height is to be used when these heights vary. Therefore, in practice and reality, the required separation distance can be determined by considering either height (Hao 2015). As a provision, this study considers the requirement of Australian Standard AS1170.4 to calculate the required gap utilising both numerical and experimental methods. The results are then compared to verify the adequacy of the standard requirement, depicted in Table 4.2.

As illustrated in Table 4.2, separation distance calculated using 1% of the taller adjacent structure always underestimates the required separation gap to prevent pounding under near-field earthquakes. It also underestimates the required separation gap to prevent pounding under far-field earthquakes, except in two cases. In the first case, the code required a separation distance of 15 mm (1% of the 15-storey frame height), which is deemed adequate to preclude pounding between 15-storey and 5-storey frames under

scaled El Centro and Hachinohe earthquakes. In the second case, the code required a separation distance of 10 mm (1% of the 10-storey frame height) as adequate to preclude pounding between 10-storey and 5-storey frames under a scaled Hachinohe earthquake.

However, the underestimation of gap values is true for both near-field and far-field if the shorter building is considered. These results indicate that the code specifications are inadequate if the shorter adjacent building is used to estimate the seismic gap under both near-field and far-field earthquakes. Moreover, the specifications are also inadequate if the height of the taller building is utilised during near-field earthquakes. The standard specifications become adequate, in some cases, if the same building is contemplated during far-field earthquakes only.

Table 4.2 Experimental, numerical and Australian Standard seismic gap for all four scaled earthquakes, in mm

	El Centro				Hachinohe				Northridge				Kobe			
	Experiment	Numerical	AS 1170.4 0.01 x H_a	AS 1170.4 0.01 x H_b	Experiment	Numerical	AS 1170.4 0.01 x H_a	AS 1170.4 0.01 x H_b	Experiment	Numerical	AS 1170.4 0.01 x H_a	AS 1170.4 0.01 x H_b	Experiment	Numerical	AS 1170.4 0.01 x H_a	AS 1170.4 0.01 x H_b
15BS adjacent to 10S	18	16	15	10	21	19	15	10	53	52	15	10	29	30	15	10
15BS adjacent to 5BS	11	9	15	5	13	10.5	15	5	27	25	15	5	17	17	15	5
10S adjacent to 5BS	12	8.5	10	5	6	5	10	5	28	31	10	5	26	24.5	10	5
15AS adjacent to 15BS	20	22.5	15	15	46	44.4	15	15	41	42.7	15	15	13	14.3	15	15
5AS adjacent to 5BS	10	8.8	5	5	5	4.2	5	5	9	8.8	5	5	24	22.8	5	5

4.3.4 Code Comparisons

As mentioned in Section 2.4, several building codes point out minimum separation gap between two adjacent buildings in order to avoid collision during an earthquake. The absolute sum (ABS) method, the square-root-of-sum-of-squares (SRSS) method and Australian Standard AS 1170.4-2007 have provided formulae to measure required separation distance, based on the maximum lateral displacement in Equations 2.25–2.26, and the height in Equation 2.30, respectively. Table 4.3 compares the calculated separation distances using ABS along with SRSS methods by considering experimental relative displacements subjected to the given excitations. The ABS method appears to be the safest, although it slightly exaggerates the final outcomes. Results given by the SRSS

method are reasonably accurate because it is not as conservative as the ABS method. These outcomes are consistent with those described by Jeng et al. (1992a), Kasai et al. (1996) and Lopez-Garcia & Soong (2009). It is worth mentioning that results obtained by the SRSS method are relatively similar to the experimental outputs. This is only true for the coupled case of 15-storey and 5-storey, when the natural frequency of both buildings are different (also described by Shrestha (2013)).

Moreover, it appears that the Australian Standard has based the gap requirement on earthquakes with far-field conditions because of the absence of active tectonic plates. Hence, the requirement should revolve around both structure and an earthquake's characteristics.

Table 4.3 Gap distance results for all four scaled earthquakes, in mm, using experimental relative displacement

	El Centro			Hachinohe			Northridge			Kobe		
	Experiment	ABS	SRSS	Experiment	ABS	SRSS	Experiment	ABS	SRSS	Experiment	ABS	SRSS
15BS adjacent to 10S	18	19	13.9	21	19.8	15.9	53	59.1	42	29	33.6	24.6
15BS adjacent to 5BS	11	11.4	8.1	13	11.9	9.3	28	30.2	23.1	17	23.1	16.8
10S adjacent to 5BS	12	10.4	7.3	6	6.6	4.7	28	30.6	23.4	26	31.9	22.7
15AS adjacent to 15BS	20	30.1	21.5	46	51.11	38	41	76	53.7	13	37.6	26.7
5AS adjacent to 5BS	10	10.8	7.7	5	6.9	4.7	9	19.4	13.7	24	30.8	21.8

As mentioned, increasing the separation gap is an expensive solution. To compromise between cost and safety, other solutions can be used as alternatives. These are highlighted as follows.

The first technique is to utilise the collision shear walls and bracing systems (Anagnostopoulos & Karamaneas 2008; Barros & Khatami 2012).

The second technique is the adoption of soft material layers made of rubber for installation at the specific locations between adjacent buildings (Raheem 2013; Sołtysik et al. 2017).

The third technique is to connect adjacent structures together with links (such as spring links, dashpot links or viscoelastic links) to produce in-phase vibrations (Jankowski & Mahmoud 2016; Richardson et al. 2013).

There are inherent advantages and disadvantages among the three techniques. Anagnostopoulos & Karamaneas (2008) and Lopez-Garcia & Soong (2009) stated that using shear walls reduces the peak displacements and number of impacts but will increase the peak impact force. Abdel Raheem (2014) and Sołtysik et al. (2017) suggested that filling the gap with rubber pad may decrease the peak impact force but will increase the number of poundings. Furthermore, Jankowski & Mahmoud (2016) and Richardson et al. (2013) stated that connecting the two adjacent structures is beneficial to the more flexible structure while increasing the responses of the stiffer structure.

4.4 **Summary**

This chapter focusses on comparing the results of the separation gap using numerical and experimental approaches to the 0.01H requirement by AS1170.4. The objective was to assess the degree of accuracy of the suggested expressions based on the specifications adhered to by the Standard.

There is uncertainty present in the Australian Earthquake Standard (AS1170.4 2007) regarding which height should be used when considering the impact of earthquakes. Specifically, it is unclear whether the height of the tall building or the height of the short building should be considered for the analysis. This ambiguity can lead to differing interpretations and potential inconsistencies in seismic design practices.

According to the results, it is observed that the standard-based separation gap prescribed in AS 1170.4-2007 is inadequate when the shorter building height in a coupled case is considered under the given earthquake excitation. This requirement also becomes inadequate when the taller building height is utilised under a near-field earthquake.

Moreover, the adequacy of the standard-based separation gap prescribed in AS 1170.4-2007 returns only if the height of the taller structure is contemplated under a far-field earthquake.

Furthermore, it can be observed that the characteristics of near-field and far-field earthquakes have significant impact on the gap requirements to prevent collision.

CHAPTER 5
OPTIMUM IMPACT STIFFNESS OF THE LINEAR VISCOELASTIC MODEL FOR SEISMIC POUNDING SIMULATION

5.1 Introduction

Pounding between adjacent structures during earthquakes poses a serious risk to neighbouring edifices. This phenomenon is attributed to the fact that adjacent buildings or bridge elements with varying dynamic characteristics tremble out of phase due to restricted or insufficient separation distance to support the relative displacement. Adjoining structures with insufficient spacing are often considered to be loose structures, without taking into account the pounding effect during earthquake loading. This neglect can lead to failure of structures. Seismic pounding causes soaring magnitude and brief interval acceleration pulses that can induce slight non-structural series of structural damage such as the partial or total collapse of buildings and bridges (Naderpour et al. 2016; Schramm & Pilkey 1996; Zheng et al. 2015). Hence, an assessment of the seismic pounding risk is imperative in order to come up with future calibration of seismic designs for adjacent structures.

Structural seismic pounding is an extreme nonlinear occurrence. It encompasses plastic deformation, local cracking or crushing, and fracturing along with friction destruction at the contact area. Given the complexity of this phenomenon, performing precise mathematical analysis can be challenging. Hence, based on assumptions, several contact models were developed to analyse and study structural pounding during a seismic activity like earthquakes. These impact models were discussed in detail in Section 2.2.

The linear viscoelastic model (see Section 2.2.3) is commonly adopted in the simulation of structural pounding because of its simplicity, which allows it to be easily be applied in most commercial computer codes or software programs as revealed by most researchers (Anagnostopoulos 1995; Khatiwada et al. 2013; Mate et al. 2012; Pant et al. 2010). A primary shortcoming of the model is related to the negative impact force observed just prior to the separation of two colliding structures, which does not have any physical clarification. This behaviour is attributed to the fact that the linear damping term of the model is triggered throughout the entire duration of the contact, assuming a uniform dissipation of energy (Goldsmith 2001b). To correct the weakness of the linear viscoelastic model, Komodromos et al. (2007) recommended a variation of the model.

The proposed model also has a significant constraint: the correct value of the impact stiffness k to be applied in the simulation cannot be determined beforehand. An impact spring with under-stiffness can result in the overlaying of adjacent structures. Conversely, using a spring of very high stiffness can lead to unrealistic high impact forces and numerical convergence problems.

As discussed in Chapter 2, several studies have shown that impact stiffness k has a great bearing on the pounding response, particularly on the structural acceleration response and the inertia force response, though the researchers proposed various methods and equations to compute the stiffness of the impact element model (Anagnostopoulos 1988; Cole et al. 2012a; Jankowski 2008a; Jaradat & Far 2020; Maison & Kasai 1992; Wada et al. 1984). To use impact stiffness in analysing structural pounding is a challenging decision since it needs to consider the unknown geometry of the impact surfaces, the uncertainty of the material properties under impact load, the variable impact velocities and other factors. There has been scant research conducted in choosing impact stiffness. Usually, the impact stiffness in the linear viscoelastic model is taken proportionally to the axial stiffness of the colliding elements. This method is usually adopted in evaluating the structural seismic pounding (Muthukumar & Desroches 2006).

The impact stiffness employed in analysing bridge pounding is taken as the axial stiffness of girder (Jankowski et al. 1998). The impact stiffness used in the building pounding analysis is taken as the axial stiffness of building slab (Maison & Kasai 1990). Cole et al. (2011b) proposed a new formula to calculate impact stiffness based on the properties of the impact members and the duration of the collision. Xu et al. (2016) developed an alternative formula for the impact rigidity of linear models and compared it to the axial rigidity formula and the Cole formula. The findings indicated that the new equation yielded more precise results than the other two formulae.

The structural response assigned to the pounding did not account for the high values of the impact stiffness coefficient. For example, Ghandil & Aldaikh (2017) established that the pounding reaction is indifferent to the coefficient of impact stiffness when its value exceeds 10^{10} N/m.

The purpose of this chapter is to develop a formula for impact stiffness in the linear viscoelastic model based on the experimental measurements of the tested coupled 15B-storey and 5B-storey frame models.

5.2 Shaking Table Test

5.2.1 Test Frames Set-up

As shown in Figure 3.15, the structural models were prepared and secured on the shaking table with the configuration of a 15B-storey structure adjacent to the 5B-storey edifice. Next, the accelerometers and laser displacement (LD) sensors were installed. In addition, a force sensor was mounted at contact level of impact. The impact pounding force, acceleration and displacement response data were obtained using the sensors. The results of the shaking table tests were applied to the scaled earthquake acceleration records (Figures 3.10(b), 3.11(b), 3.12(b) and 3.13(b)). The reference frames are based outside the shaking table. Hence, the recorded displacements are the absolute displacement time history.

5.2.2 Test Program

The coupled steel frames were tested with separation gaps of 10.5 mm, 9.7 mm, 9.5 mm, 9.3 mm and 8.5 mm with the scaled El Centro earthquake. The separation gaps were 12.5 mm, 12 mm, 11.5 mm, 11 mm and 10 mm with the scaled Hachinohe earthquake. When applying the scaled Northridge earthquake, the separation gaps were 21.8 mm, 21.4 mm, 21 mm, 19.5 mm and 18 mm. The adjacent steel frames were tested with separation gaps of 16.8 mm, 16.4 mm, 15.6 mm, 15 mm and 14 mm under the scaled Kobe earthquake. The separation distances were based on the finding listed in Chapter 4 (Jaradat & Far 2021). To detect pounding without causing any instability in the structure and to keep the elastic system response, the gaps were carefully chosen. It should be noted that no significant torsional motion was observed in any of the tests conducted.

5.3 Experimental Results

A total of more than 70 pounding experiments were carried out on the adjacent structural steel models, under various input excitations and separation gaps. To capture the pounding force, displacement and acceleration accurately, the researchers utilised a data sampling rate of 10,000 per second. The results of the shaking table tests excited under the effect of four scaled ground motion records in terms of impact force time histories (force sensor) are presented in Figures 5.5–5.8.

5.3.1 Experimental Impact Stiffness

To find out the impact model parameters, containing the impact stiffness k and impact damping C, the experimental impact force-displacement relationship was plotted; this is shown in Figures 5.1–5.4. Figures 5.1-5.4 depict the experimental measurements of the impact force-displacement relationship for varying frame heights. These measurements

were obtained by subjecting the frames to different gap conditions and acceleration time histories. The figures provide a visual representation of the relationship between the applied impact force and the resulting displacement for each specific combination of frame height, gap size, and acceleration history. The area under each loop in these figures represents the energy expended during collision. The slope of the diagram in any of the loops is a representation of the contact element stiffness.

Based on the experimental data, it was noted that an average value of ($k - experiment = 20660\ N/mm$) is a reliable presentation of the stiffness of the contact element. Conversely, the dashpot coefficient C in the contact element was derived using the coefficient of restitution, as shown in Equations 2.6–2.8. To obtain the coefficient of restitution e, the acceleration data records at the fifth floors of both the 15B-storey frame and the adjacent 5B-storey frame (where pounding occurred) were numerically integrated using the trapezoidal method to obtain the velocity time history. After the integration, the drift error and phase distortion were eliminated by using a method of Pitilakis et al. (2008), which involves multiple applications of a high-pass Butterworth filter. A MATLAB code was developed to carry out the aforementioned integration.

Algebraic values of velocities before and after the impact were determined by locating the velocity at the time step where the pounding occurred. The coefficient of restitution e was calculated from the velocities before and after each collision event using Equation 2.8. For each value of e, the impact damping ratio ξ was computed using Equation 2.7. The mean value of the calculated coefficient was predicted for the whole time history record. Thus, the linear viscoelastic model used the following experimental parameters:

$k - experiment = 20660\ N/mm$

$C - experiment = 1255\ kg/s$

$\xi = 0.078407$

$e = 0.810154$

It is worth mentioned that in order to simulate actual impacts between structures, the employed coefficient of restitution e ranges between 0.5 and 0.75 (Anagnostopoulos & Spiliopoulos 1992). Maison & Kasai (1992) recommended interval of $0.53 < e <$0.85 for typical buildings. Based on the experimental results, Guo et al. (2012) found that the

coefficient of restitution is between 0.86 and 0.96 for steel bridge structures. Thus, the computed e value is deemed an acceptable figure for steel-to-steel pounding.

5.3.2 Theoretical Formulae for Impact Stiffness

As mentioned earlier in Section 2.3, several researchers have carried out studies suggesting several assumptions for assigning stiffness to the spring element k. These values were calculated based on the current experiment as follows:

1. The contact surface was between the steel plate with 5 mm thickness and the force sensor impact cap. The impact surface area and length of steel plate are $A = 63.5mm^2$ and $L = 400mm$, respectively. The modulus of elasticity is $E = 2 \times 10^5 Mpa$ (AS/NZS3678 2011). Therefore, based on Equation 2.21, the impact stiffness parameter $k - Maison\ \&\ Kasai = \frac{200000000 \times 63.5}{400} = 31{,}750N/mm$.

2. Based on Equation 2.23 by Naserkhaki et al. (2013), $k - Naserkhaki\ et\ al = 0.0275 \times 100 = 2750N/mm$.

3. A 1/30 scale was used in this study; therefore, according to Jankowski (2008a), $k - Jankowski = 482 \times \frac{1}{30} \cong 16{,}000N/mm$.

4. Developed by Xu et al. (2016), according to Equation 2.24, $k - Xu\ et\ al. = 12{,}858\ N/mm$.

Based on the above impact stiffness k, the dashpot coefficient C in the contact element was determined using Equation 2.6. Having determined the impact stiffness parameters for the linear viscoelastic impact model (see Table 5.1), impact force time history was computed using Equation 2.5.

Table 5.1 Linear viscoelastic impact model parameters

Method	Impact Stiffness k N/mm	Impact Damping Coefficient C kg/s
Experiment	20660	1255
Maison & Kasai	31750	1556
Naserkhaki et al.	2750	458
Jankowski	16000	1104
Xu et al.	12848	990

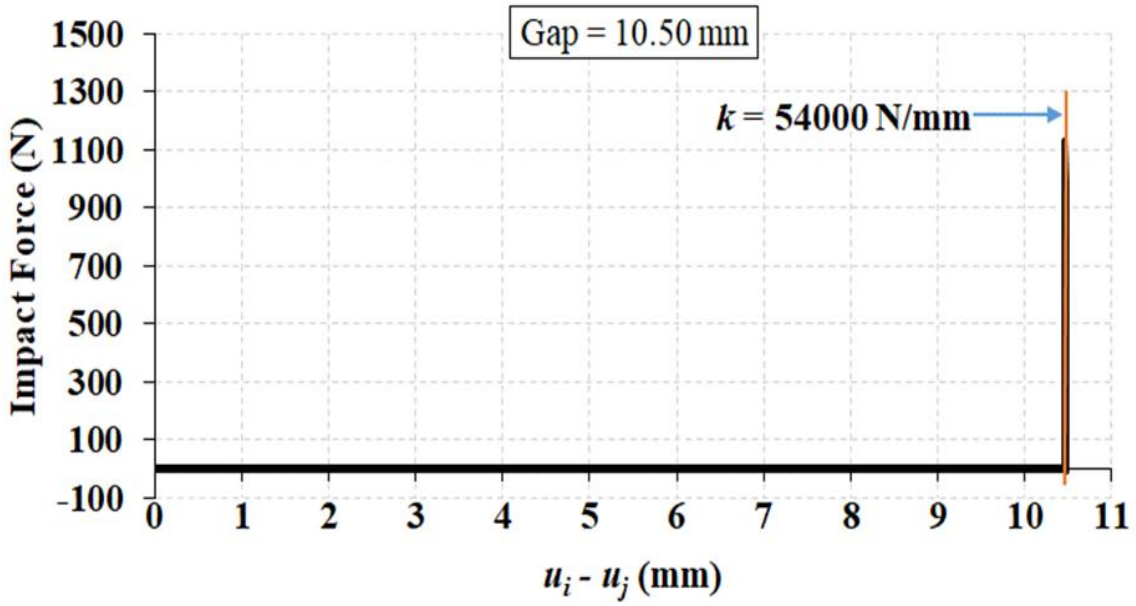

Figure 5.1(a) Fifth floor impact force–displacement relationship for pounding between 15B-storey adjacent to 5B-storey under scaled El Centro earthquake with gap equal to 10.5 mm

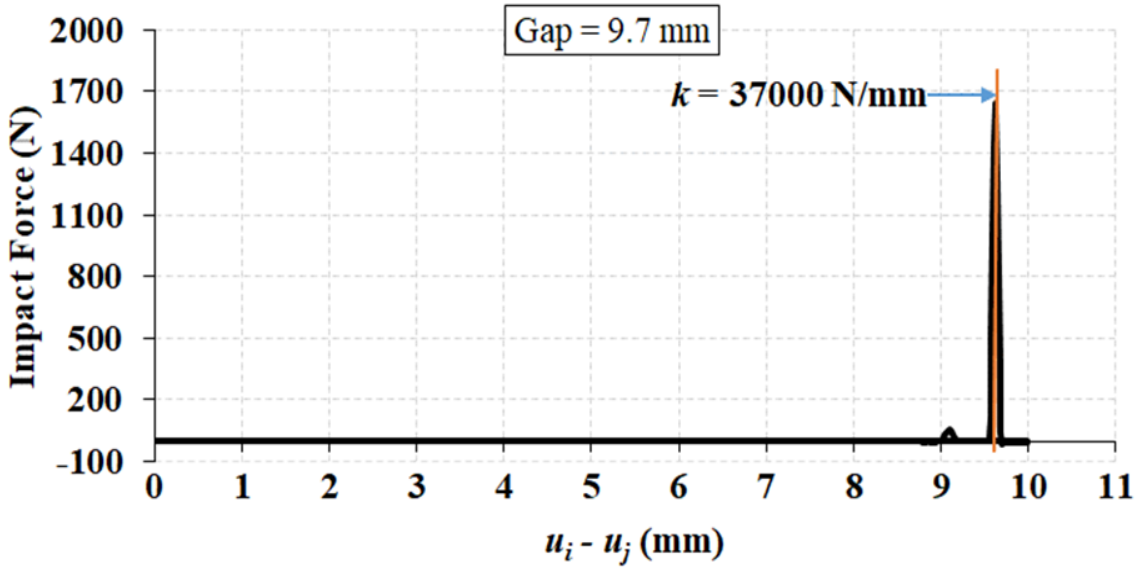

Figure 5.1(b) Fifth floor impact force–displacement relationship for pounding between 15B-storey adjacent to 5B-storey under scaled El Centro earthquake with gap equal to 9.7 mm

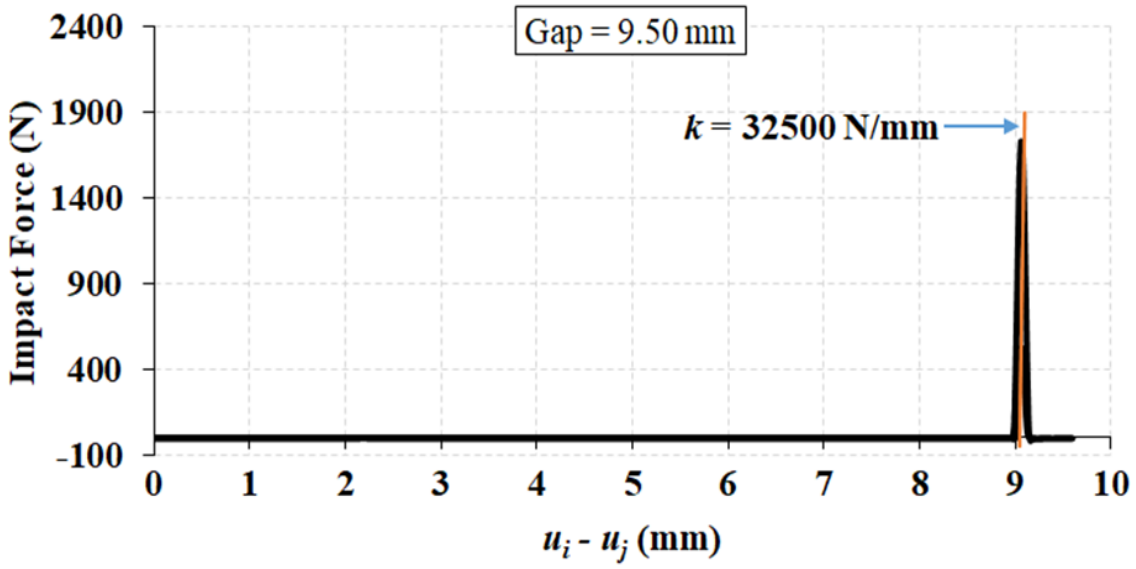

Figure 5.1(c) Fifth floor impact force–displacement relationship for pounding between 15B-storey adjacent to 5B-storey under a scaled El Centro earthquake with gap equal to 9.5 mm

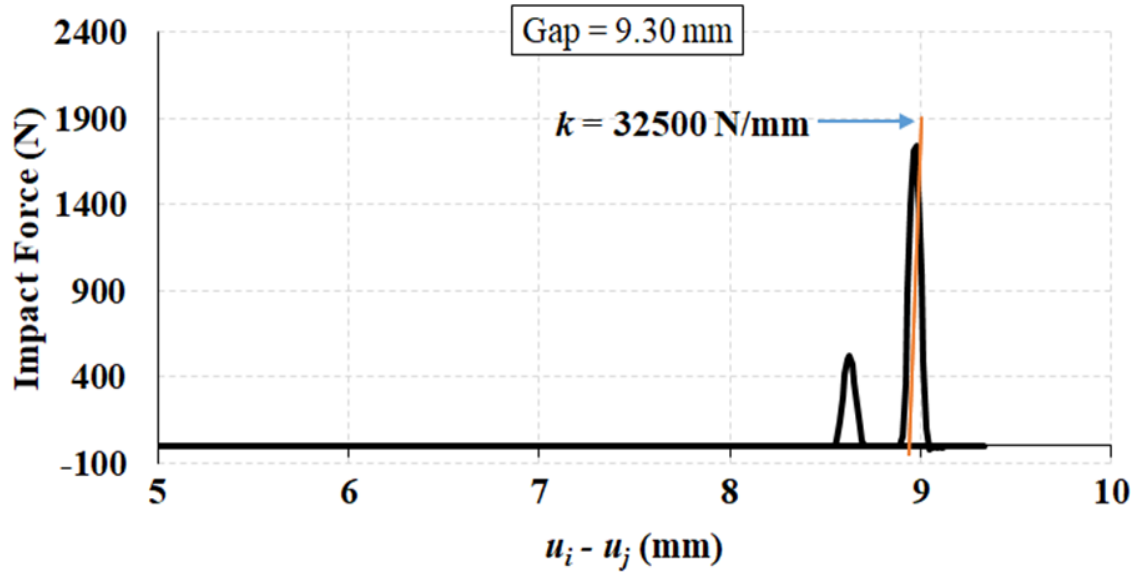

Figure 5.1(d) Fifth floor impact force–displacement relationship for pounding between 15B-storey adjacent to 5B-storey under scaled El Centro earthquake with gap equal to 9.3 mm

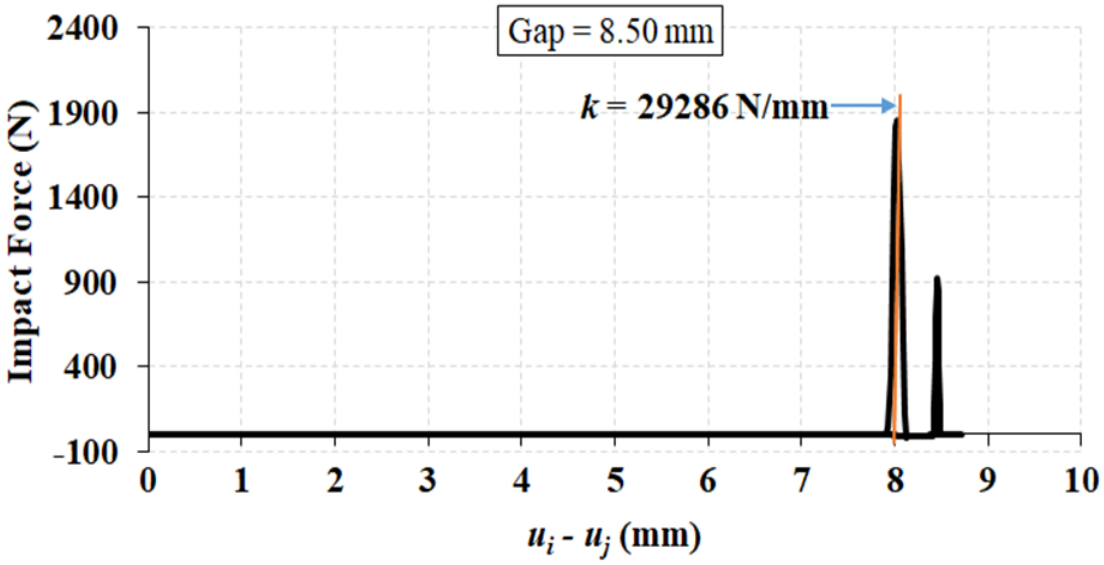

Figure 5.1(e) Fifth floor impact force–displacement relationship for pounding between 15B-storey adjacent to 5B-storey under scaled El Centro earthquake with gap equal to 8.5 mm

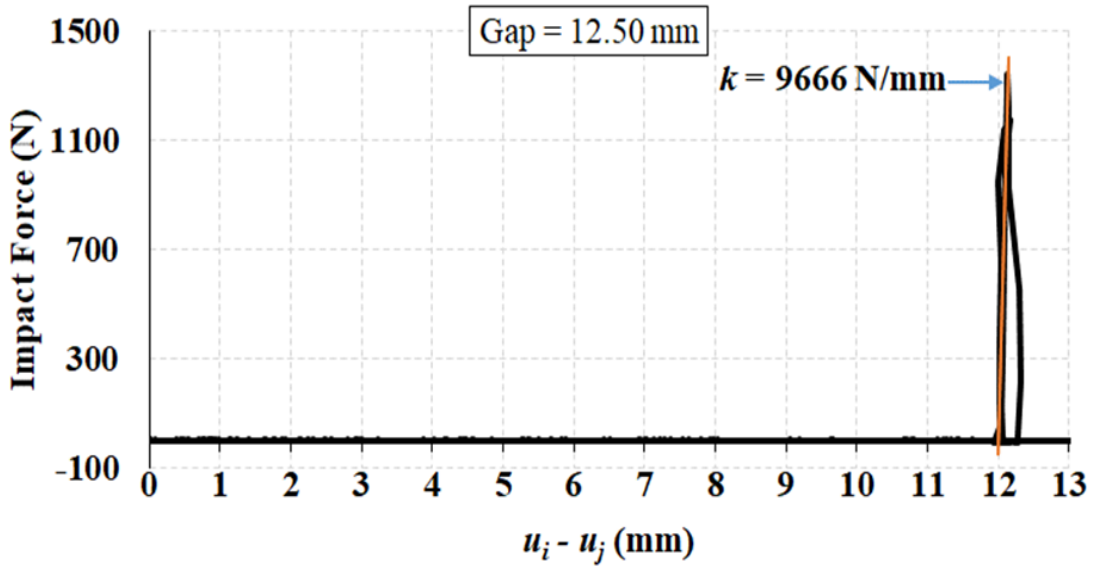

Figure 5.2(a) Fifth floor impact force–displacement relationship for pounding between 15B-storey adjacent to 5B-storey under scaled Hachinohe earthquake with gap equal to 12.5 mm

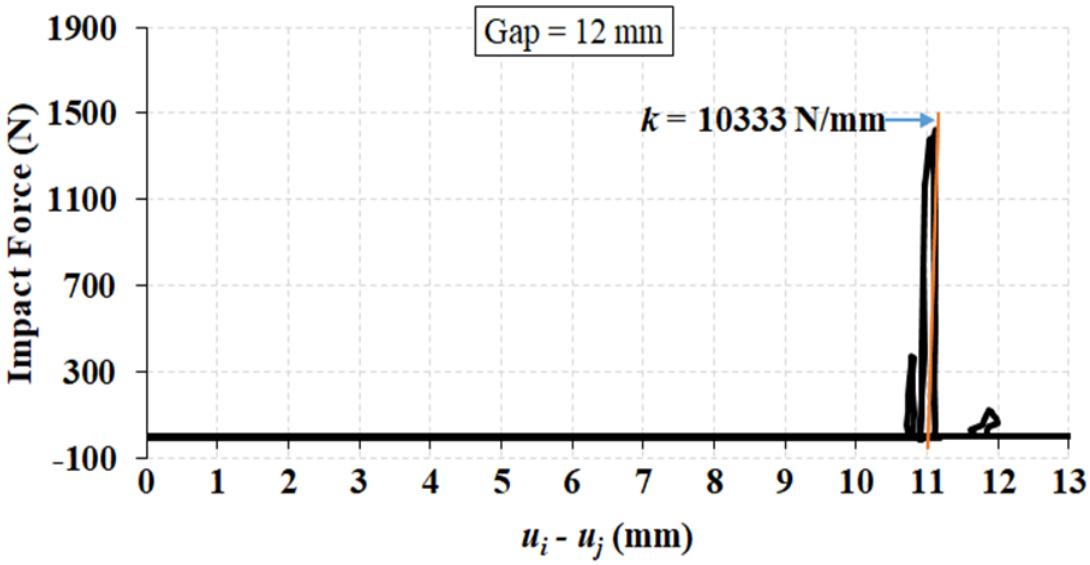

Figure 5.2(b) Fifth floor impact force–displacement relationship for pounding between 15B-storey adjacent to 5B-storey under scaled Hachinohe earthquake with gap equal to 12 mm

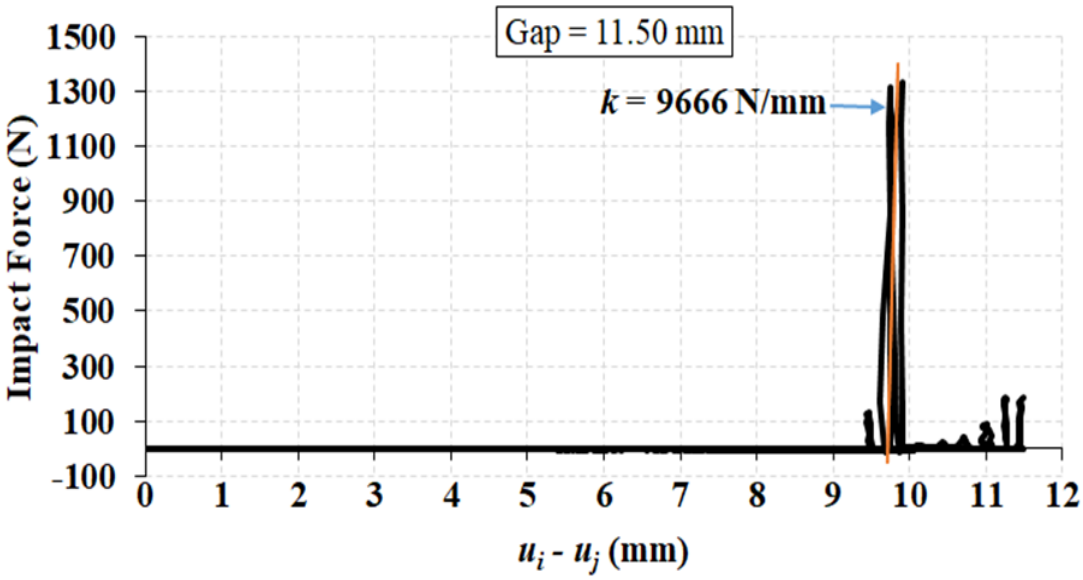

Figure 5.2(c) Fifth floor impact force–displacement relationship for pounding between 15B-storey adjacent to 5B-storey under scaled Hachinohe earthquake with gap equal to 11.5 mm

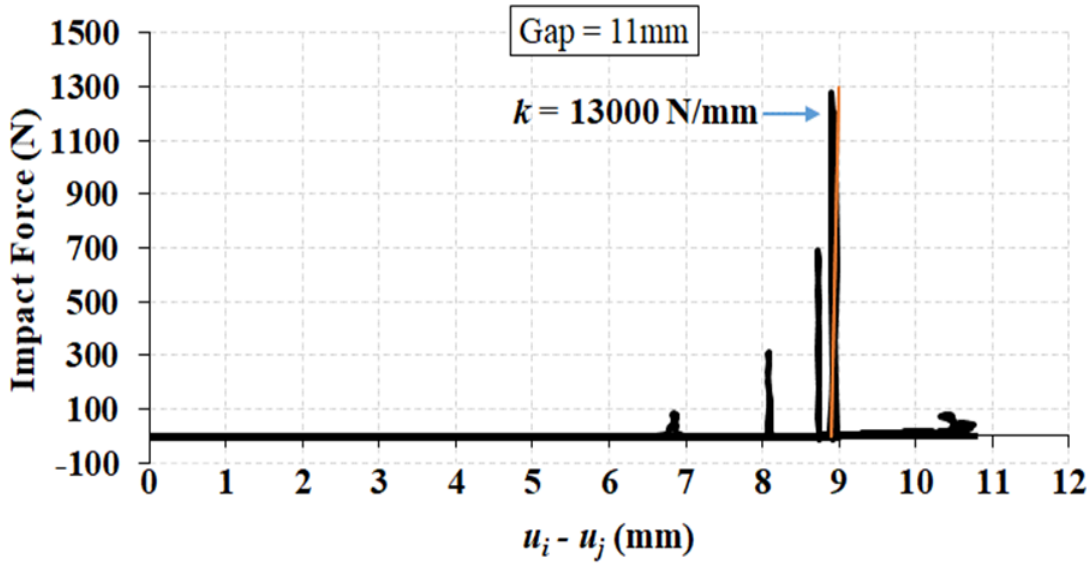

Figure 5.2(d) Fifth floor impact force–displacement relationship for pounding between 15B-storey adjacent to 5B-storey under scaled Hachinohe earthquake with gap equal to 11 mm

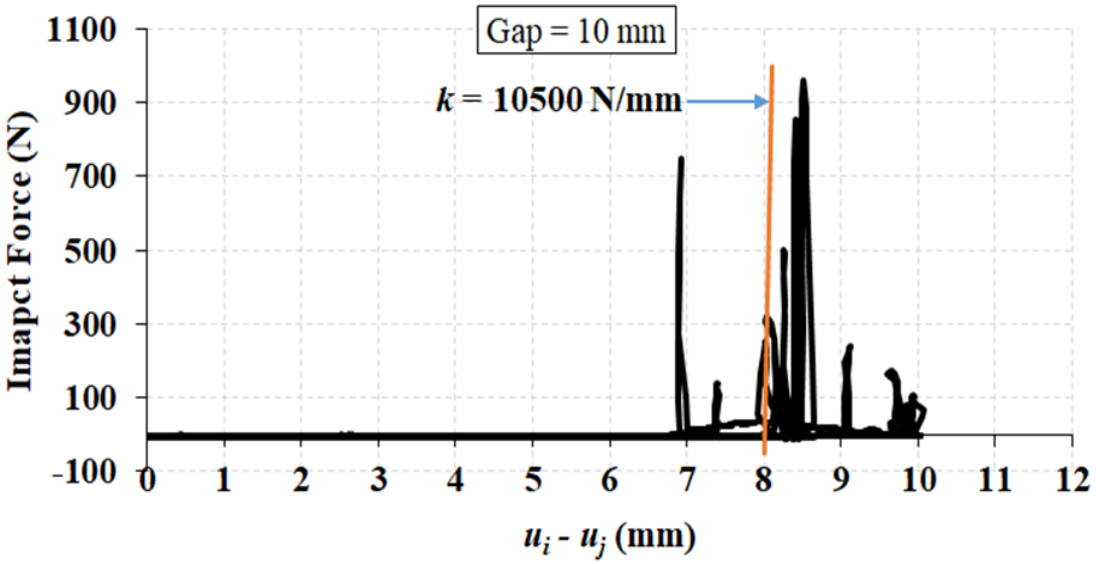

Figure 5.2(e) Fifth floor impact force–displacement relationship for pounding between 15B-storey adjacent to 5B-storey under scaled Hachinohe earthquake with gap equal to 10 mm

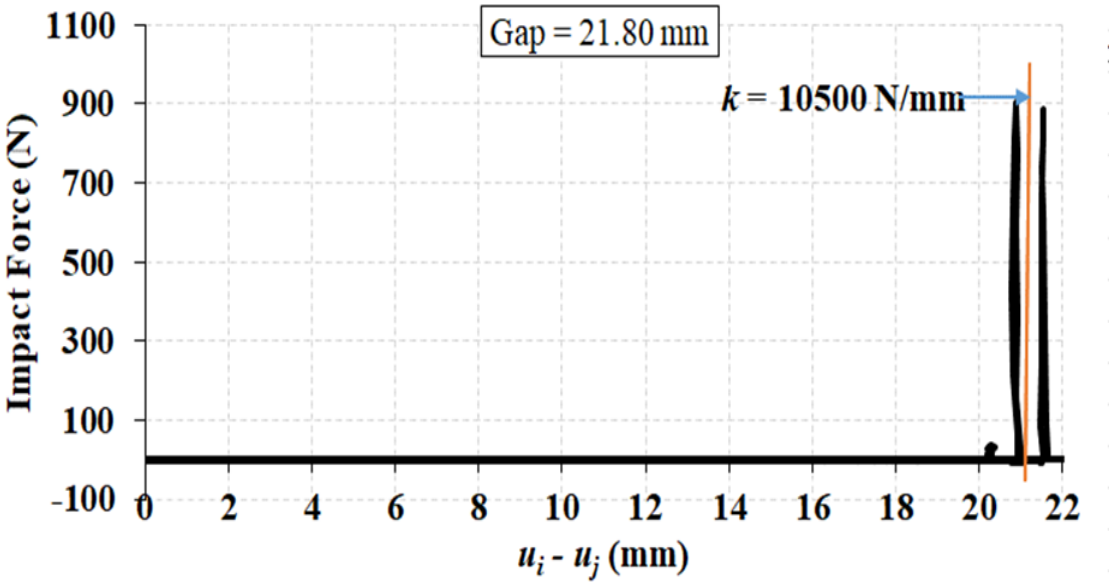

Figure 5.3(a) Fifth floor impact force–displacement relationship for pounding between 15B-storey adjacent to 5B-storey under scaled Northridge earthquake with gap equal to 21.8 mm

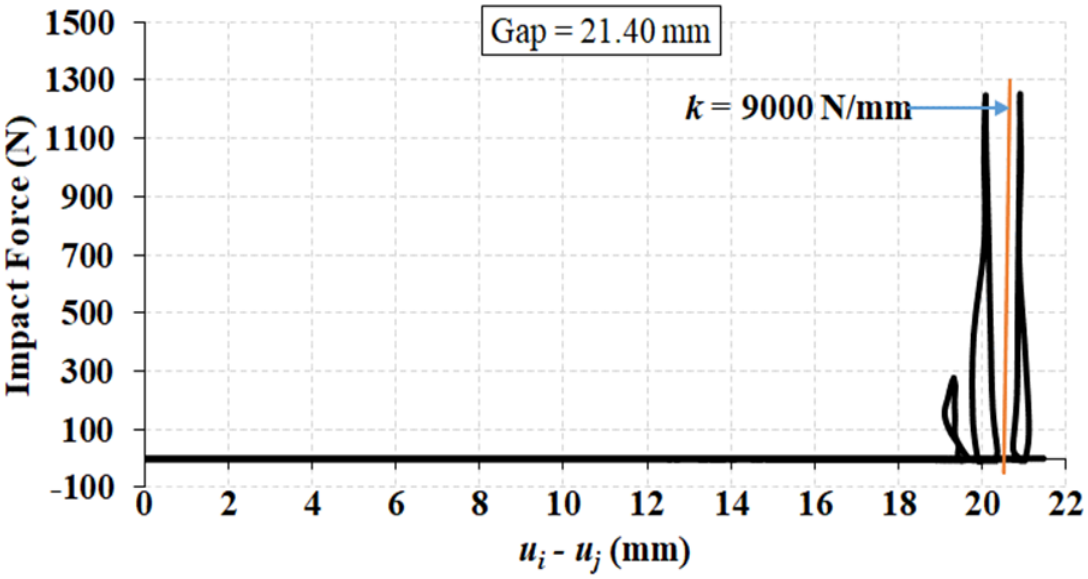

Figure 5.3(b) Fifth floor impact force–displacement relationship for pounding between 15B-storey adjacent to 5B-storey under scaled Northridge earthquake with gap equal to 21.4 mm

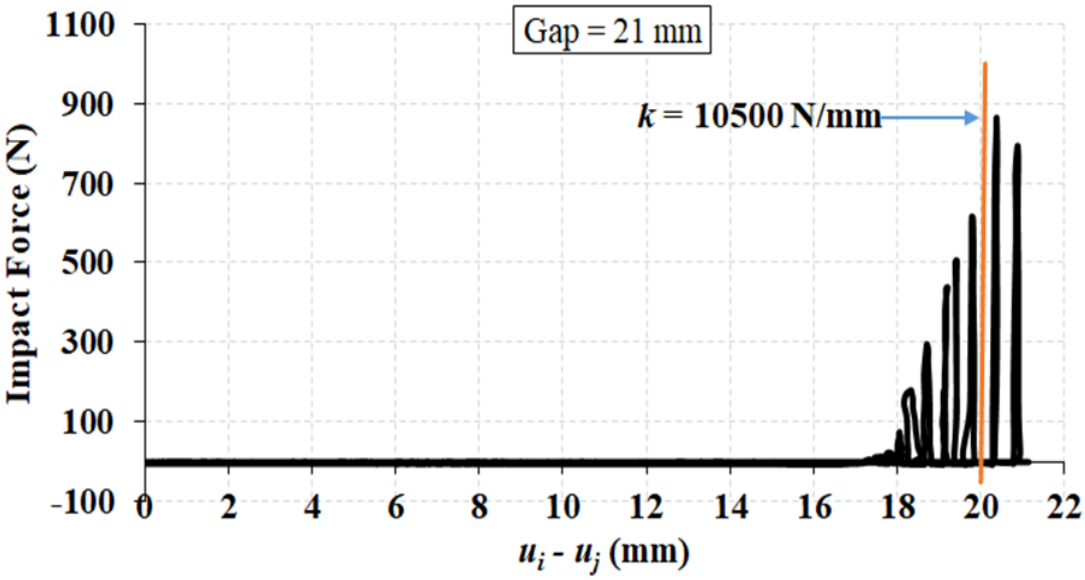

Figure 5.3(c) Fifth floor impact force–displacement relationship for pounding between 15B-storey adjacent to 5B-storey under scaled Northridge earthquake with gap equal to 21 mm

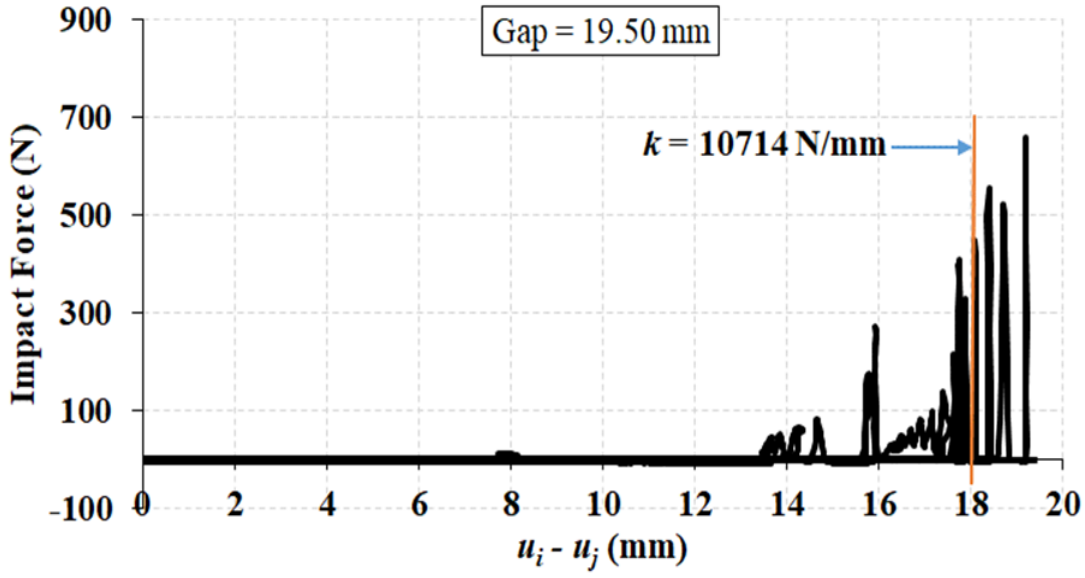

Figure 5.3(d) Fifth floor impact force–displacement relationship for pounding between 15B-storey adjacent to 5B-storey under scaled Northridge earthquake with gap equal to 19.5 mm

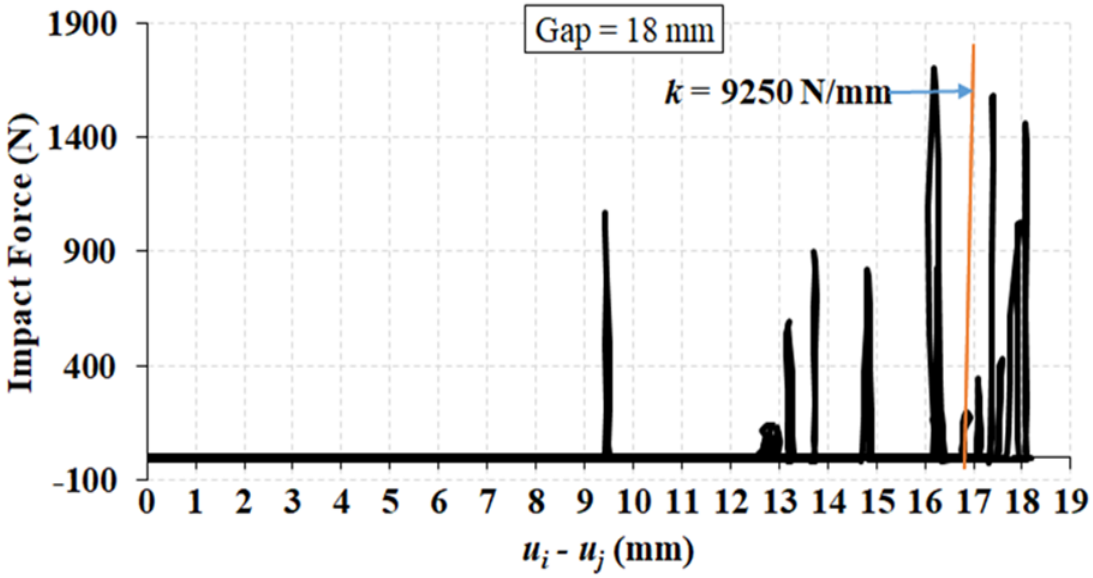

Figure 5.3(e) Fifth floor impact force–displacement relationship for pounding between 15B-storey adjacent to 5B-storey under scaled Northridge earthquake with gap equal to 18 mm

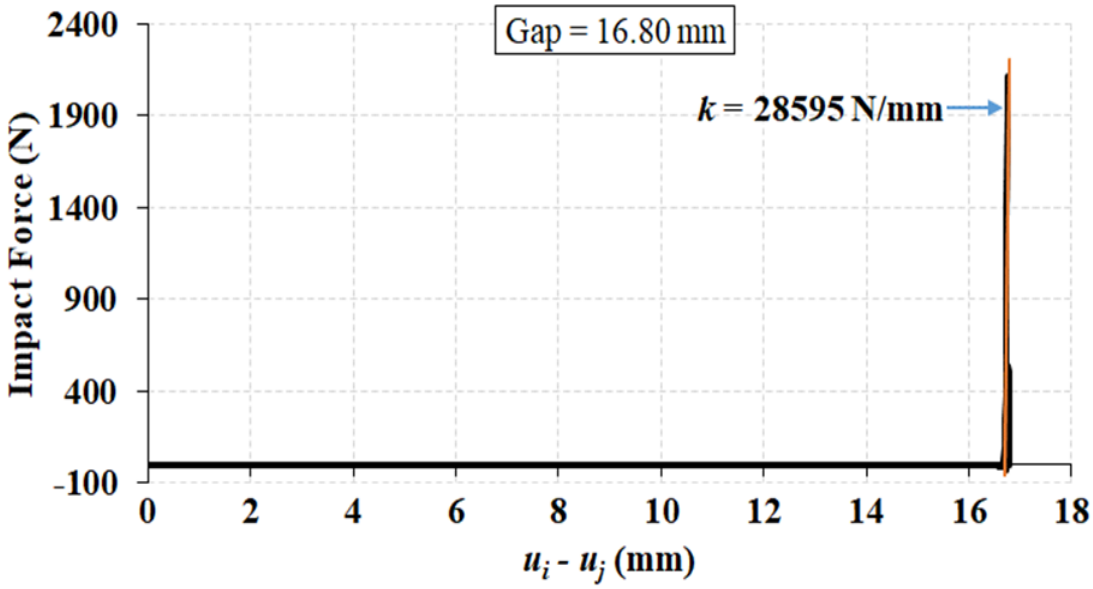

Figure 5.4(a) Fifth floor impact force–displacement relationship for pounding between 15B-storey adjacent to 5B-storey under scaled Kobe earthquake with gap equal to 16.8 mm

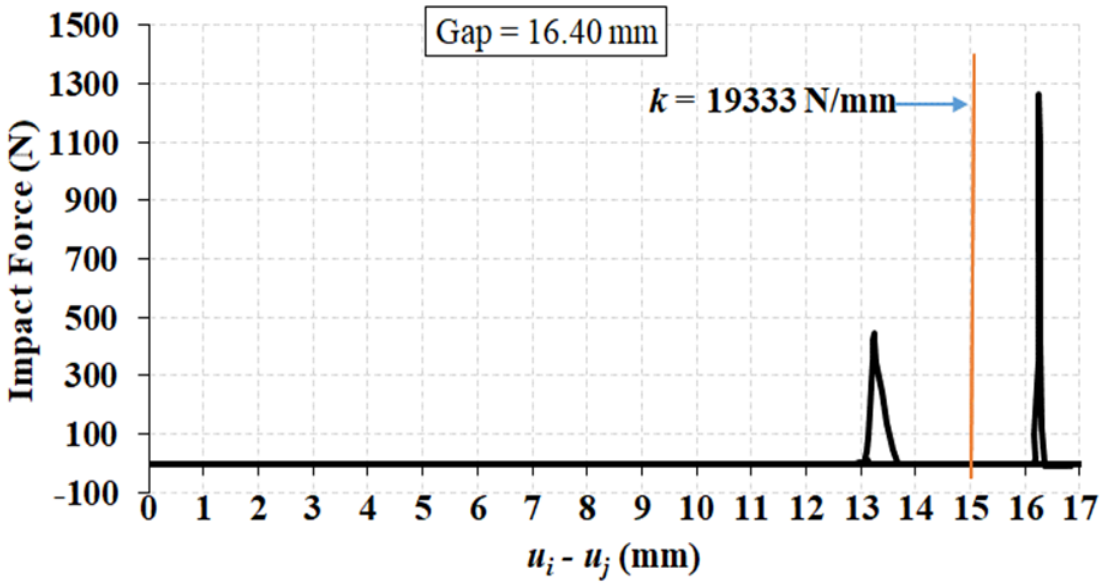

Figure 5.4(b) Fifth floor impact force–displacement relationship for pounding between 15B-storey adjacent to 5B-storey under scaled Kobe earthquake with gap equal to 16.4 mm

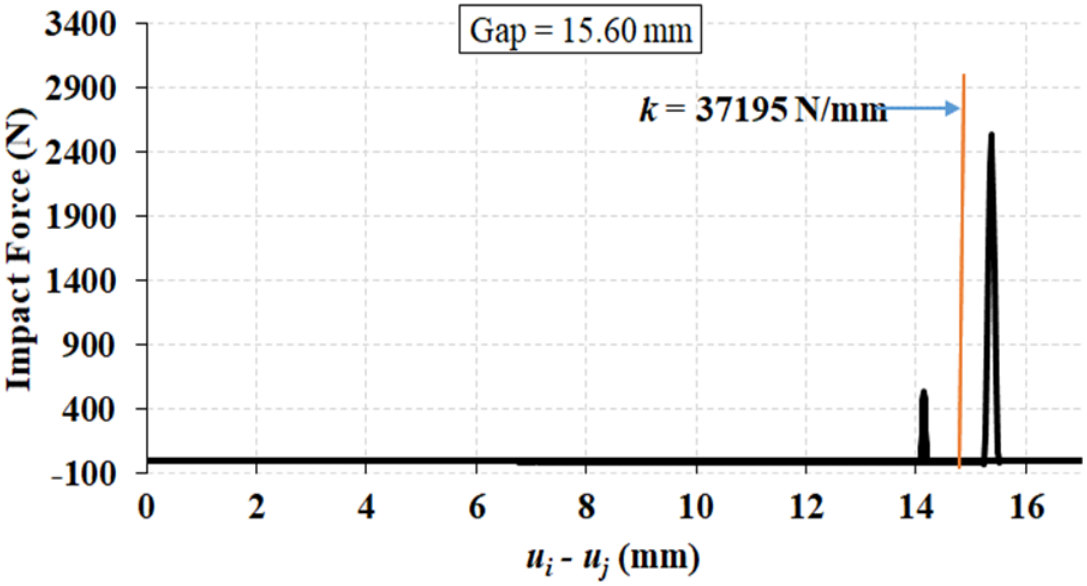

Figure 5.4(c) Fifth floor impact force–displacement relationship for pounding between 15B-storey adjacent to 5B-storey under scaled Kobe earthquake with gap equal to 15.6 mm

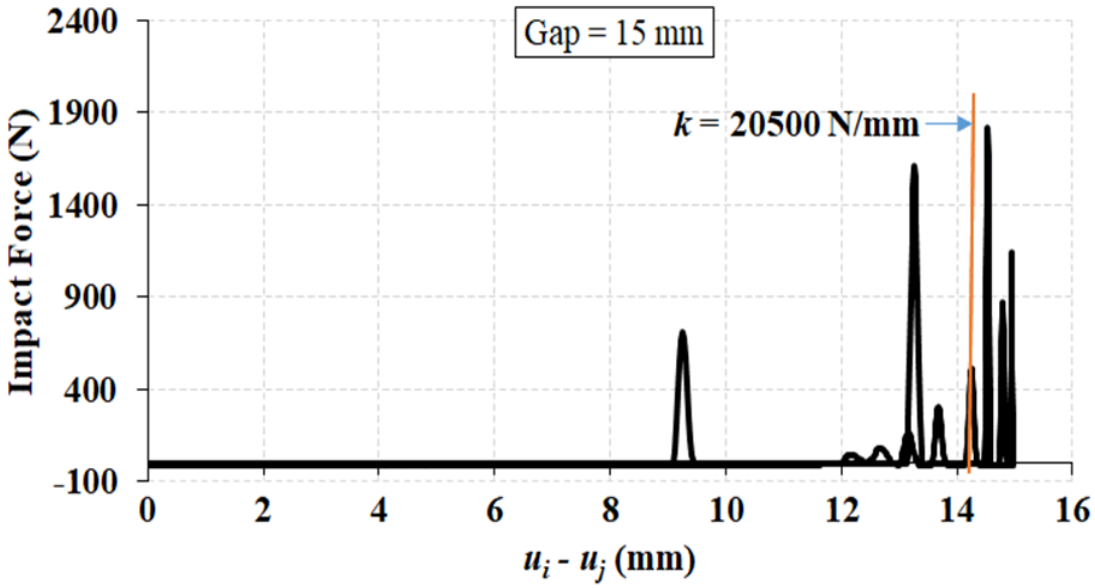

Figure 5.4(d) Fifth floor impact force–displacement relationship for pounding between 15B-storey adjacent to 5B-storey under scaled Kobe earthquake with gap equal to 15 mm

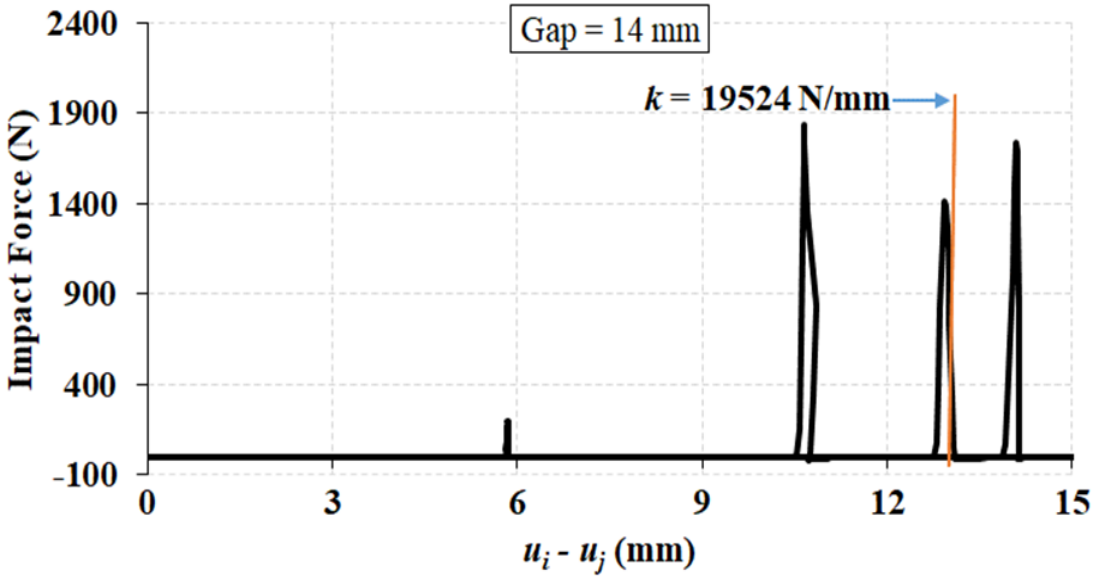

Figure 5.4(e) Fifth floor impact force–displacement relationship for pounding between 15B-storey adjacent to 5B-storey under scaled Kobe earthquake with gap equal to 14 mm

5.4 **Numerical Verification**

It is important to validate the accuracy of the experimental value ($k - experiment$). The impact stiffness value derived from the experimental measures was compared to that determined by other methods. In addition, the accuracy of the current experimental value is validated using numerical simulations of the pounding response. A comparative study was made based on five methods of determining impact stiffness: the experimental value ($k - experiment$); Maison and Kasai's formula ($k - Maison\ \&\ Kasai$); Naserkhaki et al.'s formula ($k - Naserkhaki\ et\ al.$); Jankowski's value ($k - Jankowski$); and Xu et al.'s formula ($k - Xu\ et\ al.$).

To contrast the experimental impact force with the linear viscoelastic model's impact force, with regard to the impact stiffness obtained from the five methods, impact force time history was computed using Equation 2.5. The calculation was carried out using the Excel spreadsheet and the time step for this analysis was taken as 1×10^{-4} s.

The comparison of results from the five methods for impact stiffness is presented in Figures 5.5–5.8. It can be inferred from the figures that the impact stiffness derived experimentally is evidently different from that determined by other methods. To confirm the accuracy of the proposed experimental value for impact stiffness, an evaluation of the peak impact forces from the pounding simulations using the linear viscoelastic model was conducted. The impact stiffness obtained using the five methods and similar model factors was utilised in running the numerical analysis.

The difference between the results of the experimental measurement obtained by the force sensor and that of the numerical analysis was determined by calculating the percent error (Bennett et al. 2008). The relative error of the peak impact force using the numerical simulation was obtained using the following formula:

$$PE = \frac{\left|F_{e,max} - F_{t,max}\right|}{F_{e,max}} \times 100\% \qquad 5.1$$

where PE is the percent error. $F_{e,max}$ is the maximum impact force from the experimental measurements. $F_{t,max}$ is the maximum impact force from the theoretical simulation. The relative errors of maximum impact forces from the numerical simulations, based on the linear viscoelastic model in relation to the impact stiffness derived from the five methods, are reflected in Figure 5.9. It can be deduced from Figure 5.9 that the experimental value of impact stiffness derived from the linear viscoelastic model had the least relative errors

when compared with that of the axial stiffness formula (Equation 2.21), Naserkhaki et al.'s formula (Equation 2.23), Jankowski's value and Xu et al.'s formula (Equation 2.24). In the above-mentioned formulas, researchers commonly employed single-degree-of-freedom systems to simplify the problem at hand. This approach allowed for a more straightforward analysis of the structural response. Additionally, some experimental studies encountered limitations in terms of testing technology. Specifically, there was a lack of suitable sensors available for directly measuring the impact force. This constraint may have impacted the ability to obtain precise and direct measurements of the forces involved in the impact phenomenon.

In contrast, this study diverged from the common approach of using single-degree-of-freedom systems and instead employed a multiple degree of freedom (MDOF) model to represent the adjoining structures. By utilizing an MDOF model, the study aimed to capture a more realistic and comprehensive depiction of the structural behaviour and response.

Thus, it can be stated that the impact stiffness obtained from the adopted experimental formula of the linear viscoelastic model can produce a more accurate simulation of the structural pounding than those of other formulae.

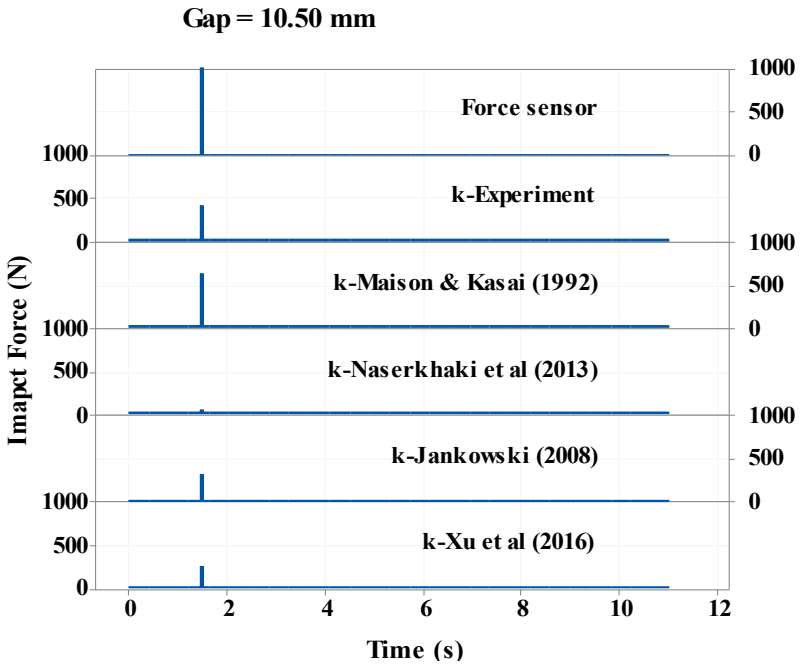

Figure 5.5(a) Experimental impact force time histories vs theoretical force with several *k* values for pounding between the coupled 15B and 5B-storeys under scaled El Centro with gap equal to 10.5 mm

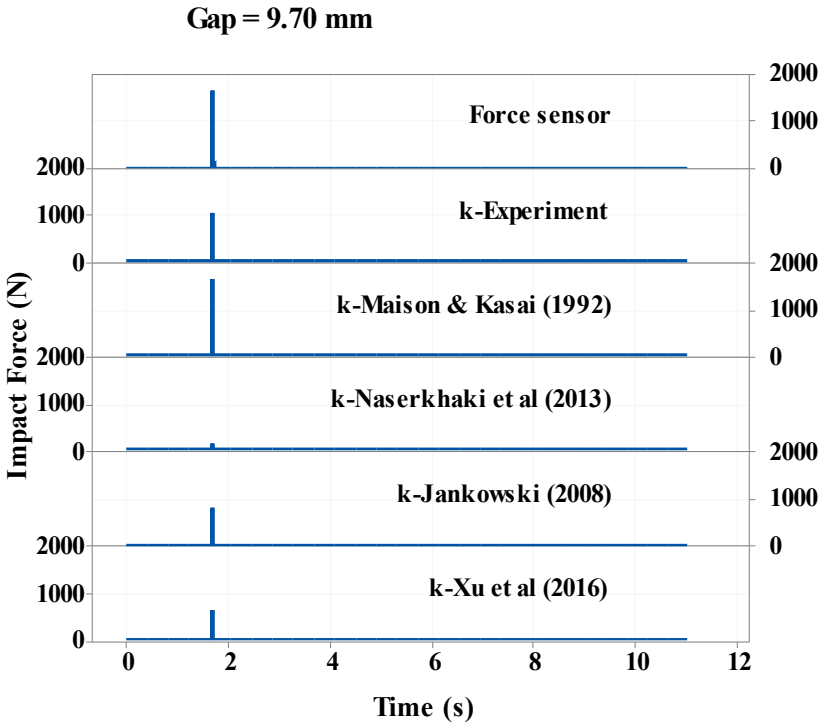

Figure 5.5(b) Experimental impact force time histories vs theoretical force with several *k* values for pounding between the coupled 15B and 5B-storeys under scaled El Centro with gap equal to 9.7 mm

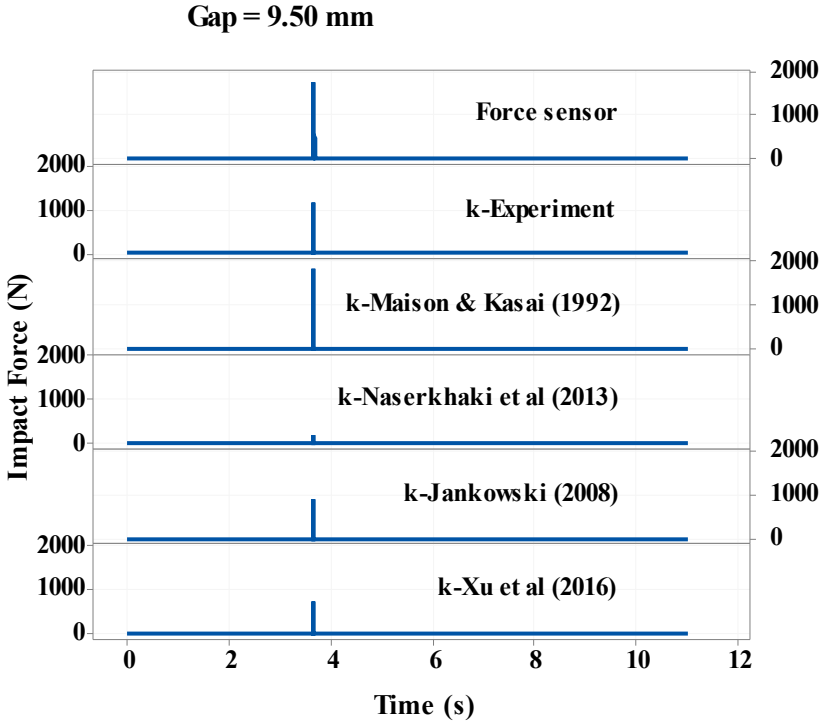

Figure 5.5(c) Experimental impact force time histories vs theoretical force with several *k* values for pounding between the coupled 15B and 5B-storeys under scaled El Centro with gap equal to 9.5 mm

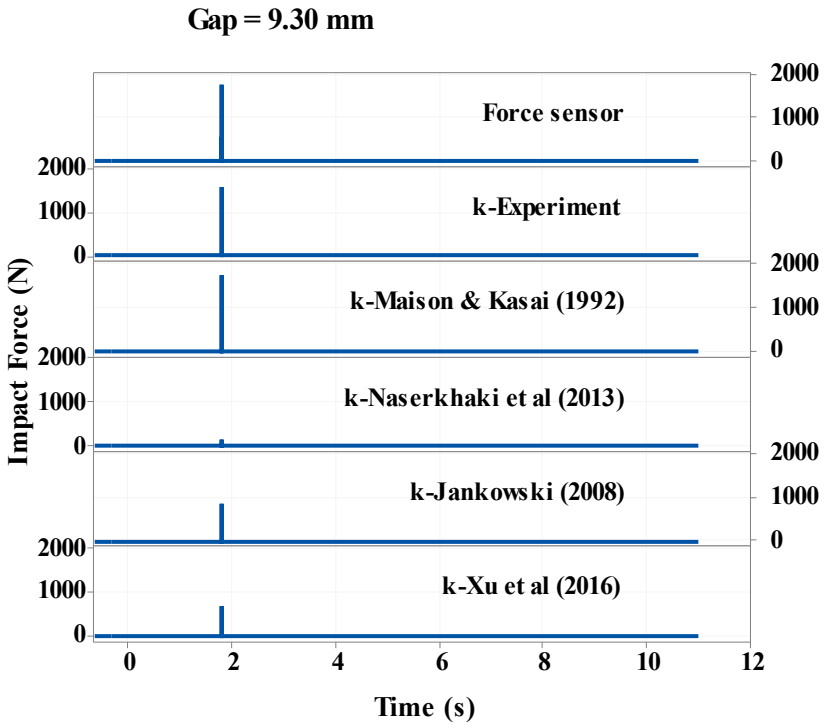

Figure 5.5(d) Experimental impact force time histories vs theoretical force with several *k* values for pounding between the coupled 15B and 5B-storeys under scaled El Centro with gap equal to 9.3 mm

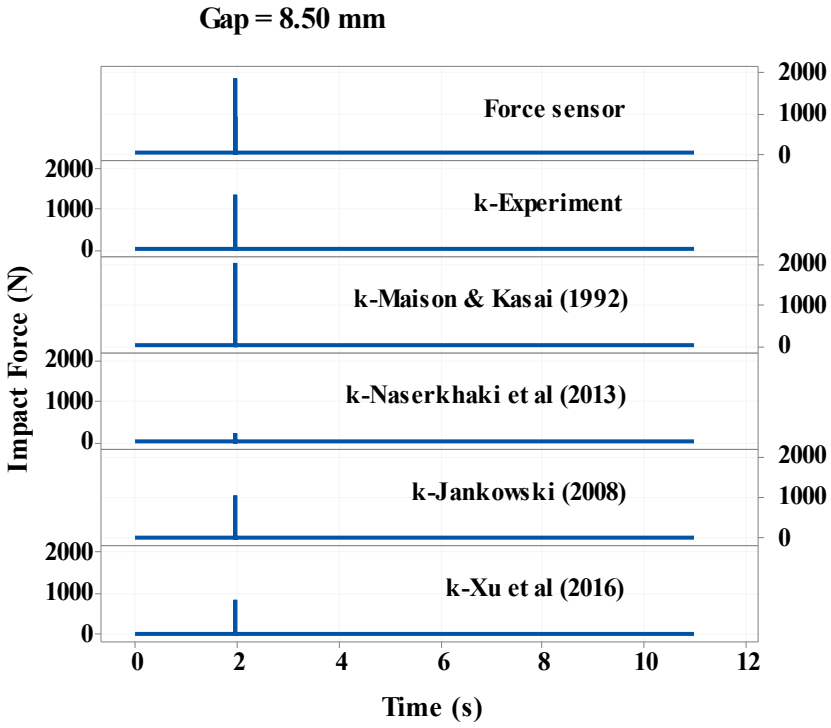

Figure 5.5(e) Experimental impact force time histories vs theoretical force with several *k* values for pounding between the coupled 15B and 5B-storeys under scaled El Centro with gap equal to 8.5 mm

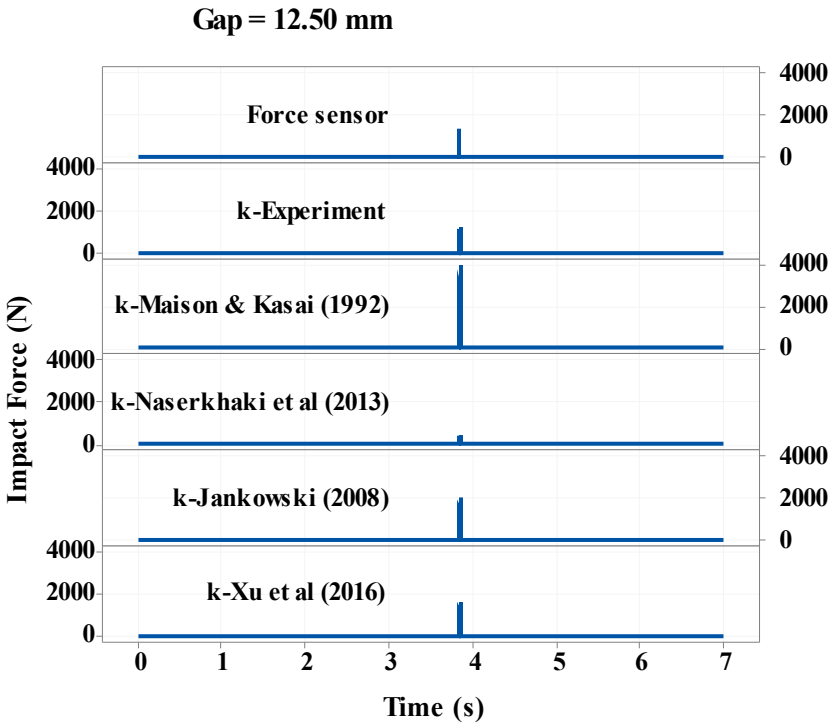

Figure 5.6(a) Experimental impact force time histories vs theoretical force with several *k* values for pounding between the coupled 15B and 5B-storeys under scaled Hachinohe with gap equal to 12.5 mm

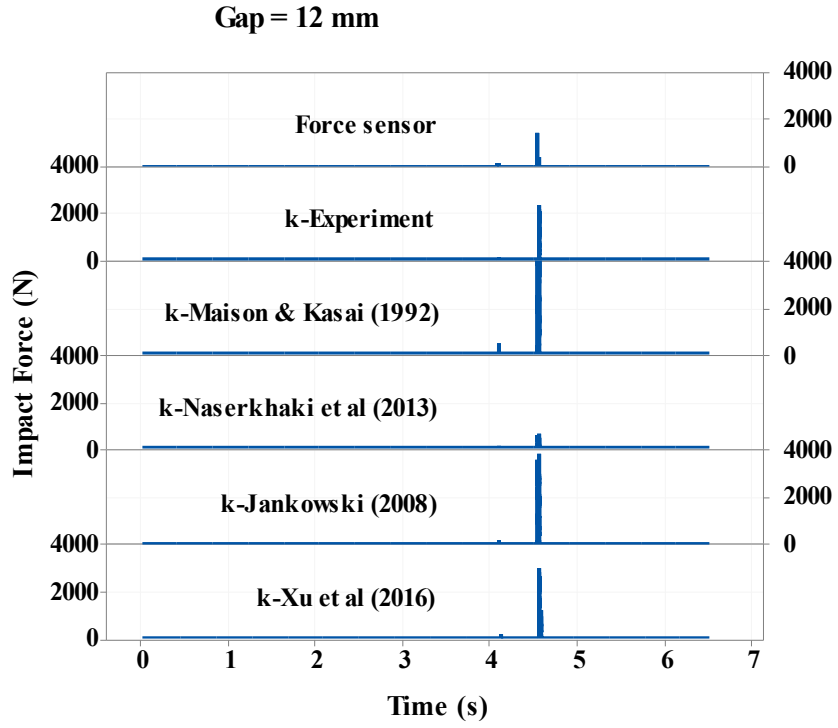

Figure 5.6(b) Experimental impact force time histories vs theoretical force with several *k* values for pounding between the coupled 15B and 5B-storeys under scaled Hachinohe with gap equal to 12 mm

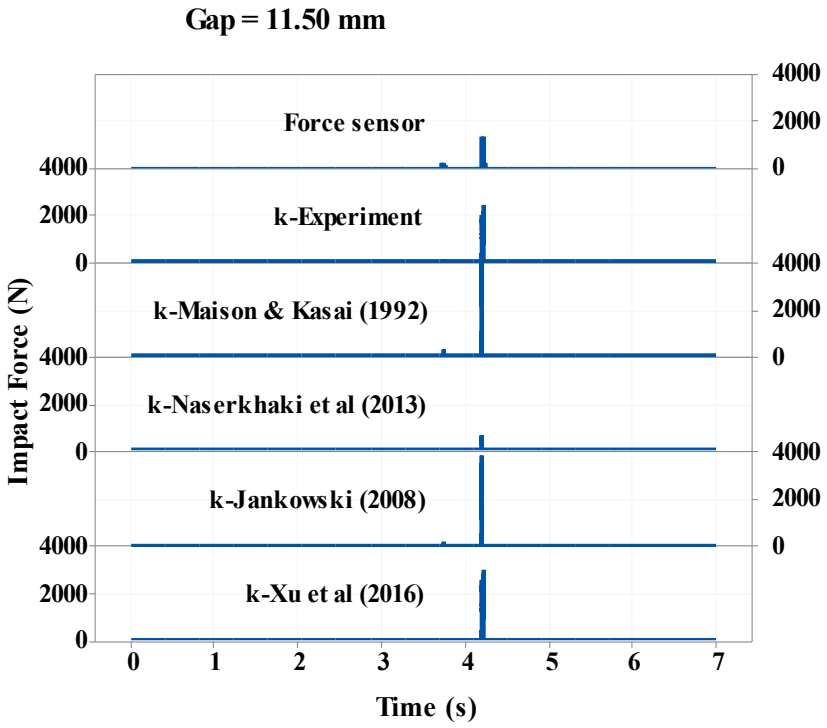

Figure 5.6(c) Experimental impact force time histories vs theoretical force with several *k* values for pounding between the coupled 15B and 5B-storeys under scaled Hachinohe with gap equal to 11.5 mm

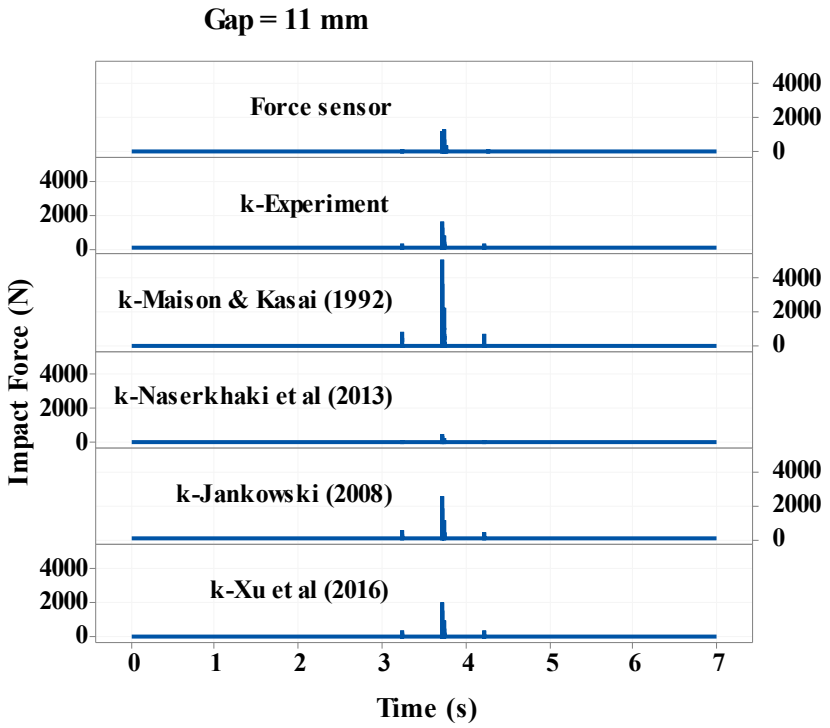

Figure 5.6(d) Experimental impact force time histories vs theoretical force with several *k* values for pounding between the coupled 15B and 5B-storeys under scaled Hachinohe with gap equal to 11 mm

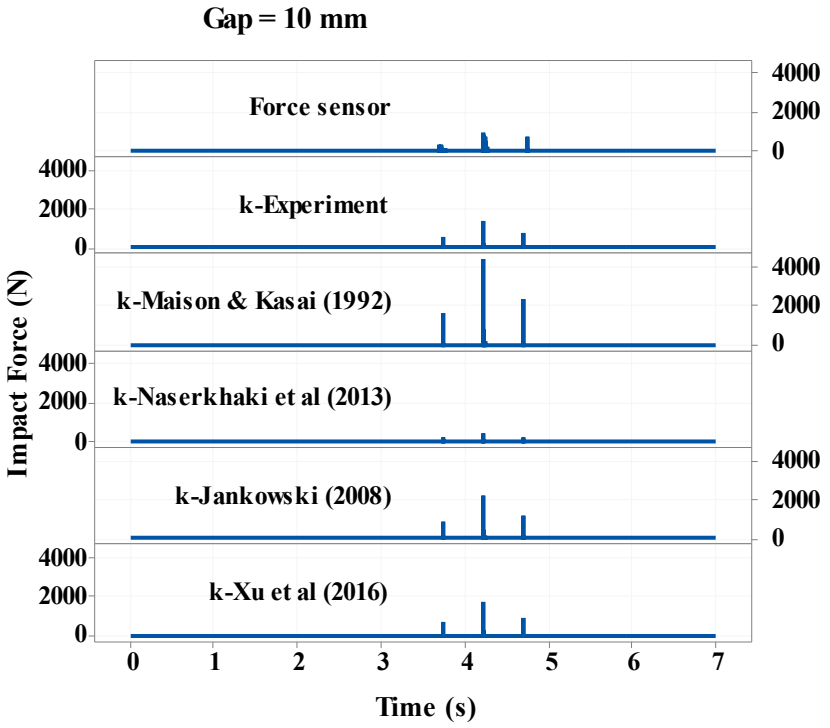

Figure 5.6(e) Experimental impact force time histories vs theoretical force with several *k* values for pounding between the coupled 15B and 5B-storeys under scaled Hachinohe with gap equal to 10 mm

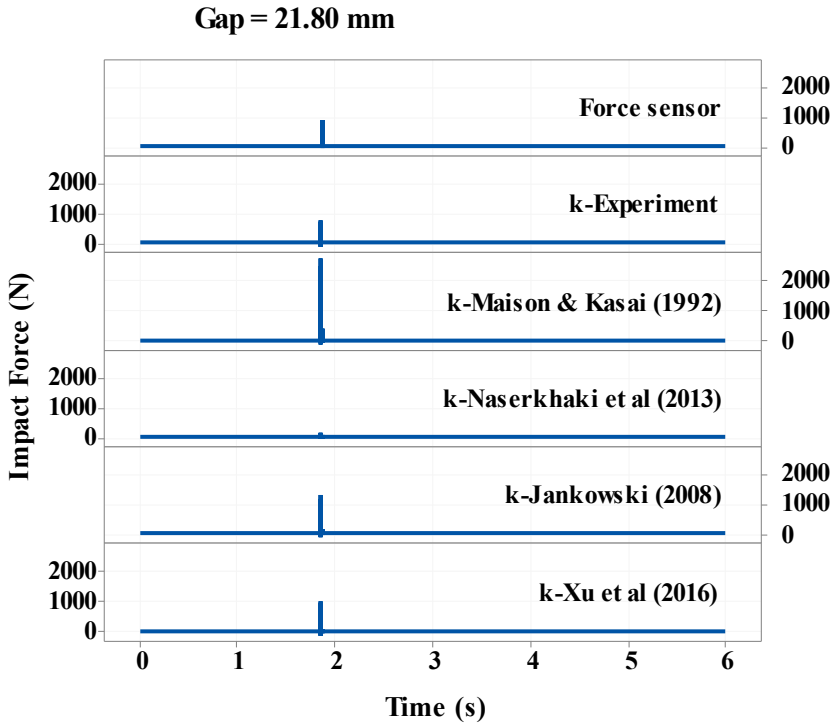

Figure 5.7(a) Experimental impact force time histories vs theoretical force with several *k* values for pounding between the coupled 15B and 5B-storeys under scaled Northridge with gap equal to 21.8 mm

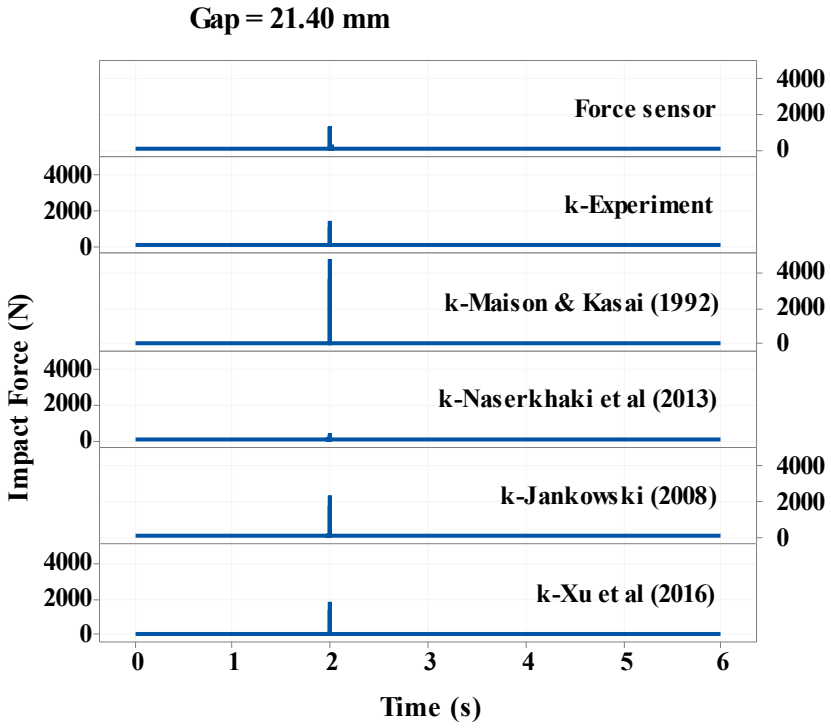

Figure 5.7(b) Experimental impact force time histories vs theoretical force with several *k* values for pounding between the coupled 15B and 5B-storeys under scaled Northridge with gap equal to 21.4 mm

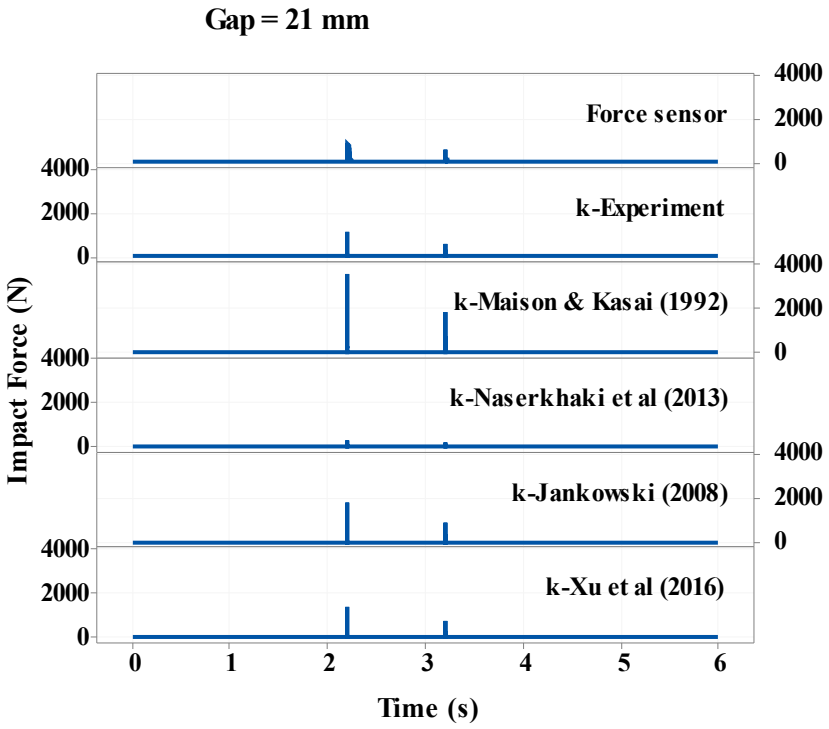

Figure 5.7(c) Experimental impact force time histories vs theoretical force with several *k* values for pounding between the coupled 15B and 5B-storeys under scaled Northridge with gap equal to 21 mm

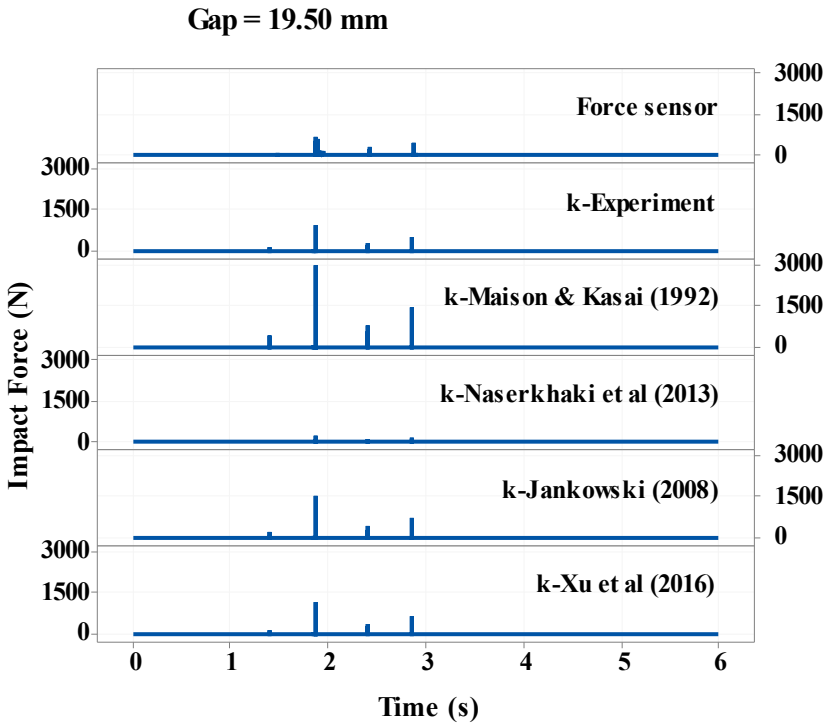

Figure 5.7(d) Experimental impact force time histories vs theoretical force with several *k* values for pounding between the coupled 15B and 5B-storeys under scaled Northridge with gap equal to 19.5 mm

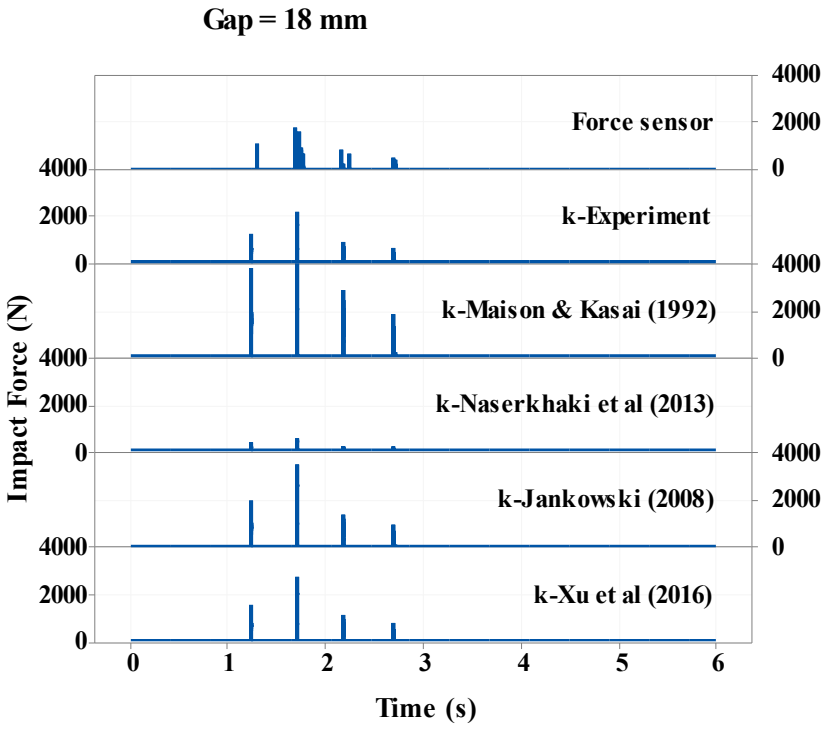

Figure 5.7(e) Experimental impact force time histories vs theoretical force with several *k* values for pounding between the coupled 15B and 5B-storeys under scaled Northridge with gap equal to 18 mm

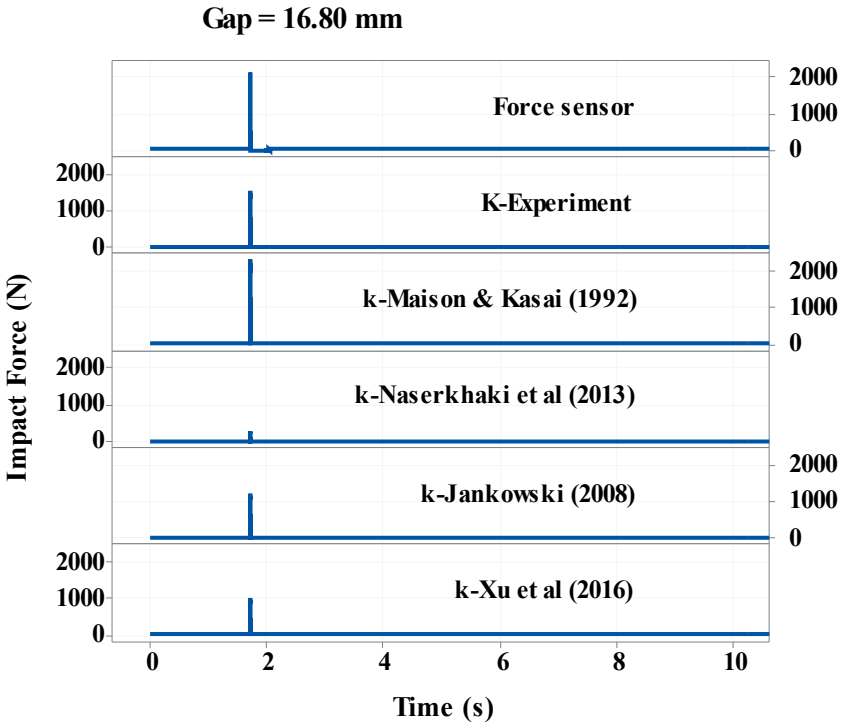

Figure 5.8(a) Experimental impact force time histories vs theoretical force with several *k* values for pounding between the coupled 15B and 5B-storeys under scaled Kobe with gap equal to 16.8 mm

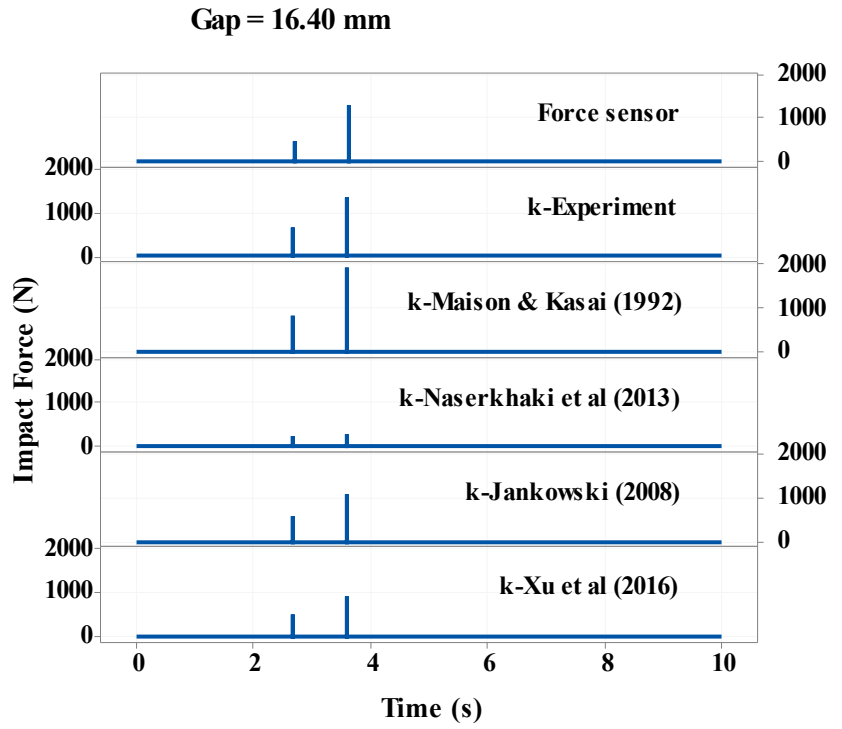

Figure 5.8(b) Experimental impact force time histories vs theoretical force with several *k* values for pounding between the coupled 15B and 5B-storeys under scaled Kobe with gap equal to 16.4 mm

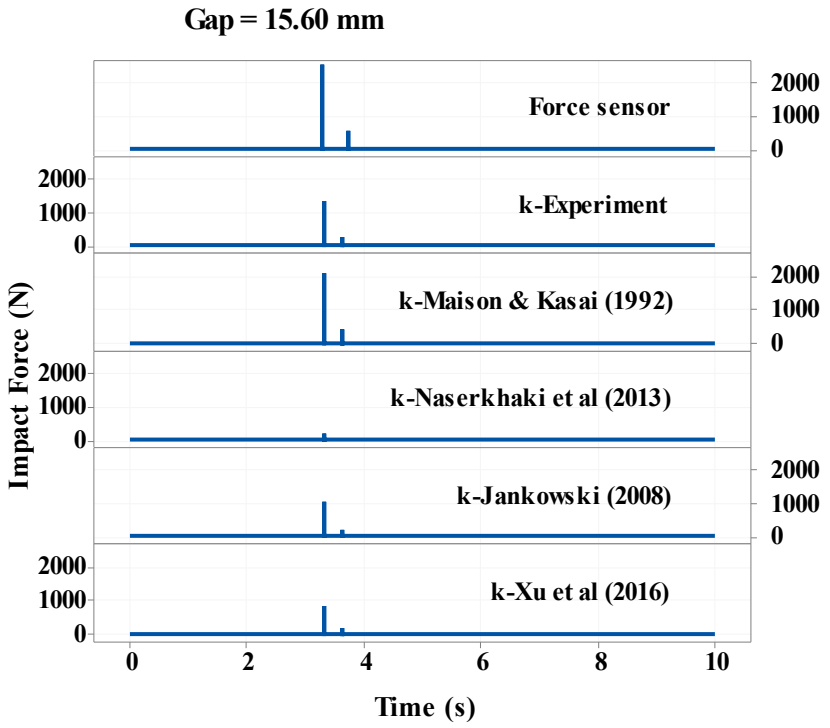

Figure 5.8(c) Experimental impact force time histories vs theoretical force with several *k* values for pounding between the coupled 15B and 5B-storeys under scaled Kobe with gap equal to 15.6 mm

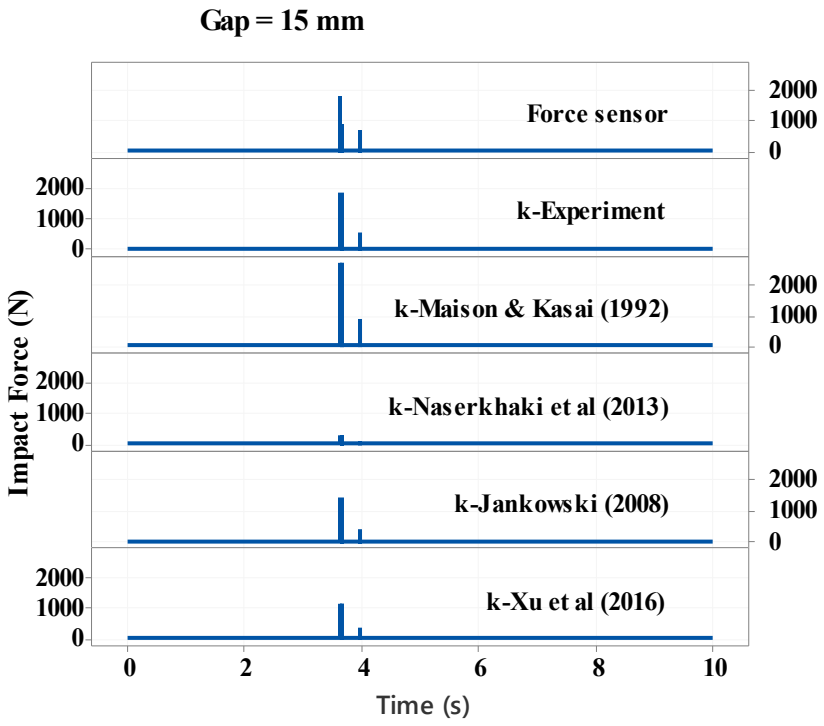

Figure 5.8(d) Experimental impact force time histories vs theoretical force with several *k* values for pounding between the coupled 15B and 5B-storeys under scaled Kobe with gap equal to 15 mm

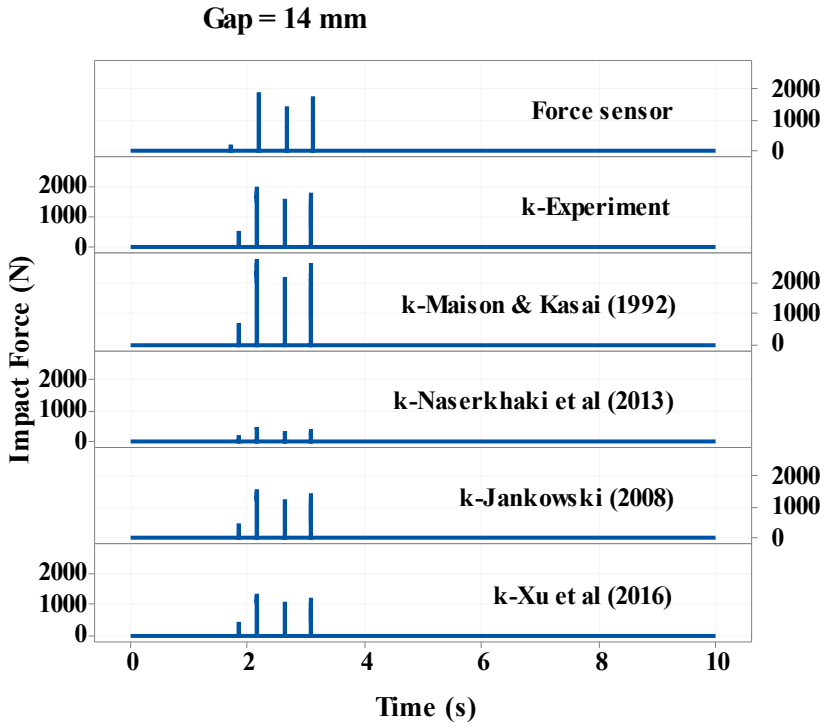

Figure 5.8(e) Experimental impact force time histories vs theoretical force with several *k* values for pounding between the coupled 15B and 5B-storeys under scaled Kobe with gap equal to 14 mm

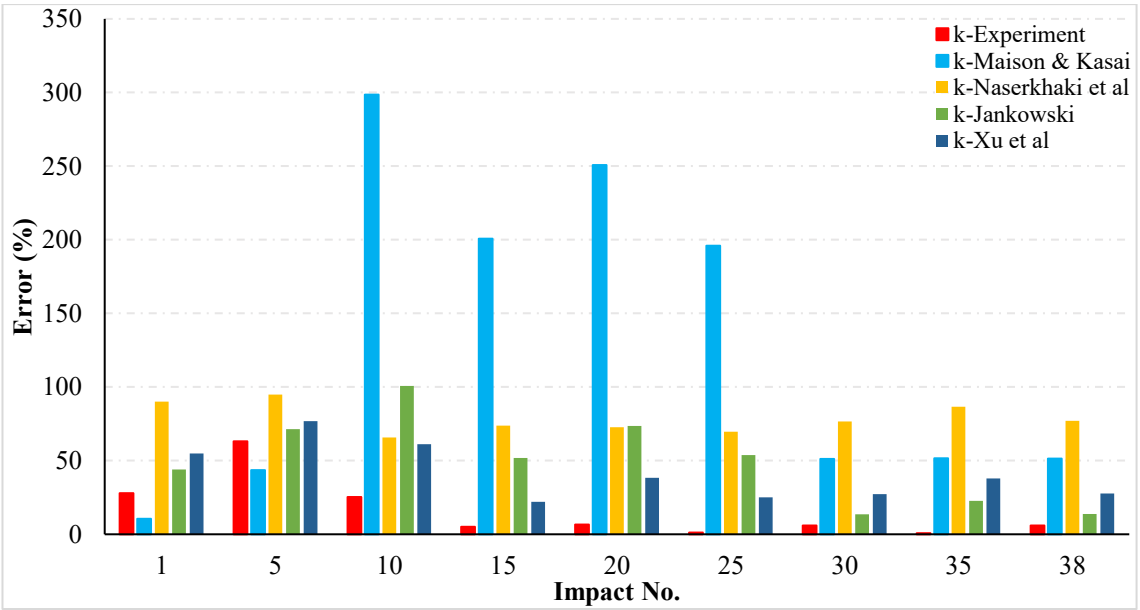

Figure 5.9 Relative errors of the peak impact forces from numerical simulations based on five kinds of methods to calculate impact stiffness.

It should be noted that, the results presented in this chapter study are valid in the case of buildings responding elastically. Furthermore, the soil–structure interaction effects are

neglected in this study, under the assumption that the soil beneath the foundations is infinitely rigid. The numerical evaluation has confirmed the acceptable level of accuracy of the adapted formula in terms of the actual engineering application. Based on the outcomes of this study, the following equation can determine the optimal rescaled impact stiffness k value:

$$k = 20.66 \times \lambda \times 30$$

which can be written as:

$$k = 620 \times \lambda \qquad 5.2$$

where λ denotes the scale factor used by the researchers, and the k value was measured by kN/mm. The value of $k - experiment$ was based on a 1/30 scale factor for single-bay moment-resisting steel frame models. If any other scale factors are employed, then Equation 4.9 will be used to calculate the new k value. For instance, if a scale of 1/8 was selected for this model, the equation result will be as shown below:

$$k = 620 \times \frac{1}{8} = 77.50\ kN/mm$$

5.5 **Summary**

In this chapter, an experimental evaluation was carried out to estimate the impact stiffness used in the linear viscoelastic impact model for pounding simulation. Multiple tests on pounding between adjacent steel frames with different heights was conducted using earthquake simulator. The results show the value of the impact stiffness using the linear viscoelastic model compared with the theoretical values advanced by other researchers. According to the results, the proposed value of $k = 620\ kN/mm$ can be scaled up based on $k = 620 \times \hat{S}$, where $\hat{S}$ presents the scale factor.

Furthermore, the k value of the experimental study was the most relevant value to the standard deviation and error rate of the numerical analysis. Therefore, the present formula for impact stiffness of the linear viscoelastic model is recommended for obtaining more reliable results in experimental and numerical simulations of earthquake-induced structural pounding.

CHAPTER 6
EXPERIMENTAL EVALUATION OF THEORETICAL IMPACT MODELS FOR SEISMIC POUNDING

6.1 Introduction

Structural failure caused by earthquake-induced pounding between two neighbouring buildings is one of the main concerns in the context of earthquake-induced structural damage. Pounding between neighboring structures is a frequently detected phenomenon during main earthquakes. Buildings with different dynamic characteristics due to different weights, stiffness and building heights are expected to strike during an earthquake. Impact forces transferred between buildings can cause unexpected damage in a possible structural collision resulting from differences in dynamic characteristics such as natural vibration periods (Anagnostopoulos & Spiliopoulos 1992; Maison & Kasai 1990). Pounding is a nonlinear occurrence.

Many studies have been conducted pertaining to structural pounding using various analytical models of impact force (see Section 2.2). The models activate a contact element when the structures come into contact. Aiming to preclude penetration between adjacent parts, a spring with high stiffness has been employed, occasionally in connection with a damper. The contact elements used comprise the linear spring model (Filiatrault et al. 1995; Maison & Kasai 1990), the linear viscoelastic model (Anagnostopoulos 1988; Anagnostopoulos & Spiliopoulos 1992; Crozet et al. 2017; Jankowski et al. 1998), the nonlinear elastic model (Abdel Raheem 2006; Chau et al. 2003; Mate et al. 2012), the nonlinear viscoelastic model (Jankowski 2005; Mate et al. 2012; Naderpour et al. 2016) and the Hertz-damp model (Muthukumar & Desroches 2006; Ye et al. 2009). With the aim to replicate correctly the impact force during contact, the Hertz-damp model has been improved and enhanced.

Despite the numerous studies conducted on pounding using the various analytical models, there are inherent weaknesses noted in the models. Energy loss during impact is not considered in the linear elastic and nonlinear elastic models. The linear viscoelastic model exhibits an initial leap of the pounding force values upon impact due to damping. Moreover, damping initiated the negative pounding forces before separation that pull the colliding structures. In the case of the nonlinear viscoelastic model, the pounding force-time curve is not easily diverged between the approaching and restitution phases of the

collision. The presence of different analytical models will provide the springboard to assess their relevance and efficacy in measuring the pounding phenomenon during earthquakes.

6.2 **Effectiveness of Different Models**

Various studies have been undertaken to determine the effectiveness of different pounding models. Komodromos et al. (2007) showed that the results of their study were similar to those of Anagnostopoulos (1988) and Jankowski (2005). Jankowski et al. (Jankowski 2008a; Jankowski et al. 2015; Mahmoud et al. 2008) concluded that the nonlinear viscoelastic model generated higher accuracy in predicting the impact force compared to the nonlinear elastic Hertz, Hertz-damp and linear viscoelastic models. Nevertheless, using the Hertz-damp model to determine the impact velocity yields higher accuracy than using the nonlinear viscoelastic model (Mahmoud et al. 2008). Khatiwada et al. (2013) concluded that the linear viscoelastic model, the modified Hertz-damp model and the nonlinear viscoelastic model were more accurate in computing the impact velocity, whereas the Hertz-damp model revealed inaccurate results. Mavronicola et al. (Mavronicola et al. 2015; Mavronicola et al. 2016) compared the efficiency of five impact models detailed in the research by (Anagnostopoulos 1988; Komodromos et al. 2007; Mahmoud & Jankowski 2011; Pant et al. 2010; Ye & Li 2009). The study outcomes indicated that the correctness of the various models depended on the analysis of the coefficient of restitution and the impact stiffness. Hence, no concluding statement will affirm one of the models as giving the most accurate results. There is a requirement for further investigation in usability and precision of the models.

Several experimental tests have been conducted to determine the validity of the models in terms of actual poundings between adjacent structures. There were a few shaking table trials administered to evaluate the efficacy of the models in terms of seismic pounding. Papadrakakis & Mouzakis (1995) conducted shaking table experiments on pounding between two 2-storey reinforced concrete buildings with zero-gap separation subject to sinusoidal and random motions. They compared the results with the predictions generated by the Lagrange multiplier method.

Shaking table test was conducted by Filiatrault et al. (1995) for pounding between adjacent 3-storey and 8-storey steel frame structures under the influence of the 1940 El Centro earthquake time history. Predictions generated by two computer programs served as the benchmark for the outcomes derived from the experiments.

Chau et al. (2003) conducted shaking table tests to examine the pounding force between two steel towers (2 metres tall), based on the harmonic excitation and ground motion from the El Centro earthquake. The experimental outcomes were compared with the theoretical prediction of nonlinear pounding using the Hertz contact law (nonlinear elastic model).

Jankowski (2007, 2010) performed an experiment to ascertain the interactions upon impact among a range of building materials, such as concrete, steel, timber and ceramic. The material's restitution coefficient was achieved through testing the impact of dropping balls. Crozet et al. (2019) executed comprehensive shaking table experiments and compared the results with the outcomes of the numerical analyses. Khatiwada et al. (2013) compared five impact force models over a comparative study. They compared the numerical simulation results with the experimental recorded displacement amplification of frames. The authors applied regular-shaped impacting slabs. The results revealed that the linear viscoelastic impact element generated positive outcomes.

This chapter aims to ascertain the efficiency of different analytical models in representing the pounding response of closely spaced adjacent structures. The adjoining structures are represented by a multiple degree of freedom (MDOF) model. Only the elastic system response is considered.

6.3 **Shaking Table Test**

6.3.1 Test Frames Set-up

As shown in Figures 3.9-3.11, the structural models were fixed and secured on the shaking table with the configuration of 15B-storey adjacent to 10-storey, 15B-storey adjacent to 5B-storey and 10-storey adjacent to 5B-storey. Subsequently, the accelerometers and laser displacement (LD) sensors were installed. An additional force sensor was mounted at the contact level of impact. The impact pounding force, acceleration and displacement response data were obtained using the sensors. The results of the shaking table tests were applied to the scaled earthquake acceleration records (Figures 3.10(b), 3.11(b), 3.12(b) and 3.13(b)). The reference frames are based outside the shaking table. Hence, the recorded displacements are the absolute displacement time history.

6.3.2 Test Program

The adjacent pairs of 10-storey and 5B-storey steel frames were tested by applying the scaled El Centro, Hachinohe, Northridge and Kobe earthquakes, with separation gaps of 6 mm, 6 mm, 20 mm and 25 mm, respectively. The separation gaps for the adjacent pairs of 15B-storey and 5B-storey structures, when applying the scaled El Centro, Hachinohe,

Northridge and Kobe earthquakes, were 11 mm, 11 mm, 20 mm and 17 mm, respectively. Moreover, the adjacent pairs of 15B-storey and 10-storey frames were tested by applying El Centro, Hachinohe, Northridge and Kobe earthquakes, with separation distances equal to 12 mm, 22 mm, 44 mm and 21 mm, respectively. It is worth mentioning that the separation distances were chosen based on the findings in Chapter 4. To detect pounding without causing any instability in the structure and to keep the elastic system response, the gaps were carefully chosen. It should be noted that no significant torsional motion was observed in any of the tests.

6.4 **Experimental Results**

A total of 45 pounding experiments were carried out on the adjacent structural steel models under various input excitations and separation gaps. To capture the pounding force, displacement and acceleration accurately, the researchers utilised a data sampling rate of 10,000 per second. The results of the shaking table tests excited under the effect of four scaled ground motion records in terms of impact force time history are presented in Figures 6.1–6.3.

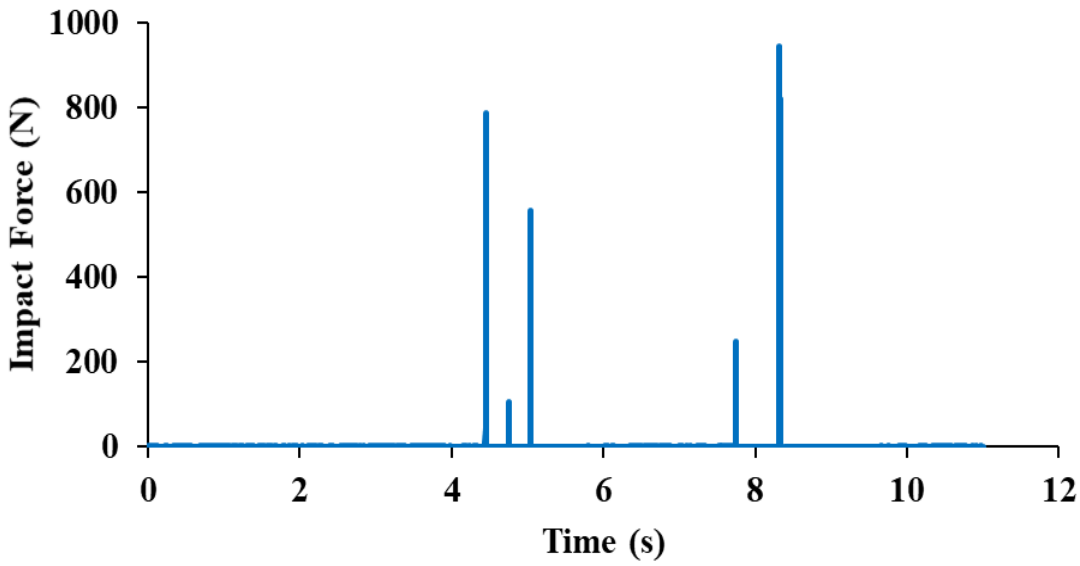

Figure 6.1(a) Fifth floor impact time histories for pounding between 10-storey frame adjacent to 5B-storey frame under scaled El Centro earthquake

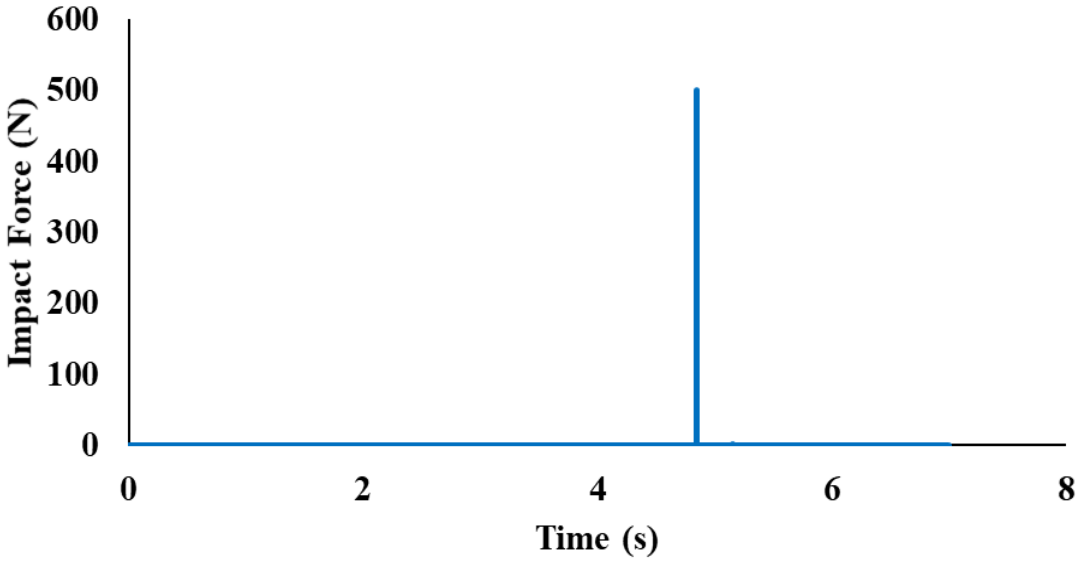

Figure 6.1(b) Fifth floor impact time histories for pounding between 10-storey frame adjacent to 5B-storey frame under scaled Hachinohe earthquake

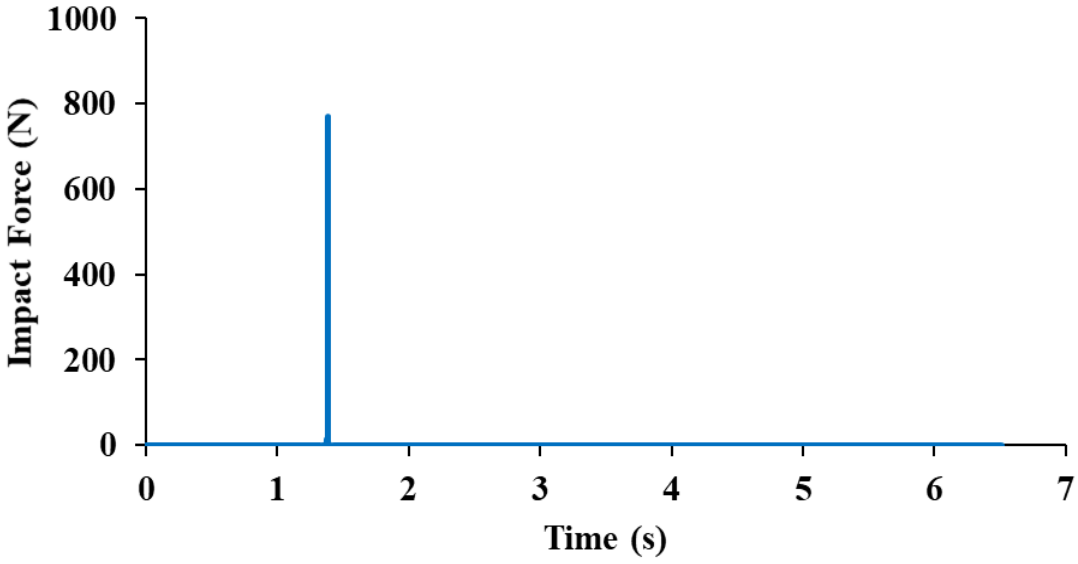

Figure 6.1(c) Fifth floor impact time histories for pounding between 10-storey frame adjacent to 5B-storey frame under scaled Northridge earthquake

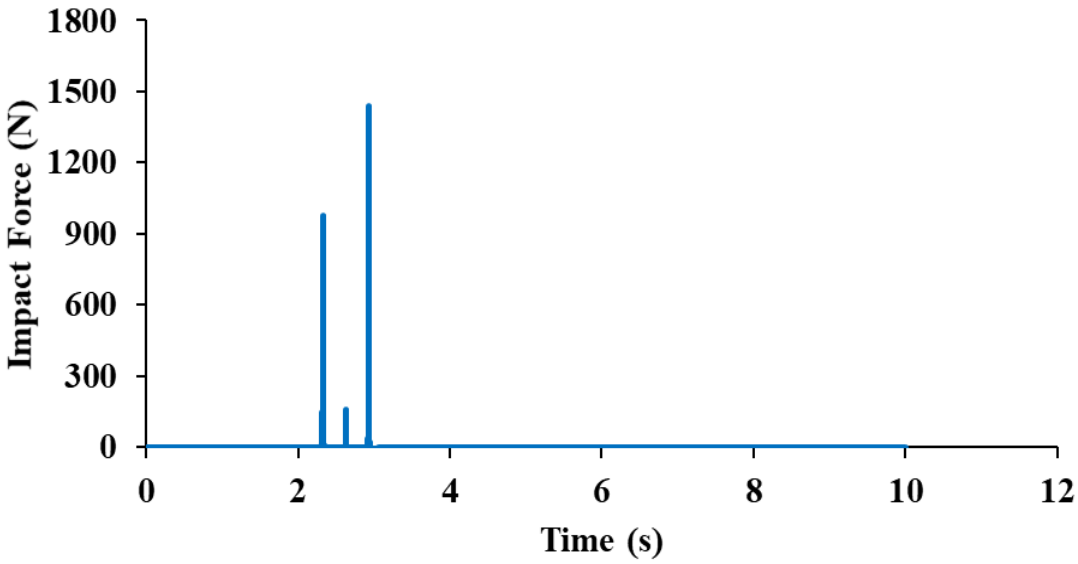

Figure 6.1(d) Fifth floor impact time histories for pounding between 10-storey frame adjacent to 5B-storey frame under scaled Kobe earthquake

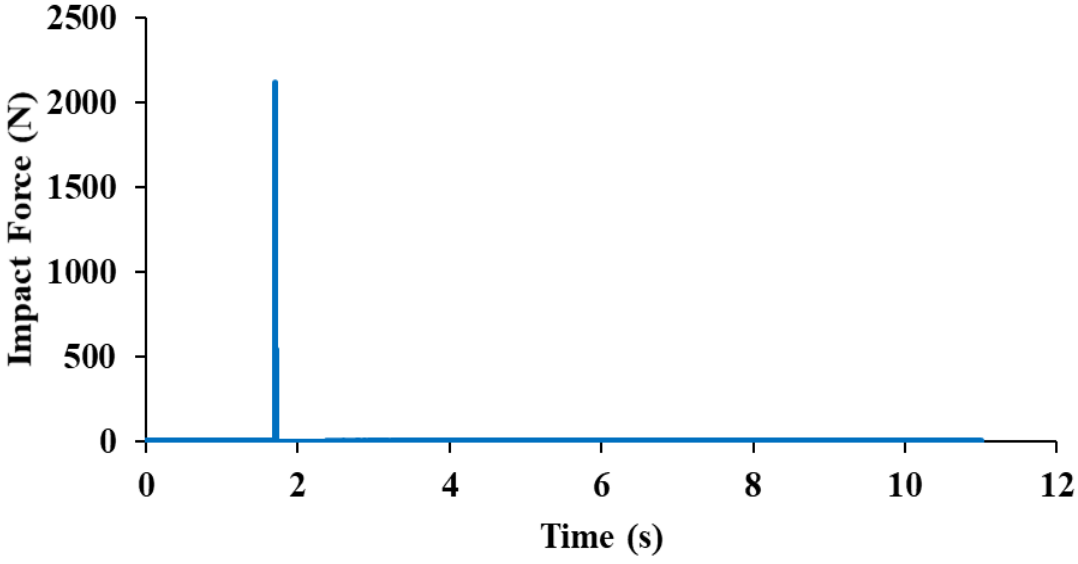

Figure 6.2(a) Fifth floor impact time histories for pounding between 15B-storey frame adjacent to 5B-storey frame under scaled El Centro earthquake

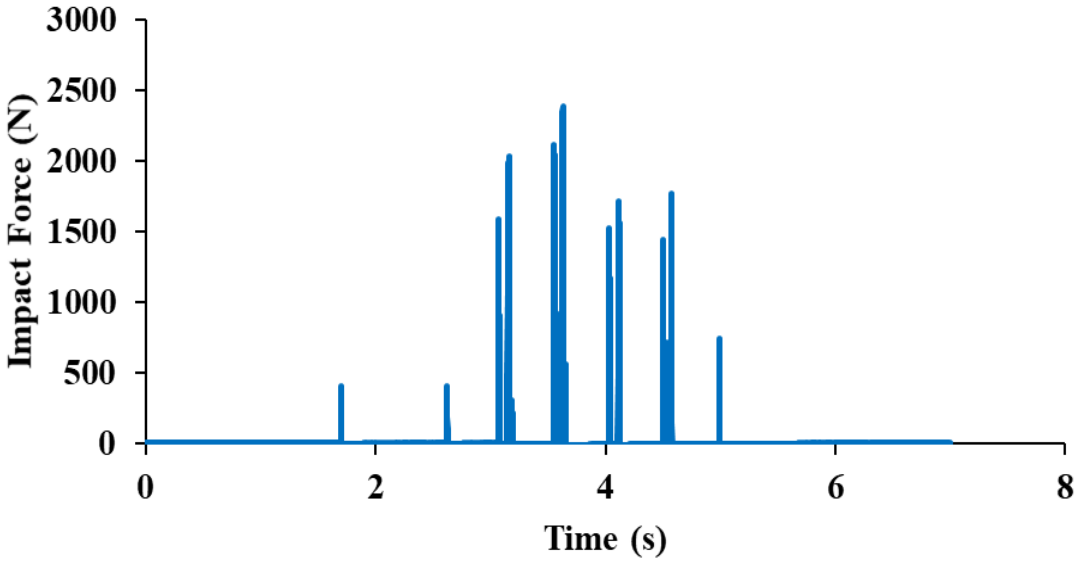

Figure 6.2(b) Fifth floor impact time histories for pounding between 15B-storey frame adjacent to 5B-storey frame under scaled Hachinohe earthquake

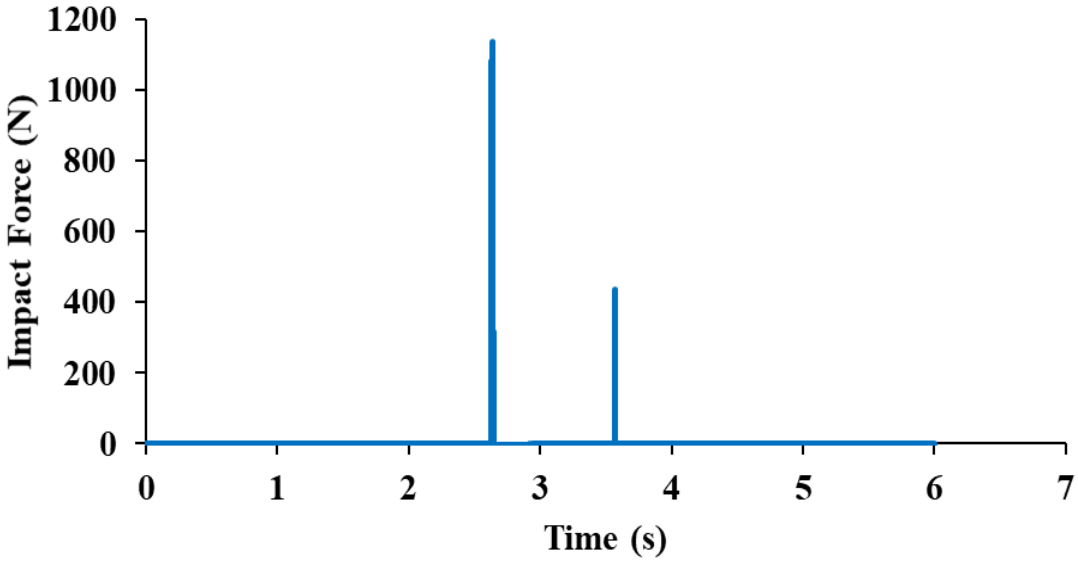

Figure 6.2(c) Fifth floor impact time histories for pounding between 15B-storey frame adjacent to 5B-storey frame under scaled Northridge earthquake

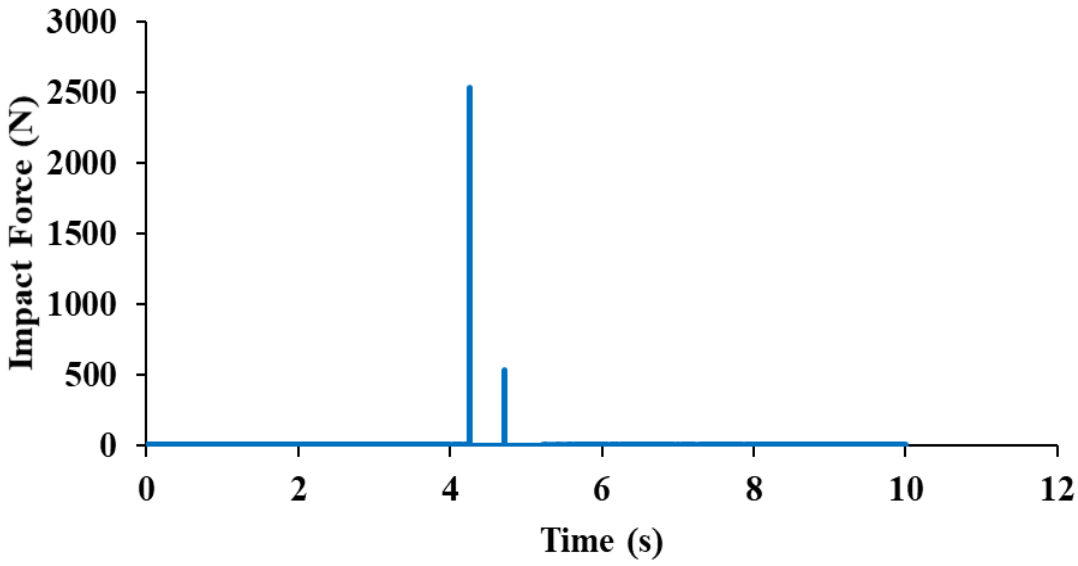

Figure 6.2(d) Fifth floor impact time histories for pounding between 15B-storey frame adjacent to 5B-storey frame under scaled Kobe earthquake

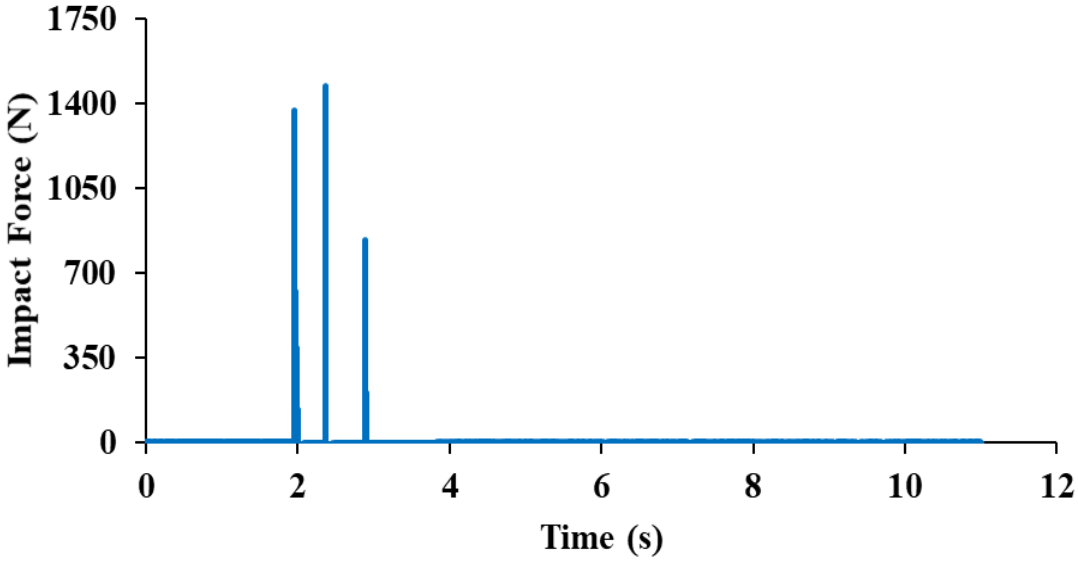

Figure 6.3(a) Tenth floor impact time histories for pounding between 15B-storey frame adjacent to 10-storey frame under scaled El Centro earthquake

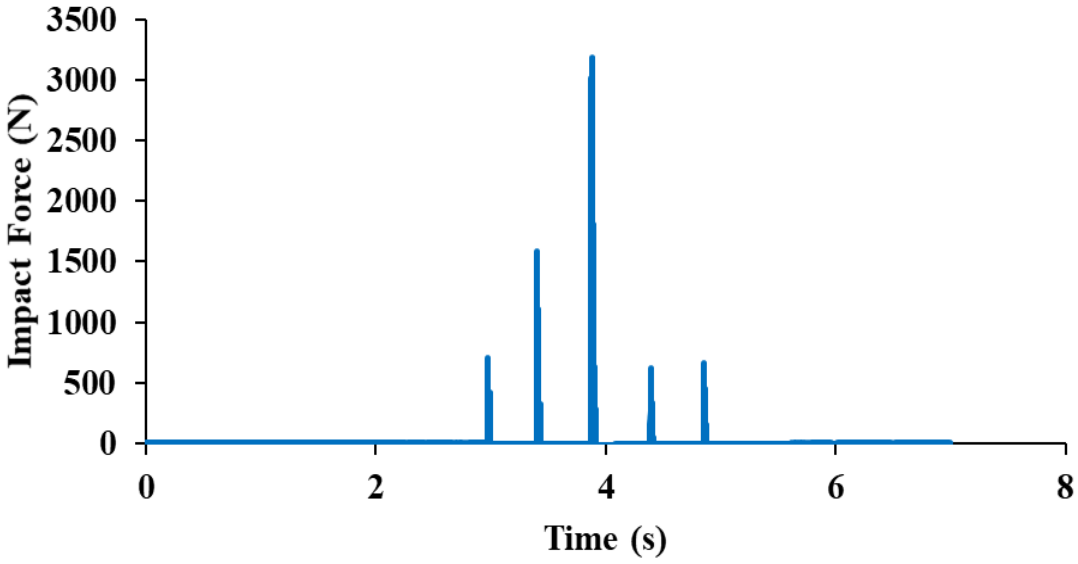

Figure 6.3(b) Tenth floor impact time histories for pounding between 15B-storey frame adjacent to 10-storey frame under scaled Hachinohe earthquake

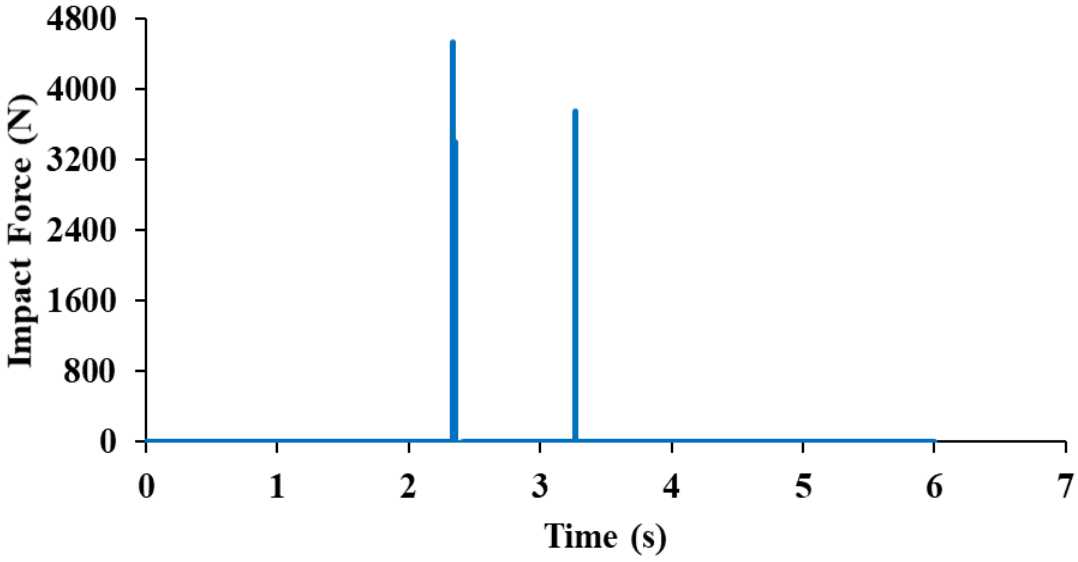

Figure 6.3(c) Tenth floor impact time histories for pounding between 15B-storey frame adjacent to 10-storey frame under scaled Northridge earthquake

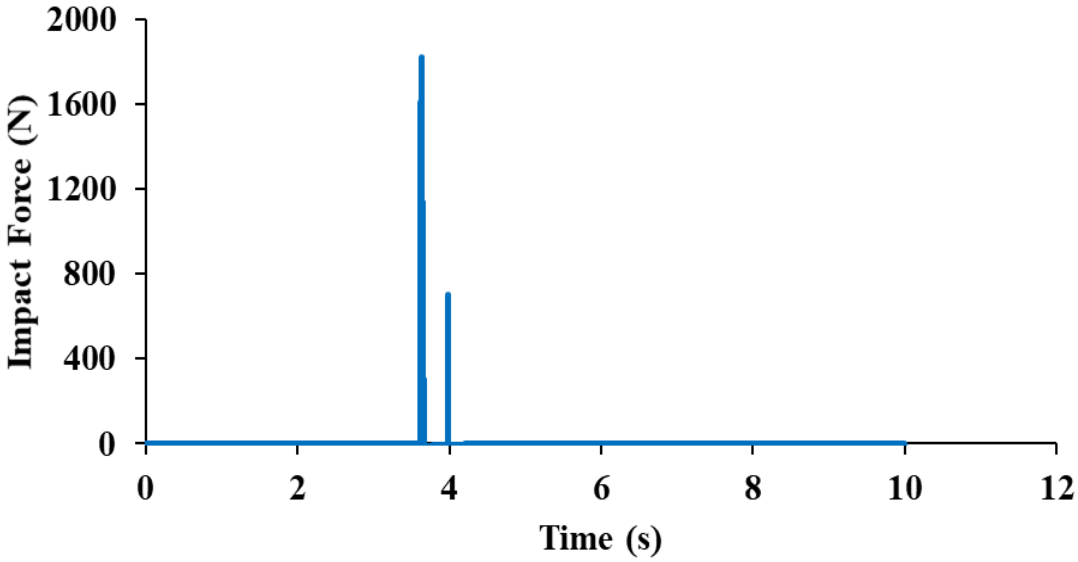

Figure 6.3(d) Tenth floor impact time histories for pounding between 15B-storey frame adjacent to 10-storey frame under scaled Kobe earthquake

6.5 **Numerical Simulation**

Pounding between the adjacent frames was modelled using five different contact element models: linear spring, linear viscoelastic, Hertz, nonlinear viscoelastic and Hertz-damp. To compare the outcomes of the contact force–based models, the impact stiffness parameters were carefully selected.

According to Chapter 5, for the linear spring and linear viscoelastic models, the stiffness value of the contact element k ($k = 20660\ N/mm$) is used in the numerical simulation. Moreover, the dashpot coefficient C, the coefficient of restitution e and the impact damping ratio ξ used for the linear viscoelastic model are as follows:

$C - experiment = 1255\ kg/s$

$\xi = 0.078407$

$r = 0.810154$

Furthermore, the impact stiffness parameter, k_h, for the Hertz and Hertz-damp models was obtained based on the material properties of the colliding structures and the contact surface geometry. In this experiment, contact surface was between steel plate of 5 mm thickness and the force sensor impact cap, as shown in Figure 3.19. The impact surface area is $63.5\ mm^2$ and the radius $R = 4.49\ mm$. The Poisson's ratio and modulus of elasticity of the impact cap are $\rho = 0.272$ and $E = 1.965 \times 10^5 MPa$, respectively

(STAINLESS 2021). The Poisson's ratio and modulus of elasticity of the steel plate are $\rho = 0.3$ and $E = 2 \times 10^5 MPa$, respectively (AS/NZS3678 2011). Therefore, based on Equation 2.10, the impact stiffness parameter $k_h = 9.772 \times 10^8 N/m^{1.5}$. The impact damping ratio time history ξ_h was obtained using Equation 2.18. (See Appendix F for a detailed drawing of the force sensor.)

Additionally, the impact stiffness parameter β for the nonlinear viscoelastic model was extracted from the experimental study carried out by Jankowski (2008a), where $\beta = 6.6 \times 10^{10} N/m^{1.5}$. Thus, the impact stiffness parameter β adopted for this study $= 6.6 \times 10^{10} \times \frac{1}{30} = 2.2 \times 10^9 N/m^{1.5}$. Using Equation 2.14 with similar steps, the impact damping ratio ξ of the linear viscoelastic model was computed as $\bar{\xi} = 0.193872$. Table 6.1 illustrates the impact stiffness parameters of the contact force–based models.

Table 6.1 Experimental values for the theoretical impact model parameters

Impact Model	Impact Stiffness	Impact Damping ratio	Coefficient of Restitution
Linear spring	20.66×10^6	-	-
Linear viscoelastic	20.66×10^6	0.078407	0.810154
Hertz	9.772×10^8	-	-
Nonlinear viscoelastic	2.2×10^9	0.193872	0.810154
Hertz-damp	9.772×10^8	-	0.810154

Notes: The units of the impact stiffness are N/m for the linear spring model and linear viscoelastic model and $N/m^{1.5}$ for the Hertz model, nonlinear viscoelastic model and Hertz-damp model.

6.6 Comparison between Numerical and Experimental Results

6.6.1 General Comparison

Having determined the impact stiffness parameters of the contact force–based models (see Table 6.1), impact force time history was computed using Equations 2.4, 2.5, 2.9, 2.12 and 2.15 for the linear spring, linear viscoelastic, Hertz, nonlinear viscoelastic and Hertz-damp models, respectively, as shown in Figures 6.4–6.6. This calculation was carried out using the Excel spreadsheet and the time step for this analysis was taken as 1×10^{-4} s. It can be observed that the analytical results closely match the experimental results, as shown in Figures 6.4–6.6, in terms of the number and exact time of impact. However, the impact force values were different.

To compare experimental impact force with theoretical force, very short time intervals were considered. These are shown in Figures 6.7–6.9. The figures illustrate the normal contact force for experimental and theoretical results within a short time. They show a

comparison between the experimental pounding force time histories and those of the predicted method using the different models. The pounding is assessed by the occurrence of far-field and near-field earthquakes.

The results show that the models did not accurately predict the pounding forces in most cases. This difference can be attributed to the difficulty of estimating the dynamic properties of the structures and accurately reproducing the contact behaviour (despite several models having been considered). Moreover, forces created by collisions generate stress waves, which propagate away from the contact region. It is difficult to analyse this problem mathematically owing to the complexity in energy transfer process during a collision (Cole et al. 2011b; Goldsmith 2001b).

The predicted trend corresponds with the experimental trend. The overestimation may be attributed to the selection of the model parameters and the prediction results may be enhanced by using optimisation techniques (Luenberger & Ye 1984). Nevertheless, the linear viscoelastic model yields the best predictions of all the models studied.

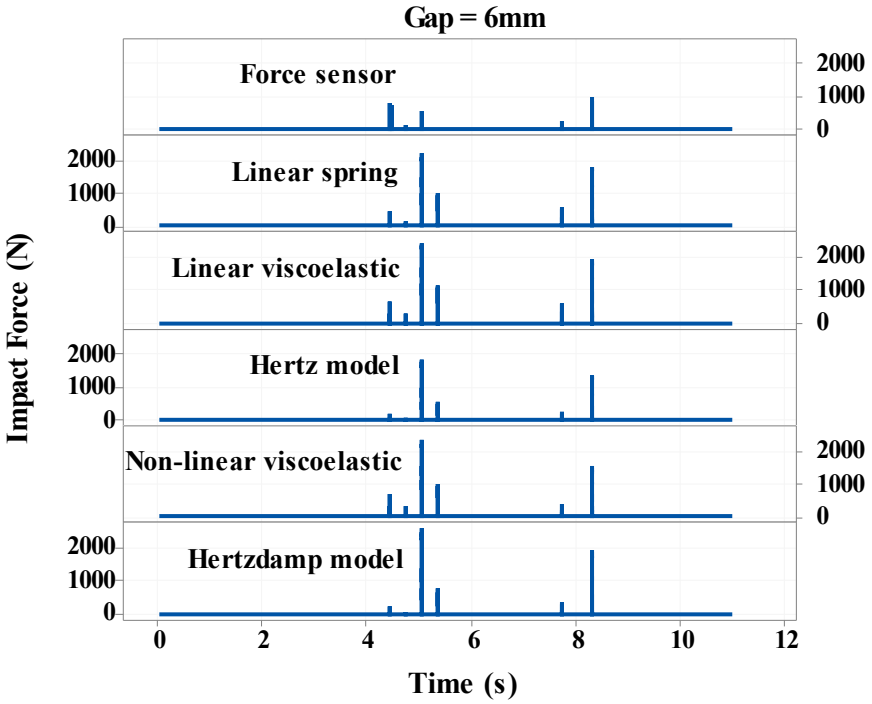

Figure 6.4(a) Experimental and theoretical impact force for pounding between 10-storey adjacent frame to 5B-storey frame (5th floor) under scaled El Centro earthquake

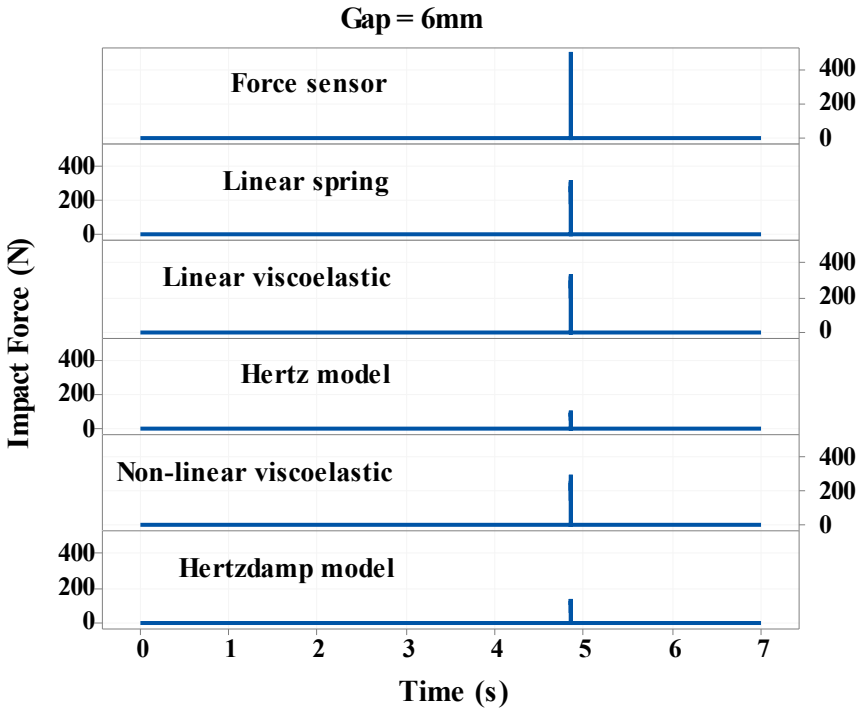

Figure 6.4(b) Experimental and theoretical impact force for pounding between 10-storey frame adjacent to 5B-storey frame (5th floor) under scaled Hachinohe earthquake

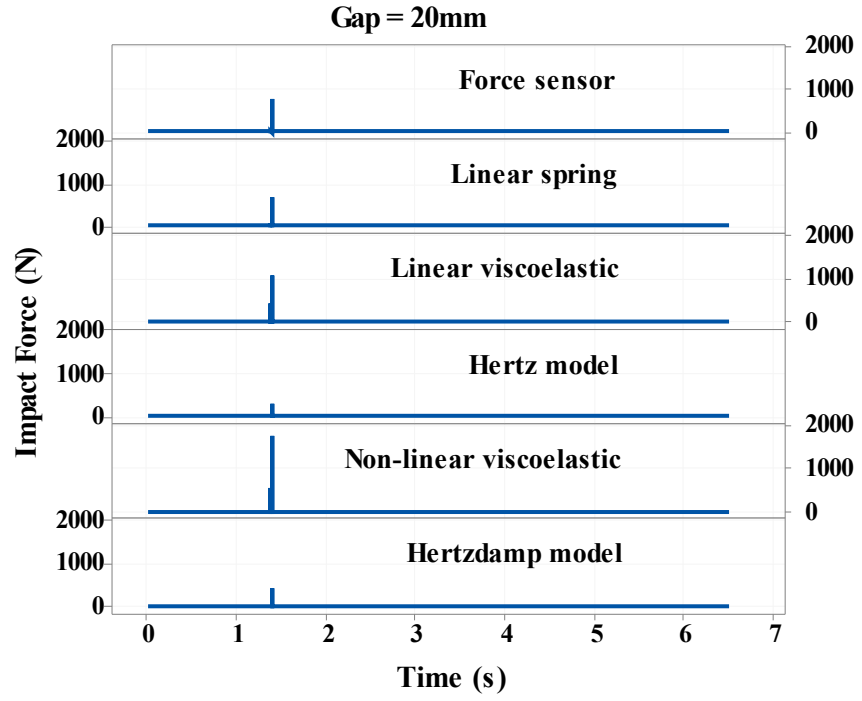

Figure 6.4(c) Experimental and theoretical impact force for pounding between 10-storey frame adjacent to 5B-storey frame (5th floor) under scaled Northridge earthquake

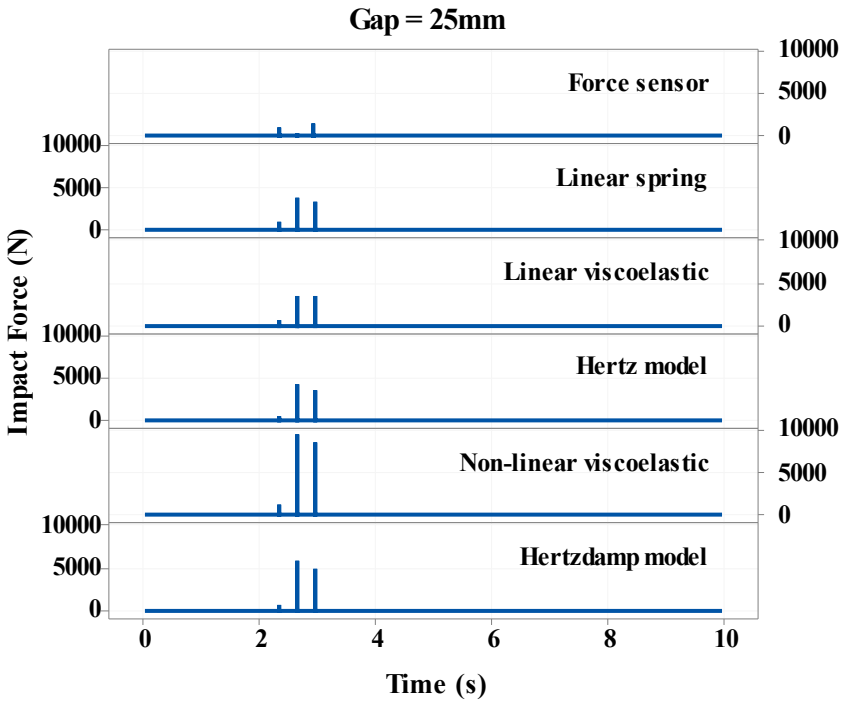

Figure 6.4(d) Experimental and theoretical impact force for pounding between 10-storey frame adjacent to 5B-storey frame (5th floor) under scaled Kobe earthquake

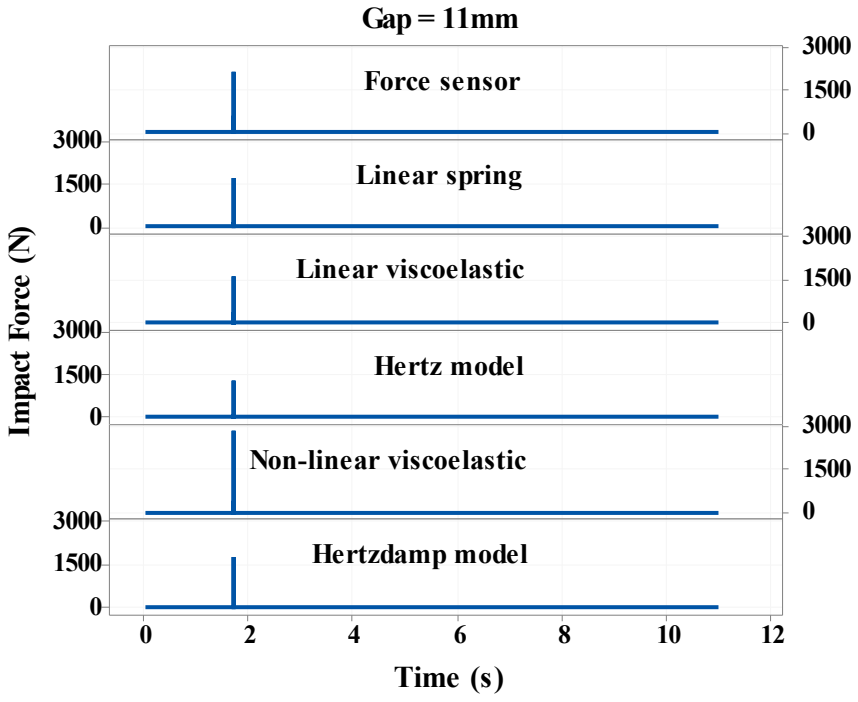

Figure 6.5(a) Experimental and theoretical impact force for pounding between 15B-storey frame adjacent to 5B-storey frame (5th floor) under scaled El Centro earthquake

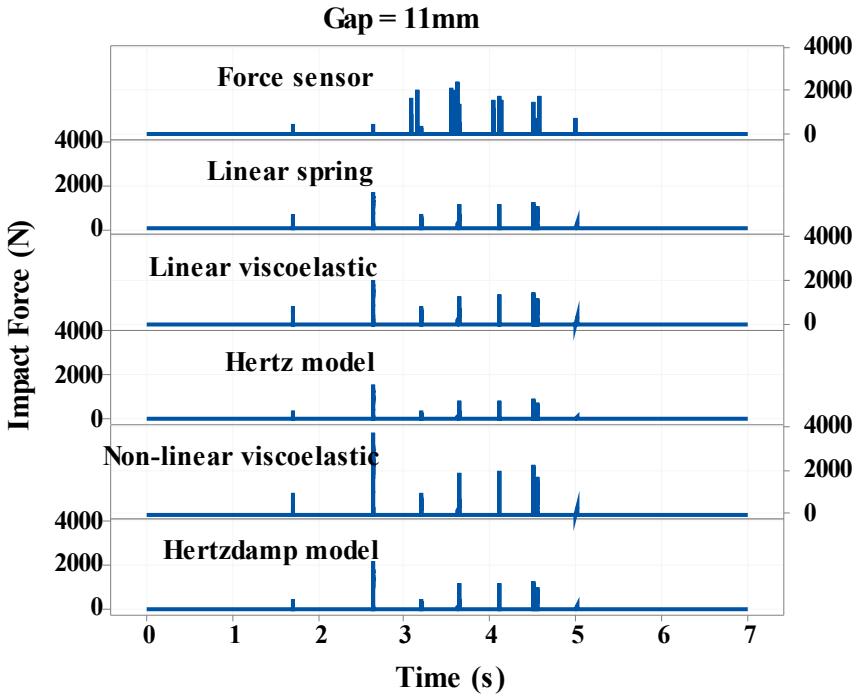

Figure 6.5(b) Experimental and theoretical impact force for pounding between 15B-storey frame adjacent to 5B-storey frame (5th floor) under scaled Hachinohe earthquake

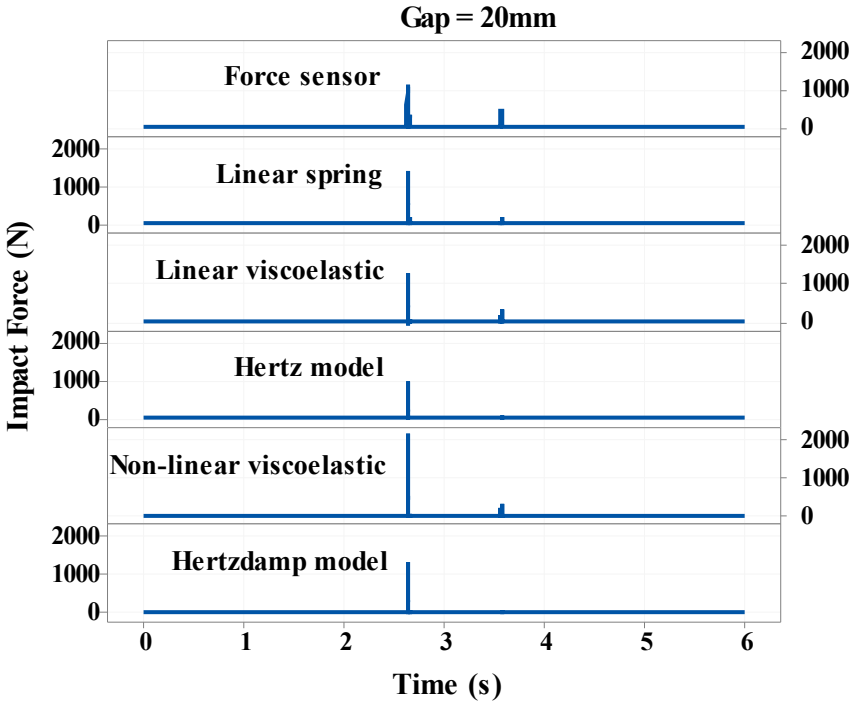

Figure 6.5(c) Experimental and theoretical impact force for pounding between 15B-storey frame adjacent to 5B-storey frame (5th floor) under scaled Northridge earthquake

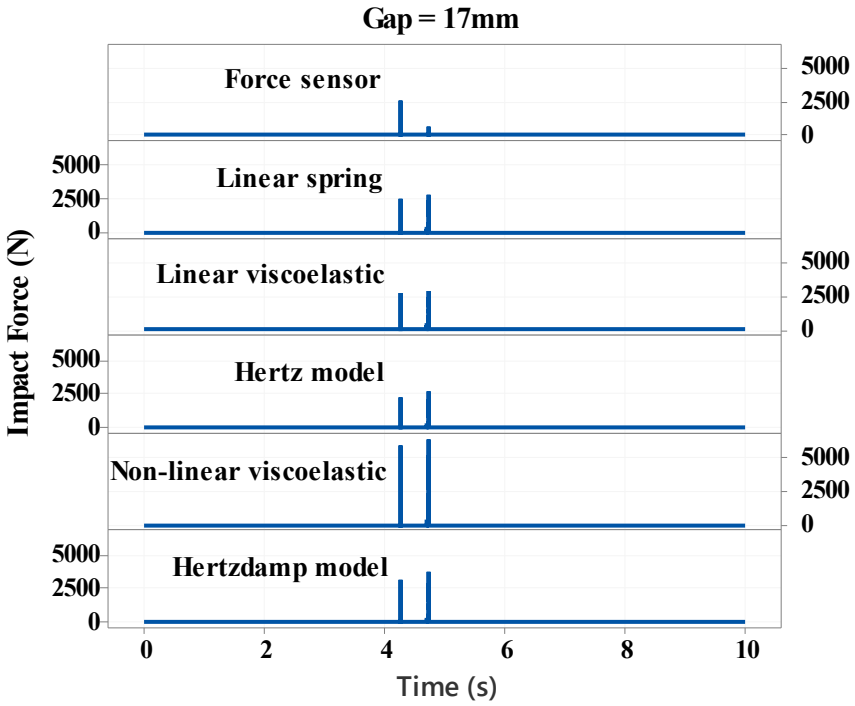

Figure 6.5(d) Experimental and theoretical impact force for pounding between 15B-storey frame adjacent to 5B-storey frame (5th floor) under scaled Kobe earthquake

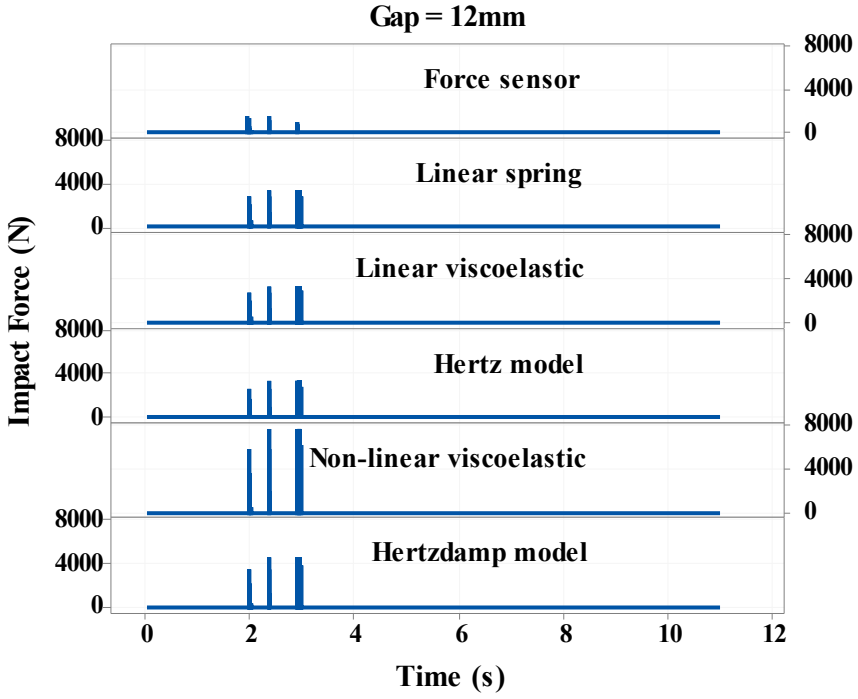

Figure 6.6(a) Experimental and theoretical impact force for pounding between 15B-storey frame adjacent to 10-storey frame (10th floor) under scaled El Centro earthquake

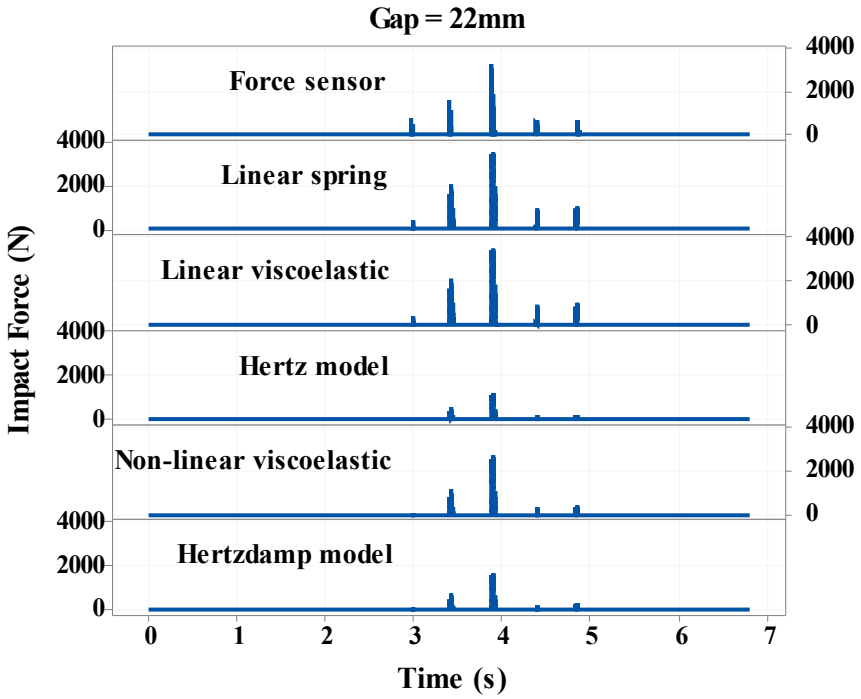

Figure 6.6(b) Experimental and theoretical impact force for pounding between 15B-storey frame adjacent to 10-storey frame (10th floor) under scaled Hachinohe earthquake

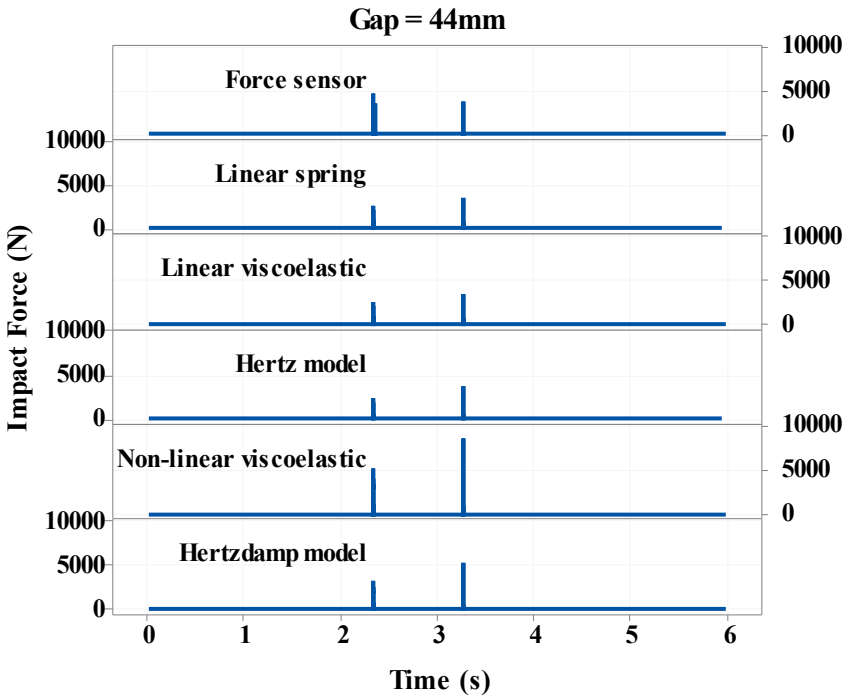

Figure 6.6(c) Experimental and theoretical impact force for pounding between 15B-storey frame adjacent to 10-storey frame (10th floor) under scaled Northridge earthquake

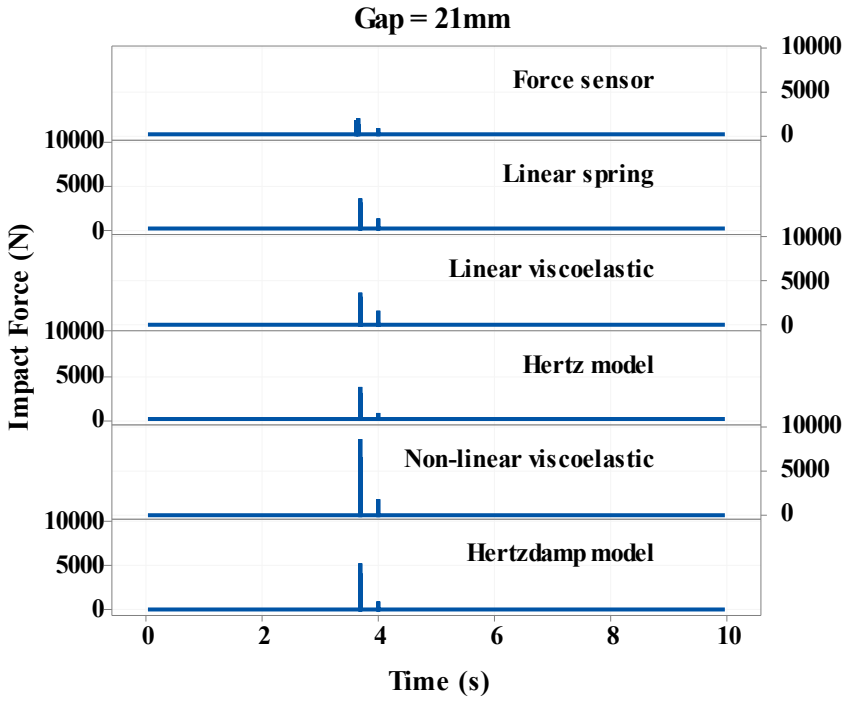

Figure 6.6(d) Experimental and theoretical impact force for pounding between 15B-storey frame adjacent to 10-storey frame (10th floor) under scaled Kobe earthquake

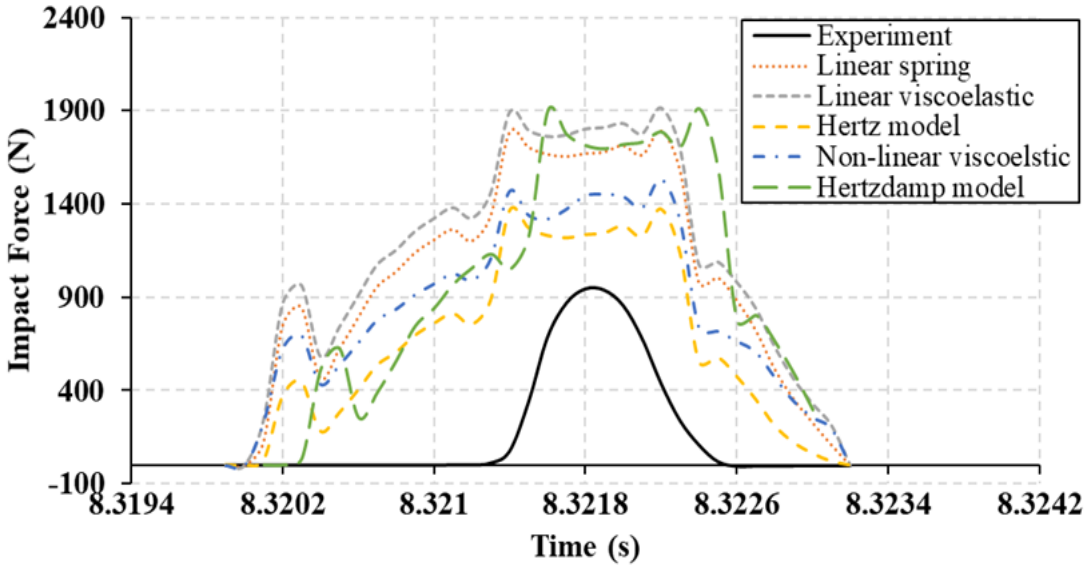

Figure 6.7(a) Experimental and theoretical normal contact force for pounding between 10-storey frame adjacent to 5B-storey frame (5th floor) under scaled El Centro earthquake

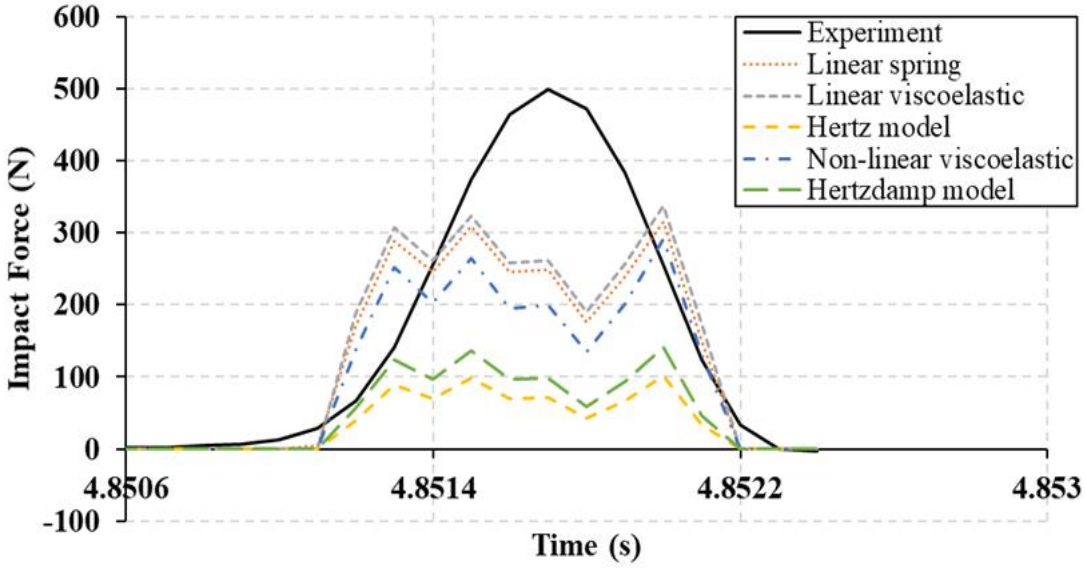

Figure 6.7(b) Experimental and theoretical normal contact force for pounding between 10-storey frame adjacent to 5B-storey frame (5th floor) under scaled Hachinohe earthquake

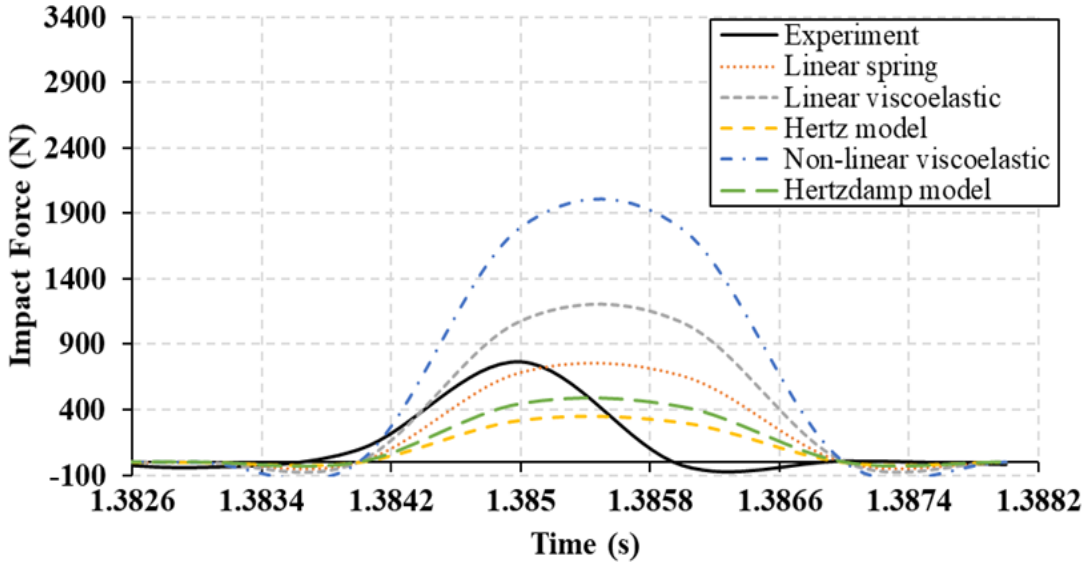

Figure 6.7(c) Experimental and theoretical normal contact force for pounding between 10-storey frame adjacent to 5B-storey frame (5th floor) under scaled Northridge earthquake

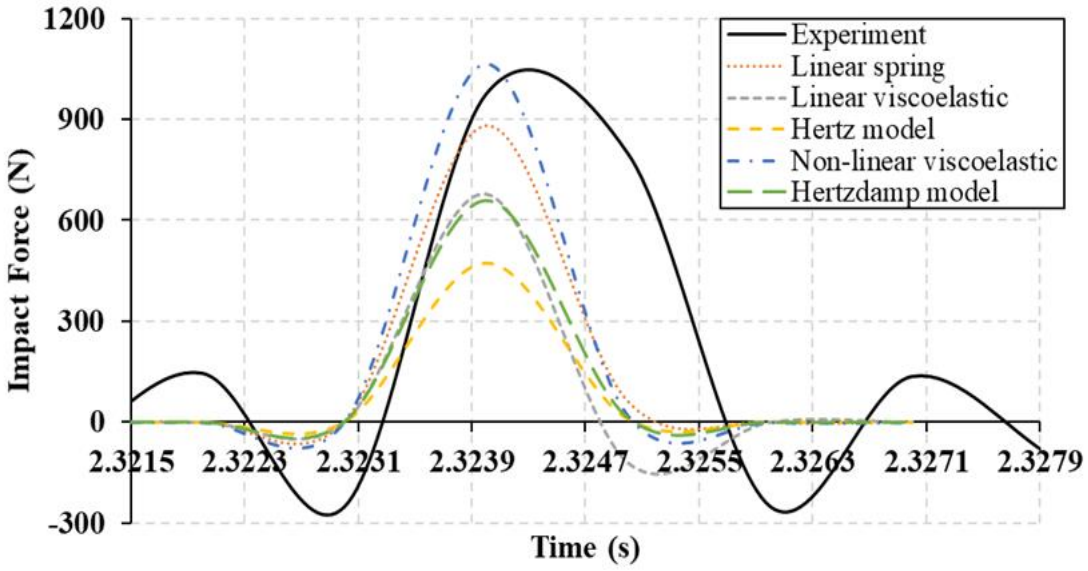

Figure 6.7(d) Experimental and theoretical normal contact force for pounding between 10-storey frame adjacent to 5B-storey frame (5th floor) under scaled Kobe earthquake

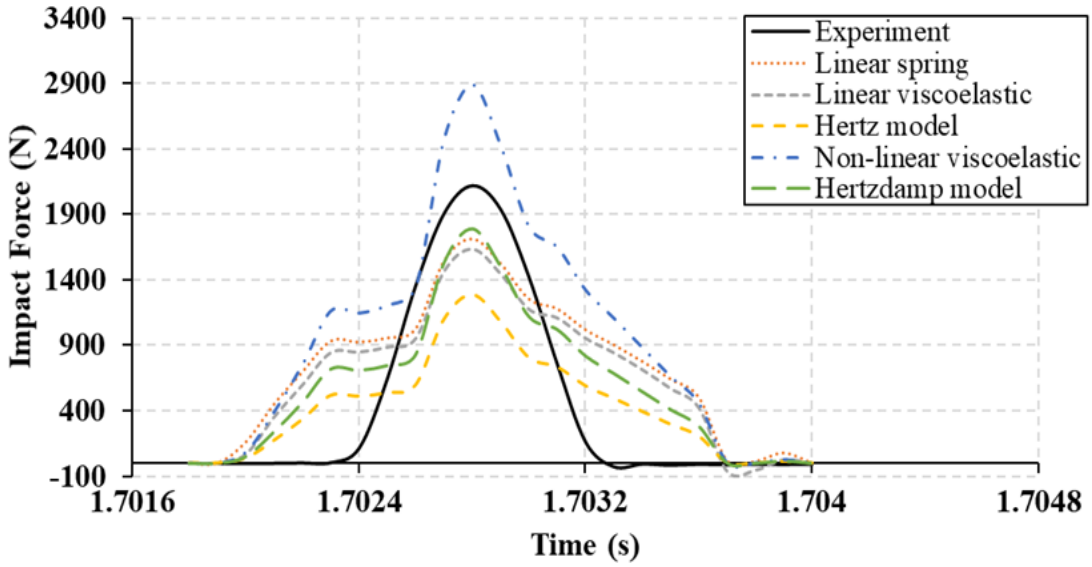

Figure 6.8(a) Experimental and theoretical normal contact force for pounding between 15B-storey frame adjacent to 5B-storey frame (5th floor) under scaled El Centro earthquake

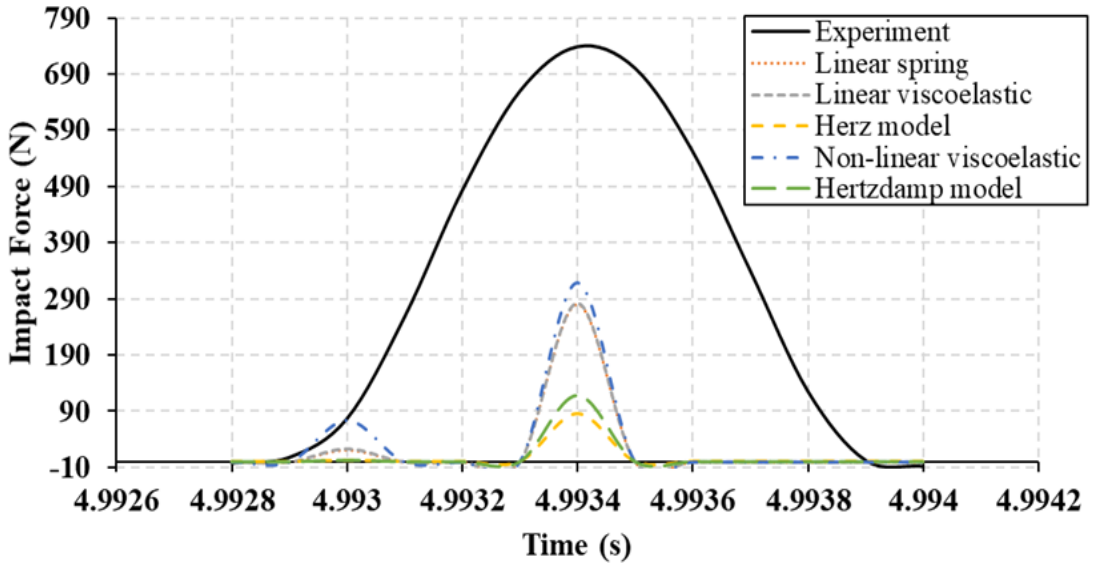

Figure 6.8(b) Experimental and theoretical normal contact force for pounding between 15B-storey frame adjacent to 5B-storey frame (5th floor) under scaled Hachinohe earthquake

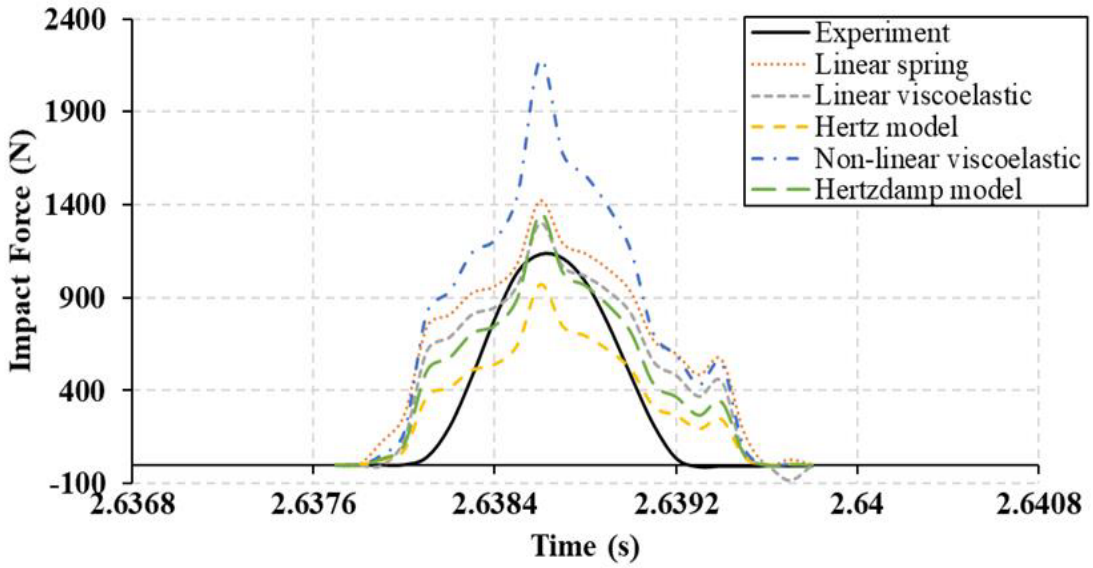

Figure 6.8(c) Experimental and theoretical normal contact force for pounding between 15B-storey frame adjacent to 5B-storey frame (5th floor) under scaled Northridge earthquake

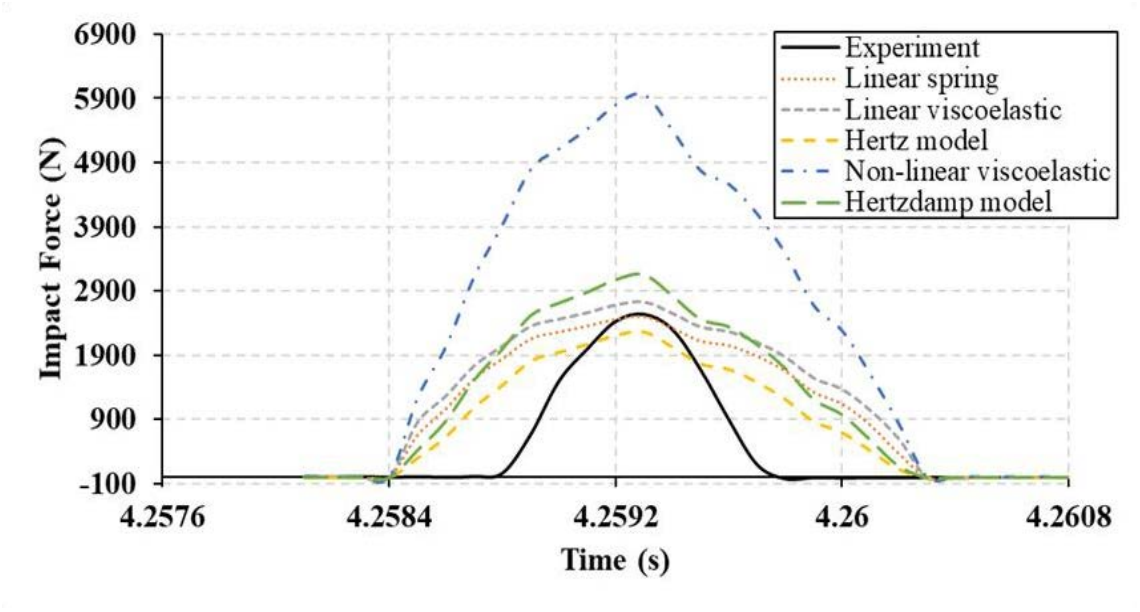

Figure 6.8(d) Experimental and theoretical normal contact force for pounding between 15B-storey frame adjacent to 5B-storey frame (5th floor) under scaled Kobe earthquake

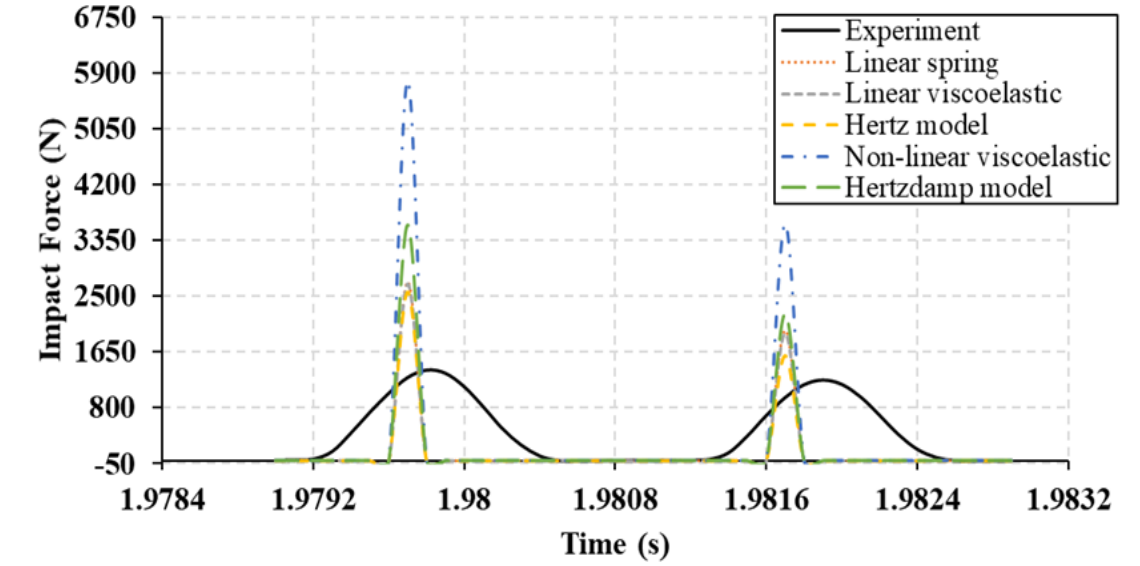

Figure 6.9(a) Experimental and theoretical normal contact force for pounding between 15B-storey frame adjacent to 10-storey frame (10th floor) under scaled El Centro earthquake

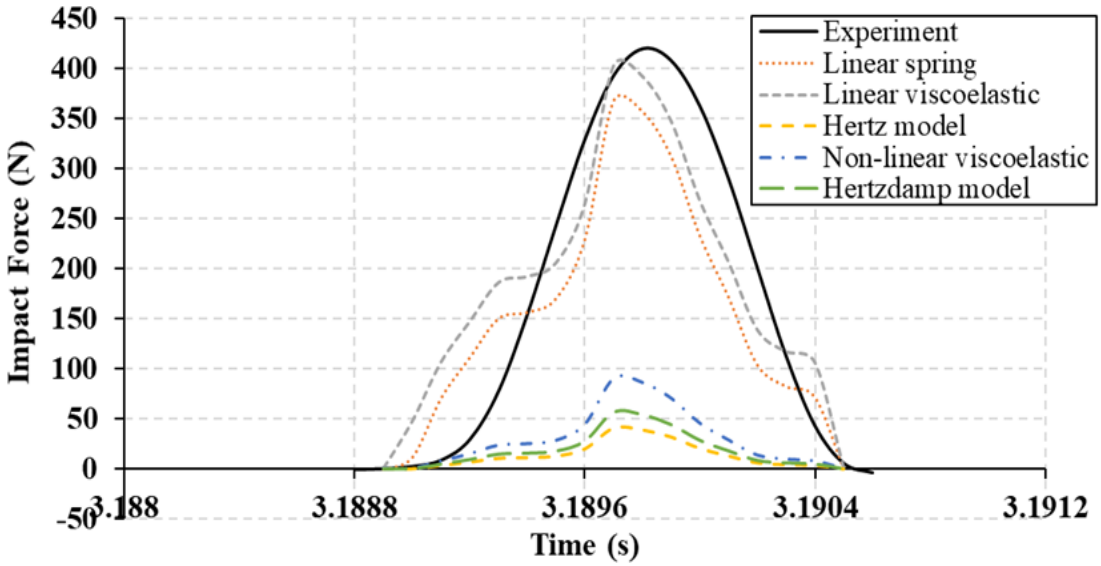

Figure 6.9(b) Experimental and theoretical normal contact force for pounding between 15B-storey frame adjacent to 10-storey frame (10th floor) under scaled Hachinohe earthquake

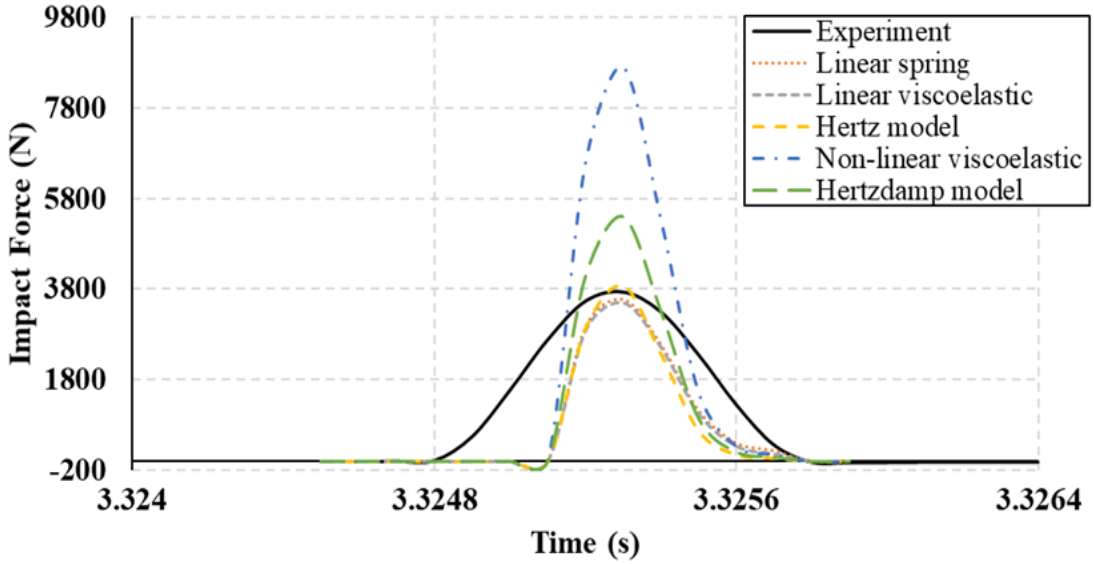

Figure 6.9(c) Experimental and theoretical normal contact force for pounding between 15B-storey frame adjacent to 10-storey frame (10th floor) under scaled Northridge earthquake

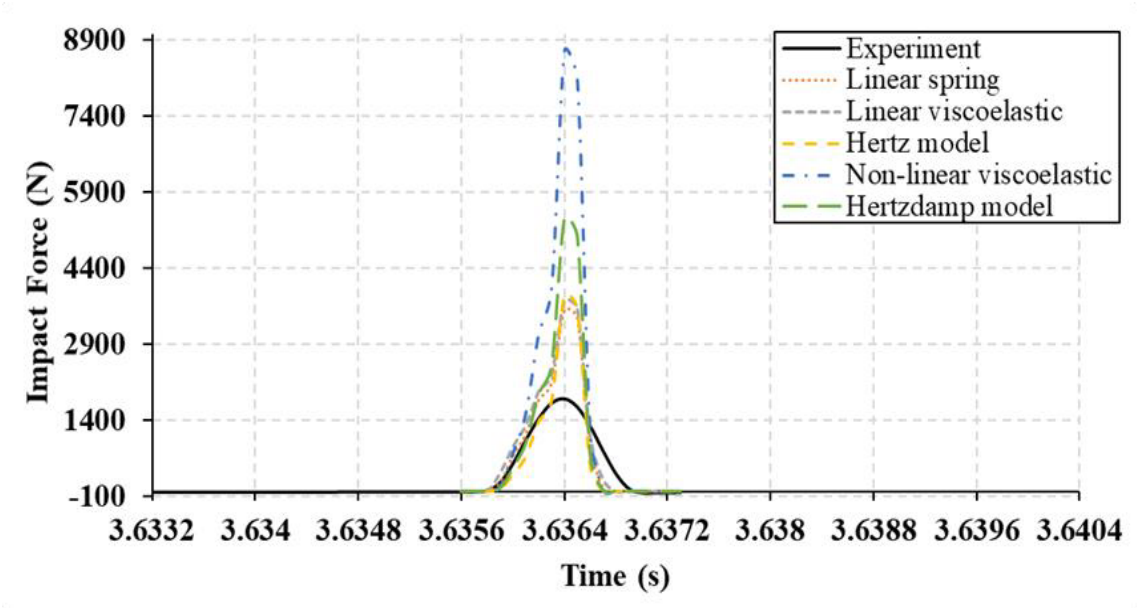

Figure 6.9(d) Experimental and theoretical normal contact force for pounding between 15B-storey frame adjacent to 10-storey frame (10th floor) under scaled Kobe earthquake

6.6.2 Comparison between Models

To select the best model, there is a need to compare the results between the theoretical impact element models with the experimental measurement. The Kolmogorov–Smirnov test was used for comparing results (Chakravarti et al. 1967, pp. 392-4).

This statistical approach was used to compare all the available impact force intervals along the time axis. The cumulative distributions for experimental measurement [$F(t_i)_e = F(t_{i-1})_e + dF(t_i)_e$, where: t_i is the ith time instant; dF_e is the impact force increment; F is the impact force; and subscript e represents the experimental data] and theoretical results [$F(t_i)_t = F(t_{i-1})_t + dF(t_i)_t$, where subscript t represents the theoretical results] were calculated, followed by the absolute difference (D) between them [$D(t_i) = |F(t_i)_t - F(t_i)_e|$]. For each theoretical model, the maximum difference was computed; this is known as the dissimilarity value [DV; $DV = \max (D(t_i))$ for $t_i = 0$ to t_f, where t_f is the final time]. This is a relatively robust measure of (dis-)similarity between two distributions. The lesser the dissimilarity, the more the curves are 'alike'.

As an example of this statistical method, Figure 6.10(a) shows a chosen interval from fifth floor impact between adjacent 15B-storey and 5B-storey frames under the Northridge acceleration record. Figure 6.10(b) reveals the cumulative values for each function; the dissimilarity values were 1535, 782, 2598, 597 and 2449 for the linear spring, linear viscoelastic, Hertz, nonlinear viscoelastic and Hertz-damp impact models, respectively. The nonlinear viscoelastic model has the lowest dissimilarity value, while

the Hertz model has the highest dissimilarity value. This means that the nonlinear viscoelastic curve is more similar to the experimental curve than the linear viscoelastic, linear spring, Hertz-damp and Hertz curves.

The same steps have been conducted for all intervals in all cases. Table 6.2 presents the dissimilarity values computed using the Kolmogorov–Smirnov method.

It is noted that there was no regular pattern identified among the models. Manual ranking was conducted for each case to determine the model with the lowest dissimilarity value. The model with the lowest dissimilarity value was ranked 1 and the one with the highest dissimilarity value was ranked 5. The sum value of all rankings under each model was calculated. The smallest sum was considered to be the most accurate and best performing model. As can be seen in Table 6.3, the smallest summation is 97 and was derived by the linear viscoelastic model. Other values of 105, 132, 130 and 136 were obtained from the linear spring, Hertz, Hertz-damp and nonlinear viscoelastic models, respectively. Previous studies revealed that the linear viscoelastic element model produces the most reliable results with fewer difficulties in numerical solution conversions, consistent with this study (Anagnostopoulos 1995; Khatiwada et al. 2013; Mate et al. 2012; Pant et al. 2010).

The linear spring model is ranked second. The model is simple and can easily be implemented in commercial software. However, the dissipated energy during impact will not be incorporated in the linear spring model. Due to high coefficients of restitution for steel-to-steel impact in this experiment ($e = 0.81$), both linear spring and linear viscoelastic models show close results and ranking. The same observation was made for the Hertz and Hertz-damp models. This is expected because the models were originally intended for highly elastic impact (high value of coefficient of restitution) (Muthukumar & Desroches 2006).

The nonlinear viscoelastic model ranked last in this comparative study. The impact stiffness parameter β used in this model was extracted from Janskowski's study as there is no clear procedure of deriving this parameter, unlike the impact stiffness parameters k and k_h, which were derived directly from this experiment. Jankowski et al. (Jankowski 2008a; Jankowski et al. 2015; Mahmoud et al. 2008) determined that the nonlinear viscoelastic model has better accuracy in predicting the impact force compared with the other models. The iterative procedure determined the impact stiffness parameter β by

equalising the maximum impact force calculated numerically vis-à-vis with the computed experimental value.

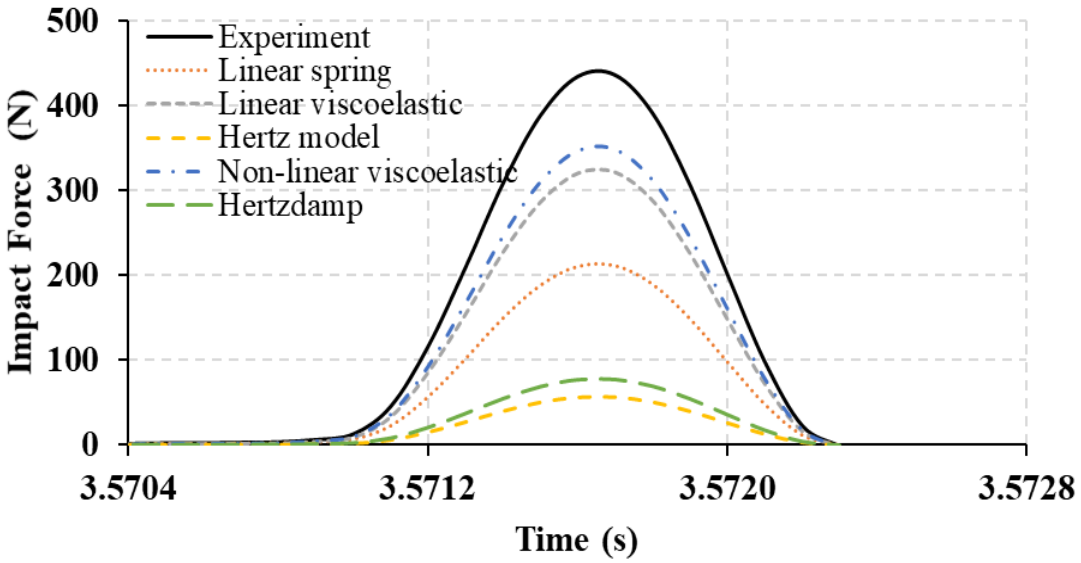

Figure 6.10(a) Experimental and theoretical normal contact force for pounding between adjacent 15B-storey and 5B-storey frames (5th floor) under scaled Northridge earthquake

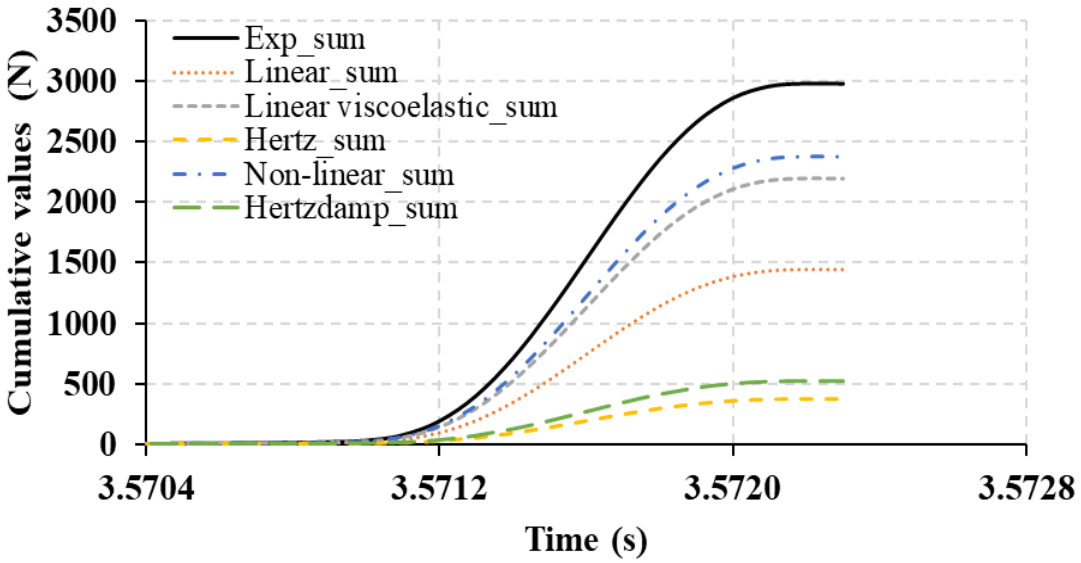

Figure 6.10(b) Cumulative values for experimental and theoretical normal contact force for pounding between adjacent 15B-storey and 5B-storey (5th floor) frames under scaled Northridge earthquake, using Kolmogorov–Smirnov test

Table 6.2 Dissimilarity values calculated by Kolmogorov–Smirnov test, units in N

		Earthquake									
		Dissimilarity values under El Centro					Dissimilarity values under Hachinohe				
	No. of Impact	Linear	Linear viscoelastic	Hertz model	Nonlinear viscoelastic	Hertz-damp	Linear	Linear viscoelastic	Hertz model	Nonlinear viscoelastic	Hertz-damp
10-storey adjacent 5B-storey	Impact 1	27324	30824	15557	21777	24099	788	669	2448	1128	2181
	Impact 2	713	367	1299	434	1124			-		
15B-storey adjacent 5B-storey	Impact 1	5979	4491	2571	11427	3132	916	2521	1438	3213	987
	Impact 2	2797	2643	2932	2578	2915	1247	820	2213	987	1993
	Impact 3			-			993	2038	1158	2294	743
	Impact 4			-			1765	2240	1715	2209	1208
	Impact 5			-			2870	1718	4852	1787	3461
	Impact 6			-			6059	9715	1627	16727	5127
	Impact 7			-			3709	3612	3866	3632	3832
15B-storey adjacent 10-storey	Impact 1	3428	3480	4092	3788	2167	588	214	2851	2577	2764
	Impact 2	6104	5893	4006	17522	8258	1964	1244	2384	2355	2375
	Impact 3	2750	2805	2718	3637	1428	4494	7113	7819	8145	6740
	Impact 4	1373	1416	1822	5513	2020	334	469	1580	1353	1700
	Impact 5	5108	5130	4416	11434	6589			-		

Table 6.2 (continued) Dissimilarity values calculated by Kolmogorov–Smirnov test, units in N

		Earthquake									
		Dissimilarity values under Northridge					Dissimilarity values under Kobe				
	No. of Impact	Linear	Linear viscoelastic	Hertz model	Nonlinear viscoelastic	Hertz-damp	Linear	Linear viscoelastic	Hertz model	Nonlinear viscoelastic	Hertz-damp
10-storey adjacent 5B-storey	Impact 1	577	1751	512	3326	382	724	935	1133	541	946
	Impact 2			-			23642	20585	22362	50529	31224
	Impact 3			-			6625	7239	5699	17160	8617
15B-storey adjacent 5B-storey	Impact 1	5946	3890	938	8921	2773	16415	20295	9910	53004	19372
	Impact 2	2564	2345	2869	2294	2827	669	923	2182	846	1672
15B-storey adjacent 10-storey	Impact 1	15683	10131	15189	15701	17510	6596	6263	7069	3000	5634
	Impact 2	9500	7763	7997	9512	10366	4500	5693	3260	17884	7861
	Impact 3	8513	5182	5402	8939	9356	4573	4230	5399	2693	4543
	Impact 4			-			3655	3146	4239	2541	3642
	Impact 5			-			3286	3022	3605	3310	3512
	Impact 6			-			1411	1154	1843	1096	1608
	Impact 7			-			6948	8805	3990	10925	6172
	Impact 8			-			2774	2031	3585	2206	3151

Note: DV = max($D(t_i)$) for $t_i = 0$ to t_f, where: t_f is the final time; $D(t_i) = |F(t_i)_t - F(t_i)_e|$; $F(t_i)_t = F(t_{i-1})_t + dF(t_i)_t$; $F(t_i)_e = F(t_{i-1})_e + dF(t_i)_e$

Table 6.3 Scale ranking for theoretical impact models

Linear	Linear viscoelastic	Hertz model	Nonlinear viscoelastic	Hertz-damp
4	5	1	2	3
3	1	5	2	4
2	1	5	3	4
3	4	2	5	1
2	3	5	1	4
3	1	2	5	4
2	3	1	5	4
4	3	1	5	2
3	2	5	1	4
1	4	3	5	2
3	1	5	2	4
2	4	3	5	1
3	5	2	4	1
3	1	5	2	4
3	4	1	5	2
3	1	5	2	4
4	3	1	5	2
3	2	5	1	4
2	4	1	5	3
1	3	5	2	4
2	3	5	4	1
3	2	1	5	4
3	4	2	5	1
1	2	3	5	4
2	3	1	5	4
2	1	5	3	4
2	1	5	3	4
1	3	4	5	2
1	2	5	3	4
3	1	2	4	5
3	1	2	4	5
3	1	2	4	5
4	3	5	1	2
2	3	1	5	4
4	2	5	1	3
4	2	5	1	3
2	1	5	3	4
3	2	5	1	4
3	4	1	5	2
3	1	5	2	4
105	**97**	**132**	**136**	**130**

Based on the data presented, all the theoretical models presented similar predictions in terms of number and time of impact. The results also showed that the impact force magnitude was overestimated by all the models in most cases. The findings indicated that any of the investigated models can be utilised to predict pounding force. However, the Hertz, nonlinear viscoelastic and Hertz-damp models are much more complicated than the linear spring and linear viscoelastic models. This is especially true in the process of computing the impact stiffness parameters, k_h and β, in real practical pounding. The impact stiffness parameter k can be derived using different methods (Anagnostopoulos 1988; Cole et al. 2012a; Jaradat & Far 2020; Maison & Kasai 1992; Wada et al. 1984). The results of this study clearly specify that researchers prefer to use the linear spring and linear viscoelastic models in future numerical modelling of floor-to-floor pounding between adjacent structures. Since the linear spring model does not take into account the energy dissipation during impact, the linear viscoelastic model is the better choice. Importantly, the linear viscoelastic model is found in many commercial design software programs.

6.7 **Summary**

In this chapter, in order to evaluate the accuracy and performance of five theoretical impact force models, shaking table tests were conducted on pounding between adjacent steel frames with different heights.

According to the comparison of the results between the predicted and experimental impact forces, all the theoretical contact element models predicted the pounding response of closely spaced structures and generated similar predictions in terms of number and time of impact. However, the magnitude of the impact force was not accurately predicted by impact models in most cases.

Moreover, the statistical analysis shows that the linear viscoelastic model appears to be the most suitable of the five models studied in this chapter for conducting pounding simulation.

CHAPTER 7
MATHEMATICAL APPROACH FOR ESTIMATION OF MINIMUM GAP BETWEEN ADJACENT BUILDINGS WITH UNEQUAL HEIGHTS

7.1 Introduction

Concern about structural pounding between adjacent structures during earthquakes has led to the study of this phenomenon in recent years. Significant incidents of building damage and/or collapse, triggered by collisions in powerful earthquakes, have occurred in many places during the past 20 years. One of the major reasons for this problem is the insufficient separation gap between adjacent buildings that allows collisions to occur during seismic excitations. The phenomenon, often called 'earthquake-induced structural pounding', affects buildings and bridges (Anagnostopoulos 1988; Favvata 2017; Jankowski 2015; Khatami et al. 2019; Miari et al. 2019; Rahman et al. 2000). Earthquake-induced structural pounding occurs when the gap between structures, or structural members, cannot cover their relative movements, and the relative lateral displacement exceeds the separation gap (Elwardany et al. 2017; Khatami et al. 2020; Sołtysik & Jankowski 2013). Hence, there is a need to make calculations to ensure that there will be adequate separation gaps between adjacent buildings to avoid structural damage or collapse during earthquakes (Anagnostopoulos 1995; Kasai & Maison 1997; Rosenblueth & Meli 1986).

To mitigate the incidence of severe building damage and/or collapse brought about by earthquake-induced structural pounding, modern building codes include seismic separation requirements for adjacent structures, particularly for locations in seismically active areas.

Building rules and regulations across different countries, as well as previous studies, proposed methods to calculate the minimum separation gaps between adjacent structures in order to mitigate the incidence of building collisions during earthquakes. This has been comprehensively explained in Sections 2.4 and 2.5. The methods given in the literature and in codes or provisions involve the determination of lateral displacements of the adjacent buildings. Hence, both buildings should be analysed.

This chapter aims to propose a simple mathematical approach that does not require complex analysis to estimate the minimum required separation distances for mid-rise steel frame buildings.

In this chapter, experimental and numerical tests were carried out using multi-linear regression analysis to develop the mathematical model capable of predicting the sufficient separation gap between adjacent structures to avoid earthquake-induced pounding. The investigation was carried out in two stages. The first stage involved a model validation study conducted with numerical and experimental comparison. In the second stage, a parametric study was conducted to investigate the effects of different building heights, building damping ratio, building frequency, building stiffness, building mass and earthquake excitations. Output analytics was done after the two investigation stages were completed. The analytics was executed with the help of a multiple linear regression model.

7.2 Stage One

7.2.1 Selected Seismic Acceleration Records

Nine scaled earthquake acceleration records were used in the analyses, as depicted in Table 7.1. The ground motion records were grouped into three levels, depending on the peak ground acceleration: low (0.1g up to 0.3g), moderate (0.3g up to 0.6g) and high (0.6g up to 0.9g) with different dominant vibration period ($\boldsymbol{T_g}$) (Abdel Raheem 2006; Muthukumar & Desroches 2004). The value of $\boldsymbol{T_g}$ can be obtained based on the calculation of Kramer (1996). In order to achieve a wide range of the period ratios ($T_5/\boldsymbol{T_g}$, $T_{10}/\boldsymbol{T_g}$ and $T_{15}/\boldsymbol{T_g}$; adjacent buildings' fundamental period over the ground motion characteristic period), the earthquake acceleration records were carefully chosen. Hachinohe, El Centro, Kobe and Northridge were implemented for the shaking table tests (Figure 3.6(b), Figure 3.7(b), Figure 3.8(b) and Figure 3.9(b)). These four earthquakes were used in Stage one, while more SAP earthquake records were added in Stage two: SAP1, SAP2, SAP3, SAP4 and SAP 5. These SAP records were extracted from SAP2000 (SAP 2000). According to the SAP2000 time history function file, these earthquakes are real earthquakes that struck California between 1971 and 1992. The earthquake acceleration time histories are shown in Figures 7.1–7.5.

7.2.2 Model Validation Study

In this investigation, only adjacent buildings with unequal height were considered, namely the coupled configurations of 15B-storey with 10-storey, 15B-storey with 5B-storey and 10-storey with 5B-storey. As discussed extensively in Chapter 4, model validation was successfully completed with a negligible difference between the experimental and the numerical required separation gap (see Table 4.2).

Table 7.1 Suite of scaled earthquake ground motion records

PGA Level	PGA (g)	Earthquake	T_g (s)
Low	0.167	SAP 1	0.095
	0.24	Hachinohe	0.233
	0.287	SAP 2	0.182
Moderate	0.349	El Centro	0.105
	0.460	SAP 3	0.091
	0.521	SAP 4	0.063
High	0.675	Kobe	0.10
	0.849	Northridge	0.146
	0.843	SAP 5	0.125

7.3 **Stage Two**

7.3.1 Selection of Structure's Parameters

In the second stage of the investigation, an intensive numerical analysis was carried out. In this stage, analyses were conducted with additional SAP earthquake records. Referring to Table 7.1, the earthquake records were categorised into three different levels – low, moderate and high. However, the SAP 5 record was not included in the numerical analyses. It was used for validation purposes. The numerical investigation was done to determine the minimum required separation gap to prevent pounding between adjacent buildings for different parametric values, such as mass, damping ratio, natural vibration frequencies, structural stiffness and peak ground acceleration records.

When the effects of one parameter are investigated, the values of the other factors are held constant. In the analysis, the basic values of the structural models' parameters were applied as depicted in Table 3.1. Initially, the adjacent structures' damping ratio was gradually increased from 1% to 5%. In each level of increase, analysis was conducted to obtain the separation gap. Then, the mass was added at the centre of each floor by 2 kg, 1 kg and 1 kg. In each level of mass increase, the analysis was done at a different damping ratio. Lastly, the structure stiffness was increased by 10% and 20%. A total of 9768 cases were obtained for the separation gap under three earthquake categories. There were 3081 cases for low PGA level, 3081 cases for moderate PGA level and 3606 cases for high PGA level. Tables 7.2, 7.3 and 7.4 illustrate the numerical separation gap for the three different PGA levels – low, moderate and high. Due to the big turnout of cases in each level, only the first and last few records are shown in the tables.

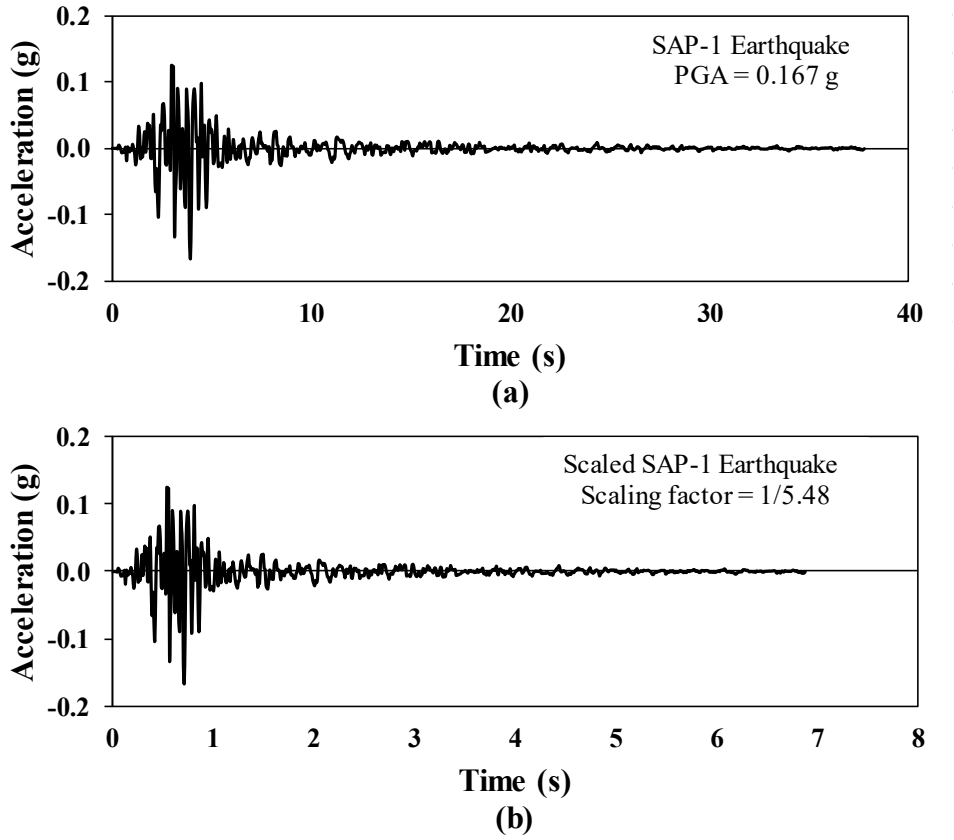

Figure 7.1 SAP-1 earthquake; (a) Original record, (b) Scaled record

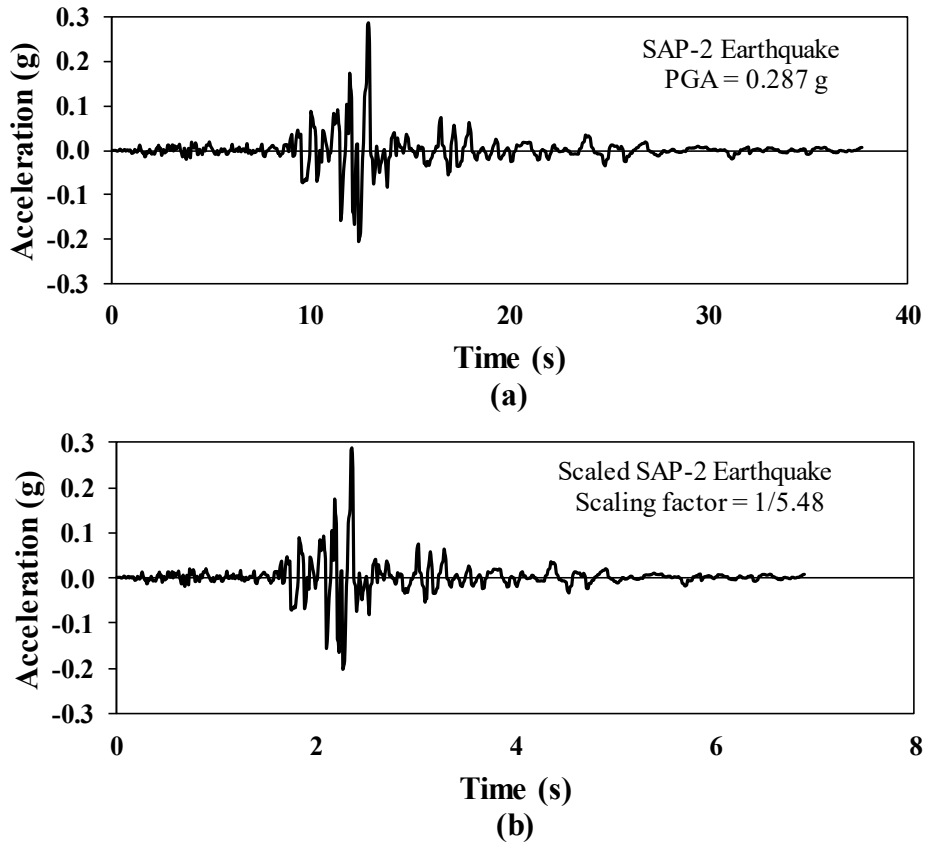

Figure 7.2 SAP-2 earthquake; (a) Original record, (b) Scaled record

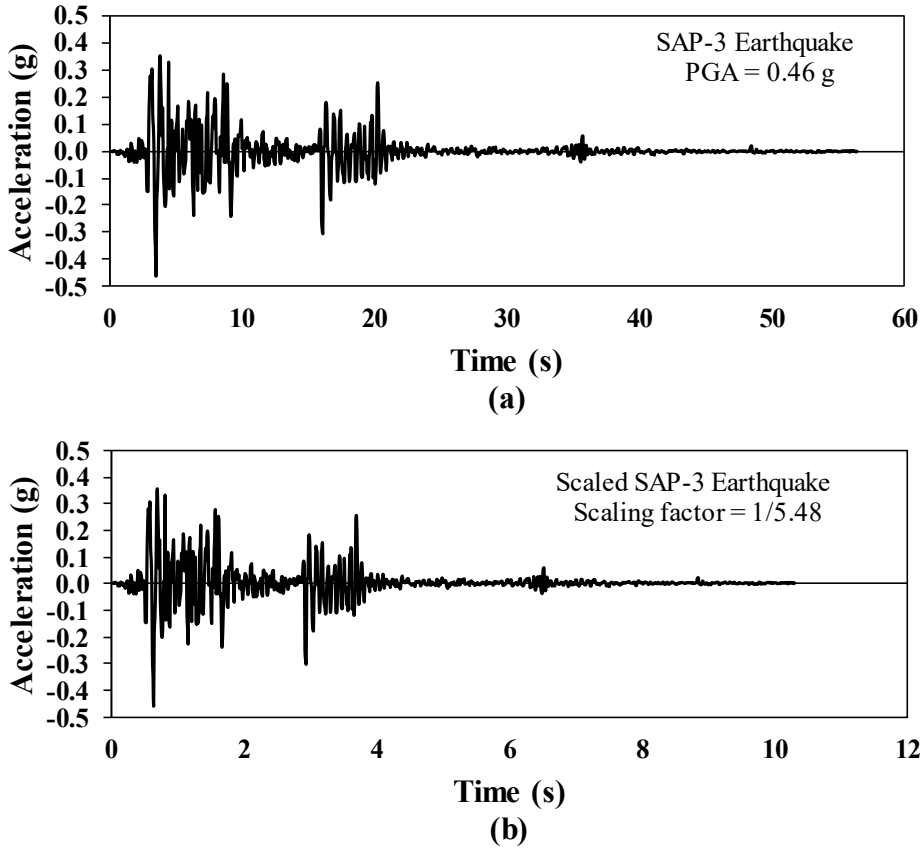

Figure 7.3 SAP-3 earthquake; (a) Original record, (b) Scaled record

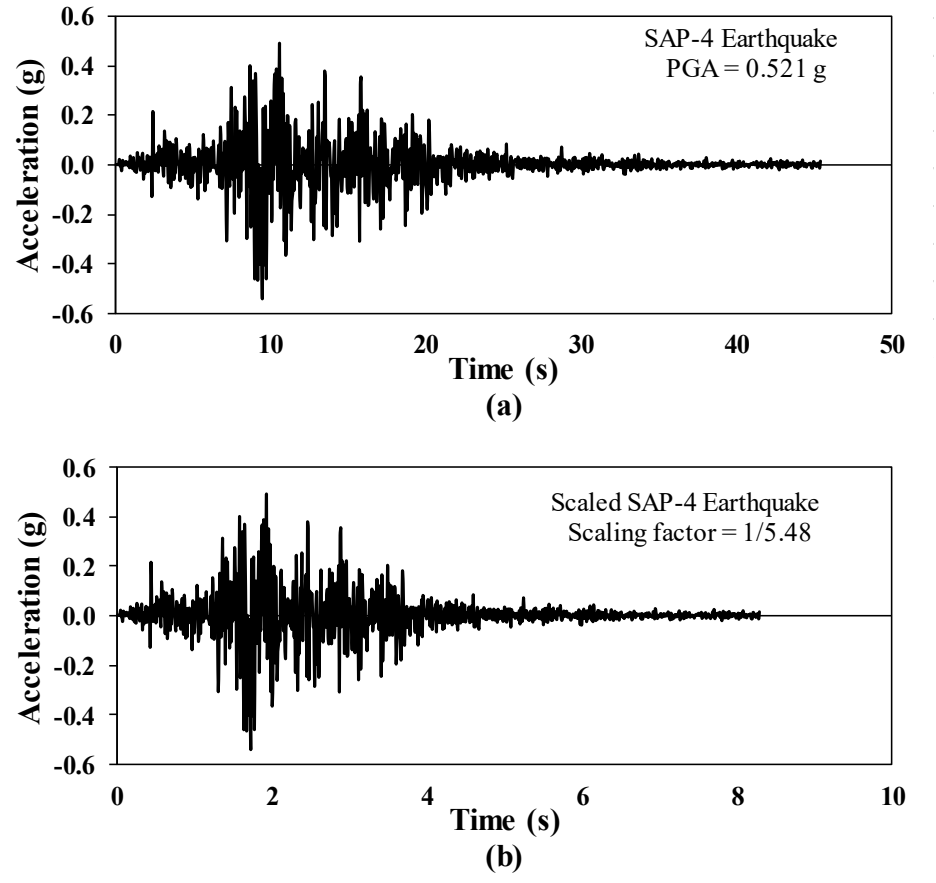

Figure 7.4 SAP-4 earthquake; (a) Original record, (b) Scaled record

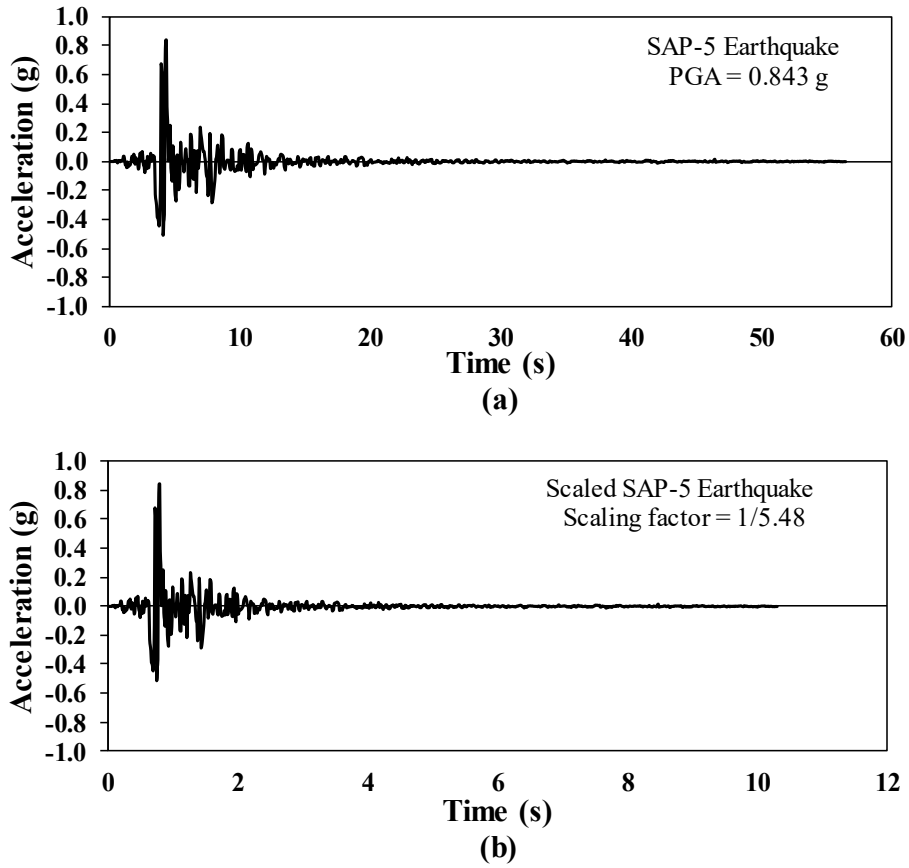

Figure 7.5 SAP-5 earthquake; (a) Original record, (b) Scaled record

7.3.2 Sensitivity Analysis for Multiple Variables

In order to create a multiple linear regression, it is essential to verify the presence of a linear association between each independent variable and the dependent variable. This involves demonstrating the significance of each variable in determining the minimum gap between structures (dependent variable). Additionally, it is crucial to assess whether the independent variables exhibit multicollinearity.

Multicollinearity occurs when there is a strong correlation between two or more independent variables in a regression mode (Kutner et al. 2005; Montgomery et al. 2009). This situation complicates the assessment of the individual impact of each independent variable on the dependent variable. The correlation values were calculated using Statistical Packages for Social Sciences (SPSS).

The correlation being conducted is known as Pearson's correlation coefficient (Pearson's r). It quantifies the relationship between two variables, ranging from -1 to +1. A value of zero indicates no relationship, while values closer to either +1 or -1 indicate a stronger relationship between the variables. In this analysis, Pearson's correlation coefficient will

be used along with a two-tailed test of significance (Kutner et al. 2005; Montgomery et al. 2009).

The information presented in Tables 7.5–7.7 provides additional insights into the correlation matrix. Table 7.5 reveals that the mass, frequency, stiffness, and height of the short building exhibit the strongest correlation with the minimum gap. The PGA as well as the mass, frequency, stiffness, and height of the tall building, display a moderate level of correlation. On the other hand, the damping values of both the tall and short buildings show a very weak correlation with the minimum gap. Consistent findings were also noticed in Tables 7.6–7.7, supporting the observations mentioned earlier. The results suggest that parameters derived from the short building hold more significance in determining the minimum gap.

The analysis indicates a high correlation between the height, frequency, stiffness, and mass of the short building. Similarly, there is a high correlation between the stiffness, height, and frequency of the tall building. These findings suggest the presence of multicollinearity among these variables.

Given that there are variables with low correlation and the presence of multicollinearity, it may be necessary to remove certain variables from the model if they are not significant predictors. However, initially, it was decided to proceed with a linear regression model that included all the independent variables. This approach allowed for the assessment of the overall impact and significance of each variable on the dependent variable before any further adjustments were made.

7.3.3 Introducing Mathematical Models

The data were collected in terms of seismic gap, as illustrated in Tables 7.2–7.4. Twelve variables are involved in this study – one dependent variable and 11 independent variables. The predictor variables are HT (height of the tall building in mm), HS (height of the short building in mm), E (earthquake peak ground acceleration in g), FT (frequency of the tall building in Hz), FS (frequency of the short building in Hz), DT (damping ratio of the tall building in %), DS (damping ratio of the short building in %), ST (stiffness of the tall building in kN/mm), SS (stiffness of the short building in kN/mm), MT (mass of the tall building in kg) and MS (mass of the short building in kg). The dependent variable is Y (minimum separation gap in mm).

A multiple linear regression analysis (MLR) was carried out to better understand the impact of the input variables on the output variables. MLR is an increasingly common statistical method used to explain the relationship between one dependent variable and two or more independent variables (Montgomery et al. 2009). The model is estimated by least squares, which yields parameter estimates such that the sum of squares of errors is minimised. The resulting prediction equation is shown as in Equation 7.1 (Kutner et al. 2005):

$$\hat{Y}_i = b_0 + b_1 x_{i,1} + b_2 x_{i,2} + \cdots + b_k x_{i,k} \quad 7.1$$

where b_0 is the intercept (constant), b_1, b_2 to b_k are the regression coefficients for each explanatory (independent) variable, $x_{i,k}$ are the explanatory (independent) variables, and Y_i is the dependent variable or real data. The goal of using MLR in this study is to model the linear relationship between the explanatory (11 independent) variables to predict the outcome of the response (one dependent) variable in determining the appropriate separation gap between adjacent structures to avoid earthquake-induced pounding.

7.3.4 Estimation of Coefficients of the Model

The values of the regression coefficients of the abovementioned model were calculated using Statistical Packages for Social Sciences (SPSS). The estimated regression coefficients for low, moderate and high levels of PGA are reflected in Tables 7.5–7.7. The standard error and t Stat values are tabulated in Tables 7.5–7.7. The standard error is a measure of the statistical accuracy of an estimate equal to the standard deviation of the distribution of coefficients or the theoretical distribution of a large population of such estimates or forecasts. The t Stat is a type of inferential statistic used to ascertain if there is a significant difference between the means of two variables. The value of the regression coefficient gives the engineer or analyst an idea of how to make predictions about one variable based on the information that is known about another variable. In this study, the (11) independent variables are the parameters used to calculate the dependent variable or outcome, which is the minimum seismic gap between adjacent structures necessary to avoid earthquake-induced pounding. Higher coefficient values of regression may signify high influence of input variables.

7.3.5 Testing the Significance of Regression Coefficients

In regression with multiple independent variables, the coefficient reveals how much the dependent variable is expected to increase when the independent variable increases, assuming all the other independent variables remain constant. The value describes the

relationship between a predictor variable and the response. To achieve this, p value is used. Based on the test, when the calculated value of $(p)$is less than 0.05 for the desired level of probability of (95%), the regression coefficient becomes significant. These conditions were satisfied for the development of the final mathematical model. It can be seen in Table 7.5 that the p value of the mass of the tall building, MT, is more than 0.05. Also, in Table 7.6, the p value of the frequency of the tall building, FT, and mass of the tall building, MT, are more than 0.05. Furthermore, in Table 7.7, the p value of the frequency of the tall building, FT, and stiffness of the short building, SS, are more than 0.05. Therefore, the abovementioned variables are statistically insignificant. Thus, they can be excluded from the mathematical model.

Table 7.2 Numerical seismic gap between adjacent buildings under low PGA level

Obs.	Height Tall mm	Height Short mm	PGA g	Frequency Tall Hz	Frequency Short Hz	Damping Tall %	Damping Short %	Stiffness Tall kN/mm	Stiffness Short kN/mm	Mass Tall kg	Mass Short kg	Numerical Min Gap mm
1	1500	1000	0.24	2.29	3.53	1	1	0.009	0.0149	104.2	72	14.14
2	1500	1000	0.24	2.29	3.53	1	2	0.009	0.0149	104.2	72	13.85
3	1500	1000	0.24	2.29	3.53	1	3	0.009	0.0149	104.2	72	13.62
4	1500	1000	0.24	2.29	3.53	1	4	0.009	0.0149	104.2	72	13.45
5	1500	1000	0.24	2.29	3.53	1	5	0.009	0.0149	104.2	72	13.33
6	1500	1000	0.24	2.29	3.09	1	0.431	0.009	0.0149	104.2	92	15.38
7	1500	1000	0.24	2.29	3.09	1	1	0.009	0.0149	104.2	92	15.04
8	1500	1000	0.24	2.29	3.09	1	2	0.009	0.0149	104.2	92	14.58
9	1500	1000	0.24	2.29	3.09	1	3	0.009	0.0149	104.2	92	14.25
10	1500	1000	0.24	2.29	3.09	1	4	0.009	0.0149	104.2	92	13.99
11	1500	1000	0.24	2.29	3.09	1	5	0.009	0.0149	104.2	92	13.77
12	1500	1000	0.24	2.29	2.92	1	0.431	0.009	0.0149	104.2	102	17.62
13	1500	1000	0.24	2.29	2.92	1	1	0.009	0.0149	104.2	102	17.11
14	1500	1000	0.24	2.29	2.92	1	2	0.009	0.0149	104.2	102	16.15
15	1500	1000	0.24	2.29	2.92	1	3	0.009	0.0149	104.2	102	15.31
16	1500	1000	0.24	2.29	2.92	1	4	0.009	0.0149	104.2	102	14.64
17	1500	1000	0.24	2.29	2.92	1	5	0.009	0.0149	104.2	102	14.21
18	1500	1000	0.24	2.29	2.78	1	0.431	0.009	0.0149	104.2	112	21.09
19	1500	1000	0.24	2.29	2.78	1	1	0.009	0.0149	104.2	112	19.13
↓						↓						↓
3061	1000	500	0.167	3.09	6.96	0.431	2	0.0149	0.0276	92	34.85	2.8
3062	1000	500	0.167	2.92	6.96	0.431	2	0.0149	0.0276	102	34.85	2.81
3063	1000	500	0.167	2.78	6.96	0.431	2	0.0149	0.0276	112	34.85	2.96
3064	1000	500	0.167	3.09	6.96	0.431	3	0.0149	0.0276	92	34.85	2.53
3065	1000	500	0.167	2.92	6.96	0.431	3	0.0149	0.0276	102	34.85	2.62
3066	1000	500	0.167	2.78	6.96	0.431	3	0.0149	0.0276	112	34.85	2.82
3067	1000	500	0.167	3.09	6.96	0.431	4	0.0149	0.0276	92	34.85	2.34
3068	1000	500	0.167	2.92	6.96	0.431	4	0.0149	0.0276	102	34.85	2.51
3069	1000	500	0.167	2.78	6.96	0.431	4	0.0149	0.0276	112	34.85	2.7
3070	1000	500	0.167	3.09	6.96	0.431	5	0.0149	0.0276	92	34.85	2.2
3071	1000	500	0.167	2.92	6.96	0.431	5	0.0149	0.0276	102	34.85	2.41
3072	1000	500	0.167	2.78	6.96	0.431	5	0.0149	0.0276	112	34.85	2.6
3073	1000	500	0.167	3.09	5.95	0.431	0.366	0.0149	0.0276	92	44.85	2.64
3074	1000	500	0.167	2.92	5.95	0.431	0.366	0.0149	0.0276	102	44.85	2.4
3075	1000	500	0.167	2.78	5.95	0.431	0.366	0.0149	0.0276	112	44.85	2.39
3076	1000	500	0.167	3.09	5.59	0.431	0.366	0.0149	0.0276	92	49.85	2.64
3077	1000	500	0.167	2.92	5.59	0.431	0.366	0.0149	0.0276	102	49.85	2.6
3078	1000	500	0.167	2.78	5.59	0.431	0.366	0.0149	0.0276	112	49.85	2.52
3079	1000	500	0.167	3.09	5.28	0.431	0.366	0.0149	0.0276	92	54.85	3.07
3080	1000	500	0.167	2.92	5.28	0.431	0.366	0.0149	0.0276	102	54.85	3.07
3081	1000	500	0.167	2.78	5.28	0.431	0.366	0.0149	0.0276	112	54.85	3.39

Table 7.3 Numerical seismic gap between adjacent buildings under moderate PGA level

Obs.	Height Tall mm	Height Short mm	PGA g	Frequency Tall Hz	Frequency Short Hz	Damping Tall %	Damping Short %	Stiffness Tall kN/mm	Stiffness Short kN/mm	Mass Tall kg	Mass Short kg	Numerical Min Gap mm
1	1500	1000	0.349	2.29	3.53	1	1	0.009	0.0149	104.24	72	14.04
2	1500	1000	0.349	2.29	3.53	1	2	0.009	0.0149	104.24	72	13.49
3	1500	1000	0.349	2.29	3.53	1	3	0.009	0.0149	104.24	72	13.06
4	1500	1000	0.349	2.29	3.53	1	4	0.009	0.0149	104.24	72	12.71
5	1500	1000	0.349	2.29	3.53	1	5	0.009	0.0149	104.24	72	12.42
6	1500	1000	0.349	2.29	3.09	1	0.431	0.009	0.0149	104.24	92	15.48
7	1500	1000	0.349	2.29	3.09	1	1	0.009	0.0149	104.24	92	15.16
8	1500	1000	0.349	2.29	3.09	1	2	0.009	0.0149	104.24	92	14.72
9	1500	1000	0.349	2.29	3.09	1	3	0.009	0.0149	104.24	92	14.35
10	1500	1000	0.349	2.29	3.09	1	4	0.009	0.0149	104.24	92	14.01
11	1500	1000	0.349	2.29	3.09	1	5	0.009	0.0149	104.24	92	13.68
12	1500	1000	0.349	2.29	2.92	1	0.431	0.009	0.0149	104.24	102	15.59
13	1500	1000	0.349	2.29	2.92	1	1	0.009	0.0149	104.24	102	15.23
14	1500	1000	0.349	2.29	2.92	1	2	0.009	0.0149	104.24	102	14.72
15	1500	1000	0.349	2.29	2.92	1	3	0.009	0.0149	104.24	102	14.28
16	1500	1000	0.349	2.29	2.92	1	4	0.009	0.0149	104.24	102	13.89
17	1500	1000	0.349	2.29	2.92	1	5	0.009	0.0149	104.24	102	13.52
18	1500	1000	0.349	2.29	2.78	1	0.431	0.009	0.0149	104.24	112	15.56
19	1500	1000	0.349	2.29	2.78	1	1	0.009	0.0149	104.24	112	15.15
↓						↓						↓
3061	1000	500	0.521	3.09	6.96	0.431	2	0.0149	0.0276	92	34.85	8.5
3062	1000	500	0.521	2.92	6.96	0.431	2	0.0149	0.0276	102	34.85	10
3063	1000	500	0.521	2.78	6.96	0.431	2	0.0149	0.0276	112	34.85	11.2
3064	1000	500	0.521	3.09	6.96	0.431	3	0.0149	0.0276	92	34.85	8.3
3065	1000	500	0.521	2.92	6.96	0.431	3	0.0149	0.0276	102	34.85	9.5
3066	1000	500	0.521	2.78	6.96	0.431	3	0.0149	0.0276	112	34.85	11.8
3067	1000	500	0.521	3.09	6.96	0.431	4	0.0149	0.0276	92	34.85	8
3068	1000	500	0.521	2.92	6.96	0.431	4	0.0149	0.0276	102	34.85	9.3
3069	1000	500	0.521	2.78	6.96	0.431	4	0.0149	0.0276	112	34.85	10.8
3070	1000	500	0.521	3.09	6.96	0.431	5	0.0149	0.0276	92	34.85	7.8
3071	1000	500	0.521	2.92	6.96	0.431	5	0.0149	0.0276	102	34.85	9
3072	1000	500	0.521	2.78	6.96	0.431	5	0.0149	0.0276	112	34.85	10.8
3073	1000	500	0.521	3.09	5.95	0.431	0.366	0.0149	0.0276	92	44.85	12.6
3074	1000	500	0.521	2.92	5.95	0.431	0.366	0.0149	0.0276	102	44.85	14.8
3075	1000	500	0.521	2.78	5.95	0.431	0.366	0.0149	0.0276	112	44.85	15.6
3076	1000	500	0.521	3.09	5.59	0.431	0.366	0.0149	0.0276	92	49.85	14.2
3077	1000	500	0.521	2.92	5.59	0.431	0.366	0.0149	0.0276	102	49.85	14
3078	1000	500	0.521	2.78	5.59	0.431	0.366	0.0149	0.0276	112	49.85	14
3079	1000	500	0.521	3.09	5.28	0.431	0.366	0.0149	0.0276	92	54.85	11.4
3080	1000	500	0.521	2.92	5.28	0.431	0.366	0.0149	0.0276	102	54.85	11.7
3081	1000	500	0.521	2.78	5.28	0.431	0.366	0.0149	0.0276	112	54.85	12

Table 7.4 Numerical seismic gap between adjacent buildings under high PGA level

Obs.	Height Tall mm	Height Short mm	PGA g	Frequency Tall Hz	Frequency Short Hz	Damping Tall %	Damping Short %	Stiffness Tall kN/mm	Stiffness Short kN/mm	Mass Tall kg	Mass Short kg	Numerical Min Gap mm
1	1500	1000	0.849	2.293	3.53	1	1	0.009	0.0149	104.24	72	63.34
2	1500	1000	0.849	2.293	3.53	1	2	0.009	0.0149	104.24	72	57.4
3	1500	1000	0.849	2.293	3.53	1	3	0.009	0.0149	104.24	72	52.92
4	1500	1000	0.849	2.293	3.53	1	4	0.009	0.0149	104.24	72	49.46
5	1500	1000	0.849	2.293	3.53	1	5	0.009	0.0149	104.24	72	46.78
6	1500	1000	0.849	2.293	3.09	1	0.43	0.009	0.0149	104.24	92	46.69
7	1500	1000	0.849	2.293	3.09	1	1	0.009	0.0149	104.24	92	44.47
8	1500	1000	0.849	2.293	3.09	1	2	0.009	0.0149	104.24	92	42.22
9	1500	1000	0.849	2.293	3.09	1	3	0.009	0.0149	104.24	92	40.86
10	1500	1000	0.849	2.293	3.09	1	4	0.009	0.0149	104.24	92	39.63
11	1500	1000	0.849	2.293	3.09	1	5	0.009	0.0149	104.24	92	38.49
12	1500	1000	0.849	2.293	2.92	1	0.43	0.009	0.0149	104.24	102	48.83
13	1500	1000	0.849	2.293	2.92	1	1	0.009	0.0149	104.24	102	46.83
14	1500	1000	0.849	2.293	2.92	1	2	0.009	0.0149	104.24	102	43.8
15	1500	1000	0.849	2.293	2.92	1	3	0.009	0.0149	104.24	102	41.28
16	1500	1000	0.849	2.293	2.92	1	4	0.009	0.0149	104.24	102	39.16
17	1500	1000	0.849	2.293	2.92	1	5	0.009	0.0149	104.24	102	37.39
18	1500	1000	0.849	2.293	2.78	1	0.43	0.009	0.0149	104.24	112	53.03
19	1500	1000	0.849	2.293	2.78	1	1	0.009	0.0149	104.24	112	50.77
↓						↓						↓
3586	1000	500	0.675	2.777	6.96	5	0.37	0.0149	0.0276	112	34.85	17.71
3587	1000	500	0.675	2.777	6.96	5	1	0.0149	0.0276	112	34.85	16.51
3588	1000	500	0.675	2.777	6.96	5	2	0.0149	0.0276	112	34.85	15.57
3589	1000	500	0.675	2.777	6.96	5	3	0.0149	0.0276	112	34.85	14.72
3590	1000	500	0.675	2.777	6.96	5	4	0.0149	0.0276	112	34.85	13.95
3591	1000	500	0.675	2.777	6.96	5	5	0.0149	0.0276	112	34.85	13.25
3592	1000	500	0.675	2.777	5.95	5	1	0.0149	0.0276	112	44.85	26.36
3593	1000	500	0.675	2.777	5.95	5	2	0.0149	0.0276	112	44.85	23.96
3594	1000	500	0.675	2.777	5.95	5	3	0.0149	0.0276	112	44.85	21.98
3595	1000	500	0.675	2.777	5.95	5	4	0.0149	0.0276	112	44.85	20.34
3596	1000	500	0.675	2.777	5.95	5	5	0.0149	0.0276	112	44.85	18.99
3597	1000	500	0.675	2.777	5.59	5	1	0.0149	0.0276	112	49.85	22.26
3598	1000	500	0.675	2.777	5.59	5	2	0.0149	0.0276	112	49.85	20.42
3599	1000	500	0.675	2.777	5.59	5	3	0.0149	0.0276	112	49.85	18.94
3600	1000	500	0.675	2.777	5.59	5	4	0.0149	0.0276	112	49.85	17.74
3601	1000	500	0.675	2.777	5.59	5	5	0.0149	0.0276	112	49.85	16.77
3602	1000	500	0.675	2.777	5.28	5	1	0.0149	0.0276	112	54.85	19.8
3603	1000	500	0.675	2.777	5.28	5	2	0.0149	0.0276	112	54.85	18.66
3604	1000	500	0.675	2.777	5.28	5	3	0.0149	0.0276	112	54.85	17.64
3605	1000	500	0.675	2.777	5.28	5	4	0.0149	0.0276	112	54.85	16.72
3606	1000	500	0.675	2.777	5.28	5	5	0.0149	0.0276	112	54.85	15.89

Table 7.5 Correlation coefficients between all variables for low PGA level

		Numerical min gap mm	Height Tall mm	Height Short mm	PGA g	Frequency Tall Hz	Frequency Short Hz	Damping Tall %	Damping Short %	Stiffness Tall kN/mm	Stiffness Short kN/mm	Mass Tall kg	Mass Short kg
Numerical min gap mm	Pearson Corre	1	.253	.481	.434	-.338	-.526	-.121	-.062	-.304	-.480	.296	.574
	Sig. (2-tailed)		.000	.000	.000	.000	.000	.000	.001	.000	.000	.000	.000
	N	3081	3081	3081	3081	3081	3081	3081	3081	3081	3081	3081	3081
Height Tall mm	Pearson Corre	.253	1	.425	-.028	-.821	-.372	.136	-.066	**-.957**	-.420	.526	.359
	Sig. (2-tailed)	.000		.000	.121	.000	.000	.000	.000	.000	.000	.000	.000
	N	3081	3081	3081	3081	3081	3081	3081	3081	3081	3081	3081	3081
Height Short mm	Pearson Corre	.481	.425	1	-.009	-.349	**-.932**	.058	-.047	-.406	**-1.00**	.224	**.884**
	Sig. (2-tailed)	.000	.000		.623	.000	.000	.001	.009	.000	.000	.000	.000
	N	3081	3081	3081	3081	3081	3081	3081	3081	3081	3081	3081	3081
PGA g	Pearson Corre	.434	-.028	-.009	1	.015	-.013	.007	.046	.027	.017	-.006	.020
	Sig. (2-tailed)	.000	.121	.623		.406	.482	.708	.010	.131	.359	.727	.263
	N	3081	3081	3081	3081	3081	3081	3081	3081	3081	3081	3081	3081
Frequency Tall Hz	Pearson Corre	-.338	-.821	-.349	.015	1	.313	-.099	.039	**.899**	.345	**-.890**	-.301
	Sig. (2-tailed)	.000	.000	.000	.406		.000	.000	.029	.000	.000	.000	.000
	N	3081	3081	3081	3081	3081	3081	3081	3081	3081	3081	3081	3081
Frequency Short Hz	Pearson Corre	-.526	-.372	-.932	-.013	.313	1	-.061	.072	.356	**.933**	-.204	**-.956**
	Sig. (2-tailed)	.000	.000	.000	.482	.000		.001	.000	.000	.000	.000	.000
	N	3081	3081	3081	3081	3081	3081	3081	3081	3081	3081	3081	3081
Damping Tall %	Pearson Corre	-.121	.136	.058	.007	-.099	-.061	1	.010	-.127	-.058	.071	.058
	Sig. (2-tailed)	.000	.000	.001	.708	.000	.001		.568	.000	.001	.000	.001
	N	3081	3081	3081	3081	3081	3081	3081	3081	3081	3081	3081	3081
Damping Short %	Pearson Corre	-.062	-.066	-.047	.046	.039	.072	.010	1	.064	.045	-.019	-.098
	Sig. (2-tailed)	.001	.000	.009	.010	.029	.000	.568		.000	.012	.287	.000
	N	3081	3081	3081	3081	3081	3081	3081	3081	3081	3081	3081	3081
Stiffness Tall kN/mm	Pearson Corre	-.304	-.957	-.406	.027	.899	.356	-.127	.064	1	.401	-.640	-.343
	Sig. (2-tailed)	.000	.000	.000	.131	.000	.000	.000	.000		.000	.000	.000
	N	3081	3081	3081	3081	3081	3081	3081	3081	3081	3081	3081	3081
Stiffness Short kN/mm	Pearson Corre	-.480	-.420	-1.00	.017	.345	.933	-.058	.045	.401	1	-.221	**-.885**
	Sig. (2-tailed)	.000	.000	.000	.359	.000	.000	.001	.012	.000		.000	.000
	N	3081	3081	3081	3081	3081	3081	3081	3081	3081	3081	3081	3081
Mass Tall kg	Pearson Corre	.296	.526	.224	-.006	-.890	-.204	.071	-.019	-.640	-.221	1	.196
	Sig. (2-tailed)	.000	.000	.000	.727	.000	.000	.000	.287	.000	.000		.000
	N	3081	3081	3081	3081	3081	3081	3081	3081	3081	3081	3081	3081
Mass Short kg	Pearson Corre	.574	.359	.884	.020	-.301	-.956	.058	-.098	-.343	-.885	.196	1
	Sig. (2-tailed)	.000	.000	.000	.263	.000	.000	.001	.000	.000	.000	.000	
	N	3081	3081	3081	3081	3081	3081	3081	3081	3081	3081	3081	3081

Table 7.6 Correlation coefficients between all variables for moderate PGA level

		Numerical min gap mm	Height Tall mm	Height Short mm	PGA g	Frequency Tall Hz	Frequency Short Hz	Damping Tall %	Damping Short %	Stiffness Tall kN/mm	Stiffness Short kN/mm	Mass Tall kg	Mass Short kg
Numerical min gap mm	Pearson Corre	1	.362	.612	.189	-.375	-.583	-.196	-.414	-.392	-.613	.299	.587
	Sig. (2-tailed)		.000	.000	.000	.000	.000	.000	.000	.000	.000	.000	.000
	N	3081	3081	3081	3081	3081	3081	3081	3081	3081	3081	3081	3081
Height Tall mm	Pearson Corre	.362	1	.425	.164	-.821	-.372	.136	-.066	**-.957**	-.420	.526	.359
	Sig. (2-tailed)	.000		.000	.000	.000	.000	.000	.000	.000	.000	.000	.000
	N	3081	3081	3081	3081	3081	3081	3081	3081	3081	3081	3081	3081
Height Short mm	Pearson Corre	.612	.425	1	.052	-.349	**-.932**	.058	-.047	-.406	**-1.00**	.224	**.884**
	Sig. (2-tailed)	.000	.000		.004	.000	.000	.001	.009	.000	.000	.000	.000
	N	3081	3081	3081	3081	3081	3081	3081	3081	3081	3081	3081	3081
PGA g	Pearson Corre	.189	.164	.052	1	-.088	.075	-.040	-.273	-.160	-.043	.037	-.119
	Sig. (2-tailed)	.000	.000	.004		.000	.000	.027	.000	.000	.018	.040	.000
	N	3081	3081	3081	3081	3081	3081	3081	3081	3081	3081	3081	3081
Frequency Tall Hz	Pearson Corre	-.375	-.821	-.349	-.088	1	.313	-.099	.039	**.899**	.345	**-.890**	-.301
	Sig. (2-tailed)	.000	.000	.000	.000		.000	.000	.029	.000	.000	.000	.000
	N	3081	3081	3081	3081	3081	3081	3081	3081	3081	3081	3081	3081
Frequency Short Hz	Pearson Corre	-.583	-.372	-.932	.075	.313	1	-.061	.072	.356	**.933**	-.204	**-.956**
	Sig. (2-tailed)	.000	.000	.000	.000	.000		.001	.000	.000	.000	.000	.000
	N	3081	3081	3081	3081	3081	3081	3081	3081	3081	3081	3081	3081
Damping Tall %	Pearson Corre	-.196	.136	.058	-.040	-.099	-.061	1	.010	-.127	-.058	.071	.058
	Sig. (2-tailed)	.000	.000	.001	.027	.000	.001		.568	.000	.001	.000	.001
	N	3081	3081	3081	3081	3081	3081	3081	3081	3081	3081	3081	3081
Damping Short %	Pearson Corre	-.414	-.066	-.047	-.273	.039	.072	.010	1	.064	.045	-.019	-.098
	Sig. (2-tailed)	.000	.000	.009	.000	.029	.000	.568		.000	.012	.287	.000
	N	3081	3081	3081	3081	3081	3081	3081	3081	3081	3081	3081	3081
Stiffness Tall kN/mm	Pearson Corre	-.392	-.957	-.406	-.160	.899	.356	-.127	.064	1	.401	-.640	-.343
	Sig. (2-tailed)	.000	.000	.000	.000	.000	.000	.000	.000		.000	.000	.000
	N	3081	3081	3081	3081	3081	3081	3081	3081	3081	3081	3081	3081
Stiffness Short kN/mm	Pearson Corre	-.613	-.420	-1.00	-.043	.345	.933	-.058	.045	.401	1	-.221	**-.885**
	Sig. (2-tailed)	.000	.000	.000	.018	.000	.000	.001	.012	.000		.000	.000
	N	3081	3081	3081	3081	3081	3081	3081	3081	3081	3081	3081	3081
Mass Tall kg	Pearson Corre	.299	.526	.224	.037	-.890	-.204	.071	-.019	-.640	-.221	1	.196
	Sig. (2-tailed)	.000	.000	.000	.040	.000	.000	.000	.287	.000	.000		.000
	N	3081	3081	3081	3081	3081	3081	3081	3081	3081	3081	3081	3081
Mass Short kg	Pearson Corre	.587	.359	.884	-.119	-.301	-.956	.058	-.098	-.343	-.885	.196	1
	Sig. (2-tailed)	.000	.000	.000	.000	.000	.000	.001	.000	.000	.000	.000	
	N	3081	3081	3081	3081	3081	3081	3081	3081	3081	3081	3081	3081

Table 7.7 Correlation coefficients between all variables for high PGA level

		Numerical min gap mm	Height Tall mm	Height Short mm	PGA g	Frequency Tall Hz	Frequency Short Hz	Damping Tall %	Damping Short %	Stiffness Tall kN/mm	Stiffness Short kN/mm	Mass Tall kg	Mass Short kg
Numerical min gap mm	Pearson Corre	1	.260	.657	.434	-.270	-.621	-.121	-.232	-.282	-.657	.210	.570
	Sig. (2-tailed)		.000	.000	.000	.000	.000	.000	.000	.000	.000	.000	.000
	N	3606	3606	3606	3606	3606	3606	3606	3606	3606	3606	3606	3606
Height Tall mm	Pearson Corre	.260	1	.476	.000	-.830	-.445	.101	-.032	**-.966**	-.476	.534	.436
	Sig. (2-tailed)	.000		.000	1.000	.000	.000	.000	.056	.000	.000	.000	.000
	N	3606	3606	3606	3606	3606	3606	3606	3606	3606	3606	3606	3606
Height Short mm	Pearson Corre	.657	.476	1	.000	-.395	**-.934**	.048	-.067	-.460	**-1.00**	.254	**.915**
	Sig. (2-tailed)	.000	.000		1.000	.000	.000	.004	.000	.000	.000	.000	.000
	N	3606	3606	3606	3606	3606	3606	3606	3606	3606	3606	3606	3606
PGA g	Pearson Corre	.434	.000	.000	1	.000	-.004	.000	.000	.000	.000	.000	.000
	Sig. (2-tailed)	.000	1.000	1.000		1.000	.805	1.000	1.000	1.000	1.000	1.000	1.000
	N	3606	3606	3606	3606	3606	3606	3606	3606	3606	3606	3606	3606
Frequency Tall Hz	Pearson Corre	-.270	-.830	-.395	.000	1	.369	-.067	.026	**.900**	.395	**-.888**	-.362
	Sig. (2-tailed)	.000	.000	.000	1.000		.000	.000	.113	.000	.000	.000	.000
	N	3606	3606	3606	3606	3606	3606	3606	3606	3606	3606	3606	3606
Frequency Short Hz	Pearson Corre	-.621	-.445	-.934	-.004	.369	1	-.045	.031	.430	**.934**	-.238	**-.967**
	Sig. (2-tailed)	.000	.000	.000	.805	.000		.007	.061	.000	.000	.000	.000
	N	3606	3606	3606	3606	3606	3606	3606	3606	3606	3606	3606	3606
Damping Tall %	Pearson Corre	-.121	.101	.048	.000	-.067	-.045	1	-.003	-.098	-.048	.039	.044
	Sig. (2-tailed)	.000	.000	.004	1.000	.000	.007		.847	.000	.004	.020	.008
	N	3606	3606	3606	3606	3606	3606	3606	3606	3606	3606	3606	3606
Damping Short %	Pearson Corre	-.232	-.032	-.067	.000	.026	.031	-.003	1	.031	.067	-.017	-.061
	Sig. (2-tailed)	.000	.056	.000	1.000	.113	.061	.847		.065	.000	.308	.000
	N	3606	3606	3606	3606	3606	3606	3606	3606	3606	3606	3606	3606
Stiffness Tall kN/mm	Pearson Corre	-.282	-.966	-.460	.000	.900	.430	-.098	.031	1	.460	-.639	-.421
	Sig. (2-tailed)	.000	.000	.000	1.000	.000	.000	.000	.065		.000	.000	.000
	N	3606	3606	3606	3606	3606	3606	3606	3606	3606	3606	3606	3606
Stiffness Short kN/mm	Pearson Corre	-.657	-.476	-1.00	.000	.395	.934	-.048	.067	.460	1	-.254	**-.915**
	Sig. (2-tailed)	.000	.000	.000	1.000	.000	.000	.004	.000	.000		.000	.000
	N	3606	3606	3606	3606	3606	3606	3606	3606	3606	3606	3606	3606
Mass Tall kg	Pearson Corre	.210	.534	.254	.000	-.888	-.238	.039	-.017	-.639	-.254	1	.233
	Sig. (2-tailed)	.000	.000	.000	1.000	.000	.000	.020	.308	.000	.000		.000
	N	3606	3606	3606	3606	3606	3606	3606	3606	3606	3606	3606	3606
Mass Short kg	Pearson Corre	.570	.436	.915	.000	-.362	-.967	.044	-.061	-.421	-.915	.233	1
	Sig. (2-tailed)	.000	.000	.000	1.000	.000	.000	.008	.000	.000	.000	.000	
	N	3606	3606	3606	3606	3606	3606	3606	3606	3606	3606	3606	3606

Table 7.8 Estimated regression coefficients of mathematical model for low PGA level

Independent Variable	Unstandardised Coefficients		t-Stat	P-value
	B	Std. Error		
(Constant)	460	25.67	17.94	1.66E-68
Height of the tall building, HT	-0.01	0.00	-10.57	1.14E-25
Height of the short building, HS	-0.28	0.02	-17.28	6.82E-64
Earthquake peak ground acceleration, E	71	1.69	42.24	1.01E-307
Frequency of the tall building, FT	-3.83	0.77	-4.97	7.12E-07
Frequency of the short building, FS	1.32	0.16	8.19	3.93E-16
Damping ratio of the tall building, DT	-0.57	0.04	-14.75	1.23E-47
Damping ratio of the short building, DS	-0.17	0.04	-4.72	2.42E-06
Stiffness of the tall building, ST	-902	127.52	-7.08	1.81E-12
Stiffness of the short building, SS	-11082	641.44	-17.28	6.64E-64
Total mass of the tall building, MT	-0.02	0.01	-1.93	0.0543
Total mass of the short building, MS	0.17	0.01	21.60	2.09E-96

Table 7.9 Estimated regression coefficients of mathematical model under moderate PGA level

Independent Variable	Unstandardised Coefficients		t-Stat	P-value
	B	Std. Error		
(Constant)	434	19.22	22.59	1.15E-104
Height of the tall building, HT	-0.004	0.00	-5.53	3.50E-08
Height of the short building, HS	-0.26	0.01	-21.37	1.49E-94
Earthquake peak ground acceleration, E	12.3	0.79	15.57	1.12E-52
Frequency of the tall building, FT	-0.85	0.58	-1.47	0.142
Frequency of the short building, FS	0.76	0.12	6.40	1.83E-10
Damping ratio of the tall building, DT	-0.64	0.03	-22.12	1.08E-100
Damping ratio of the short building, DS	-0.84	0.03	-30.59	1.25E-179
Stiffness of the tall building, ST	-578	94.98	-6.09	1.286E-09
Stiffness of the short building, SS	-10500	476.87	-22.02	6.98E-100
Total mass of the tall building, MT	0.01	0.01	1.21	0.228
Total mass of the short building, MS	0.07	0.01	11.60	1.73E-30

Table 7.10 Estimated regression coefficients of mathematical model under high PGA level

Independent Variable l	Unstandardised Coefficients		t-Stat	P-value
	B	Std. Error		
(Constant)	58.8	5.96	9.88	9.61E-23
Height of the tall building, HT	-0.02	0.00	-12.38	1.61E-34
Height of the short building, HS	0.026	0.00	25.49	7E-132
Earthquake peak ground acceleration, E	48.87	0.99	49.25	0
Frequency of the tall building, FT	-0.37	1.16	-0.31	0.75
Frequency of the short building, FS	-4.39	0.26	-17.05	1.04E-62
Damping ratio of the tall building, DT	-0.995	0.06	-16.80	5.04E-61
Damping ratio of the short building, DS	-1.36	0.06	-23.73	8.6E-116
Stiffness of the tall building, ST	-1611	192.74	-8.36	9.12E-17
Stiffness of the short building, SS	0.0	0.00	65535.00	0.18
Total mass of the tall building, MT	0.006	0.01	0.45	#NUM!
Total mass of the short building, MS	-0.244	0.01	-18.79	3.15E-75

7.3.6 Deriving the Mathematical Model

The statistically significant coefficients were selected from Tables 7.5–7.7 in order to develop the mathematical models. The mathematical model is used to predict the minimum separation gap needed to avoid pounding between adjacent buildings by substituting the above significant coefficient values in Equation 7.1. Based on the results of the regression analysis, the following linear equations are established and proposed:

For low PGA level:

$$\hat{Y}_1 = 460 - 0.01 \times HT - 0.28 \times HS + 71 \times E - 3.83 \times FT + 1.32 \times FS - 0.57 \times DT - 0.17 \times DS - 902 \times ST - 11082 \times SS + 0.17 \times MS \quad 7.2$$

For moderate PGA level:

$$\hat{Y}_1 = 434 - 0.004 \times HT - 0.26 \times HS + 12.3 \times E + 0.76 \times FS - 0.64 \times DT - 0.84 \times DS - 578 \times ST - 10500 \times SS + 0.07 \times MS \quad 7.3$$

For high PGA level:

$$\hat{Y}_1 = 58.8 - 0.02 \times HT + 0.026 \times HS + 48.87 \times E - 4.39 \times FS - 0.99 \times DT - 1.36 \times DS - 1611 \times ST + 0.006 \times MT - 0.244 \times MS \quad 7.4$$

where $\hat{Y}_1$ is the predicted data (the predicted minimum separation gap using Equation 7.2, 7.3 or 7.4).

There are 11 independent variables, for which frequency, mass and stiffness depend on each other. These parameters were obtained individually using the experimental model. The MLR analysis was done by excluding, in certain cases, the frequency and keeping mass and stiffness, excluding stiffness and keeping frequency and mass, or excluding mass and keeping frequency and stiffness. These steps were carried out in order to minimise the mathematical model's variables and to increase its accuracy. Sections 7.3.3 and 7.3.4 have been repeated for excluding stiffness and mass then frequency and stiffness. Tables 7.8 and 7.9 illustrate the regression coefficients for low PGA level, excluding stiffness and mass, and frequency and stiffness. Tables 7.10 and 7.11 illustrate the regression coefficients for moderate PGA level, excluding stiffness and mass, and frequency and stiffness. Tables 7.12 and 7.13 illustrate the regression coefficients for high PGA level, excluding stiffness and mass, and frequency and stiffness.

The new mathematical equations for low PGA level are:

$$\hat{Y}_2 = 23 - 0.005 \times HT + 57.77 \times E - 4.08 \times FT - 1.7 \times FS - 0.57 \times DT - 0.138 \times DS \quad 7.5$$

$$\hat{Y}_3 = -14 - 0.0023 \times HS + 57 \times E - 0.59 \times DT + 0.04 \times MT + 0.13 \times MS \quad 7.6$$

The new mathematical equations for moderate PGA level are:

$$\hat{Y}_2 = 16 - 0.002 \times HT + 0.008 \times HS + 3 \times E - 2.2 \times FT - 0.24 \times FS - 0.65 \times DT - 0.91 \times DS \quad 7.7$$

$$\hat{Y}_3 = 2 + 0.001 \times HT + 0.007 \times HS + 4 \times E - 0.66 \times DT - 0.87 \times DS + 0.02 \times MT + 0.03 \times MS \quad 7.8$$

The new mathematical equations for high PGA level are:

$$\hat{Y}_2 = -0.83 - 0.009 \times HT + 0.024 \times HS + 49 \times E - 3.4 \times FT - 0.6 \times FS - DT - 1.2 \times DS \quad 7.9$$

$$\hat{Y}_3 = -24 - 0.005 \times HT + 0.03 \times HS + 49 \times E - DT - 1.2 \times DS + 0.04 \times MT - 0.07 \times MS \quad 7.10$$

where $\hat{Y}_2$ and $\hat{Y}_3$ is the predicted data (the predicted minimum separation gap).

Table 7.11 SPSS regression analysis output for low PGA level, excluding stiffness & mass

Independent Variable	Unstandardised Coefficients		t-Stat	P-value
	B	Std. Error		
(Constant)	23	1.668	13.823	3.3E-42
Height of the tall building, HT	-0.005	0.001	-8.796	2.3E-18
Height of the short building, HS	-0.001	0.001	-1.129	0.26
Earthquake peak ground acceleration, E	57.8	1.650	35.018	2.3E-226
Frequency of the tall building, FT	-4.08	0.237	-17.209	1.96E-63
Frequency of the short building, FS	-1.7	0.113	-15.306	5.0E-51
Damping ratio of the tall building, DT	-0.57	0.044	-13.160	1.6E-38
Damping ratio of the short building, DS	-0.14	0.039	-3.522	0.00043

Table 7.12 SPSS regression analysis output for low PGA level, excluding frequency & stiffness

Independent Variable	Unstandardised Coefficients		t-Stat	P-value
	B	Std. Error		
(Constant)	-14	0.59	-23.86	1.3E-55
Height of the tall building, HT	-0.0001	0.00	-0.38	0.7
Height of the short building, HS	-0.0023	0.00	-4.18	2.9E-05
Earthquake peak ground acceleration, E	57	1.58	35.94	1.7E-36
Damping ratio of the tall building, DT	-0.59	0.04	-14.22	1.6E-44
Damping ratio of the short building, DS	-0.06	0.04	-1.71	0.087
Total mass of the tall building, MT	0.04	0.00	15.52	2.4E-52
Total mass of the short building, MS	0.13	0.01	24.77	1.0E-65

Table 7.13 SPSS regression analysis output for moderate PGA level, excluding stiffness & mass

Independent Variable	Unstandardised Coefficients		t-Stat	P-value
	B	Std. Error		
(Constant)	16	1.16	14.06	1.5E-43
Height of the tall building, HT	-0.002	0.00	-3.82	0.00014
Height of the short building, HS	0.008	0.00	13.74	9.3E-42
Earthquake peak ground acceleration, E	3	0.73	4.16	3.3E-05
Frequency of the tall building, FT	-2.2	0.17	-12.80	1.4E-36
Frequency of the short building, FS	-0.24	0.09	-2.74	0.006
Damping ratio of the tall building, DT	-0.65	0.03	-20.84	2.3E-90
Damping ratio of the short building, DS	-0.91	0.03	-30.54	3.6E-79

Table 7.14 SPSS regression analysis output for moderate PGA level, excluding frequency & stiffness

Independent Variable	Unstandardised Coefficients		t-Stat	P-value
	B	Std. Error		
(Constant)	2	0	5	6.0E-06
Height of the tall building, HT	0.001	0.00	3.04	0.0024
Height of the short building, HS	0.007	0.00	14.64	5.9E-47
Earthquake peak ground acceleration, E	4	0.73	5.61	2.2E-08
Damping ratio of the tall building, DT	-0.66	0.03	-21.21	2.5E-93
Damping ratio of the short building, DS	-0.87	0.03	-29.12	7.4E-65
Total mass of the tall building, MT	0.02	0.00	12.19	2.0E-33
Total mass of the short building, MS	0.03	0.00	7.01	2.8E-12

Table 7.15 SPSS regression analysis output for high PGA level, excluding stiffness & mass

Independent Variable	Unstandardised Coefficients		t-Stat	P-value
	B	Std. Error		
(Constant)	-0.83	2.46	-0.3	0.74
Height of the tall building, HT	-0.009	0.001	-11	4.7E-28
Height of the short building, HS	0.024	0.001	22	1.5E-99
Earthquake peak ground acceleration, E	49	1	47	0
Frequency of the tall building, FT	-3.4	0.3	-10.1	1.3E-23
Frequency of the short building, FS	-0.6	0.2	-3.5	0.0004
Damping ratio of the tall building, DT	-1.0	0.1	-15.7	1.6E-53
Damping ratio of the short building, DS	-1.2	0.1	-20.6	2.5E-89

Table 7.16 SPSS regression analysis output for high PGA level, excluding frequency & stiffness

Independent Variable	Unstandardised Coefficients		t-Stat	P-value
	B	Std. Error		
(Constant)	-24	1	-24	4.3E-99
Height of the tall building, HT	-0.005	0.00	-8.71	4.6E-18
Height of the short building, HS	0.03	0.00	36.33	1.8E-96
Earthquake peak ground acceleration, E	49	1	47	0
Damping ratio of the tall building, DT	-1.0	0.06	-15.87	6.6E-55
Damping ratio of the short building, DS	-1.2	0.06	-20.47	3.2E-88
Total mass of the tall building, MT	0.04	0.00	8.82	1.7E-18
Total mass of the short building, MS	-0.07	0.01	-8.31	1.3E-16

7.3.7 Cross-validation Technique

Cross-validation is a statistical method of evaluating how the results of a projected model will validate the real data set. The technique is used when one intends to evaluate and compare how precise a predictive model is when applied to real data (Shao 1993). In this study, two methods of cross-validation were used in Equations 7.11 and 7.12. The mean square error (MSE) represents how close a regression line is to a set of points (the distances are the 'errors'). MSE provides the average squared difference between the outputs and targets. The other method is the mean absolute error (MAE), which is the measure of errors between paired observations expressing the same phenomenon. MAE is the magnitude of difference between the prediction of an observation and actual data or true value of that observation. Lower values mean better performance of the mathematical model (zero means no error). MSE is expressed in Equation 7.11, while MAE is shown in Equation 7.12:

$$MSE = \sum \left(Y_i - \hat{Y}_i\right)^2 / N \tag{7.11}$$

$$MAE = \sum \left|Y_i - \hat{Y}_i\right| / N \tag{7.12}$$

where Y_i is the actual data, $\hat{Y}_i$ is the predicted data (the predicted minimum separation gap using the mathematical model) and N is the number of observations. Table 7.14 shows the MSE and MAE for the above developed mathematical models under different PGA intensity.

Table 7.17 MSE and MAE comparison of the developed mathematical models

	Low PGA Level		Moderate PGA Level		High PGA Level	
	MSE	MAE	MSE	MAE	MSE	MAE
$\hat{Y}_1$	31.11	4.97	11.71	2.93	30.42	4.67
$\hat{Y}_2$	13.3	2.67	7.09	1.84	30.28	4.39
$\hat{Y}_3$	12.02	2.47	6.59	1.82	38.85	4.59

Based on the values of MSE and MAE in Table 7.14, the mathematical model revealed that the lowest value for MSE and MAE is the best-fit model. Therefore, for low, moderate and high PGA levels, the most suitable models are indicated as in Equations 7.6, 7.8 and 7.9, respectively. In the succeeding sections, the different developed models will be validated for the structural parameters.

7.4 **Validation**

In order to validate the method for other structural parameters, the study was extended to buildings with different heights, masses and stiffness of each storey for both buildings. This section describes a demonstrative example of the validation analysis conducted for a 12-storey building adjacent to an 8-storey building and a 10-storey building adjacent to an 8-storey building (Figure 7.6). The adjacent buildings were exposed to the SAP 2 earthquake record (PGA = 0.287 g), the SAP 3 earthquake record (PGA = 0.46 g) and the SAP 5 earthquake record (PGA = 0.843 g) for low, moderate and high PGA levels, respectively. The 12-storey and 8-storey buildings were designed in similar steps as in the previous models. In the analysis, the following basic values of the structural model's parameters were applied: for the 12-storey building, height = 1200 mm, natural frequency = 2.984 Hz, stiffness = 0.0125 kN/mm and mass = 84.5 kg; for the 8-storey building, height = 800 mm, natural frequency = 4.317 Hz, stiffness = 0.0185 kN/mm and mass = 58 kg. Then, similar steps were applied to those in Section 7.3.1 to obtain a numerical minimum separation gap.

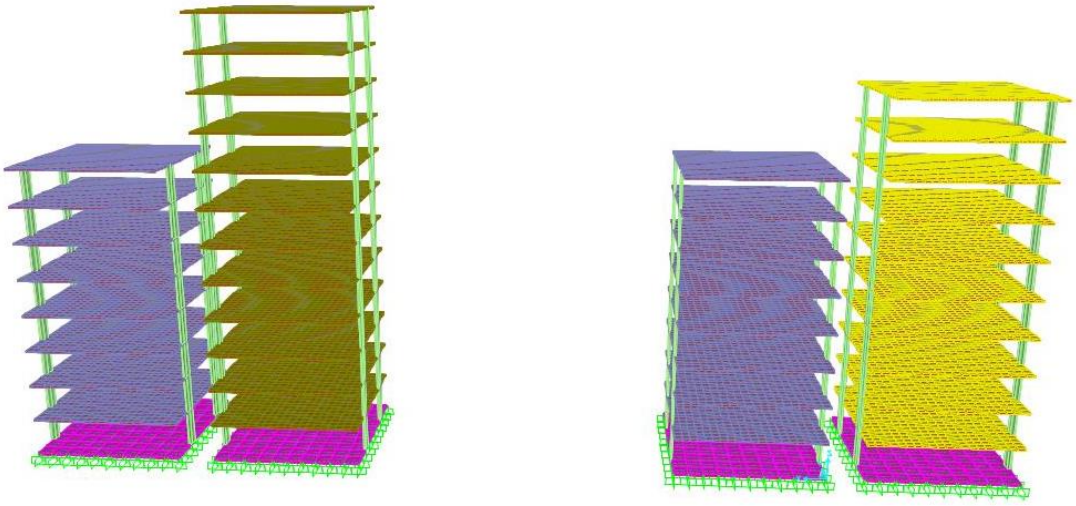

(a) (b)

Figure 7.6 3D numerical model of the structural models in SAP2000; (a) 12-storey adjacent to 8-storey, (b) 10-storey adjacent to 8-storey

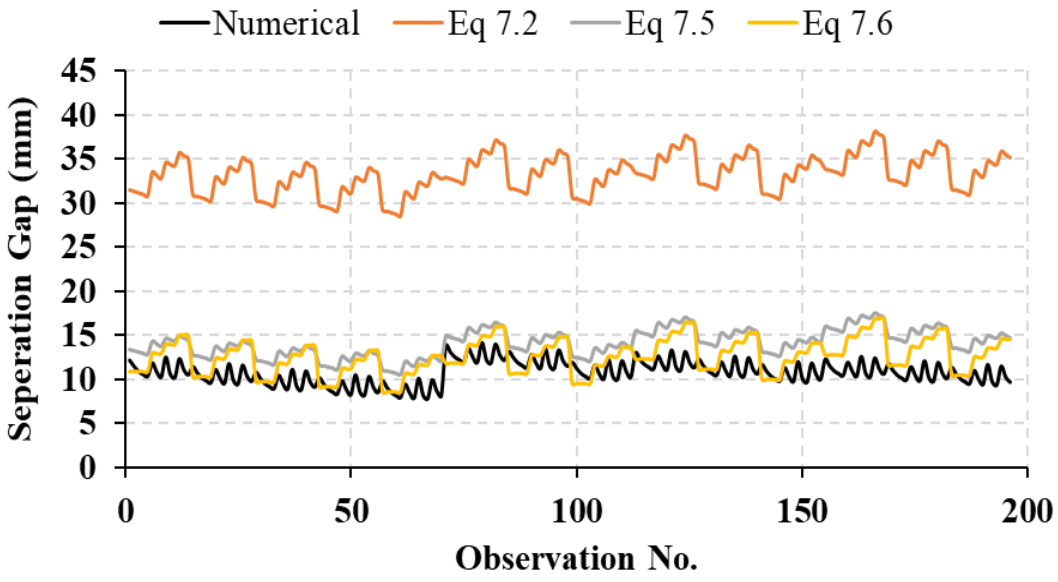

Figure 7.7 (a) Example of the results of the validation analysis for low PGA level under SAP 2 earthquake for the adjacent 12-storey and 8-storey buildings

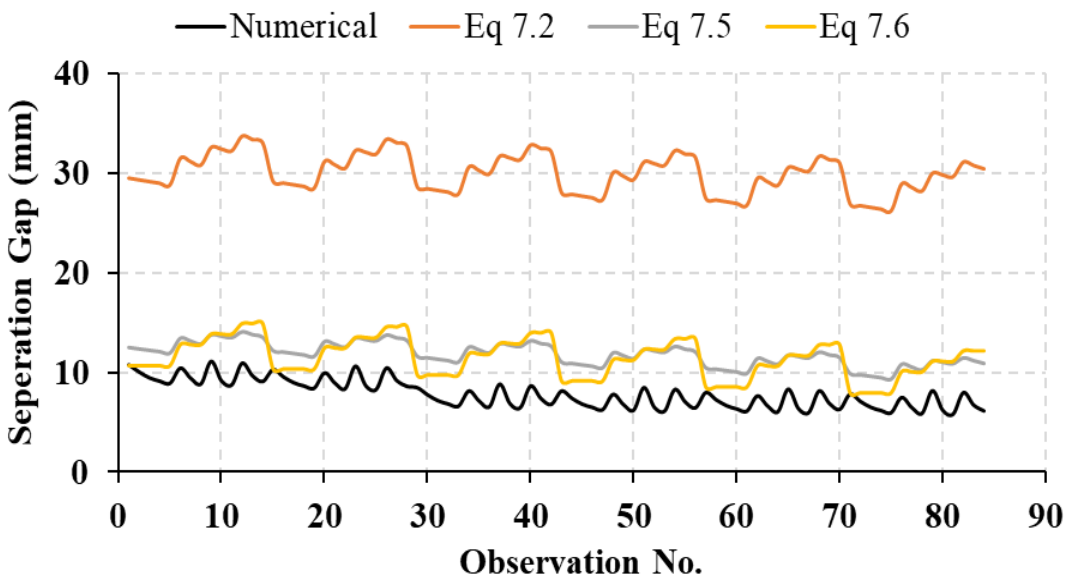

Figure 7.7(b) Example of the results of the validation analysis for low PGA level under SAP 2 earthquake for the adjacent 10-storey and 8-storey buildings

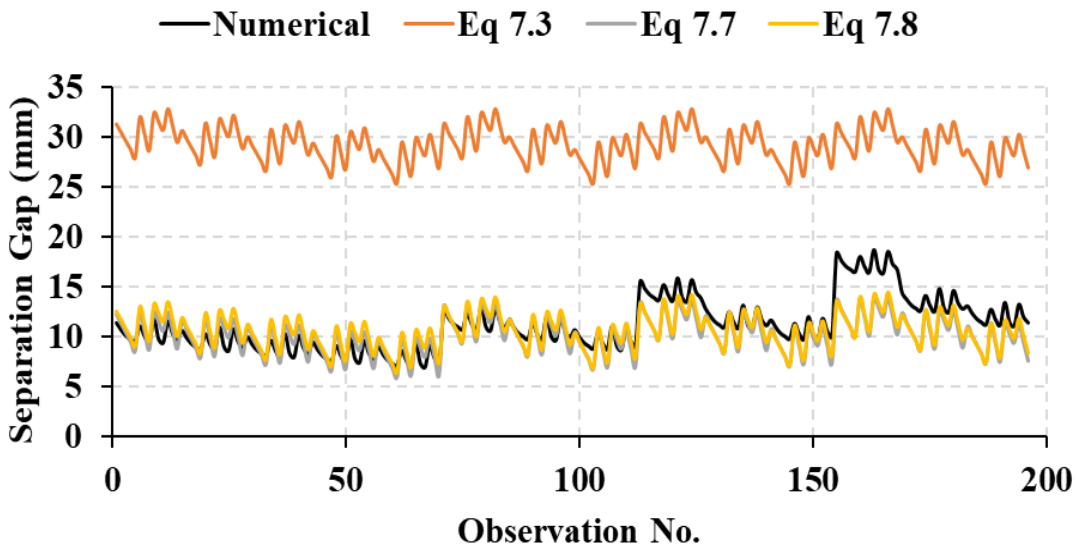

Figure 7.8(a) Example of the results of the validation analysis for moderate PGA level under SAP 3 earthquake for the adjacent 12-storey and 8-storey buildings

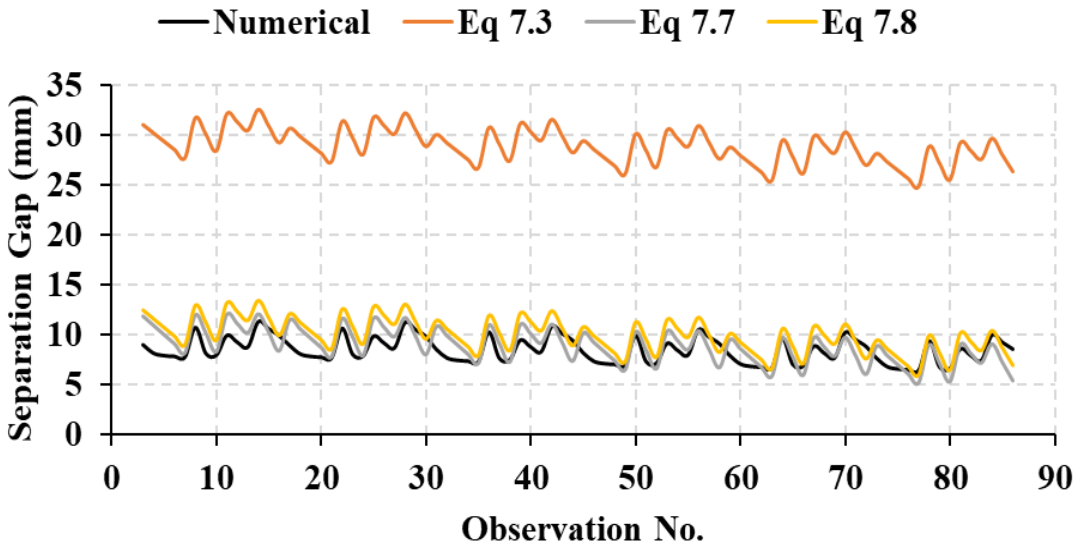

Figure 7.8(b) Example of the results of the validation analysis for moderate PGA level under SAP 3 earthquake for the adjacent 10-storey and 8-storey buildings

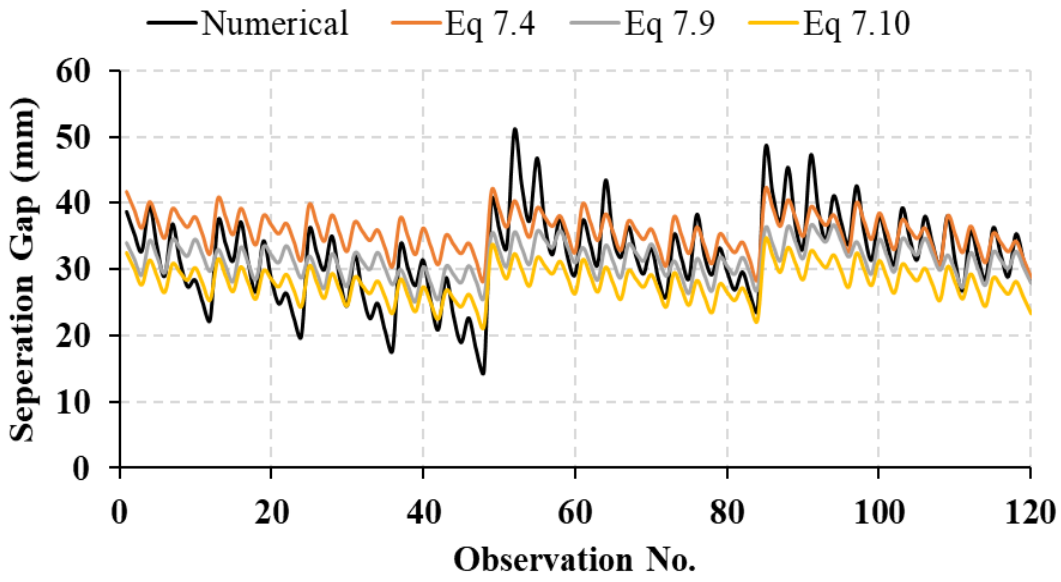

Figure 7.9(a) Example of the results of the validation analysis for high PGA level under SAP 5 earthquake for the adjacent 12-storey and 8-storey buildings

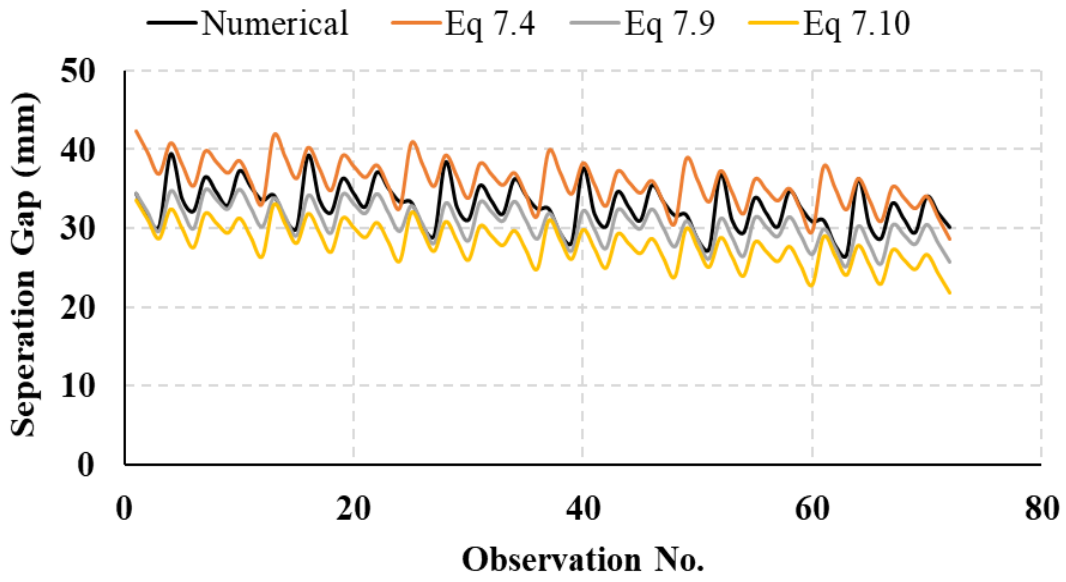

Figure 7.9(b) Example of the results of the validation analysis for high PGA level under SAP 5 earthquake for the adjacent 10-storey and 8-storey buildings

Figure 7.7 shows the separation gap obtained between 12-storey adjacent to 8-storey buildings and 10-storey adjacent to 8-storey buildings exposed to the SAP 2 earthquake record. It can be seen that the predicted separation gaps using Equation 7.2 are too far from the actual numerical data, while the predicted data using Equations 7.5 and 7.6 are close to the actual numerical data. The calculated MSE and MAE for Equations 7.5 and 7.6 in the 12-storey adjacent to 8-storey buildings are (30, 6.03) and (24.3, 4.5), respectively, while the MSE and MAE for Equations 7.5 and 7.6 in the 10-storey adjacent to 8-storey buildings are (16.8, 4.3) and (16.4, 3.6), respectively. Equations 7.5 and 7.6 give very close values of MSE and MAE. Therefore, for simplicity, Equation 7.5 is to be used as the best-fit mathematical model to predict the minimum separation gap for a low PGA level area.

Figure 7.8 depicts the separation gap obtained under the SAP 3 earthquake acceleration record between 12-storey adjacent to 8-storey buildings and 10-storey adjacent to 8-storey buildings. It is apparent that the predicted separation gap using Equation 7.3 is far from the actual numerical data, whereas the predicted data using Equations 7.7 and 7.8 are close to the actual numerical data. The MSE and MAE for Equations 7.7 and 7.8 in 12-storey adjacent to 8-storey buildings are (0.83, 1.53) and (1.94, 1.57) respectively, while the MSE and MAE for Equations 7.7 and 7.8 in 10-storey adjacent to 8-storey buildings are (1.87, 1.13) and (3.63, 1.66) respectively. Equation 7.7 gives the lowest

MSE and MAE. Thus, Equation 7.7 is the best-fit mathematical model to predict the minimum separation gap for a moderate PGA level area.

Figure 7.9 illustrates the separation gap obtained between 12-storey adjacent to 8-storey buildings and 10-storey adjacent to 8-storey buildings exhibited in the SAP 5 earthquake record. Apparently, Equations 7.4, 7.9 and 7.10 predicted the separation gap well. The MSE and MAE for Equations 7.4, 7.9 and 7.10 in 12-storey adjacent to 8-storey buildings are (33.57, 4.6), (24.83, 3.96) and (37.55, 5.25), respectively, while the MSE and MAE for Equations 7.4, 7.9 and 7.10 in 10-storey adjacent to 8-storey buildings are (42.04, 3.49), (28.5, 5.73) and (18.05, 6.72), respectively. Equation 7.9 gives the lowest MSE and MAE. Accordingly, Equation 7.9 is the best-fit mathematical model to predict the minimum separation gap for a high PGA level area.

7.5 **Regression Model Improvements**

The regression model can be enhanced in many instances by increasing or reducing factors and interactions in the analysis selection (Cox 1984). In order to enhance the accuracy and improve the prediction of the developed mathematical models, a series of methods were carried out until a better fit model was developed. Review of the previous section indicates that the mathematical models for low and high PGA levels can be enhanced to improve their accuracy, whereas, the mathematical model output for the moderate PGA level was accurate since the MAE and MSE were very low. Hence, there is no need for any improvements.

7.5.1 Low PGA Level

From the above analysis, the selected mathematical model for low PGA level is expressed in Equation 7.5. The researchers introduced a new variable to be used in the regression analysis: squared value of the earthquake peak ground acceleration, $\boldsymbol{E^2}$. This variable was used after many trials were conducted. The new regression coefficients are illustrated in Table 7.15. The enhanced mathematical model is expressed in Equation 7.13. The values of MSE and MAE for the equation were reduced from 13.3 to 9.67 and from 2.67 to 2.14, respectively.

Table 7.18 SPSS regression analysis output of the enhanced mathematical model for low PGA level

Independent Variable	Unstandardised Coefficients		t-Stat	P-value
	B	Std. Error		
(Constant)	-50.7	2.76	-18.37	1.3E-71
Height of the tall building, HT	-0.0028	0.00	-5.45	5.3E-08
Height of the short building, HS	0.0066	0.00	9.59	1.8E-21
Earthquake peak ground acceleration, E	600	17.35	34.64	3.2E-22
Frequency of the tall building, FT	-3.59	0.21	-17.40	9.6E-65
Frequency of the short building, FS	-0.46	0.11	-4.36	1.3E-05
Damping ratio of the tall building, DT	-0.64	0.04	-16.93	1.5E-61
Damping ratio of the short building, DS	-0.5	0.04	-13.94	7.4E-43
Squared earthquake peak ground acceleration, E^2	-1210	38.53	-31.41	4.3E-88

$$\hat{Y}_i = -50.7 - 0.0028 \times HT + 0.0066 \times HS + 600 \times E - 3.59 \times FT - 0.46 \times FS - 0.64 \times DT - 0.5 \times DS - 1210 \times E^2 \quad 7.13$$

To validate the new enhanced model, Section 7.4 will be repeated for low PGA level exposed to the SAP 2 earthquake record. It is evident in Figure 7.10 that the predicted separation gap using Equation 7.13 is closer to the actual numerical data compared to the prediction by Equation 7.5. The calculated MSE and MAE for Equation 7.13 in 12-storey adjacent to 8-storey buildings are (2.65, 1.2), while the MSE and MAE for Equation 7.13 in 10-storey adjacent to 8-storey buildings are (1.22, 0.96). These very low values of error indicate that the enhanced model performs well and its accuracy has improved.

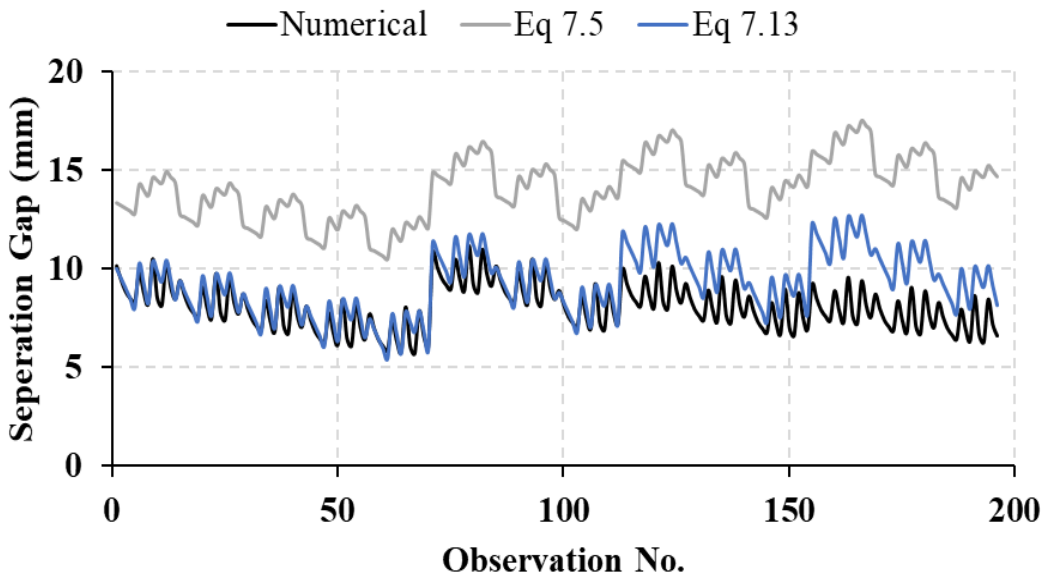

Figure 7.10(a) Validation analysis for low PGA level for the enhanced model under SAP 2 earthquake for the adjacent 12-storey and 8-storey buildings

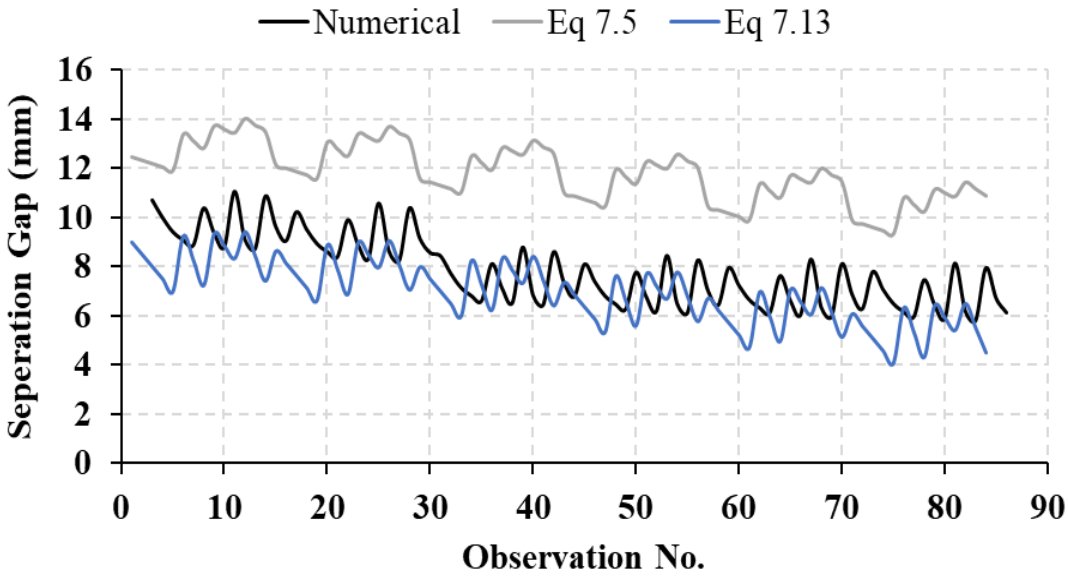

Figure 7.10(b) Validation analysis for low PGA level for the enhanced model under SAP 2 earthquake for the adjacent 10-storey and 8-storey buildings

7.5.2 High PGA Level

Based on the aforementioned analysis, the selected mathematical model for high PGA level is reflected in Equation 7.9. Polynomial regression is a special case of multiple linear regression, which approximates the relationship between the independent and dependent variables depicted as an nth degree polynomial (Ostertagová 2012). Referring to Equation 7.9, the dependent variable output, $\hat{Y}_2$, was used as an independent variable in this polynomial equation, as shown in Figure 7.11. Therefore, the enhanced mathematical

model is expressed in Equation 7.14. The values of MSE and MAE for the equation have dropped from 30.28 to 15.74 and from 4.39 to 3.05, respectively.

$$\hat{Y}_i = 0.054 \times \hat{Y}_2{}^2 - 1.64 \times \hat{Y}_2 + 29.06 \qquad 7.14$$

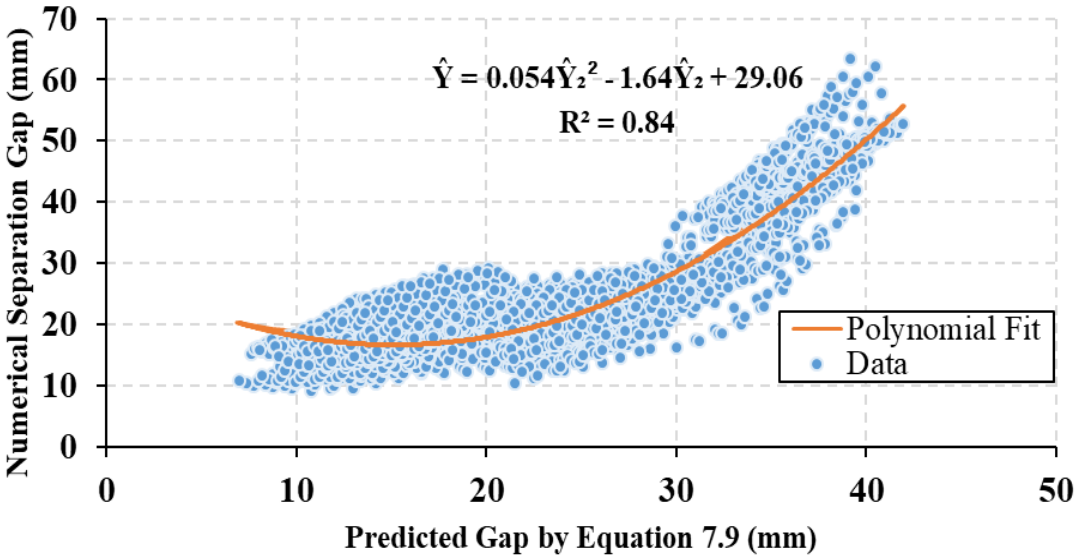

Figure 7.11 Scatter chart between numerical gap and predicted gap using Equation 7.9

To validate the new enhanced model, the procedure defined in Section 7.4 will be repeated for high PGA level exposed to the SAP 5 earthquake record. It is apparent in Figure 7.12 that the predicted separation gap using Equation 7.14 is closer to the actual numerical data compared to the prediction by Equation 7.9. The calculated MSE and MAE for Equation 7.14 in 12-storey adjacent to 8-storey buildings are (19.36, 3.59), while the MSE and MAE for Equation 7.14 in 10-storey adjacent to 8-storey buildings are (24.11, 3.19). The reasonably low values of error indicate that the new enhanced model performs better and the accuracy has improved.

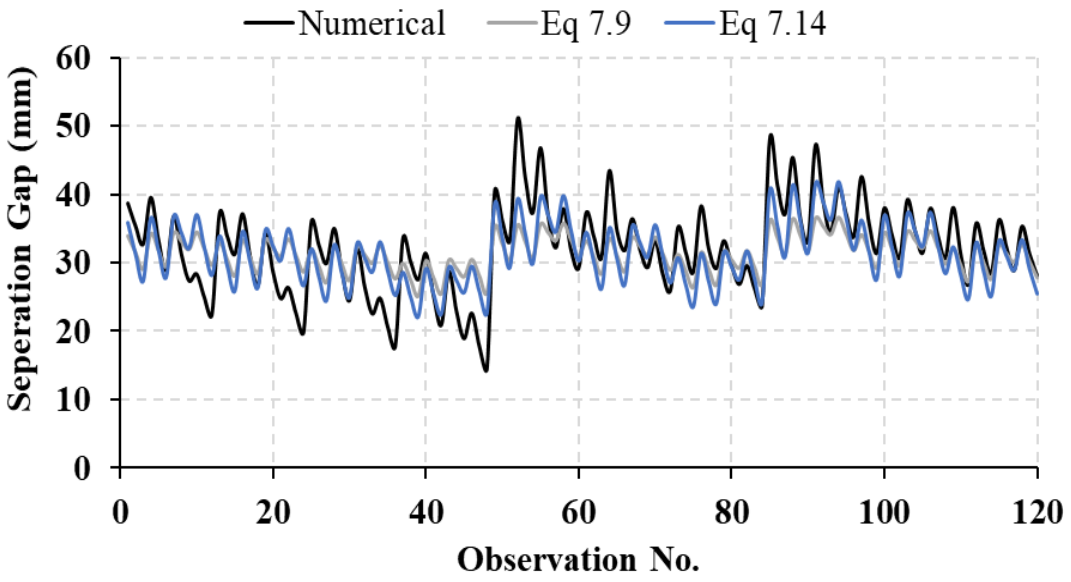

Figure 7.12(a) Validation analysis for high PGA level for the enhanced model under SAP 5 earthquake for the adjacent 12-storey and 8-storey buildings

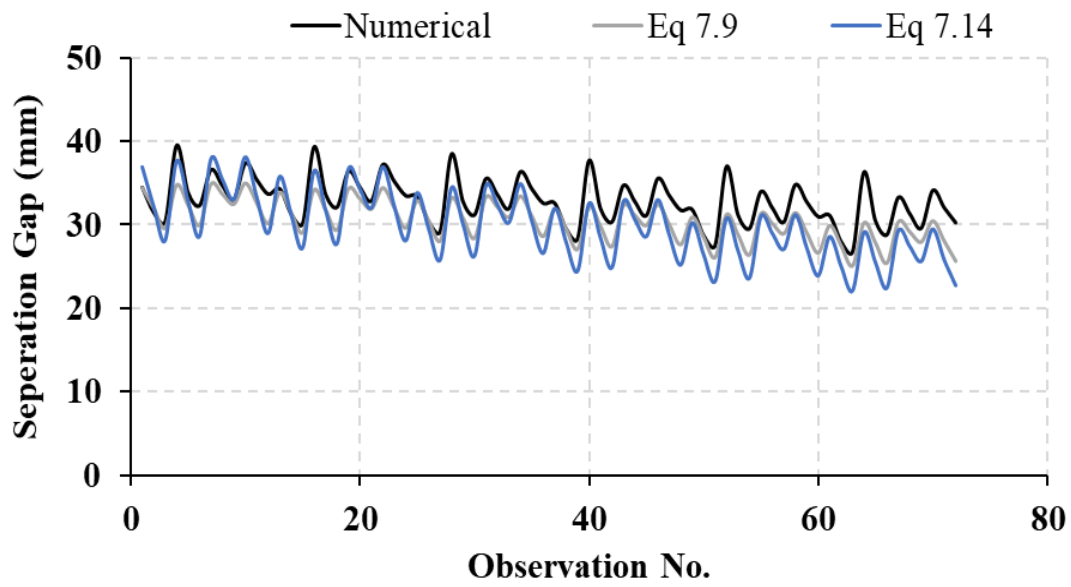

Figure 7.12(b) Validation analysis for high PGA level for the enhanced model under SAP 5 earthquake for the adjacent 10-storey and 8-storey buildings

7.6 **Simplified Procedure for Practical Application**

Numerous research works have been conducted to mitigate the incidence of pounding hazards during earthquakes. One of the objectives is to develop processes for assessing sufficient separation distance between structures to avoid contact during seismic excitations (Penzien 1997). The minimum separation gap is clearly defined in most recent seismic-resistant design codes, such as UBC 1997, Eurocode 2005, IBC 2009 and

AS1170.4. The aim for this provision is to improve the seismic performance of current edifices with insufficient in-between space and to establish adequate techniques to lessen the pounding effects on structural members.

Earthquake-induced structural pounding between adjacent edifices is a complicated phenomenon involving plastic deformations at contact points, local cracking or crushing, fracturing due to impact, friction and other effects. The complex phenomenon makes mathematical modelling and analysis a little difficult for this type of situation. Within this context, there is a need to formulate simple but accurate mathematical procedures for determining sufficient separation gaps of building structures to avoid structural pounding.

7.6.1 Full-Scale Proposed Approach

In this study, the geometric scaling factor (λ) of 1:30 is implemented for experimental shaking table and numerical tests on the scaled building models as mentioned earlier. Moreover, the scaling relationship between the natural frequency of the model (f_m) and natural frequency of the prototype (f_p) (Tabatabaiefar & Mansoury 2016) is described as below.

$$\frac{f_m}{f_p} = \lambda^{-0.5} = 5.48 \tag{7.15}$$

The mathematical models to be used in a full scale are described as follows:

For low PGA level:

$$\begin{aligned} \hat{Y}_i = 30 \times (&-50.7 - 0.0028 \times \frac{HT}{30} + 0.0066 \times \frac{HS}{30} + 600 \times E \\ &- 3.59 \times FT \times 5.48 - 0.46 \times FS \times 5.48 - 0.64 \times DT \\ &- 0.5 \times DS - 1210 \times E^2) \\ S = -1521 &- 0.0028 \times HT + 0.0066 \times HS + 18000 \times E - 590.2 \times FT \\ &- 75.6 \times FS - 19.2 \times DT - 15 \times DS - 36300 \times E^2 \end{aligned} \tag{7.16}$$

For moderate PGA level:

$$\begin{aligned} \hat{Y}_2 = 30 \times (&16 - 0.002 \times \frac{HT}{30} + 0.008 \times \frac{HS}{30} + 3 \times E - 2.2 \times FT \times 5.48 \\ &- 0.24 \times FS \times 5.48 - 0.65 \times DT - 0.91 \times DS) \\ S = 480 &- 0.002 \times HT + 0.008 \times HS + 90 \times E - 361.7 \times FT - 39.5 \times FS - \\ &19.5 \times DT - 27.3 \times DS \end{aligned} \tag{7.17}$$

For high PGA level:

$$\hat{Y}_2 = 30 \times (-0.83 - 0.009 \times \frac{HT}{30} + 0.024 \times \frac{HS}{30} + 49 \times E - 3.4 \times FT \times 5.48 - 0.6 \times FS \times 5.48 - DT - 1.2 \times DS)$$

$$S = -24.9 - 0.009 \times HT + 0.024 \times HS + 720 \times E - 559 \times FT - 98.6 \times FS - 30 \times DT - 36 \times DS \quad 7.18$$

In the high PGA level, the value of S that was derived from Equation 7.18 will be replaced with the value of $\hat{Y}_2$ in Equation 7.14. This is essential in the high PGA level only.

7.6.2 Worked Example

In order to estimate the separation gap between two adjacent buildings using Equations 7.16, 7.17 and 7.18 in the real environment, structural engineers should first determine the structural characteristics including the height of the tall and short structure (HT, HS), the fundamental natural frequency of the tall and short structure (FT, FS) and the structural damping ratio of the tall and short structure (DT, DS). To determine the level of seismicity of the area, Equation 7.16 is suggested for low PGA level, Equation 7.17 is recommended for moderate PGA level, and Equations 7.18 and then 7.14 are proposed for high PGA level.

Let us assume a 13-storey building will be built next to an existing 7-storey building in Sydney, Australia. The heights of the tall and short buildings are $HT = 39\ m$ and $HS = 21\ m$.

To estimate the building vibration period for the 13-storey and 7-storey buildings, the following equation given in the Australian Standard (AS1170.4 2007) code is used:

$$T = 1.25 k_t h^{0.75} \quad 7.19$$

where *T* is the fundamental natural translational period of the structure, k_t depends on the structural type (it is 0.11 for moment-resisting steel frames and 0.075 for moment-resisting concrete frames) and h is the height from the base of the structure to the uppermost seismic weight or mass, in metres.

Thus, the natural frequencies of the 13-storey and 7-storey buildings are 0.466 Hz and 0.7414 Hz, respectively.

$$T_{13} = 1.25 \times 0.11 \times 39^{0.75} = 2.1458\ sec \Rightarrow f_{13} = 0.466\ Hz$$

$$T_7 = 1.25 \times 0.11 \times 21^{0.75} = 1.3488\ sec \Rightarrow f_7 = 0.7414\ Hz$$

For the purpose of this example, a damping ratio of 5% is used for the two multistorey buildings. Furthermore, the Sydney Basin region is considered a low-risk seismic area. Present evaluation of earthquake risks in the Sydney area points out that, on average, there is a ten percent probability of ground acceleration surpassing 0.11g in 100 (Denham 1992). However, in the above equations, values lower than 0.2g are ignored due to the very low level of PGA, which will have no impact or a very low impact on the structures. Equation 7.16 is used to calculate the separation gap for low PGA level only. This is the only level that should be considered in the Sydney example. In calculating the separation gap between the two buildings in this example, the value of the PGA used was 0.2g. The separation gap of 154.32 mm was derived based on this equation. In contrast, the separation gap according to the Australian Standard was found as in Equation 2.30. The calculated value of the separation gap when based on the height of the tall building is 390 mm and when based on the height of the short building is 210 mm. The calculations are anchored on the Australian Standard, as expressed in Equation 2.30.

As can be gleaned from the example, the Australian Standard is safe enough based on the low level of PGA. In other countries, high PGA levels necessitate the inclusion of multiple variables to achieve a more accurate computation of the separation gap.

It is important to note that the proposed mathematical models presented in this study are specifically applicable to mid-rise steel frame buildings with unequal heights, assuming elastic structural response. Additionally, it is worth mentioning that soil-structure interaction was not considered in this study. The analysis proceeded under the assumption that the soil beneath the foundations is infinitely rigid. These assumptions and limitations should be taken into account when applying the findings of the study to real-world scenarios or when considering the broader context of soil-structure interaction.

7.6.3 Suggested Standard for Australia

In this section, recommendations are made to remove the ambiguity in the Australian Earthquake Standard (AS1170.4 2007) regarding which height to be used – the height of the tall building or the height of the short building. Table 7.16 presents the estimated regression coefficients for a low level of PGA. As concluded in Chapter 4, Australia is a low PGA seismicity region.

Table 7.19 SPSS regression analysis output for low PGA level, using building heights only

Independent Variable	Unstandardised Coefficients		t-Stat	P-value
	B	Std. Error		
(Constant)	0	#N/A	#N/A	#N/A
Height of the tall building, HT	0.0013	0.000197	6.710093	2.31E-11
Height of the short building, HS	0.0098	0.000373	26.12235	4.9E-136

The mathematical model is used to predict the minimum separation gap needed to avoid pounding between adjacent buildings by substituting the above significant coefficient values in Equation 7.1. Based on the results of the regression analysis, the following linear equation is developed and proposed:

$$S = 0.0013 \times HT + 0.0098 \times HS \qquad 7.20$$

However, the error values for Equation 7.20 compared with Equation 7.13 are higher. The MSE and MAE for Equation 7.20 are 21.20 and 3.30, respectively.

Referring to the example in Section 7.6.2, the separation gap between the adjacent 13-storey and 7-storey buildings is:

$$S = 0.0013 \times 39000 + 0.0098 \times 21000$$
$$= 256.50\ mm$$

7.7 Summary

In this chapter, in order to estimate the minimum separation gaps needed between mid-rise steel frame buildings to avoid potential collision during seismic excitation, experimental and numerical investigations were carried out focussing on using multiple regression analysis to develop mathematical equations.

The earthquake characteristics, the parameters of the buildings and numerical separation gaps have been defined as inputs in the regression analysis.

According to the results, the separation gap is directly proportional to the height of the short building (HS) and the earthquake peak ground acceleration (E). Moreover, the computed separation gap is inversely proportional to the height of the tall building (HT), frequency of the tall building (FT), frequency of the short building (FS), damping ratio of the tall building (DT) and damping ratio of the short building (DS).

Furthermore, it is observed that the proposed mathematical model developed in this investigation can be successfully used to determine the required minimal distance

between two adjacent buildings to prevent their collisions during different seismic excitations.

Therefore, this study is suggested as a reference for engineers that will provide them with validated mathematical equations with which they can estimate the minimum required separation gap between adjacent buildings to avoid earthquake-induced pounding.

CHAPTER 8
CONCLUSIONS AND RECOMMENDATIONS

8.1 Conclusions

Earthquake-induced pounding is a phenomenon that has been detected in almost every major earthquake since the 1960s. Pounding between adjacent buildings happens due to inadequate separation and the different dynamic properties of the structures. This usually causes local damage and, in some extreme cases, total collapse of structures. Building pounding has long been recognised as an urban seismic hazard due to its occurrence in almost all major earthquakes; for example, Mexico City, 1985, Loma Prieta, 1989 and Christchurch, 2011. Surveys conducted after major earthquakes have acknowledged numerous building arrangements that are especially exposed to pounding damage.

In order to avoid earthquake-induced pounding during severe earthquakes, minimum separation gap between adjacent buildings were recommended by building codes in seismically active zones. Australian Standard AS1170.4 requires 1% of the building height as a minimum separation gap between buildings to preclude pounding. Thus, it is essential to examine the adequacy of this specification. Additionally, an effective formula designed for estimating the seismic gap is needed for avoiding earthquake-induced pounding between buildings during various ground motions.

Furthermore, when simulating the structural response, the stiffness of the spring in the impact element has been considered as one of the main significant factors when the impact force during collision of adjacent buildings is calculated. Defining effective and realistic stiffness value is vital in numerical simulation of impact forces due to pounding between neighbouring buildings in order to attain realistic results. Therefore, modelling of impact is a tremendously challenging task. Thus, accurate numerical impact model is vital if a precise structural response has to be simulated.

In this study, testing was conducted on an independent lab platform at the UTS civil laboratories. Shaking table tests were performed on coupled steel structural models, with different configuration and gaps, under the effect of four scaled earthquake time histories. Experimental data were measured using accelerometers, laser displacement and force sensors. A full nonlinear time history dynamic analysis was performed on the scaled structural models to produce numerical results. Based on the numerical results and experimental measurements conducted in this report, it can be concluded that:

- The standard-based separation gap prescribed in AS 1170.4-2007 is inadequate when the shorter building height in a coupled case is considered under the given earthquake excitation. This requirement also becomes inadequate when the taller building height is utilised under a near-field earthquake.
- The standard-based separation gap prescribed in AS 1170.4-2007 is only adequate if the height of the taller structure is contemplated under a far-field earthquake.
- The ABS method is the most reliable method in determining the separation gap. However, it tends to overestimate the values.
- The SRSS method produces more veracious results while overestimating the values at times.
- The SRSS method is conservative when the natural frequencies of both structures are close to each other and reasonably accurate for determining the separation gap if the natural frequencies are different.
- The earthquake characteristics of near-field and far-field earthquakes have significant impact on the gap requirements necessary to prevent collision.
- Lateral displacement response due to pounding will be decreased in both adjacent buildings only when the fundamental period of both buildings and the dominant period of the ground motion are closely aligned.
- Compared to the no-pounding state, building top floor pounding can reduce the lateral displacement over the entire building height, whereas pounding at building mid-height can increase the peak lateral displacement response over the entire building height.
- The proposed impact stiffness value of $k = 620\ kN/mm$ can be scaled up based on $k = 620 \times \hat{S}$, where $\hat{S}$ presents the scale factor. The formula was formulated as a result of comparing the theoretical and experimental findings. The theoretical study presents numerical analysis that utilised various earthquakes with different k values.
- The proposed impact stiffness (k value) of the experimental study was the most relevant value to the standard deviation and error rate of the numerical analysis.
- All the theoretical contact models predicted the pounding response of closely spaced structures and generated similar predictions in terms of number and time of impact. However, the models did not accurately predict the magnitude of pounding force in most cases. This difference can be attributed to difficulty in

evaluating the dynamic properties of the structures and inability of the models to accurately simulate the contact behaviour.

- The pounding impact force depends on the earthquake characteristics and the relationship between the buildings' natural frequencies.
- The analytical results are more sensitive to the identification of the dynamic characteristics of the structures and to the accurate representation of the contact conditions.
- Pounding force time history depends substantially on a number of factors, such as the masses of the colliding structures, their relative velocities before impact, structural material properties, contact surface geometry and previous impact history.
- The linear viscoelastic model appears to be the most suitable model for conducting pounding simulation among the five models investigated in this study.
- Experimental measurements showed congruence with the theoretical models when the adjacent stiff and rigid steel frame (5B-storey) collides with more a flexible frame (15B-storey). However, there was incongruence and overestimation when the adjacent flexible frames collide (15B-storey adjacent to 10-storey).
- The proposed mathematical model developed in this study can be successfully used to determine the required minimal distance between two adjacent buildings to prevent their collisions during different seismic excitations.
- Some parameters have a greater impact on the separation gaps when compared with other parameters. The parameter of HS has a higher impact than HT, and DS has a higher impact than DT. These prove that short building characteristics play a major role in ascertaining the minimum separation gap needed to avoid pounding between adjacent structures during earthquakes.
- Practical application of the proposed mathematical model for simulation purposes in predicting adequate separation gaps between adjacent buildings to avoid earthquake-induced pounding requires knowledge of the model's parameters.
- The proposed mathematical equations are suggested as a reference for engineers that will enable them to estimate the minimum required separation gap between adjacent buildings.

8.2 **Recommendations and Future Works**

This research work has focussed on investigating the problem of earthquake-induced pounding between adjacent steel frames, modelled as fixed-base structures. Additional numerical and experimental studies and enhancements are recommended to make this research work more inclusive for practical applications. Future research work is recommended in the following areas:

1. numerical and experimental investigations (those outlined in this research) into pounding between adjacent multistorey structures, considering soil–structure interaction
2. further experiments on seismic pounding between concrete structures (recommended for future impact element model comparison)
3. developing a novel impact model that could more efficiently simulate pounding between different building categories.
4. further studies to quantify the effect of the impact damping ratio and the coefficient of restitution on impact modelling for different arrangements of colliding structures.
5. more extensive experimental studies to evaluate the range of the model's parameters more accurately for various types of structures with different material and contact surface geometry properties
6. further studies considering the pounding scenario of slab-to-column collision (floor-to-column collision). This research considers slab-to-slab collision (floor-to-floor collision) only.
7. The study solely focused on a specific type of frame, namely the moment-resisting steel frame. Other types of frames, such as ordinary moment frames, intermediate moment frames, and braced frames, were not taken into account. Consequently, it is recommended that future studies address this limitation and consider the inclusion of different frame types to broaden the scope of research.

REFERENCES

Abdel Raheem, S.E. 2006, 'Seismic pounding between adjacent building structures', *Electronic Journal of Structural Engineering*, vol. 6, pp. 66-74.

Abdel Raheem, S.E. 2014, 'Mitigation measures for earthquake induced pounding effects on seismic performance of adjacent buildings', *Bulletin of Earthquake Engineering*, vol. 12, no. 4, pp. 1705-24.

Anagnostopoulos, S. 1995, 'Earthquake induced pounding: State of the art', *Proceedings of the 10th European Conference on Earthquake Engineering*, vol. 2, Balkema: Rotterdam, pp. 897-905.

Anagnostopoulos, S. 1996, 'Building pounding re-examined: how serious a problem is it', *11th World Conference on Earthquake Engineering*, Pergamon, Elsevier Science Oxford, UK, p. 2108.

Anagnostopoulos, S. & Karamaneas, C. 2008, 'Use of collision shear walls to minimize seismic separation and to protect adjacent buildings from collapse due to earthquake-induced pounding', *Earthquake engineering & structural dynamics*, vol. 37, no. 12, pp. 1371-88.

Anagnostopoulos, S.A. 1988, 'Pounding of buildings in series during earthquakes', *Earthquake Engineering & Structural Dynamics*, vol. 16, no. 3, pp. 443-56.

Anagnostopoulos, S.A. 2004, 'Equivalent viscous damping for modeling inelastic impacts in earthquake pounding problems', *Earthquake Engineering & Structural Dynamics*, vol. 33, no. 8, pp. 897-902.

Anagnostopoulos, S.A. & Spiliopoulos, K.V. 1992, 'An investigation of earthquake induced pounding between adjacent buildings', *Earthquake engineering & structural dynamics*, vol. 21, no. 4, pp. 289-302.

AS1170.4 2007, 'Structural Design Actions Part 4: Earthquake Actions in Australia', *Australian Standards, Sydney*.

AS/NZS3678 2011, 'Structural steel—Hot-rolled plates, floorplates and slabs', *Australian Standards, Sydney*

ASCE 2013, 'Minimum Design Loads for Buildings and Other Structures (ASCE/SEI 7–10)', *American Society of Civil Engineers, USA*.

Barbato, M. & Tubaldi, E. 2013, 'A probabilistic performance-based approach for mitigating the seismic pounding risk between adjacent buildings', *Earthquake Engineering & Structural Dynamics*, vol. 42, no. 8, pp. 1203-19.

Barros, R.C. & Khatami, S.M. 2012, 'Seismic response effect of shear walls in reducing pounding risk of reinforced concrete buildings subjected to near-fault ground motions', *Proceedings of the fifthteenth World Conference on Earthquake Engineering. Lisbon, Portugal*.

Bennett, J.O., Briggs, W.L. & Badalamenti, A. 2008, *Using and understanding mathematics: A quantitative reasoning approach*, Pearson Addison Wesley Reading.

Chakravarti, I.M., Laha, R.G. & Roy, J. 1967, *Handbook of methods of applied statistics*, vol. I, Wiley Online Library, New York.

Chau, K.T., Wei, X.X., Guo, X. & Shen, C.Y. 2003, 'Experimental and theoretical simulations of seismic poundings between two adjacent structures', *Earthquake Engineering and Structural Dynamics*, vol. 32, no. 4, pp. 537-54.

Chopra, A. 2007, *Dynamics of Structures. 3rd edition*, Prentice Hall, New Jersey.

Cole, G., Chouw, N. & Dhakal, R. 2011a, 'Building and bridge pounding damage observed in 2011 Christchurch earthquake'.

Cole, G., Dhakal, R., Carr, A. & Bull, D. 2010a, 'Building pounding state of the art: Identifying structures vulnerable to pounding damage', *2010 NZSEE Conference*, University of Canterbury. Civil and Natural Resources Engineering, Christchurch, New Zealand.

Cole, G., Dhakal, R., Carr, A. & Bull, D. 2010b, 'Interbuilding pounding damage observed in the 2010 Darfield earthquake', *Bulletin of the New Zealand Society for Earthquake Engineering*, vol. 43, no. 4, pp. 382-6.

Cole, G., Dhakal, R., Carr, A. & Bull, D. 2011b, 'An investigation of the effects of mass distribution on pounding structures', *Earthquake Engineering & Structural Dynamics*, vol. 40, no. 6, pp. 641-59.

Cole, G., Dhakal, R., Carr, A. & Bull, D. 2012a, '3D Modelling of Building Pounding Including Diaphragm Flexibility', *PROCEEDINGS OF THE FIFTHTEENTH WORLD CONFERENCE ON EARTHQUAKE ENGINEERING*, LISBON, PORTUGAL.

Cole, G.L., Dhakal, R.P. & Turner, F.M. 2012b, 'Building pounding damage observed in the 2011 Christchurch earthquake', *Earthquake Engineering & Structural Dynamics*, vol. 41, no. 5, pp. 893-913.

Council, B.S.S. & Council, A.T. 1997, *NEHRP guidelines for the seismic rehabilitation of buildings*, vol. 1, Federal Emergency Management Agency.

Cox, D.R. 1984, 'Interaction', *International Statistical Review/Revue Internationale de Statistique*, pp. 1-24.

Crozet, V., Politopoulos, I. & Chaudat, T. 2019, 'Shake table tests of structures subject to pounding', *Earthquake Engineering & Structural Dynamics*, vol. 48, no. 10, pp. 1156-73.

Crozet, V., Politopoulos, I., Yang, M., Martinez, J. & Erlicher, S. 2017, 'Influential Structural Parameters of Pounding between Buildings during Earthquakes', *Procedia engineering*, vol. 199, pp. 1092-7.

Degg, M. 1992, 'Some implications of the 1985 Mexican earthquake for hazard assessment', *Geohazards*, Springer, pp. 105-14.

Degg, M.R. 1989, 'Earthquake hazard assessment after Mexico (1985)', *Disasters*, vol. 13, no. 3, pp. 237-46.

Denham, D. 1992, 'Earthquake attack in the Sydney Basin: What is the risk?', *Exploration Geophysics*, vol. 23, no. 4, pp. 579-87.

Doğan, M. & Günaydin, A. 2009, 'Pounding Of Adjacent RC Buildings During Seismıc Loads', *Eskişehir Osmangazi Üniversitesi Mühendislik ve Mimarlık Fakültesi Dergisi*, vol. 22, no. 1, pp. 129-45.

Dossogne, T., Masset, L., Peeters, B. & Noël, J. 2019, 'Nonlinear dynamic model upgrading and updating using sine-sweep vibration data', *Proceedings of the Royal Society A*, vol. 475, no. 2229, p. 20190166.

Elwardany, H., Seleemah, A. & Jankowski, R. 2017, 'Seismic pounding behavior of multi-story buildings in series considering the effect of infill panels', *Engineering Structures*, vol. 144, pp. 139-50.

Eurocode-8 2005, 'Design of structures for earthquake resistance-part 1: general rules, seismic actions and rules for buildings', *Brussels: European Committee for Standardization*

Far, H. 2019, 'Dynamic behaviour of unbraced steel frames resting on soft ground', *Steel Construction*, vol. 12, no. 2, pp. 135-40.

Far, H. & Flint, D. 2017, 'Significance of using isolated footing technique for residential construction on expansive soils', *Frontiers of Structural and Civil Engineering*, vol. 11, no. 1, pp. 123-9.

Favvata, M.J. 2017, 'Minimum required separation gap for adjacent RC frames with potential inter-story seismic pounding', *Engineering Structures*, vol. 152, pp. 643-59.

Filiatrault, A. & Cervantes, M. 1995, 'Separation between buildings to avoid pounding during earthquakes', *Canadian Journal of Civil Engineering*, vol. 22, no. 1, pp. 164-79.

Filiatrault, A., Wagner, P. & Cherry, S. 1995, 'Analytical prediction of experimental building pounding', *Earthquake engineering & structural dynamics*, vol. 24, no. 8, pp. 1131-54.

Flores, P. & Lankarani, H.M. 2016, *Contact force models for multibody dynamics*, vol. 226, Springer, Switzerland.

Garcia, D.L. 2004, 'SEPARATION BETWEEN ADJACENT NONLINEAR STRUCTURES FOR PREVENTION OF SEISMIC POUNDING', 2004 Aug 01.

GB50011 2001, 'Code for Seismic Design of Buildings (2001 Edition)', *China Building Industry Publisher, Beijing*.

Ghandil, M. & Aldaikh, H. 2017, 'Damage-based seismic planar pounding analysis of adjacent symmetric buildings considering inelastic structure–soil–structure interaction', *Earthquake Engineering & Structural Dynamics*, vol. 46, no. 7, pp. 1141-59.

Goldsmith, W. 2001a, *Impact*, Courier Corporation.

Goldsmith, W. 2001b, 'Impact: the theory and physical behaviour of colliding solids, 2001', *Nineola, NY: Dover Publications*.

Guo, A., Cui, L. & Li, H. 2012, 'Impact stiffness of the contact-element models for the pounding analysis of highway bridges: experimental evaluation', *Journal of Earthquake Engineering*, vol. 16, no. 8, pp. 1132-60.

Hao, H. 2015, 'Analysis of seismic pounding between adjacent buildings', *Australian Journal of Structural Engineering*, vol. 16, no. 3, pp. 208-25.

Hao, H., Bi, K., Chouw, N. & Ren, W.-X. 2013, 'State-of-the-art review on seismic induced pounding response of bridge structures', *Journal of Earthquake and Tsunami*, vol. 7, no. 03, p. 1350019.

Hao, H. & Liu, X. 1998, 'Estimation of required separations between adjacent structures under spatial ground motions', *Journal of earthquake Engineering*, vol. 2, no. 02, pp. 197-215.

Hatzigeorgiou, G.D. 2010, 'Damping modification factors for SDOF systems subjected to near-fault, far-fault and artificial earthquakes', *Earthquake Engineering & Structural Dynamics*, vol. 39, no. 11, pp. 1239-58.

Hong, H.P., Wang, S.S. & Hong, P. 2003, 'Critical building separation distance in reducing pounding risk under earthquake excitation', *Structural Safety*, vol. 25, no. 3, pp. 287-303.

IBC 2009, 'International building code', *International Code Council, Country Club Hills, Illinois. USA*.

ISC 2005, 'Iranian code of practice for seismic resistant design of buildings', *Standard*, vol. 30, p. 31.

Isobe, D., Ohta, T., Inoue, T. & Matsueda, F. 2012, 'Seismic pounding and collapse behavior of neighboring buildings with different natural periods', *Natural Science*, vol. 4, no. 28A, pp. 686-93.

Jankowski, R. 2005, 'Non-linear viscoelastic modelling of earthquake-induced structural pounding', *Earthquake engineering & structural dynamics*, vol. 34, no. 6, pp. 595-611.

Jankowski, R. 2006, 'Pounding force response spectrum under earthquake excitation', *Engineering Structures*, vol. 28, no. 8, pp. 1149-61.

Jankowski, R. 2007, 'Theoretical and experimental assessment of parameters for the non-linear viscoelastic model of structural pounding', *Journal of theoretical and applied mechanics*, vol. 45, pp. 931-42.

Jankowski, R. 2008a, 'Comparison of numerical models of impact force for simulation of earthquake-induced structural pounding', *International Conference on Computational Science*, Springer, Kraków, POLAND, pp. 710-7.

Jankowski, R. 2008b, 'Earthquake-induced pounding between equal height buildings with substantially different dynamic properties', *Engineering Structures*, vol. 30, no. 10, pp. 2818-29.

Jankowski, R. 2009, 'Non-linear FEM analysis of earthquake-induced pounding between the main building and the stairway tower of the Olive View Hospital', *Engineering Structures*, vol. 31, no. 8, pp. 1851-64.

Jankowski, R. 2010, 'Experimental study on earthquake-induced pounding between structural elements made of different building materials', *Earthquake Engineering & Structural Dynamics*, vol. 39, no. 3, pp. 343-54.

Jankowski, R. 2015, 'Pounding between superstructure segments in multi-supported elevated bridge with three-span continuous deck under 3D non-uniform earthquake excitation', *Journal of Earthquake and Tsunami*, vol. 9, no. 04, p. 1550012.

Jankowski, R. 2016, 'Pounding between Inelastic Three-Storey Buildings under Seismic Excitations', *Key Engineering Materials*, vol. 665, Trans Tech Publ, pp. 121-4.

Jankowski, R. & Mahmoud, S. 2016, 'Linking of adjacent three-storey buildings for mitigation of structural pounding during earthquakes', *Bulletin of Earthquake Engineering*, vol. 14, no. 11, pp. 3075-97.

Jankowski, R., Seleemah, A., El-Khoriby, S. & Elwardany, H. 2015, 'Experimental study on pounding between structures during damaging earthquakes', *Key Engineering Materials*, vol. 627, pp. 249-52.

Jankowski, R., Wilde, K. & Fujino, Y. 1998, 'Pounding of superstructure segments in isolated elevated bridge during earthquakes', *Earthquake engineering & structural dynamics*, vol. 27, no. 5, pp. 487-502.

Jaradat, Y. & Far, H. 2020, 'Optimum Stiffness Values for Impact Element Models to Determine Pounding Forces between Adjacent Buildings', *Structural Engineering and Mechanics*, vol. 77, no. 2, pp. 293-304.

Jaradat, Y. & Far, H. 2021, 'Project Title: Seismic Behaviour of High-rise and Mid-rise Buildings', <https://www.youtube.com/channel/UCchETciW6Dmzzpxys7mg4Ew>.

Jeng, V., Kasai, K. & Jagiasi, A. 1992a, 'The separation to avoid seismic pounding', *Proc., 10th World Conf. on Earthquake Engeering*.

Jeng, V., Kasai, K. & Maison, B.F. 1992b, 'A spectral difference method to estimate building separations to avoid pounding', *Earthquake spectra*, vol. 8, no. 2, pp. 201-23.

Jeng, V. & Tzeng, W.L. 2000, 'Assessment of seismic pounding hazard for Taipei City', *Engineering Structures*, vol. 22, no. 5, pp. 459-71.

K-Karamodin, A. & H-Kazemi, H. 2010, 'Semi-active control of structures using neuro-predictive algorithm for MR dampers', *Structural Control and Health Monitoring: The Official Journal of the International Association for Structural Control and Monitoring and of the European Association for the Control of Structures*, vol. 17, no. 3, pp. 237-53.

Karayannis, C.G. & Favvata, M.J. 2005a, 'Earthquake-induced interaction between adjacent reinforced concrete structures with non-equal heights', *Earthquake engineering & structural dynamics*, vol. 34, no. 1, pp. 1-20.

Karayannis, C.G. & Favvata, M.J. 2005b, 'Inter-story pounding between multistory reinforced concrete structures', *Structural Engineering and Mechanics, An Int'l Journal*, vol. 20, no. 5, pp. 505-26.

Karayannis, C.G. & Favvata, M.J. 2008, 'Non-linear static versus dynamic analyses for the interaction of structures', *7th European Conference on Structural Dynamics, EURODYN*.

Karayannis, C.G. & Naoum, M.C. 2017a, 'Inter-story pounding and torsional effect due to interaction between adjacent multistory RC buildings', *COMPDYN, 6th ECCOMAS Thematic Conference on Computational Methods in Structural Dynamics and Earthquake Engineering, Greece*.

Karayannis, C.G. & Naoum, M.C. 2017b, 'Torsion effect due to asymmetric pounding between multistory RC buildings', *COMPDYN 2017, 6th ECCOMAS Thematic Conference on Computational Mechanics in Structural Dynamics and Earthquake Engineering, Rhodes Island, Greece, 15-17 June*.

Karayannis, C.G. & Naoum, M.C. 2018, 'Torsional behavior of multistory RC frame structures due to asymmetric seismic interaction', *Engineering Structures*, vol. 163, pp. 93-111.

Kasai, K., Jagiasi, A.R. & Jeng, V. 1996, 'Inelastic vibration phase theory for seismic pounding mitigation', *Journal of Structural Engineering*, vol. 122, no. 10, pp. 1136-46.

Kasai, K. & Maison, B.F. 1997, 'Building pounding damage during the 1989 Loma Prieta earthquake', *Engineering Structures*, vol. 19, no. 3, pp. 195-207.

Kazemi, F., Mohebi, B. & Yakhchalian, M. 2020, 'Predicting the seismic collapse capacity of adjacent structures prone to pounding', *Canadian Journal of Civil Engineering*, vol. 47, no. 6, pp. 663-77.

Khatami, S.M., Naderpour, H., Barros, R.C., Jakubczyk-Gałczyńska, A. & Jankowski, R. 2019, 'Effective formula for impact damping ratio for simulation of earthquake-induced structural pounding', *Geosciences*, vol. 9, no. 8, p. 347.

Khatami, S.M., Naderpour, H., Barros, R.C., Jakubczyk-Gałczyńska, A. & Jankowski, R. 2020, 'Determination of peak impact force for buildings exposed to structural pounding during earthquakes', *Geosciences*, vol. 10, no. 1, p. 18.

Khatiwada, S. & Chouw, N. 2014, 'Limitations in simulation of building pounding in earthquakes', *International journal of protective structures*, vol. 5, no. 2, pp. 123-50.

Khatiwada, S., Chouw, N. & Butterworth, J. 2013, 'Evaluation of numerical pounding models with experimental validation', *Bulletin of the New Zealand Society for Earthquake Engineering*, vol. 46, no. 3, pp. 117-30.

Komodromos, P., Polycarpou, P.C., Papaloizou, L. & Phocas, M.C. 2007, 'Response of seismically isolated buildings considering poundings', *Earthquake Engineering & Structural Dynamics*, vol. 36, no. 12, pp. 1605-22.

Kramer, S.L. 1996, *Geotechnical earthquake engineering*, Prentice Hall, New Jersey, USA.

Kutner, M.H., Nachtsheim, C.J., Neter, J. & Li, W. 2005, 'Applied linear statistical models', Fifth Edition edn, McGraw-Hill New York.

Lankarani, H.M. & Nikravesh, P.E. 1992, 'Hertz contact force model with permanent indentation in impact analysis of solids', *18th Annual ASME Design Automation Conference*, Publ by ASME, pp. 391-5.

Leibovich, E., Rutenberg, A. & Yankelevsky, D. 1996, 'On eccentric seismic pounding of symmetric buildings', *Earthquake engineering & structural dynamics*, vol. 25, no. 3, pp. 219-33.

Li, P., Liu, S. & Lu, Z. 2017, 'Studies on pounding response considering structure-soil-structure interaction under seismic loads', *Sustainability*, vol. 9, no. 12, p. 2219.

Lin, J.H. 1997, 'Separation distance to avoid seismic pounding of adjacent buildings', *Earthquake engineering & structural dynamics*, vol. 26, no. 3, pp. 395-403.

Lin, J.H. & Weng, C.C. 2001, 'Spectral analysis on pounding probability of adjacent buildings', *Engineering Structures*, vol. 23, no. 7, pp. 768-78.

Lin, J.H. & Weng, C.C. 2002, 'A study on seismic pounding probability of buildings in Taipei metropolitan area', *Journal of the Chinese Institute of Engineers*, vol. 25, no. 2, pp. 123-35.

López-Almansa, F. & Kharazian, A. 2018, 'New formulation for estimating the damping parameter of the Kelvin-Voigt model for seismic pounding simulation', *Engineering Structures*, vol. 175, pp. 284-95.

Lopez-Garcia, D. & Soong, T.T. 2009, 'Assessment of the separation necessary to prevent seismic pounding between linear structural systems', *Probabilistic Engineering Mechanics*, vol. 24, no. 2, pp. 210-23.

Luenberger, D.G. & Ye, Y. 1984, *Linear and nonlinear programming*, vol. 2, Springer Switzerland.

Mahmoud, S., Chen, X. & Jankowski, R. 2008, 'Structural pounding models with Hertz spring and nonlinear damper', *Journal of Applied Sciences*, vol. 8, no. 10, pp. 1850-8.

Mahmoud, S. & Jankowski, R. 2011, 'Modified linear viscoelastic model of earthquake-induced structural pounding', *Iranian Journal of Science and Technology, Transactions of Civil and Environmental Engineering*, vol. 35, pp. 55-62.

Maison, B.F. & Kasai, K. 1990, 'Analysis for a type of structural pounding', *Journal of Structural Engineering*, vol. 116, no. 4, pp. 957-77.

Maison, B.F. & Kasai, K. 1992, 'Dynamics of pounding when two buildings collide', *Earthquake Engineering & Structural Dynamics*, vol. 21, no. 9, pp. 771-86.

Mate, N., Bakre, S. & Jaiswal, O. 2012, 'Comparative study of impact simulation models for linear elastic structures in seismic pounding', *15th World Conference on Earthquake Engineering*, Lisbon, Portugal.

Mavronicola, E., Polycarpou, P.C. & Komodromos, P. 2015, 'The effect of modified linear viscoelastic impact models on the pounding response of a base isolated building with adjacent structures', *5th International Conference on Computational Methods in Structural Dynamics and Earthquake Engineering*, Crete Island, Greece.

Mavronicola, E.A., Polycarpou, P.C. & Komodromos, P. 2016, 'Effect of planar impact modeling on the pounding response of base-isolated buildings', *Frontiers in Built Environment*, vol. 2, p. 11.

Miari, M., Choong, K.K. & Jankowski, R. 2019, 'Seismic pounding between adjacent buildings: Identification of parameters, soil interaction issues and mitigation measures', *Soil Dynamics and Earthquake Engineering*, vol. 121, pp. 135-50.

Montgomery, D.C., Runger, G.C. & Hubele, N.F. 2009, *Engineering statistics*, Fourth Edition edn, John Wiley & Sons.

Muthukumar, S. & Desroches, R. 2006, 'A Hertz contact model with non-linear damping for pounding simulation', *Earthquake engineering & structural dynamics*, vol. 35, no. 7, pp. 811-28.

Naderpour, H., Barros, R.C., Khatami, S.M. & Jankowski, R. 2016, 'Numerical Study on Pounding between Two Adjacent Buildings under Earthquake Excitation', *Shock and Vibration*, vol. 2016.

Naderpour, H., Khatami, S.M. & Barros, R.C. 2017, 'Prediction of critical distance between two MDOF systems subjected to seismic excitation in terms of artificial neural networks', *Periodica Polytechnica Civil Engineering*, vol. 61, no. 3, pp. 516-29.

Naserkhaki, S., Aziz, A., Farah, N. & Pourmohammad, H. 2012, 'Parametric study on earthquake induced pounding between adjacent buildings', *Structural Engineering and Mechanics*, vol. 43, no. 4, pp. 503-26.

Naserkhaki, S., El-Richa, M., Abdul Azizb, F.N.A. & Pourmohammadc, H. 2013, 'Separation gap, a critical factor in earthquake induced pounding between adjacent buildings', *Asian Journal of Civil Engineering*, vol. 14, no. 6, pp. 881-98.

NBCC 2010, 'National Building Code of Canada', *National Research Council, Ottawa*.

Noman, M., Alam, B., Fahad, M., Shahzada, K. & Kamal, M. 2016, 'Effects of pounding on adjacent buildings of varying heights during earthquake in Pakistan', *Cogent Engineering*, vol. 3, no. 1, p. 1225878.

Ostertagová, E. 2012, 'Modelling using polynomial regression', *Procedia Engineering*, vol. 48, pp. 500-6.

Pant, D.R., Wijeyewickrema, A.C. & Ohmachi, T. 2010, 'Seismic pounding between reinforced concrete buildings: A study using two recently proposed contact element models', *14th European Conference on Earthquake Engineering*, Ohrid, Republic of Macedonia.

Papadrakakis, M. & Mouzakis, H.P. 1995, 'Earthquake simulator testing of pounding between adjacent buildings', *Earthquake engineering & structural dynamics*, vol. 24, no. 6, pp. 811-34.

Papagiannopoulos, G.A. & Hatzigeorgiou, G.D. 2011, 'On the use of the half-power bandwidth method to estimate damping in building structures', *Soil Dynamics and Earthquake Engineering*, vol. 31, no. 7, pp. 1075-9.

Penzien, J. 1997, 'Evaluation of building separation distance required to prevent pounding during strong earthquakes', *Earthquake engineering & structural dynamics*, vol. 26, no. 8, pp. 849-58.

Pitilakis, D., Dietz, M., Wood, D.M. & Modaressi, A. 2008, 'Numerical simulation of dynamic soil–structure interaction in shaking table testing', *Soil dynamics and earthquake Engineering*, vol. 28, no. 6, pp. 453-67.

Polycarpou, P.C. & Komodromos, P. 2010, 'Earthquake-induced poundings of a seismically isolated building with adjacent structures', *Engineering Structures*, vol. 32, no. 7, pp. 1937-51.

Polycarpou, P.C., Papaloizou, L. & Komodromos, P. 2014, 'An efficient methodology for simulating earthquake-induced 3D pounding of buildings', *Earthquake engineering & structural dynamics*, vol. 43, no. 7, pp. 985-1003.

Raheem, S.E.A. 2013, 'Mitigation Measures for Seismic Pounding Effects on Adjacent Buildings Responses ', paper presented to the *4th ECCOMAS Thematic Conference*, Kos Island, Greece, 12–14 June 2013.

Raheem, S.E.A., Fooly, M.Y., Omar, M. & Zaher, A.K.A. 2019, 'Seismic pounding effects on the adjacent symmetric buildings with eccentric alignment', *Earthquakes and Structures*, vol. 16, no. 6, pp. 715-26.

Raheem, S.E.A., Fooly, M.Y., Shafy, A.G., Abbas, Y.A., Omar, M., Latif, M. & Mahmoud, S. 2018, 'Seismic pounding effects on adjacent buildings in series with different alignment configurations', *Steel and Composite Structures*, vol. 28, no. 3, pp. 289-308.

Rahman, A.M., Carr, A.J. & Moss, P.J. 2000, 'Structural pounding of adjacent multi-storey structures considering soil flexibility effects', *12th World Conference on earthquake engineering, Article*.

Rezavandi, A. & Moghadam, A.S. 2007, 'Experimental and numerical study on pounding effects and mitigation techniques for adjacent structures', *Advances in Structural Engineering*, vol. 10, no. 2, pp. 121-34.

Richardson, A., Walsh, K. & Abdullah, M. 2013, 'Closed-form design equations for controlling vibrations in connected structures', *Journal of Earthquake Engineering*, vol. 17, no. 5, pp. 699-719.

Romão, X., Costa, A., Paupério, E., Rodrigues, H., Vicente, R., Varum, H. & Costa, A. 2013, 'Field observations and interpretation of the structural performance of constructions after the 11 May 2011 Lorca earthquake', *Engineering Failure Analysis*, vol. 34, pp. 670-92.

Rosenblueth, E. & Meli, R. 1986, 'The 1985 earthquake: Causes and effects in Mexico City', *Concrete International*, vol. 8, no. 5, pp. 23-34.

SAP, C. 2000, 'Integrated software for structural analysis and design', *Analysis reference manual*.

Schramm, U. & Pilkey, W.D. 1996, 'Optimal design of structures under impact loading', *Shock and Vibration*, vol. 3, no. 1, pp. 69-81.

Shakya, K., Wijeyewickrema, A.C. & Ohmachi, T. 2008, 'Mid-column seismic pounding of reinforced concrete buildings in a row considering effects of soil', *14th World Conference on Earthquake Engineering*, pp. 12-7.

Shao, J. 1993, 'Linear model selection by cross-validation', *Journal of the American statistical Association*, vol. 88, no. 422, pp. 486-94.

Shrestha, B. 2013, 'Effects of separation distance and nonlinearity on pounding response of adjacent structures', *International Journal of Civil and Structural Engineering*, vol. 3, no. 3, p. 603.

Shrestha, B. & Hao, H. 2018, 'Building Pounding Damages Observed during the 2015 Gorkha Earthquake', *Journal of Performance of Constructed Facilities*, vol. 32, no. 2, p. 04018006.

Skrekas, P., Sextos, A. & Giaralis, A. 2014, 'Influence of bi-directional seismic pounding on the inelastic demand distribution of three adjacent multi-storey R/C buildings', *Earthquakes and Structures*, vol. 6, no. 1, pp. 71-87.

Sołtysik, B., Falborski, T. & Jankowski, R. 2017, 'Preventing of earthquake-induced pounding between steel structures by using polymer elements-experimental study', *Procedia Engineering*, vol. 199, pp. 278-83.

Sołtysik, B. & Jankowski, R. 2013, 'Non-linear strain rate analysis of earthquake-induced pounding between steel buildings', *International Journal of Earth Sciences and Engineering*, vol. 6, pp. 429-33.

Sołtysik, B. & Jankowski, R. 2015, 'Building damage due to structural pounding during earthquakes', *Journal of Physics: Conference Series*, vol. 628, IOP Publishing, p. 012040.

STAINLESS, P. 2021, *PRECIPITATION HARDENING GRADES*, viewed 20/08/2021, <https://www.pennstainless.com/resources/product-information/stainless-grades/precipitation-hardening-grades/17-4ph-h900/>.

Tabatabaiefar, H.R. & Mansoury, B. 2016, 'Detail design, building and commissioning of tall building structural models for experimental shaking table tests', *The Structural Design of Tall and Special Buildings*, vol. 25, no. 8, pp. 357-74.

Tabatabaiefar, S.H.R., Fatahi, B. & Samali, B. 2014, 'Numerical and experimental investigations on seismic response of building frames under influence of soil-structure interaction', *Advances in Structural Engineering*, vol. 17, no. 1, pp. 109-30.

TBC 1997, 'Construction and Planning Administration', *Ministry of Interior, Seismic Provisions, Taiwan Building Code.*

Valles-Mattox, R. & Reinhorn, A. 1996, 'Evaluation, prevention and mitigation of pounding effects in building structures', *Eleventh World Conference on Earthquake Engineering*, Acapulco, Mexico.

Van Mier, J. & Lenos, S. 1991, 'Experimental analysis of the load-time histories of concrete to concrete impact', *Coastal engineering*, vol. 15, no. 1-2, pp. 87-106.

Wada, A., Shinozaki, Y. & Nakamura, N. 1984, 'Collapse of building with expansion joints through collision caused by earthquake motion', *Proceedings of 8th WCEE*, vol. 4, San Francisco, USA pp. 855-63.

Wang, S. & Hong, H. 2006, 'Quantiles of critical separation distance for nonstationary seismic excitations', *Engineering structures*, vol. 28, no. 7, pp. 985-91.

Wibowo, A., Kafle, B., Kermani, A.M., Lam, N.T., Wilson, J.L. & Gad, E.F. 2008, 'Damage in the 2008 China earthquake', *Procs. of Australian Earthquake Engineering Society Conference*, Ballarat, Australia, pp. 1-8.

Xu, X., Xu, X., Liu, W. & Zhou, D. 2016, 'A new formula of impact stiffness in linear viscoelastic model for pounding simulation', *Shock and Vibration*, vol. 2016.

Yaghmaei-Sabegh, S. & Jalali-Milani, N. 2012, 'Pounding force response spectrum for near-field and far-field earthquakes', *Scientia Iranica*, vol. 19, no. 5, pp. 1236-50.

Yaghmaei-Sabegh, S. & Tsang, H. 2011, 'An updated study on near-fault ground motions of the 1978 Tabas, Iran, earthquake (Mw= 7.4)', *Scientia Iranica*, vol. 18, no. 4, pp. 895-905.

Ye, K. & Li, L. 2009, 'Impact analytical models for earthquake-induced pounding simulation', *Frontiers of Architecture and Civil Engineering in China*, vol. 3, no. 2, pp. 142-7.

Ye, K., Li, L. & Zhu, H. 2009, 'A note on the Hertz contact model with nonlinear damping for pounding simulation', *Earthquake Engineering & Structural Dynamics*, vol. 38, no. 9, pp. 1135-42.

Zheng, Y., Xiao, X., Zhi, L. & Wang, G. 2015, 'Evaluation on impact interaction between abutment and steel girder subjected to nonuniform seismic excitation', *Shock and Vibration*, vol. 2015.

APPENDIX A

Detailed drawings of scaled experimental steel frame models

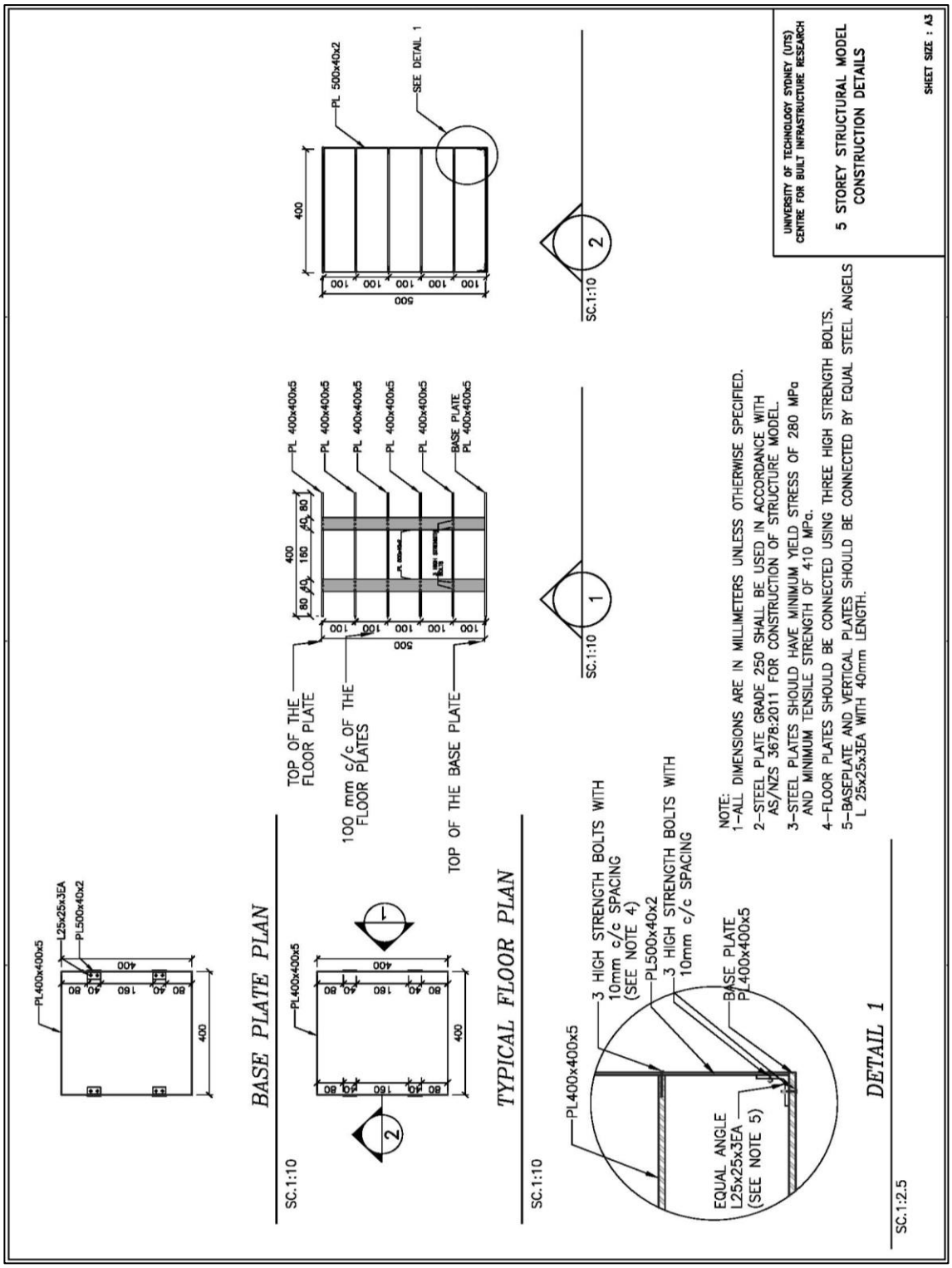

Figure A.1 Construction detail drawings of 5-storey structural model

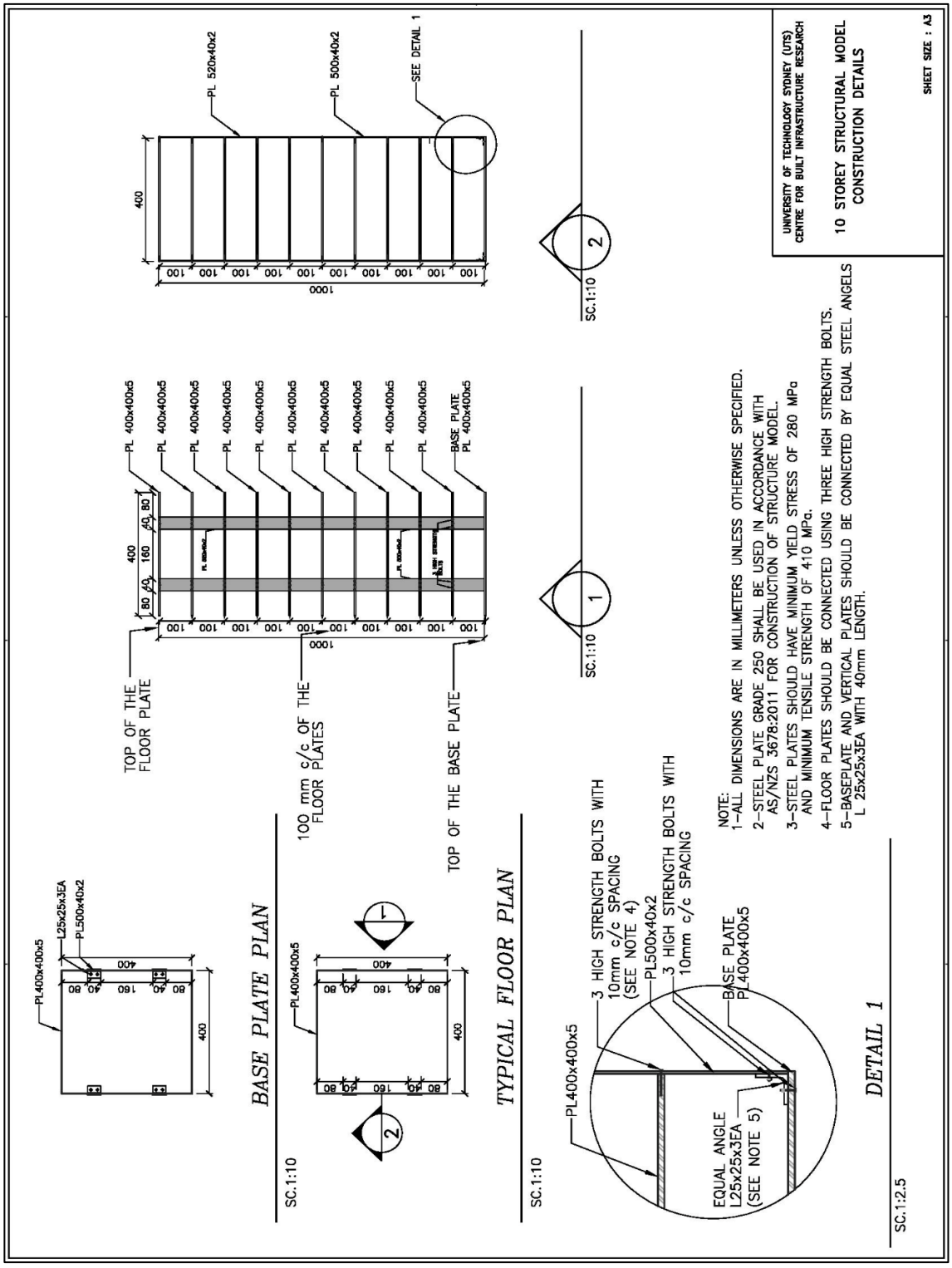

Figure A.2 Construction detail drawings of 10-storey structural model

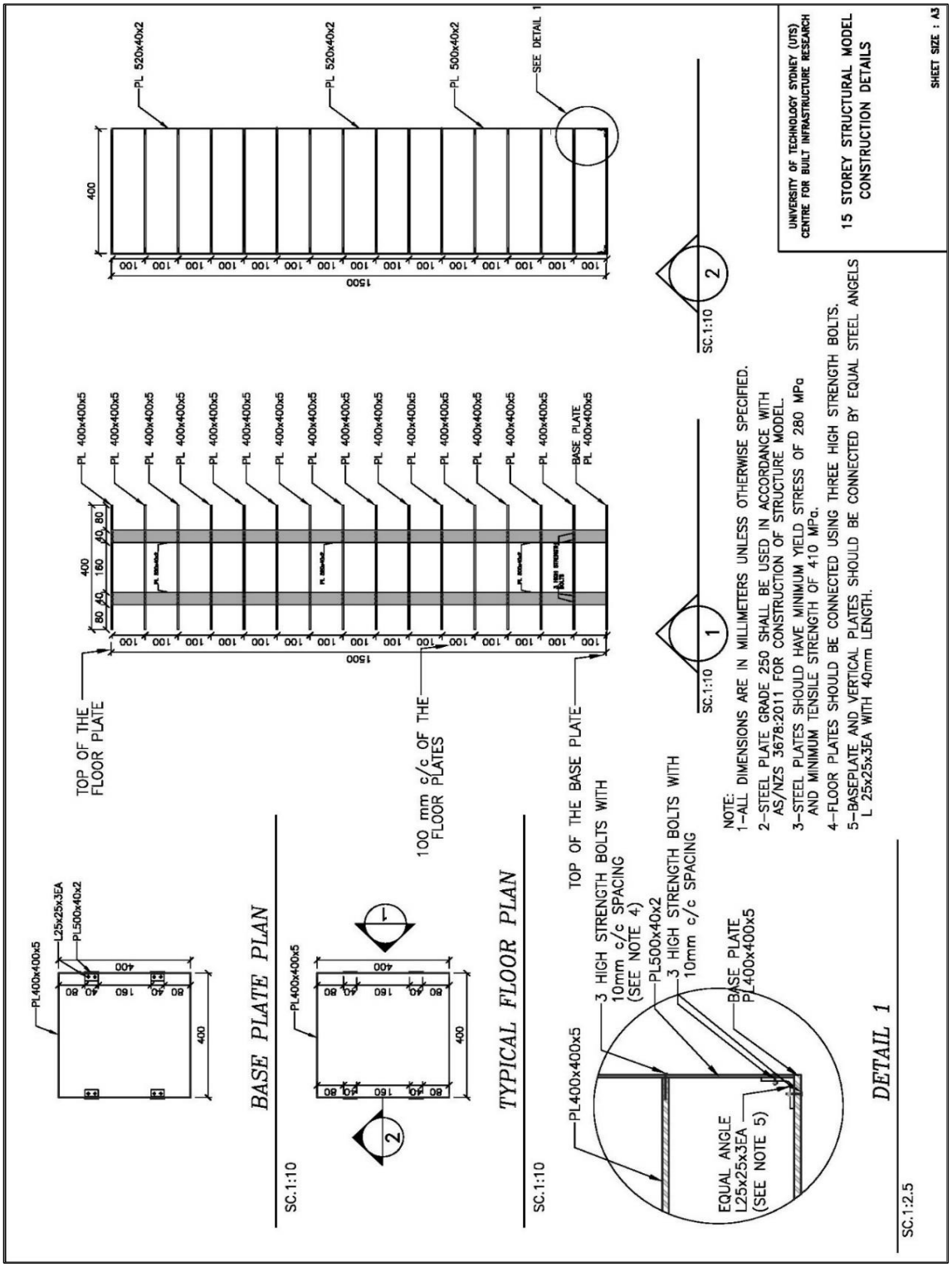

Figure A.3 Construction detail drawings of 15-storey structural model

APPENDIX B

Material stress–strain curve plot

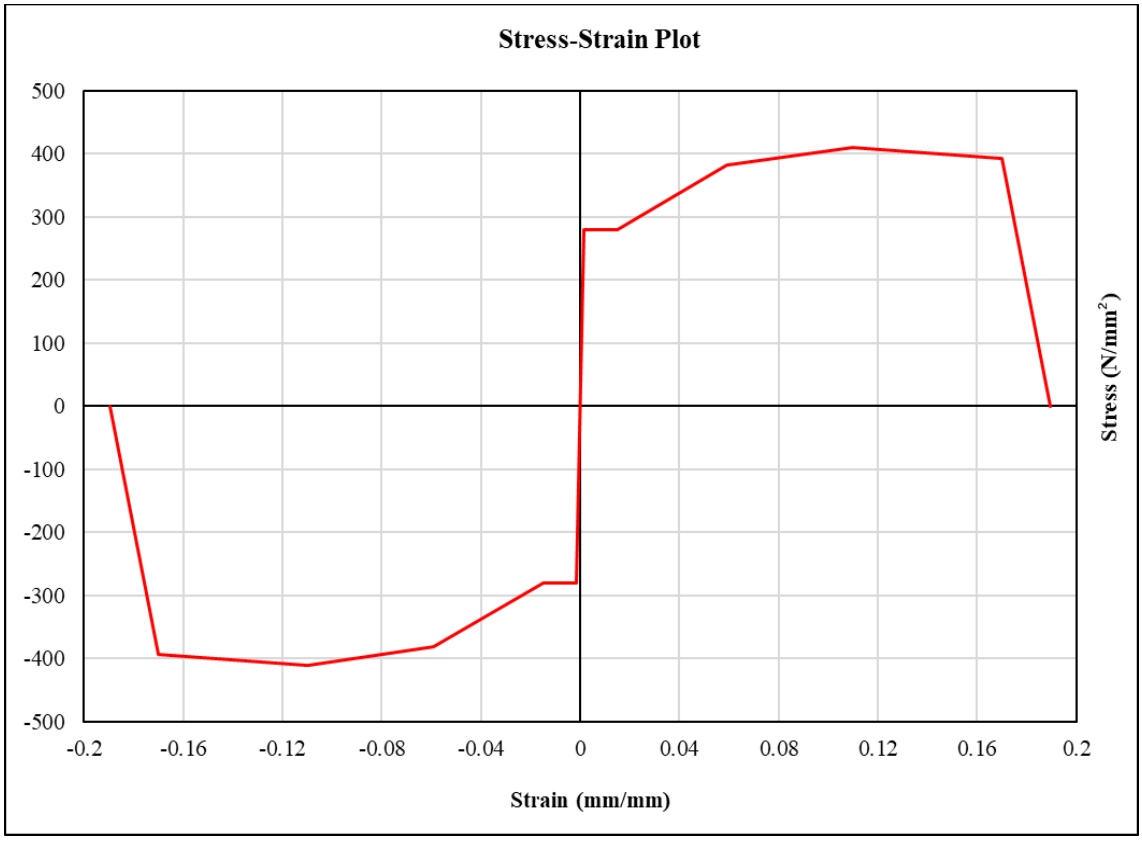

Figure B.1 Stress–strain relationship for steel

Default values of the strain parameters, i.e. strain at onset of strain hardening, strain at maximum stress, strain at rupture and final slope (0.015, 0.11, 0.17 and -0.1, respectively), have been used in this study to accurately simulate the inelastic material behaviour.

APPENDIX C

Load-deflection relationships for scaled experimental steel frame models

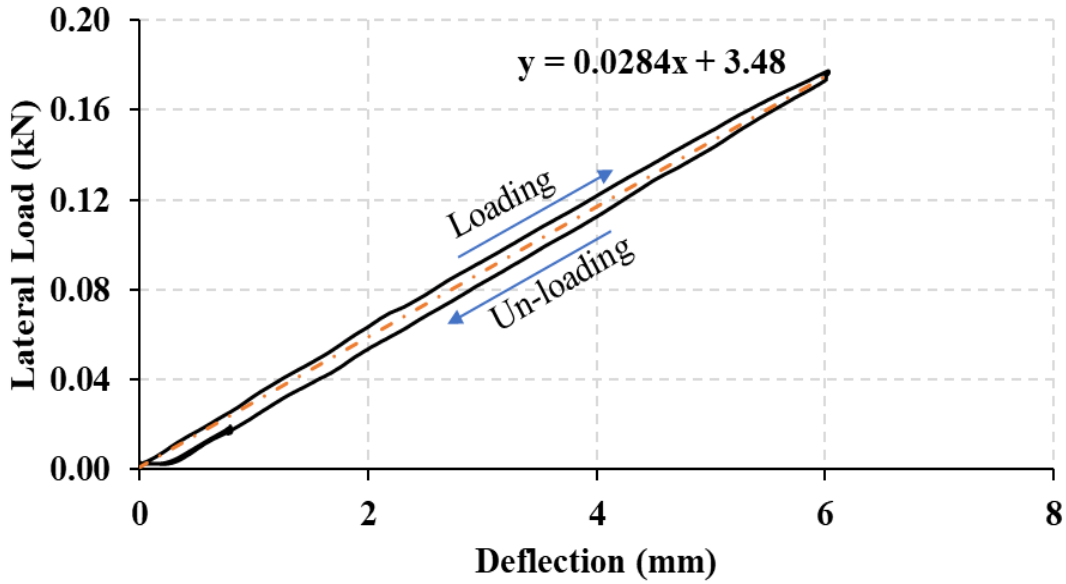

Figure C.1 Load-deflection curve for the 5A-storey frame

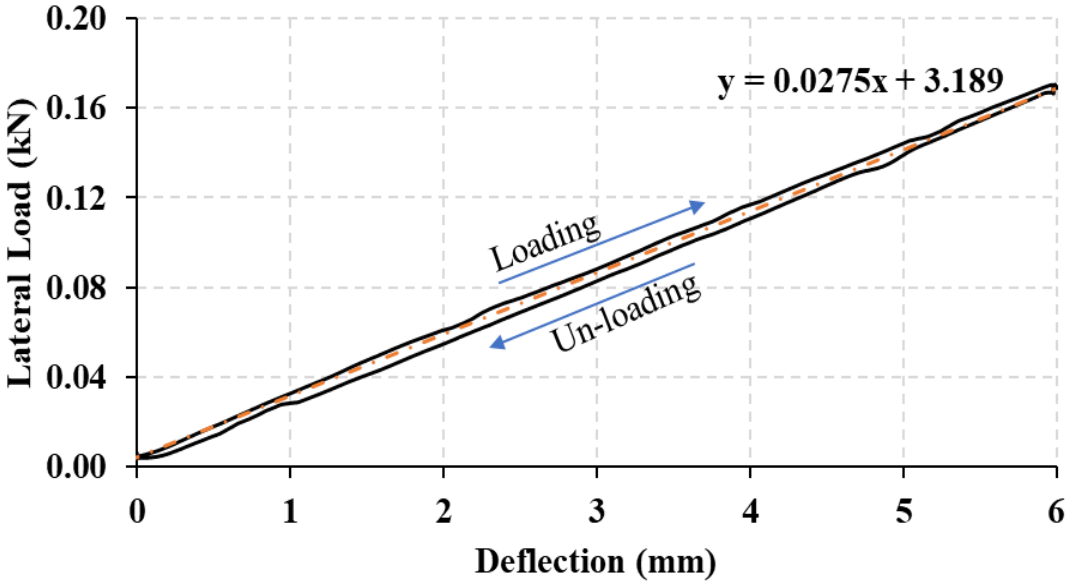

Figure C.2 Load-deflection curve for the 5B-storey frame

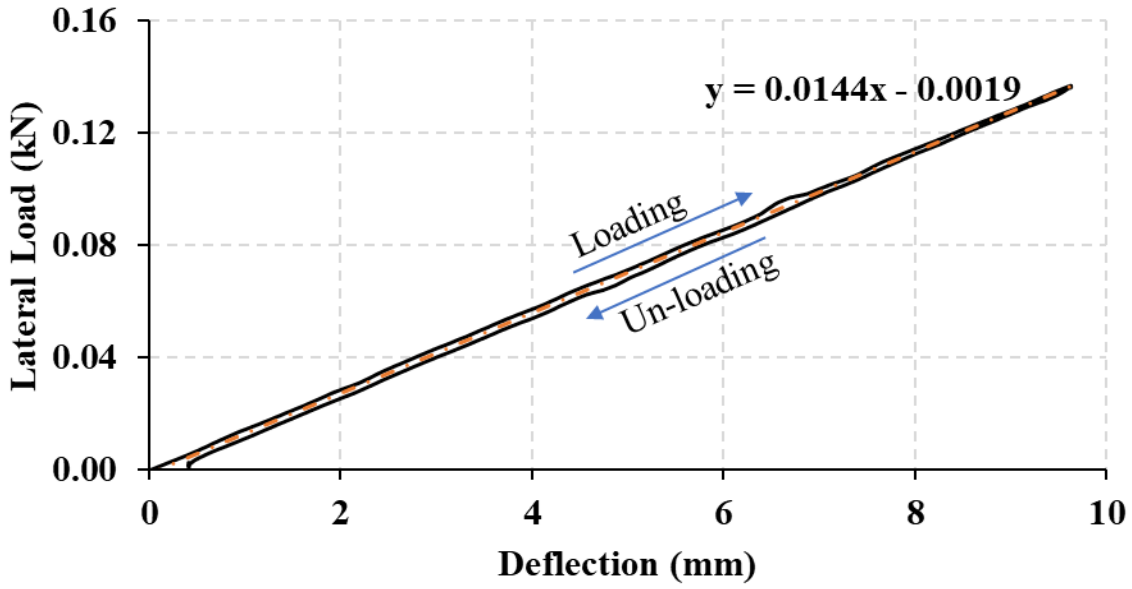

Figure C.3 Load-deflection curve for the 10-storey frame

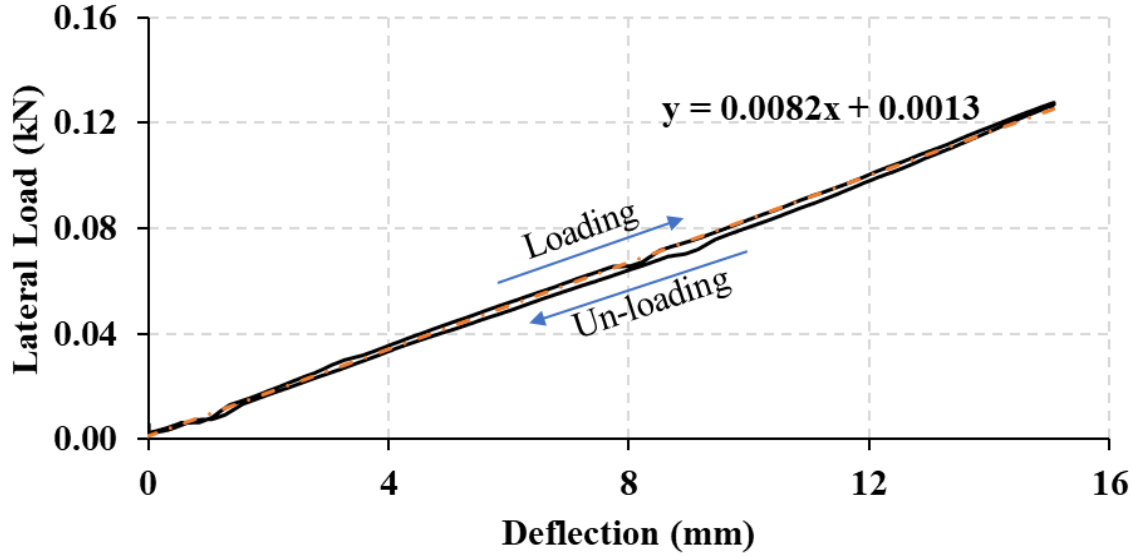

Figure C.4 Load-deflection curve for the 15A-storey frame

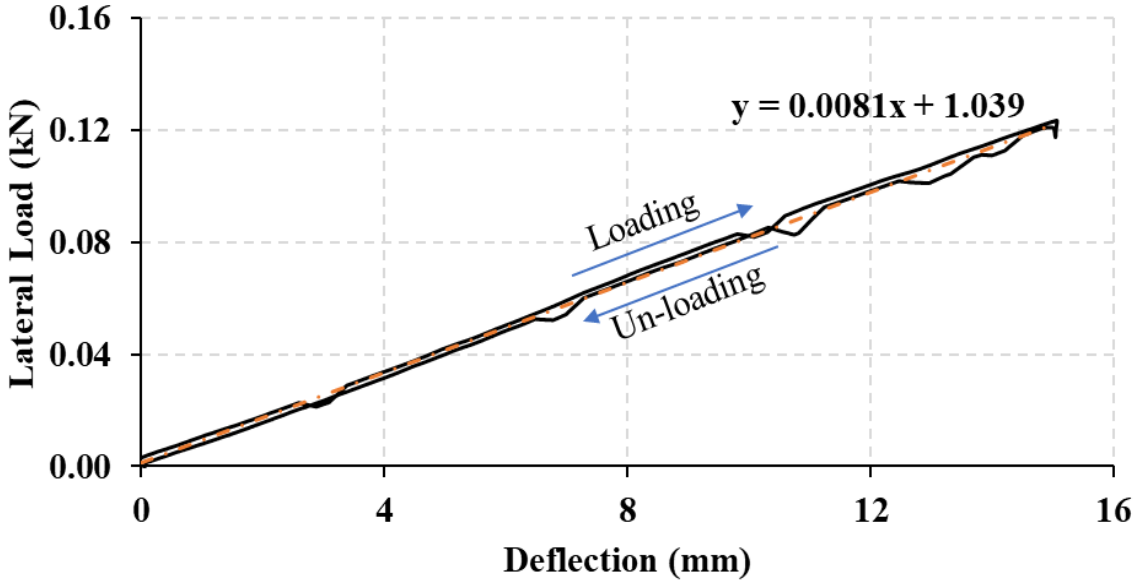

Figure C.5 Load-deflection curve for the 15B-storey frame

APPENDIX D

Acceleration time history measured on all experimental vs sine-sweep excitations

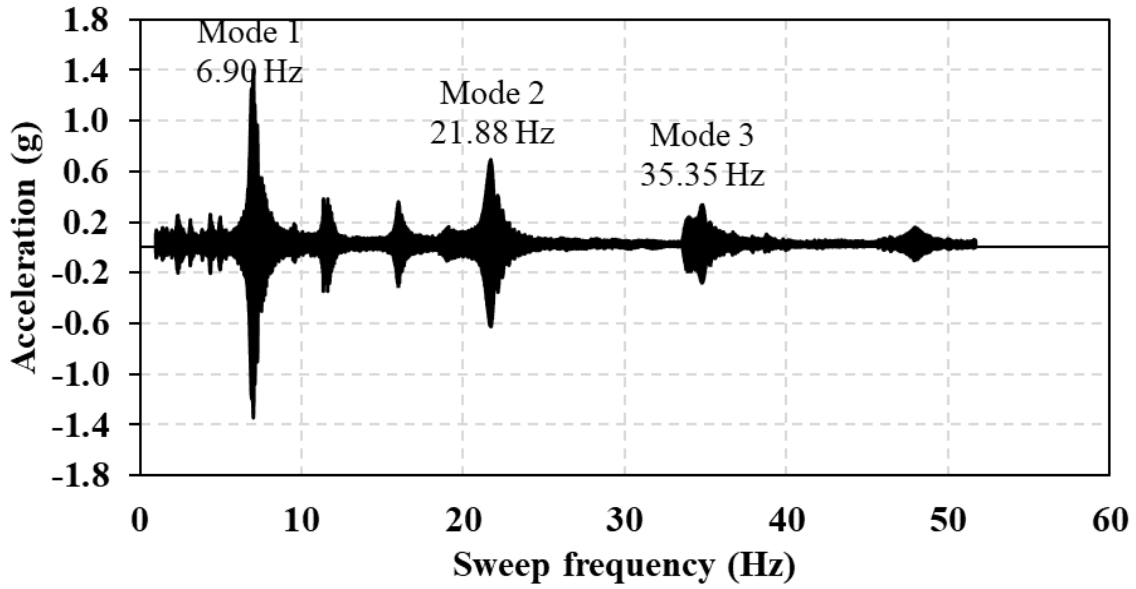

Figure D.1 Acceleration time history measured on 5A-storey frame vs sine-sweep excitation

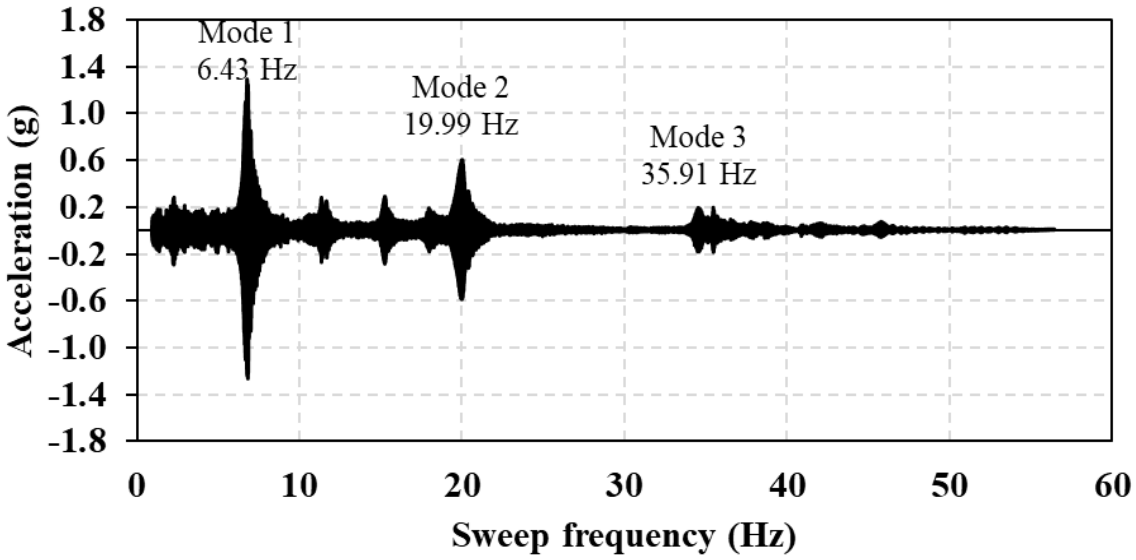

Figure D.2 Acceleration time history measured on 5B-storey frame vs sine-sweep excitation

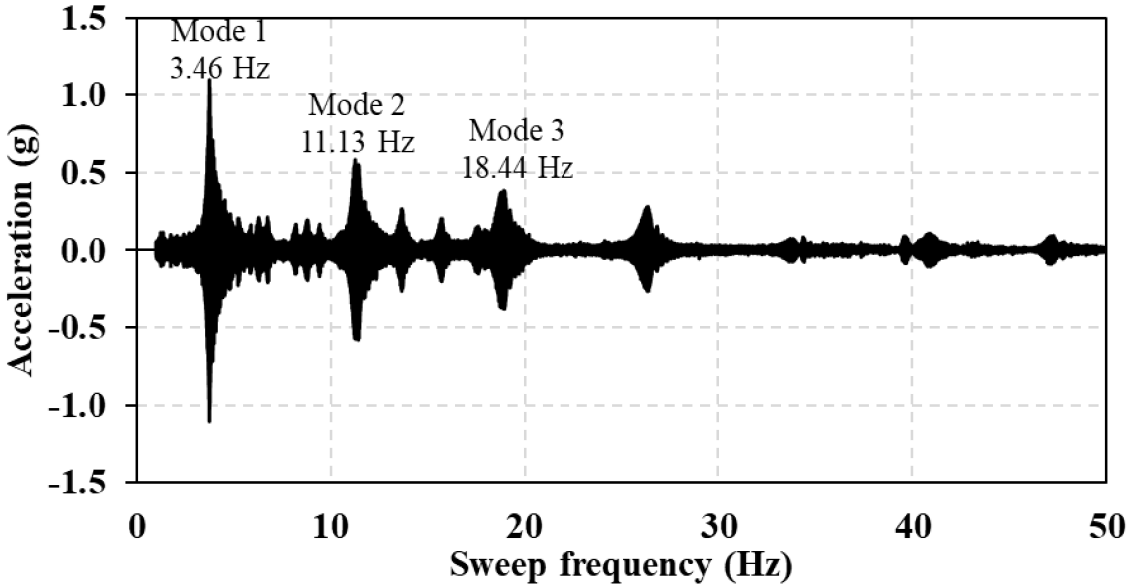

Figure D.3 Acceleration time history measured on 10-storey frame vs sine-sweep excitation

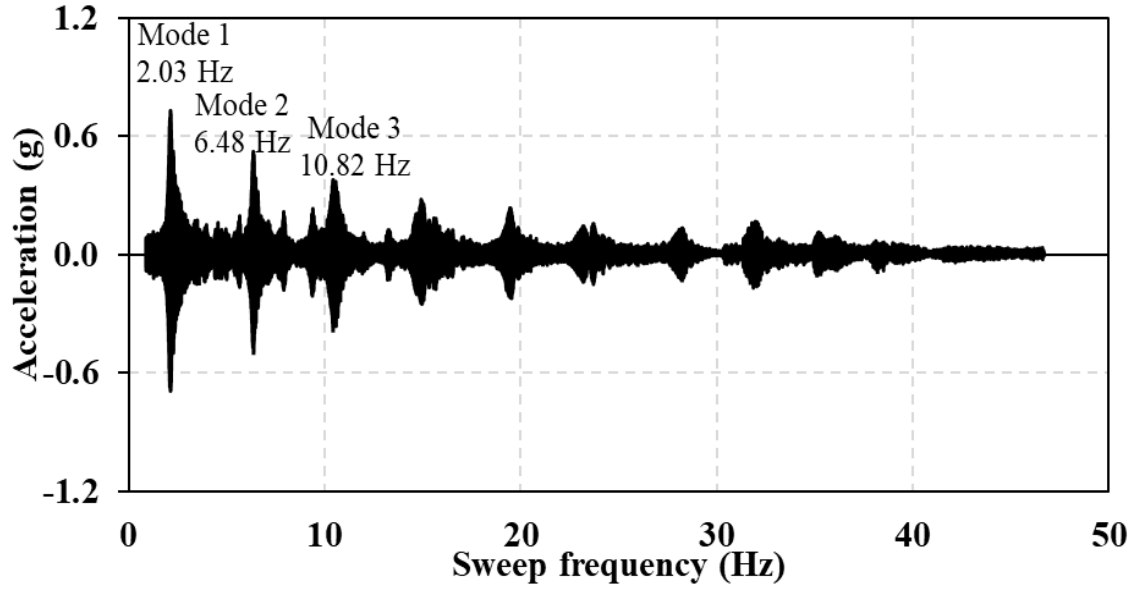

Figure D.4 Acceleration time history measured on 15A-storey frame vs sine-sweep excitation

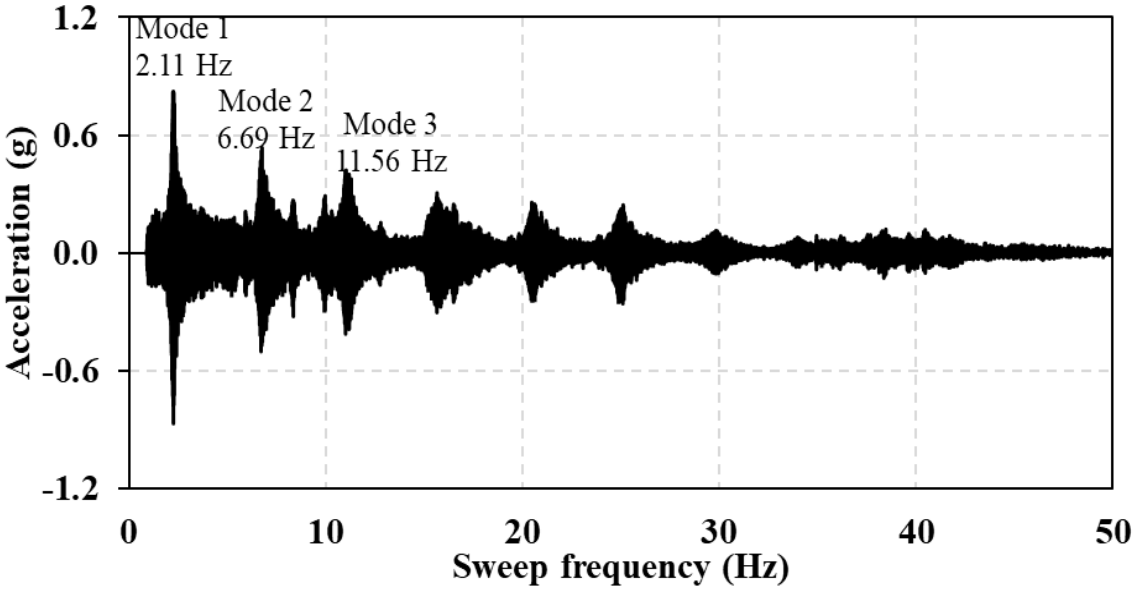

Figure D.5 Acceleration time history measured on 15B-storey frame vs sine-sweep excitation

APPENDIX E

Experimental and numerical acceleration time histories for the top floor of each frame model

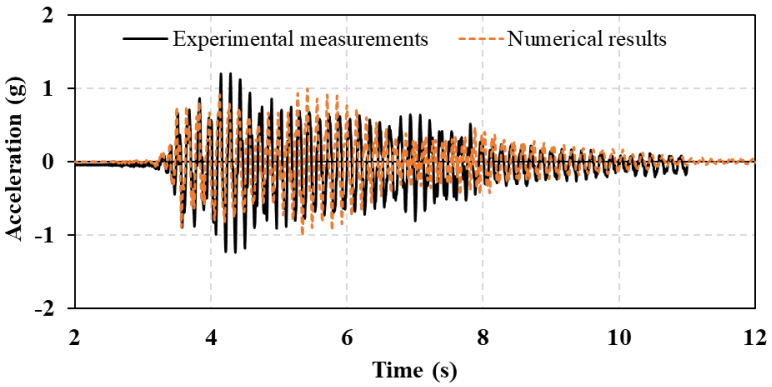

(a)

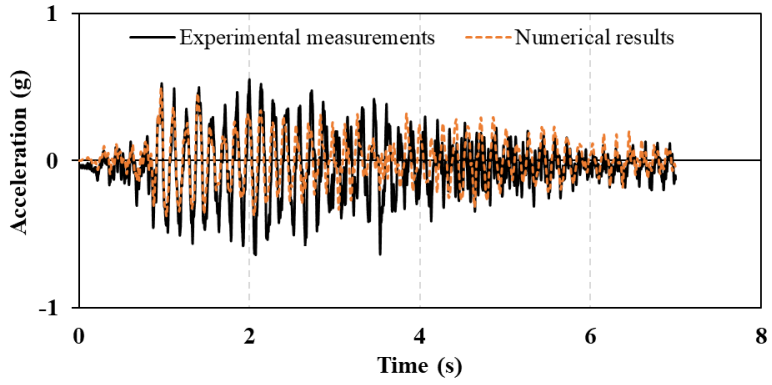

(b)

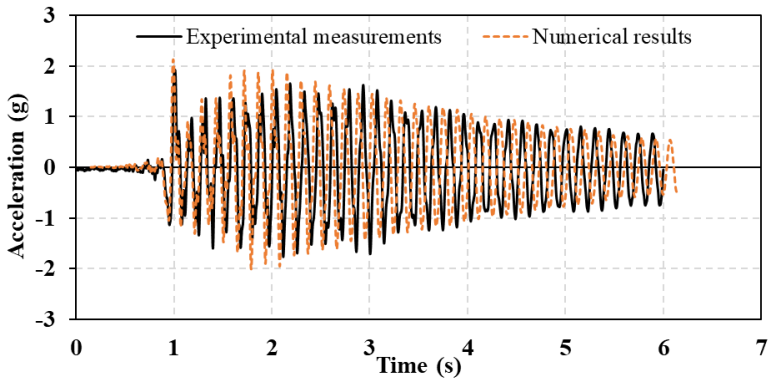

(c)

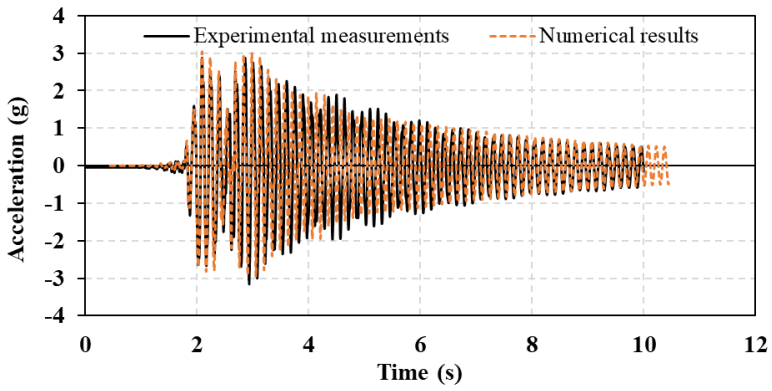

(d)

Figure E.1 Experimental and numerical acceleration time histories for 5A-storey frame (top floor) under scaled: a) El Centro earthquake; b) Hachinohe earthquake; c) Northridge earthquake; d) Kobe earthquake

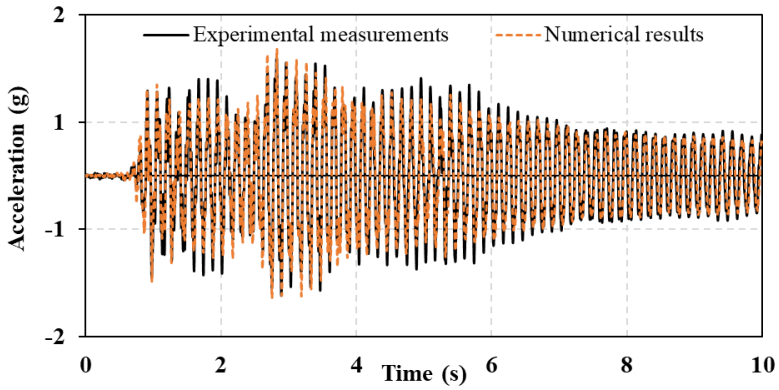

(a)

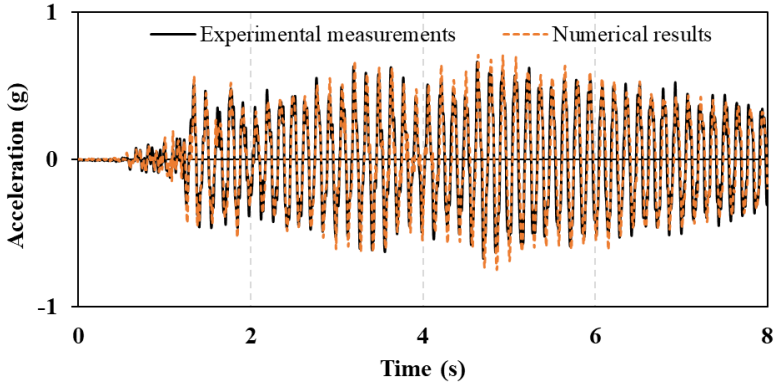

(b)

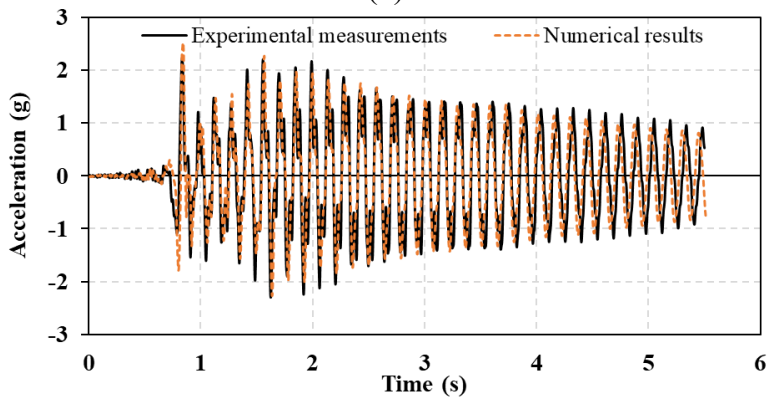

(c)

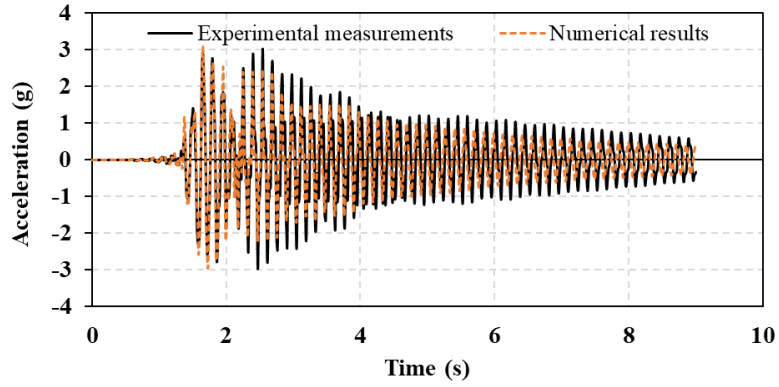

(d)

Figure E.2 Experimental and numerical acceleration time histories for 5B-storey frame (top floor) under scaled: a) El Centro earthquake; b) Hachinohe earthquake; c) Northridge earthquake; d) Kobe earthquake

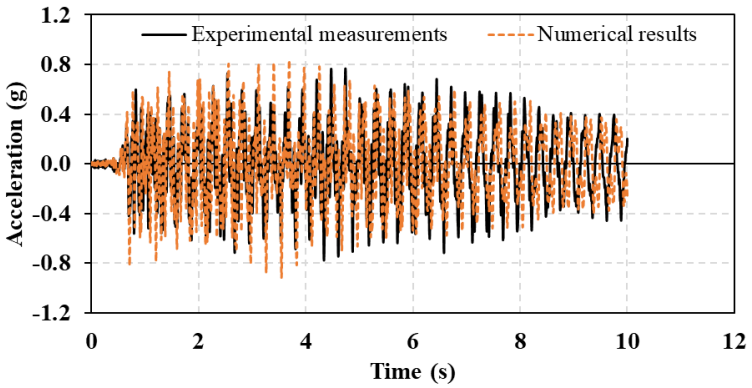

(a)

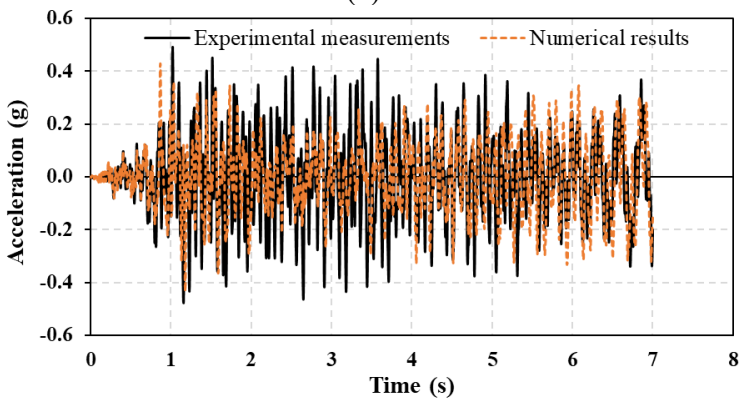

(b)

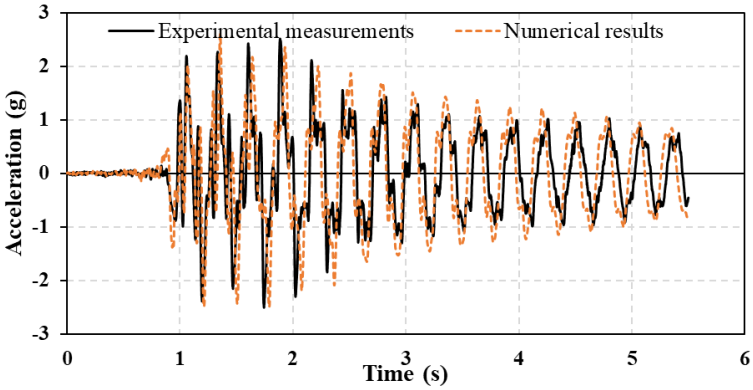

(c)

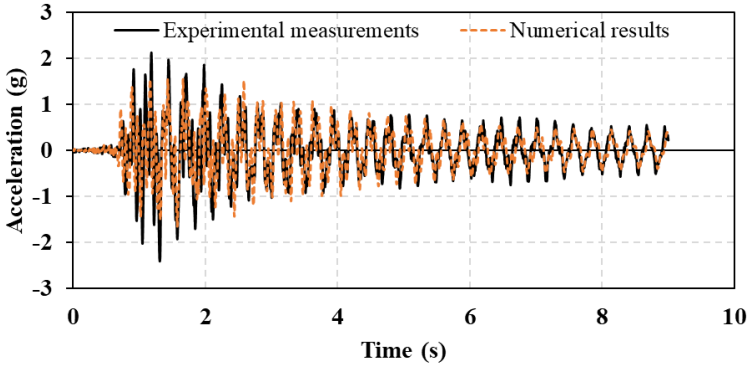

(d)

Figure E.3 Experimental and numerical acceleration time histories for 10-storey frame (top floor) under scaled: a) El Centro earthquake; b) Hachinohe earthquake; c) Northridge earthquake; d) Kobe earthquake

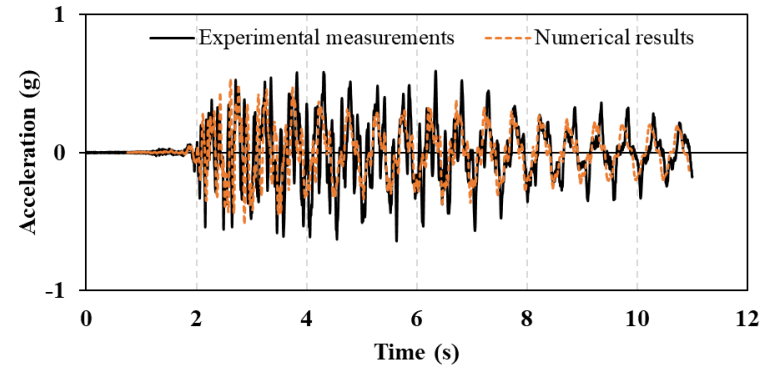

(a)

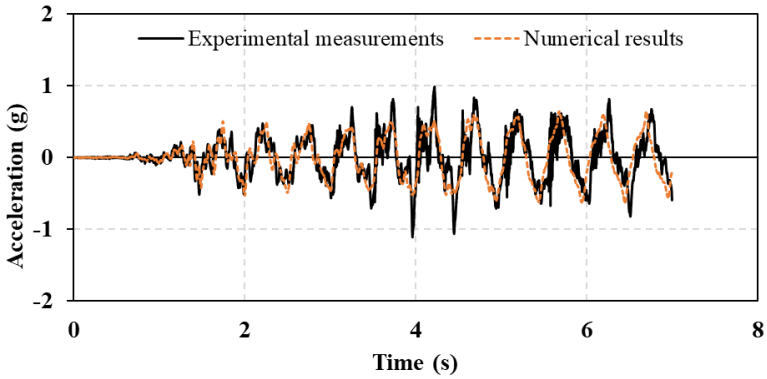

(b)

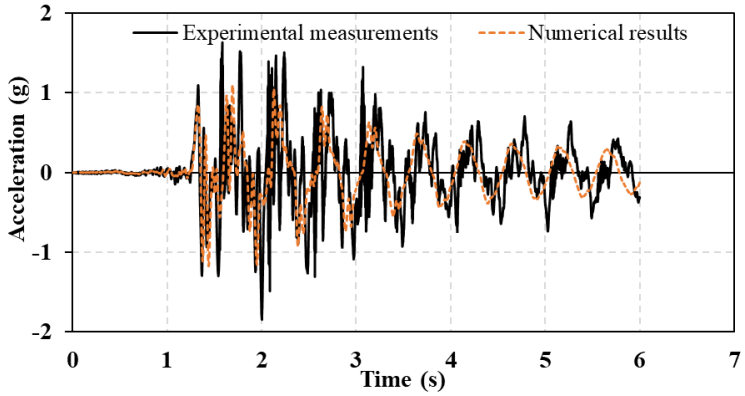

(c)

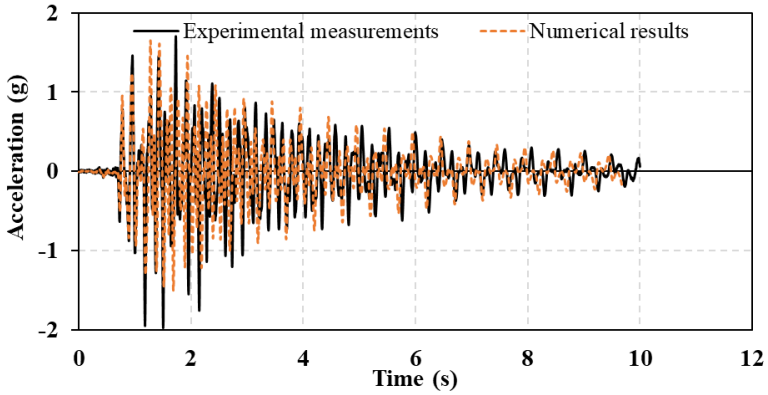

(d)

Figure E.4 Experimental and numerical acceleration time histories for 15A-storey frame (top floor) under scaled; a) El Centro earthquake; b) Hachinohe earthquake; c) Northridge earthquake; d) Kobe earthquake

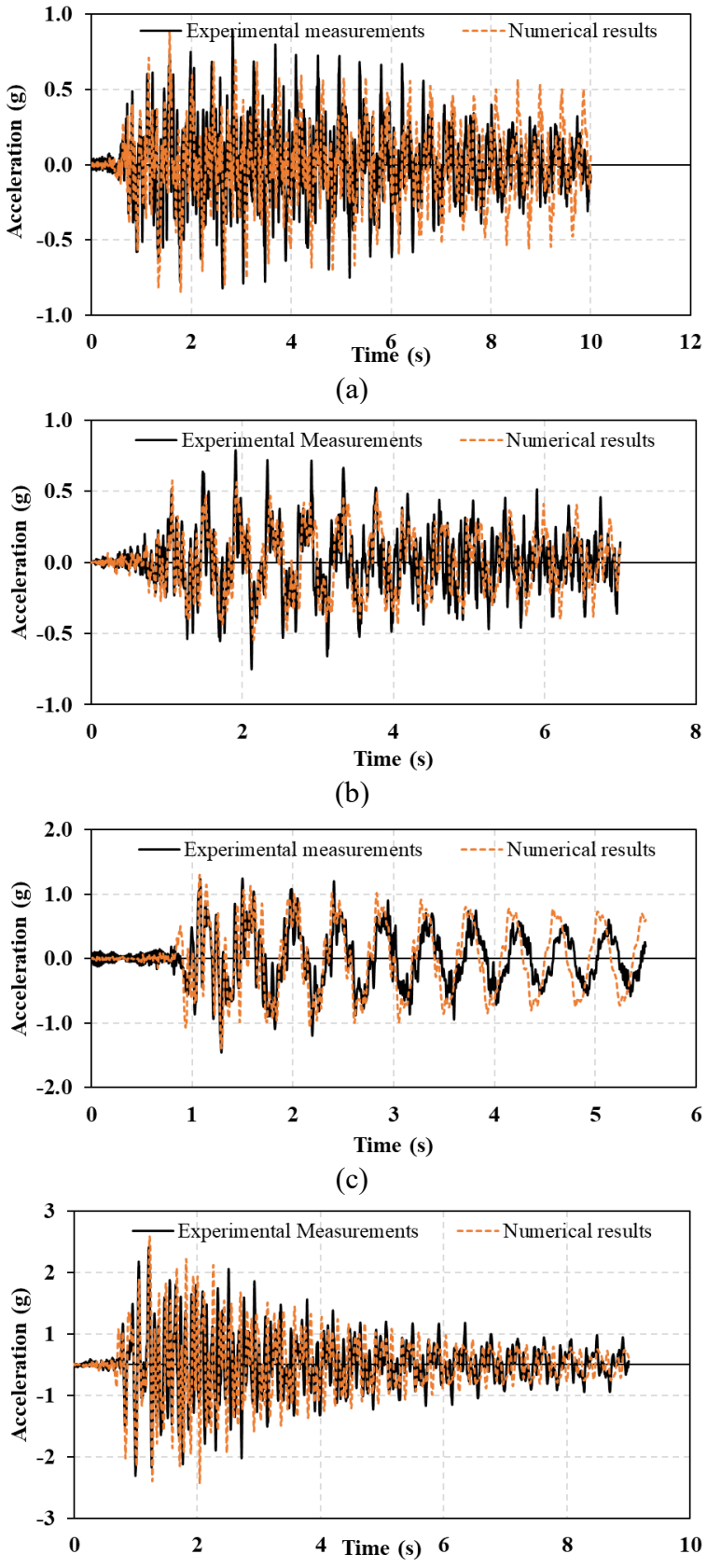

Figure E.5 Experimental and numerical relative displacement time histories for 15B-storey frame (top floor) under scaled: a) El Centro earthquake; b) Hachinohe earthquake; c) Northridge earthquake; d) Kobe earthquake

APPENDIX F

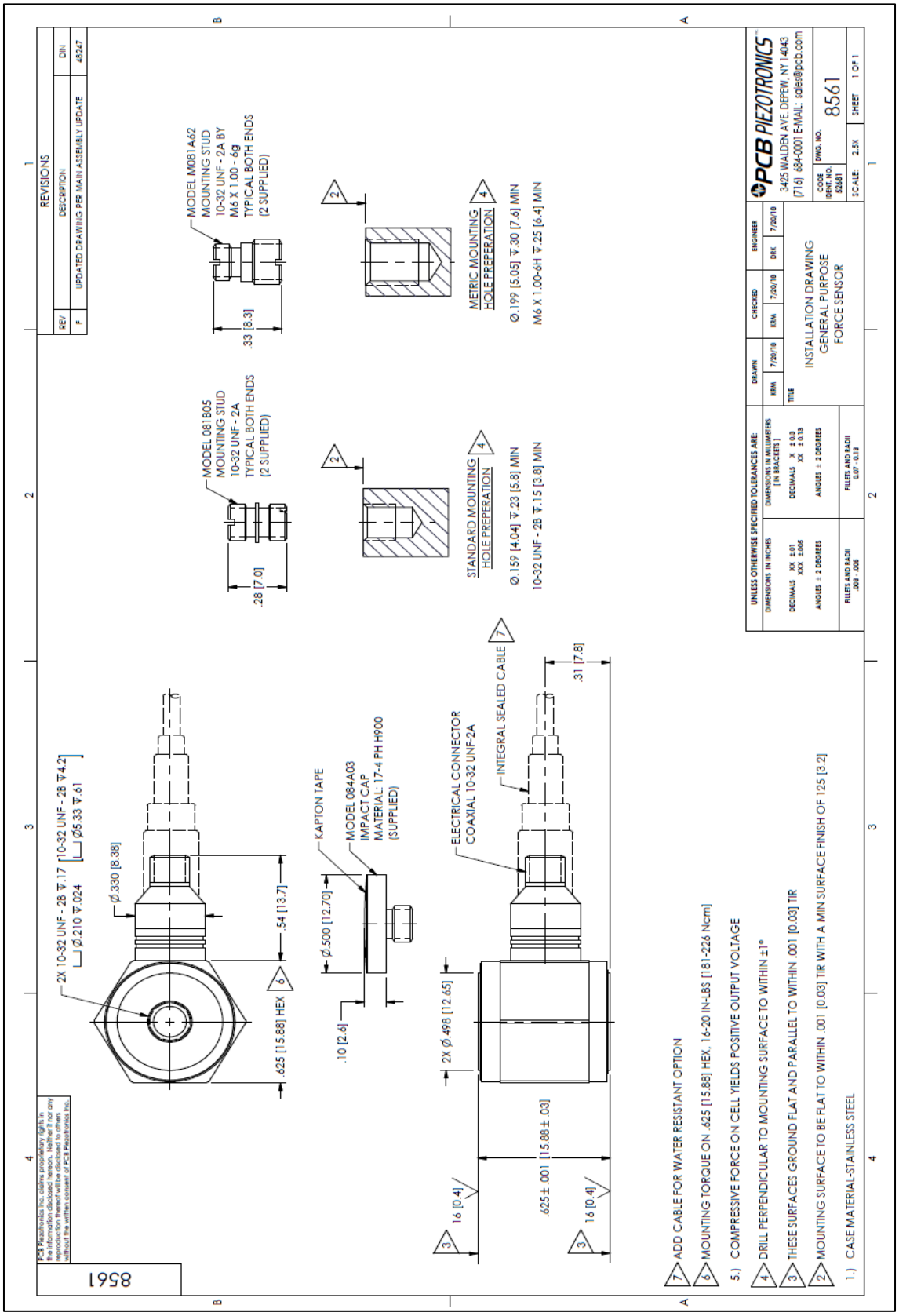

Figure F.1 Force sensor model PCB 208C05 detail drawing